Distribution and spatial statistics of pockmarks above the Smeaheia CO2 storage area:

Evaluating Quaternary sediments as a secondary seal

Elias Heimdal Leon

Master thesis
Structural Geology and Tectonics
60 credits

Department of Geosciences
The Faculty of Mathematics and Natural Sciences

UNIVERSITY of OSLO

April 2019

[Tittelblad]

(samme tekst som på forsiden, men studenten står friere i utformingen)

2019

Distribution and spatial statistics of pockmarks above the Smeaheia CO_2 storage area: Evaluating Quaternary sediments as a secondary seal

Elias Heimdal Leon

Supervisors: Alvar Braathen, Mark J. Mulrooney and Jonathon L. Osmond

http://www.duo.uio.no/

Print: Reprosentralen, University of Oslo

Abstract

Preface

This thesis is submitted to the Department of Geosciences, University of Oslo (UiO), following the master's programme in Geosciences consisting of 120 ECTS credits with subcategory: Structural geology and tectonics. The thesis is supervised by Professor Alvar Braathen (UiO), Postdoctoral Fellow Mark J. Mulrooney (UiO) and Doctoral Research Fellow Johnathon L. Osmond (UiO).

Contents

List of figures

Chapter 1

1 Introduction

The ability to capture and store CO_2 in geological formations may become an essential measure for mitigating and reducing current and future global greenhouse gas emissions. Norway has considerable experience in storing CO_2 in geological structures, for example in the Sleipner West field, central North Sea, where CO_2 has been separated from produced gas, injected and stored 1000m below the surface in the Utsira Formation since 1996.

Additionally, CO_2 extracted from liquefied natural gas (LNG) production and treatment of the Snøhvit field in the Barents Sea, is injected and stored in formations 2600 meters below the seabed (NPD, 2011). In 2014, the Norwegian government presented Proposition 1 S (2014-2015) to the Norwegian Parliament to develop strategies for CO_2 storage in Norway (Ministry of Petroleum and Energy, 2014, 2016a). The responsibility of developing technologies for full-scale carbon capture and storage (CCS) solution was given to the state enterprise Gassnova SF (Gassnova, 2015). One prospect identified for potential storage of CO_2 was identified 4 km east of the Troll East gas field offshore the west coast of Norway. This subsurface prospect is referred to as Smeaheia (Figure 1.2). This section will introduce the prospect area and the aim of the thesis.

1.1 The Smeaheia CO_2 prospect area

In 2016, Gassnova SF awarded a contract to Statoil ASA to conduct a feasibility study regarding CO_2 storage on the Norwegian Continental Shelf (Ministry of Petroleum and Energy, 2016b). The proposed Smeaheia area extends over the Norwegian blocks 32/1 and 32/4, between UTM31 60°34 - 60°49 N latitude and 3°55 - 4°32 E longitude ED50 datum (Figure 1.2). It covers a surface area of about 445 km² in the Norwegian Channel (also called the Norwegian Trench in older papers), a prominent seabed feature within the North Sea (Hjelstuen et al. , 2012). Two injection prospects have been proposed in the area; the Alpha to the west and the Beta to the east seen in Figure 1.2. Both candidates are confined laterally by the north-south trending Vette Fault Zone (VFZ) and Øygarden Fault Complex (ØFC). In 1996 and 2008, two petroleum exploration wells tested if hydrocarbons had accumulated in the prospected localities, but showed no sign of hydrocarbon charge (see Figure 1.2 dry wells 32/4-1 and 32/2-1; Kinn et al., 1997).

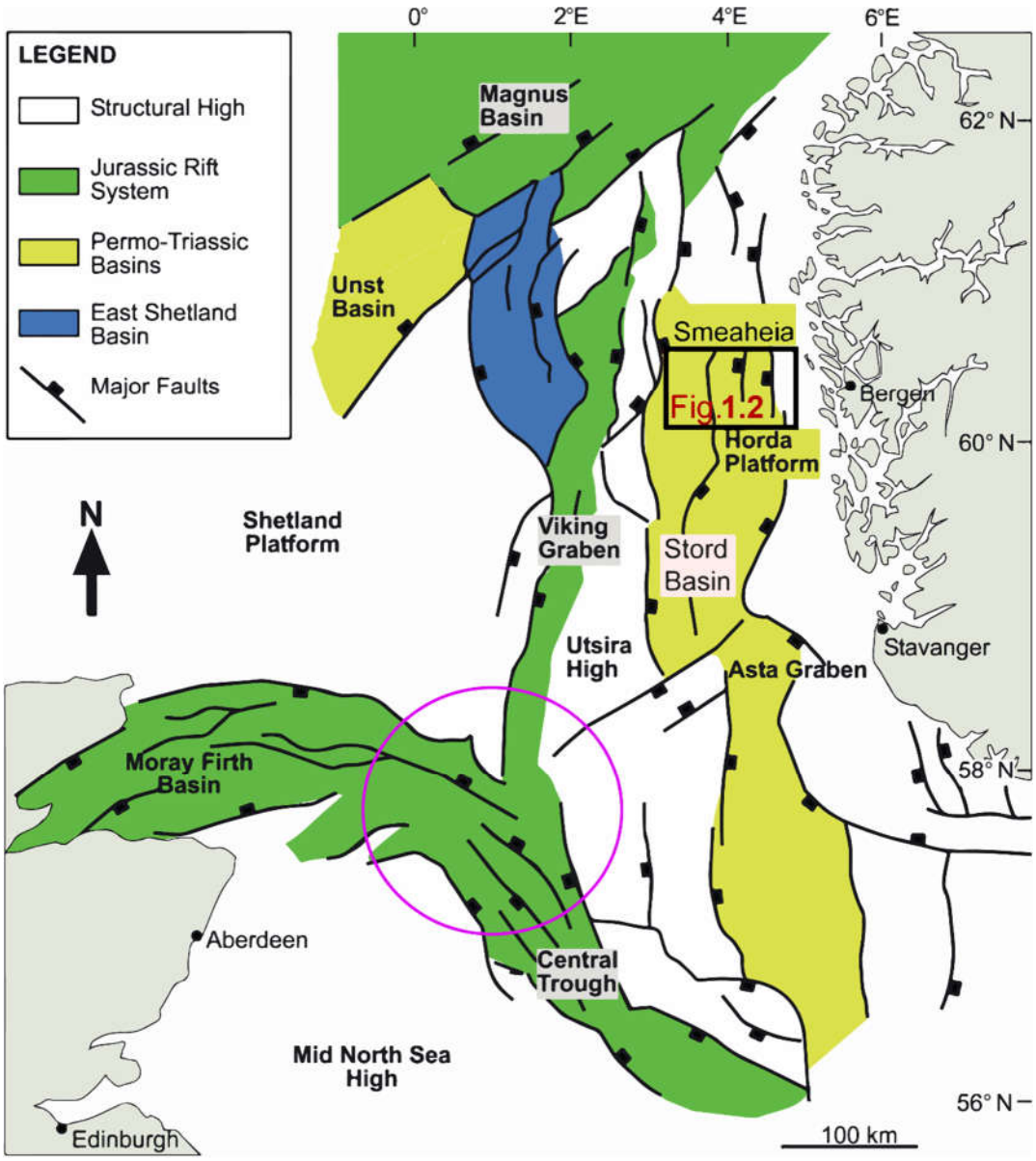

Figure 1.1: Map of the North Sea showing primary structural elements and the study area indicated by the black box. The magenta circle shows the triple junction area in the North Sea. These are structures from rift phases explained in chapter 2 Geological setting. Modified from Domínguez (2007) and Færseth (1996).

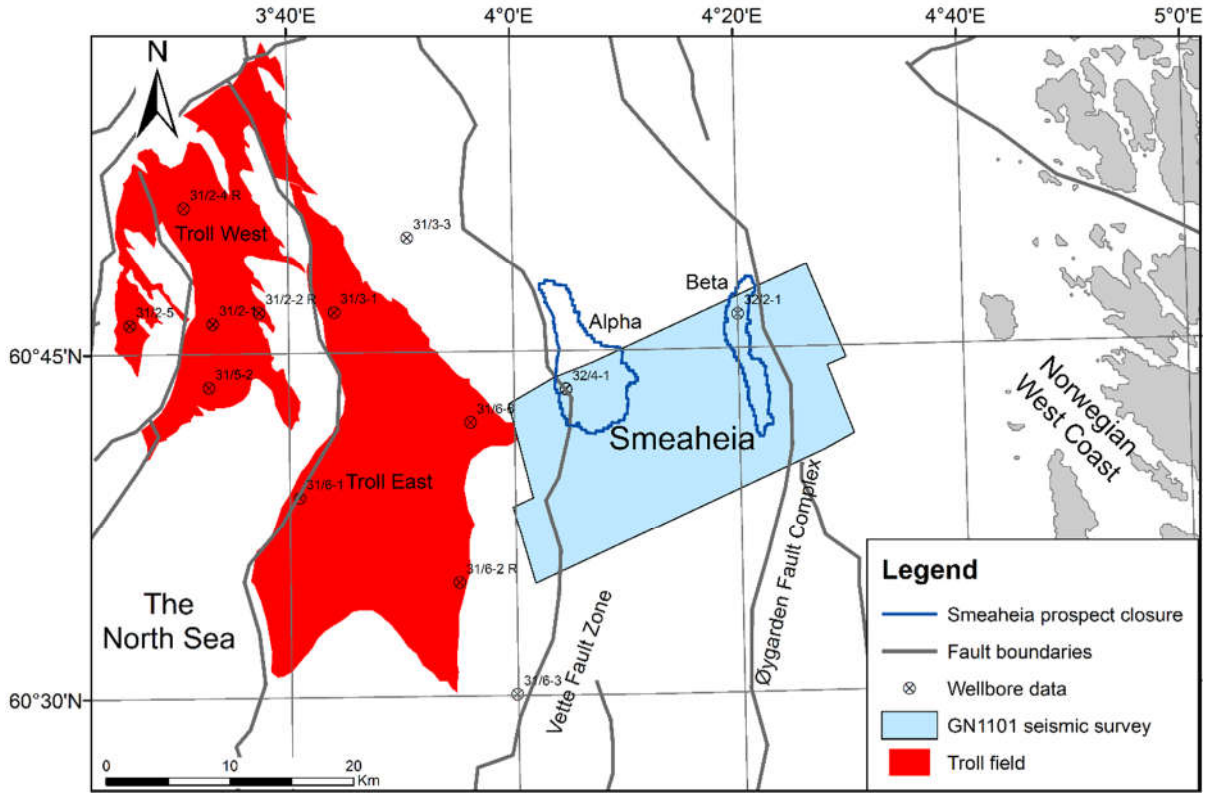

Figure 1.2: Detailed map showing the study area located offshore western Norway, and east of the Troll East gas field. The regional location is shown in Figure 1.1. The Smeaheia area is bounded by the Vette Fault zone to the west and the Øygarden Fault Complex to the east. Prospective CO_2 – water contacts (dark blue lines) are shown for fill-to-spill scenarios of the Alpha and Beta closure.

1.2 Geological concepts

This section introduces relevant geological concepts regarding necessary petroleum geology, CCS, shallow marine geology, and other geological processes impacting the study area. A summary of past research on pockmarks will subsequently serve as a point of reference for later.

1.2.1 Concepts from petroleum geology

1.2.1.1 Reservoirs

Firstly, to consider a geological formation as a reservoir there must be rocks with a fraction of voids, or pore spaces, to retain fluids (water, oil, gas) for storage. The percentage of void compared to the total volume of rock is called porosity (Craig, 2004), and one of the most common rocks found with good porosity is well sorted, clean sandstone (Bjørlykke, 2015). A reservoir needs the ability to let fluids flow through the porous rock. This ability is called permeability and depends on the number of interconnected pores, their geometry and size, capillaries and fractures (see Figure 1.3; Nolen-Hoeksema, 2014).

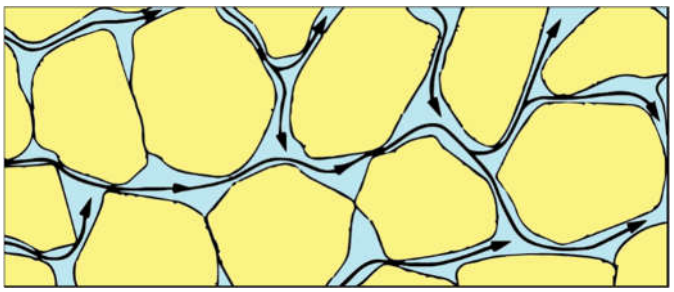

Figure 1.3: Connected pores in blue gives the rock its permeability and allows fluid to flow through (black arrows). Modified from Nolen-Hoeksema (2014).

Further, the porous formation needs to be vertically and laterally confined to prevent the fluids from escaping. The term “seal” refers to a rock unit that prevents flow, although all rocks have the intrinsic ability to be permeable for single and multiphase fluids (Cartwright et al., 2007). The minimum capillary pressure determines the threshold; the pressure which the fluids start to permeate the cap rock pore space. Shales and other tight rocks have narrow pore diameters and therefore have high capillary threshold pressures, which makes them suitable as sealing formation. (Busch & Müller, 2011).

1.2.1.2 Trapping

The formation overlying a reservoir needs to be a low porosity and permeability rock in order to trap fluids from escaping. This overlying rock is called a cap rock or top seal and is usually composed of shales (Bjørlykke, 2015; NPD, 2011). Moreover, the geometry of the caprock is crucial in order to form a trapping structure. Figure 1.4 shows different structures forming a trap.

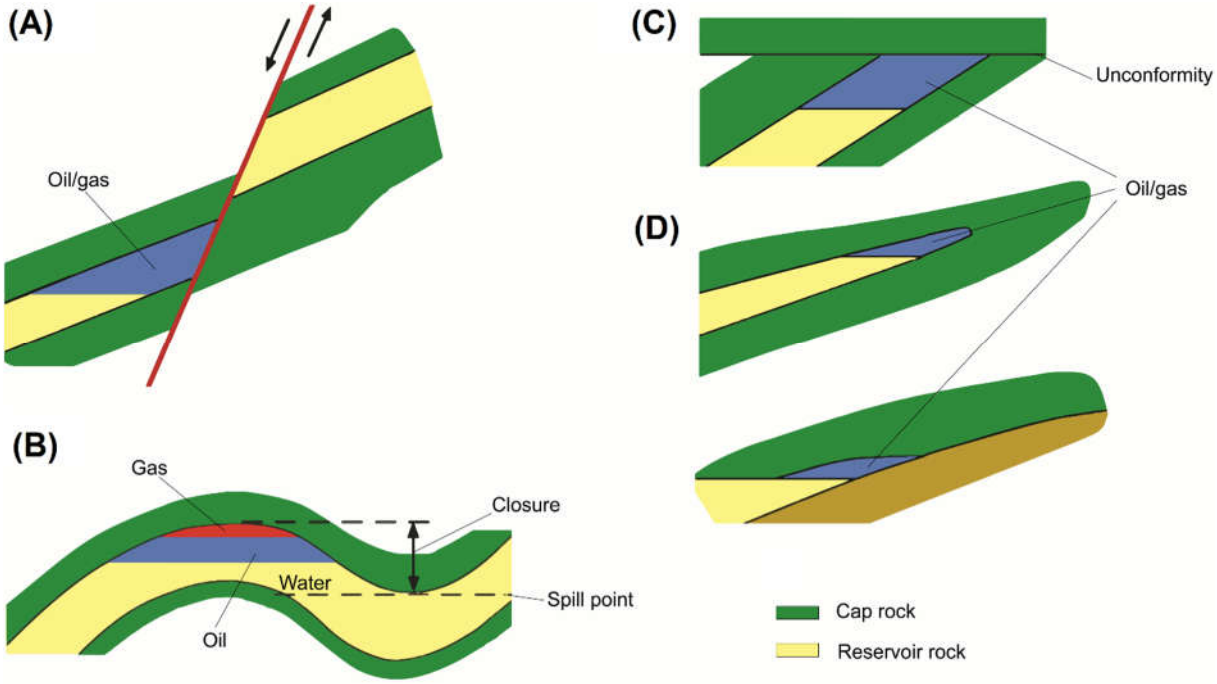

Figure 1.4: Trapping structures. (A): A fault-controlled trap. (B): An anticlinal fold making a trap. Arrow marks the height of the closure. If oil volume exceeds the spill point, it will escape up along the bedding to the right. (C): Combinations of the stratigraphic and structural. (D): Stratigraphic traps. Modified from Bjørlykke (2015).

1.2.1.2.1 Structural trapping

In fault-controlled traps (Figure 1.4A) the stratigraphic layers are separated by the fault making impermeable beds juxtapose to permeable ones. This type of seal could emerge on both sides of the reservoir unit, consequently trapping and storing fluids in the rock volume (Bjørlykke, 2015).

Anticlinal structure can confine fluids due to their geometric form (Figure 1.4B). A closure is defined by the maximum hydrocarbon column a structure can hold before leaking at the spill points. Therefore, spill points are potential leakage pathways (Bjørlykke, 2015).

1.2.1.2.2 Stratigraphic trapping

In comparison to structural traps, assessment of stratigraphic traps is made by features related to facies changes. These features, seen in Figure 1.4D, occur where a sandstone pinches out. Laterally and vertically adjacent less permeable rock units can effectively trap fluids within the sandier facies. In Figure 1.4C a sandstone is in contact with an unconformity, forming a stratigraphic trap.

1.2.1.3 Migration

Petroleum expulsion can migrate from source rock into nearby reservoir rocks; a feature called *primary migration* while further migration along carrier beds are called *secondary migration* (Bjørlykke, 2015b). Such petroleum migration is driven by buoyancy due to density difference with water (Bjørlykke, 2015).

1.2.2 CO_2 reservoirs

In order to successfully inject and store CO_2 within the subsurface a high-quality storage formation (reservoir) must be overlain or surrounded by a relatively impermeable cap rock (seal), both of which should be arranged to form a kind of trap. In general, trapping of the CO_2 occurs in four ways throughout the storage process; these include 1) structural, 2) residual, 3) solubility, 4) and mineral trapping. It must be noted that the amount to which a given trapping mechanism contributes to the volume of storage for a given location changes depending on the specific geologic conditions and the methods or procedures used during injection operations. In other words, one storage site may allow for more CO_2 to be sequestered by structural trapping, while residual trapping may be more dominant for another site a few kilometres away.

When searching exploring for potential CO_2 sites, suitable storage formations are often considered first, followed by the qualification of the seal and the way the CO_2 will be confined. Unlike in petroleum geology, the term structural trapping in CCS (1) is used to describe both stratigraphic and structural traps, as it serves to only describe pure buoyancy trapping of the CO_2. Therefore, structural trapping is generally the first step in storage capacity estimation and is much easier to predict compared to the other types of CCS trapping (2 through 4).As the CO_2 plume migrates away from the injection well, residual trapping will

capture CO_2 in the pore space of the rock by water capillary pressure. In solubility trapping, the CO_2 will as time passes, dissolve slowly in saline water or residual oil found in the rock formation over time. The mineral composition of the reservoir rock is important as the dissolved CO_2 must chemically reacts chemically with certain available cations to form new stable minerals. This is called mineral trapping and is the most secure form for storage. The process may take thousands of years to transform all the CO_2 into a carbonaceous rock (NPD, 2011). Prime conditions will turn a CO_2 deposit into minerals within a 100-10000-year period. Consequently, CO_2 storage reservoirs need to be sealing for the same amount of time (Hellevang, 2015).

1.2.3 Pockmarks

1.2.3.1 Historical documentation of pockmarks

The traditional definition of pockmarks is that they are:

"Shallow seabed depressions, typically several tens of metres across and few metres deep that are generally formed in soft, fine-grained seabed sediments." (Judd & Hovland, 2007).

Pockmarks are erosive features on the seabed, and come in different shapes and range of sizes (Judd & Hovland, 2007). Pockmarks were first described in King & MacLean (1970) after the use of echo sounder and side-scan sonar of the offshore Canadian continental shelf, and when pockmarks first were reported, King & MacLean (1970) wrote:

"We favour a hypothesis in which the main agent responsible for the formation of pockmarks is either ascending gas or water." King & MacLean (1970)

Subsequently reports from the North Sea and other parts of the world showed that the seabed is profoundly scared with pockmarks. Today, it is accepted that they are indicators of dynamic fluid seepage from the seabed. Judd & Hovland (2007) used the term *fluid* to include liquids and gases, as both these are substances that can flow freely and are not solid. This definition will also be used in this text.

The preservation of pockmarks depends on the ability for the affected sediments to mould and hold a trace of the seepage eruption. However, the term seepage covers a range of scenarios, from the explosive escape of fluids leaving physical perturbation to sea bottom sediments to

the microscopic emergence of tiny bubbles of gas, where the only evidence on the seabed is chemical. Seabed seepages will occur in diverse environments such as the deep ocean, superseding slopes or on the continental shelf. Also, they may originate from a variety of sources such as volcanic or hydrothermal, groundwater or hydrocarbons (Hovland & Judd, 1988).

In 1971 a bathymetric survey conducted between Oslo and Bergen found pockmarks along most of the Norwegian Channel (Van Weering et al., 1973; Judd & Hovland, 2007). Later work confirms that pockmarks are present throughout the area covered lying on the latest sediment cover (Judd & Hovland, 2007). Hydrocarbon exploration industry has been interested in pockmarks for the potential hazards they could bring to seabed installations, and surrounding pipelines (Judd & Hovland, 2007).

1.2.3.2 The formation of pockmarks

The original conceptual model for pockmark formation in Figure 1.5: Conceptual model for pockmarks formation. (A): Fluid pressure builds up in the shallow layer below the seabed and the excess pressure is relieved by the doming. (B): Eventually, pore fluid pressure causes the seabed sediments to yield, erupting and fluidising the sediments. Fluid and sediments are ejected into the water column. (C): Fine-grained sediments are suspended in the water and transported away by currents. Modified from Figure 1.5 was presented by Hovland & Judd (1988) in which a typical seep scenario within a petroleum-bearing sedimentary basin is explained. This model applies to the formation of pockmarks in sedimentary basins such as the North Sea.

Buoyant fluids g accumulate in temporary reservoirs while migration pathways are established. These temporary reservoirs can fill up and fluids overspill to higher reservoirs. Overpressure in the reservoir is then needed for fluids to breach the confining layer above and continue the migrating to shallower sediments as seen in Figure 1.6 (Judd & Hovland, 2007). Such reservoir will consequently be affected by lithostatic pressure changes. Changes to the lithostatic pressure can be initiated by several geological events such as sedimentation, erosion, loading and unloading of glacial ice sheets or other tectonics movements.

In sediment near the seabed, pore pressure will increase and produce areas of dome-shaped swelling (seen in Figure 1.5 A). Migrating gas will eventually find pathways along small fractures created by the doming stresses. Consequently, the fluid escaping to the seabed will result in a violent burst as the lithostatic pressure drops to zero (Figure 1.5 B). Escaping gases

will have a considerable volume change and expand as they rise. In Figure 1.5 C, the model shows the result of sediment failure by fluidisation around the edge of the newly formed pockmark where a gas-sediment plume emerges (Hovland & Judd, 1988).

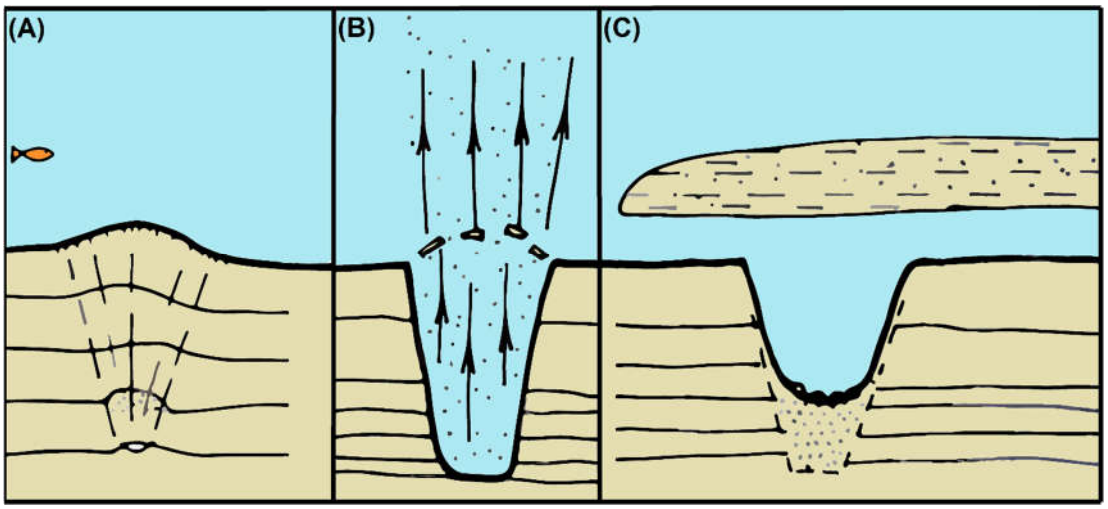

Figure 1.5: Conceptual model for pockmarks formation. (A): Fluid pressure builds up in the shallow layer below the seabed and the excess pressure is relieved by the doming. (B): Eventually, pore fluid pressure causes the seabed sediments to yield, erupting and fluidising the sediments. Fluid and sediments are ejected into the water column. (C): Fine-grained sediments are suspended in the water and transported away by currents. Modified from Hovland & Judd *(*1988*)*.

Fluid escape is a temporal event. For there to be continuous seepage, there must be a permanent link to a deeper reservoir. The alternative is cyclic seepage periods of activity and dormancy. During these dormant periods, the newly formed pockmarks will gradually fill in by side-wall slumping, and the shallow reservoirs recharged with fluids (see Figure 1.6; Hovland & Judd, 1988).

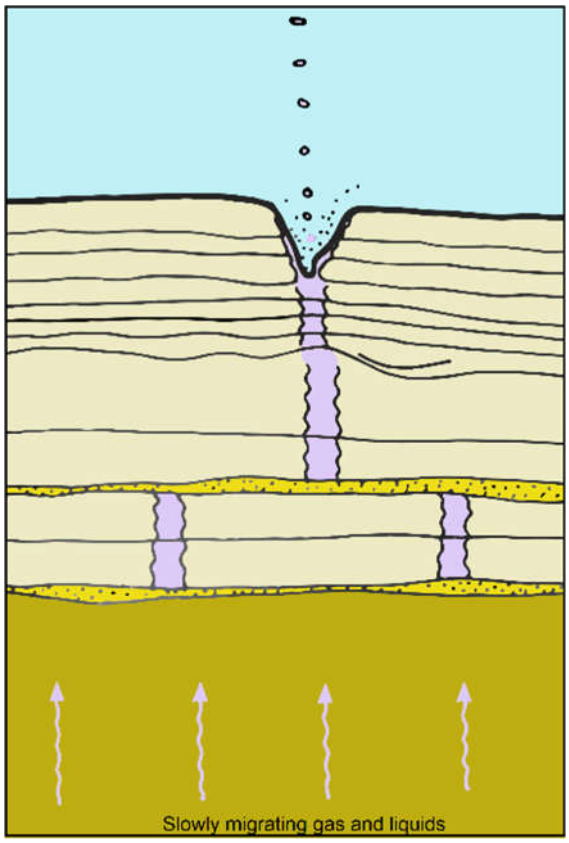

Figure 1.6: Migrating fluids will temporarily accumulate in reservoirs before escaping through established migration pathways. Fluid escape is a temporal event that can happen periodically or continuously. Overpressure is required to escape the reservoir. Modified from *Hovland & Judd (1988)*.

After a pathway is established on the seabed, subsequent gas escape will likely be of a smaller scale, and any gas build-up in the area around it will naturally find its path through it. In this way, the first pockmarks will serve as gas-drainage cells. The pockmarks density and unit sizes will depend on the established migration path which has further dependencies on features like sediment thickness, strength and permeabilities (Hovland & Judd, 1988). Therefore, pockmark distribution can help define subsurface migration pathways and event history.

1.2.3.3 Glacial effects on pockmark formation

Given the Quaternary history of the glaciation of the northern hemisphere, ice-age effects must be taken into consideration in the formation of pockmarks. Several glacial processes can in stimulate pockmark genesis including permafrost, ice sheets and icebergs and gas hydrates (Judd & Hovland, 2007).

Permafrost can reduce seabed sediment permeability, conceivably down to no permeability. Evidence from drilling in permafrost has shown that gas can be confined and contain significant amounts of microbial methane under permafrost conditions (Bondarev et al., 1993) as cited in Judd & Hovland (2007).

Research from Newfoundland Grand Banks, the Barents and the Norwegian Seas, have shown that there is a greater abundance of pockmarks inside iceberg ploughmarks than elsewhere on the seabed. Excavation of an iceberg plough on land has shown localised minor faults and fissures around stress zones (see Figure 1.7). A clear explanation was not found then, but a possible interpretation is that iceberg ploughs can increase the permeability enough for the gas to exploit the new migration paths (Thomas & Connell, 1985) as cited in Judd & Hovland (2007).

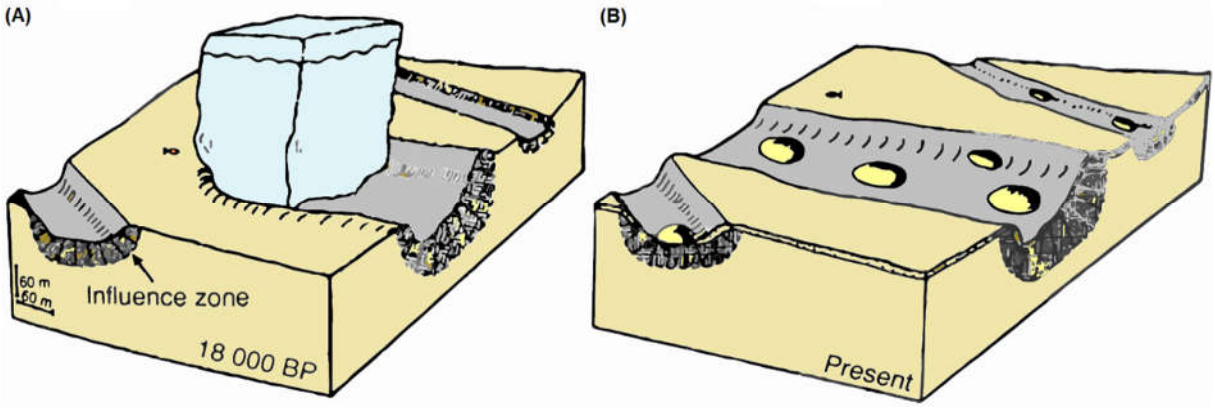

Figure 1.7: Pockmarks in iceberg furrows. (A): An iceberg ploughing through the seabed and disturbing the sediments. Localised minor faults and fissures are created in the influence zone (B): Present or after the glaciation scenario. Modified from Hovland & Judd (1988).

1.2.3.4 Pockmarks in the North and Barents seas

This section is an overview of historical pockmark research conducted in the North and Barents seas that will serve as a comparison for the results section of this thesis.

One of the first study describing pockmarks in the Norwegian Channel was Hovland (1981). A 3 km corridor was studied on the Western Slope (part of the Troll area today) and into the Norwegian Channel, intersecting the southwestern extent of the Smeaheia area. It was conducted with high-resolution side-scan sonar and sub-bottom profiler. Pockmarks were identified and characterised as dish-shaped depressions that occur in soft, silty clays ranging from 2-300 m in diameter with a density of 40-50 per km², as well as pockmark groups of 40-50 m in diameter (medium-sized) in connection to a larger parent pockmark. The next year Hovland (1982) studied a smaller area of 3.1 km², of what is known today as the middle of Troll East. It was conducted with high-resolution side-scan sonar and deep-towed boomer. The mean density of pockmarks here was 30 per km² with some pockmarks having asymmetric shapes. Columnar disturbances under many of the buried pockmarks were also observed (Hovland, 1982).

Investigations in the area an area in the Norwegian Central North Sea, part of the Viking Graben and the northern part of the Utsira High was presented in Fichler et al., (2005). The target was larger depressions in Quaternary strata studied by 3D seismic data and aeromagnetic data. They found several crater-shaped depressions ranging from 300-500 m in diameter and depth from 20-300 m. Some of the craters were found near the initiation of sub-glacial meltwater drainage channels features. Conclusions, based on previous similar crater discoveries, pointed to pockmark formation by melted gas hydrates.

The study of pressure accumulations in the skirt and outer annuli of the Troll A Platform in the Troll field, lead to a study presented in Tjelta et al., (2007). The study was conducted with high-resolution bathymetry and ROV surveys. Pockmark density in the Troll area was calculated to 15-25 per km². Conclusions suggest pockmarks here were formed by focused gas and fluid flow 10 ka ago.

Further investigations on pockmarks, based on the Troll A Platform and the Troll field research, is continued in Forsberg et al., (2007). Conducted with a high-resolution multibeam survey of the seabed and ROV surveys, in addition to 3D and high-resolution 2D seismic

data. Conclusions here shows methane-derived authigenic carbonate (MDAC) crust on the pockmarks, suggesting the expulsion of methane formed them. The position of the methane hydrates was proposed to be in unit 3 (see Figure 2.9), before melting at the end of the last glaciation. Post-glacial ocean currents gave the pockmarks asymmetrical shapes and kept them from infill.

One of the few studies to only use 3D seismic data is Ostanin et al., (2013). The seismic survey used covered 970 km² in the SW Barents Sea, and the investigation was on the potential migration pathway above the Snøhvit and Albatross gas field. An overall of 297 pockmarks was found (pockmarks density about 3 per km²) and classified as large for those up to 100m wide, giant for those between 100-300m wide, and mega-pockmarks for those of 1-2 km width. The study also investigated buried depressions, and several of them were identified at the Base of the Quaternary with linkage to deeper and shallower faults alongside seismic pipes. They inferred a minimum of two fluid and gas events in the area: one event previous or late Weichselian period affecting the Base of the Quaternary, then followed by the end of the Last Glacial Maximum (LGM) between about 17-16 ka BP responsible for the seabed pockmarks.

The next two papers are subsets of each other and are a continuation or is an extended part of the research done in Forsberg et al. (2007). In Mazzini et al., (2016) they investigated about 15000 km² of the Troll East field with a high-resolution multibeam survey in addition to detailed ROV data from six complex pockmarks. More than 7000 pockmarks were found in this field with an average of 35-100 m in width. No indication of seepage activity suggested pockmark carbonates were a result of paleo methane seepage, connected to gas hydrate dissociation. Further investigation in Mazzini et al., (2017) confirms that a total of 7243 pockmarks were found in an area of about 600 km² (pockmarks density ~12 per km²). Point pattern analysis was also conducted over an area of 296 km² from the bathymetry data and with 3189 pockmarks. Results from average nearest neighbor (ANN) analysis showed an observed distance of 173m, compared to expected 152.4 m which suggest dispersed pockmark patterns.

1.3 Study motivations, aims and objectives

This thesis assesses pockmarks in the Quaternary sediments above the Smeaheia area using 3D seismic data. The distribution of pockmarks on the seabed and within the shallow subsurface can often be correlated to deeper geological features, such as stratigraphic subcrops or faults, and suggest potential buoyant fluid migration pathways and events. Therefore, the chief scientific aim is to improve our understanding of pockmark origin and relative Quaternary fluid migration events at Smeaheia. To achieve this, pockmarks are mapped and statistical data about their distribution and morphology are compiled from different seismic horizons from the seabed to the base of the Quaternary. Glacier marks along these horizons are also mapped and provide additional information about the pockmark distribution.

Overall, the results from this work are used to infer how past fluid migration has affected Quaternary sediments at Smeaheia and to, provide insight about how well the Quaternary interval could act as a secondary seal if CO_2 injected into a storage formation at depth were to leak towards the surface.

Chapter 2

2 Geological setting

This chapter will describe the geological setting of the Smeaheia area as part of the geological developments in the northern North Sea. It describes the tectonic events from the Permo-Triassic to the Late Jurassic-Cretaceous rift stages, into the glacier events of the Quaternary. The final section presents the stratigraphic groups and formations.

2.1 The northern North Sea Basin and Smeaheia area

2.1.1 Tectonic framework and master faults of the Horda Platform

Smeaheia lies in the northern North Sea on the Norwegian Continental Shelf, which is within the Horda Platform and close to the eastern flank of the Central Viking Graben (see Figure 2.1; Gabrielsen & Koestler, 1987). The geology of the Horda Platform is the result of the tectonic and depositional evolution of the North Sea rift system, which commenced during the final closure of the Iapetus Ocean and the collision between Baltica and Laurentia (Christiansson et al., 2000; Gabrielsen et al., 2010). By the Mid-Silurian (~420 Ma) Baltica was converging and experiencing sinistral transpression with the Greenland margin of Laurentia (Soper et al., 1992). Subsequent to the closure, the Caledonides experienced extensional collapse (Soper et al., 1992; Christiansson et al., 2000; Gabrielsen et al., 2010).

By late Carboniferous-Permian, the reorganisation of the Laurentian-Baltic plate developed into the rift system in northwest Europe (Gabrielsen et al., 2010). Entering the end of the Early Permian, rift activity in northwest Europe decreased, and thermal relaxation of the lithosphere set in. In response, the central and southern North Sea began to subside and developed large depocenters such as Northern and Southern Permian Basins (see Figure 1.1; Ziegler, 1992; Gabrielsen et al., 2010). Subsidence persisted throughout the Permian, and the extension of the crust caused the development of a system of large half-grabens, with N-S striking rotated fault blocks (Gabrielsen et al., 2010). The Permian rifting continued into the Triassic and is referred to as the Permo-Triassic rift phase. A second phase occurred in the Late Jurassic-Cretaceous, where many original Permo-Triassic structures were reactivated (ref)

The Horda Platform is a N-S trending structural high and about 300 km along the eastern margin of the Norwegian North Sea. It is bounded to the east by the Øygarden Fault Complex and plays a vital role in controlling the sedimentary basin at depth (Færseth, 1996; Duffy et al., 2015; Whipp et al., 2014). The northern part of the platform consists of a network of faults; a set of N-S striking faults, active both in the Permo-Triassic and Late Jurassic-Cretaceous rift phase, and a second set of NW-SE striking fault, active only during the Jurassic-Cretaceous rift phase (Whipp et al., 2014; Duffy et al., 2015). The N-S striking set consists of basement-involved faults and including the Svartalv, Tusse, Vette Fault Zone (VFZ), and the Øygarden Fault Complex (ØFC), where the latter two acts as master faults at the Smeaheia area (see Figure 2.1;Figure 2.1 Duffy et al., 2015). These two faults are westward dipping with throws of 3–5 km, and bound up to 60 km long easterly rotated half grabens (Færseth, 1996; Whipp et al., 2014). The other set of NW-SE striking faults are shorter, about 2–10 km long and exhibit lower displacement (30–100m at Troll field), and are strata-bound to post-Upper Triassic stratigraphy and below the Base Quaternary Unconformity (Whipp et al., 2014; Duffy et al., 2015).

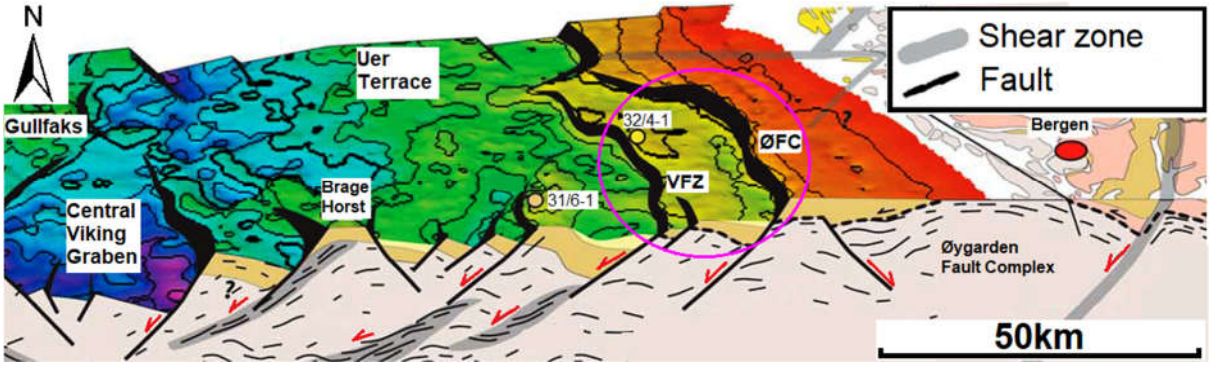

Figure 2.1: 3D view of the eastern flank of the Central Viking Graben and the Horda Platform. Smeaheia area is highlighted in the magenta circle with segments of the VFZ and ØFC. Modified from Fazlikhani et al., (2017).

2.2 Paleozoic to Mesozoic events

2.2.1 Triassic to Cretaceous rift stages

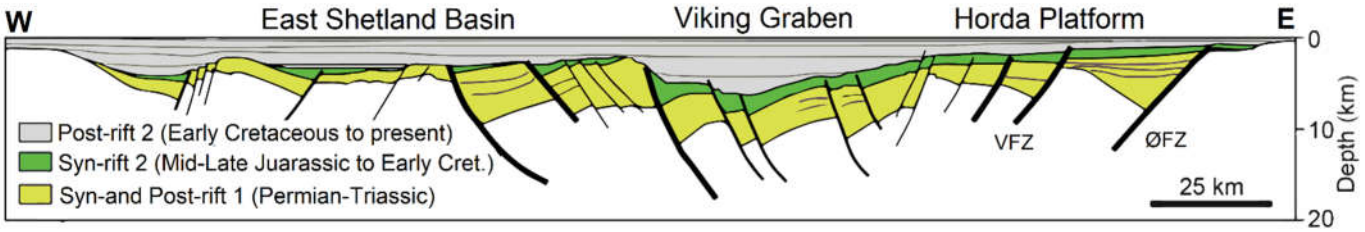

Figure 2.2: Regional interpretation of the structures from a west to east transect in the northern North Sea. Coloured strata show syn-rift and post-rift deposits. Modified from Duffy et al., (2015) after models in Færseth et al., (1996).

The Permian rift stage spread into the Viking, and Central Grabens, the Horda-Egersund half-graben and Moray Firth- Witch Ground graben systems and was followed by a prolonged phase of subsidence until the Middle Jurassic. During the Bajocian and Bathonia, a large volcanic thermal dome developed at the triple junction between these graben systems and

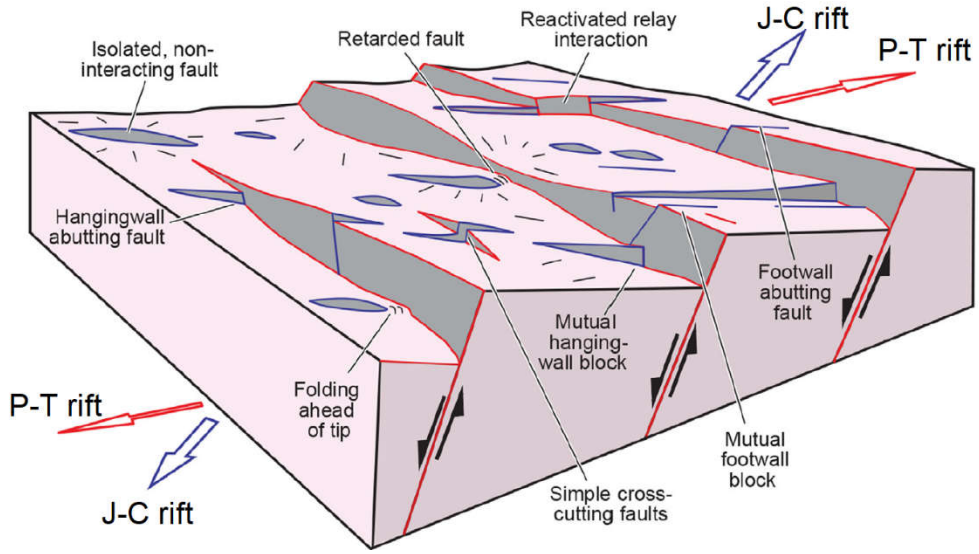

Figure 2.3: Conceptual fault network model in a multiphase rift showing typical locations of, and styles of interaction between non-colinear faults. The model assumes that the extension direction in the first rift phase (Permian-Triassic P-T), and the second rift phase (Late Jurassic-Cretaceous J-C) are different and that faults developed in the P-T rift are reactivated during the J-C rift. Modified from Duffy et al., (2015).

provided erosional sediments to the subsiding basins, whereas in the northern North Sea subsidence increased due to renewed E-W oriented extension (Ziegler, 1992; Gabrielsen et al., 2010).

The contemporaneous rifting partly reactivated the older Permian-Triassic faults, influencing the general structural pattern of the North Sea Basin, which resulted in segmentation and regional subsidence of opposing polarities (Odinsen et al., 2000). Rifting reached its peak during the Late Jurassic period, but by this time the fault activity had been reduced to a few faults along the graben margin (Odinsen et al., 2000). These changes in the internal graben relief evolved into the graben topography observed in seismic stratigraphy today, with platforms, sub-platforms, platform margins, and graben features (see Figure 2.2; Odinsen et al., 2000).

While the rotated fault block crests influenced depositional patterns and the environment in this period, the subsidence pattern created wedges of sand, shale and coal that were products of large fluvial-deltaic depositional systems along the mainland (Gabrielsen et al., 2010; NPD, 2014). Post-rift subsidence proceeded for approximately 70 Myrs., transforming the northern North Sea into a vast and shallow basin (Faleide et al., 2002; Gabrielsen et al., 2010). Interpretation in Figure 2.2Figure 2.2 shows how half-graben structures in the region have been filled with syn-sedimentary deposits during both rift stages. In Figure 2.3Figure 2.3 a conceptual fault system model illustrates the different fault directions and a fault structure that was the foundation for the Cenozoic sediments.

2.3 Cenozoic events

2.3.1 Paleogene uplift and subsidence

In the early Paleogene period, a new uplift event took place. This has been attributed to the development of the Icelandic mantle plume and the onset of seafloor spreading in the North Atlantic as the continents broke up (Gabrielsen et al., 2010). The igneous thermal event influenced the Shetland Platform more than the northern parts of the North Sea, and continent separation and uplift ceased by the end of the Paleocene. The North Sea Basin then entered ta tectonic quiescent with a followed by rapid subsidence (Ziegler, 1992; Faleide et al., 2002).

Regional subsidence in the Central and Viking Graben deepened the basin and created accommodation space for more than 3 km of sediments in the central part of the North Sea Basin (Anell et al., 2012). Simultaneously, the Norwegian mainland east of the Øygarden Fault Complex experienced uplift, hence developing the North Sea into an epicontinental

basin (Gabrielsen et al., 2010; Anell et al., 2012). Eustatic sea-level changes during the period are debated, nevertheless as climate changed from sub-tropical in the early Paleogene to a cold temperate environment in the late Paleogene, sea-level fell approximately 100-150 m (Anell et al., 2012).

Polygonal faults intersect the Paleocene to Early Eocene successions of the northern Horda Platform. Stratigraphically, these faults affect the Rogaland Group which thins out westwards (Whipp et al., 2014). Restoration suggests an extension in the SW-NE direction (Clausen et al., 1999). Some polygonal faults also developed in the overlying Neogene strata (see section 2.3.2).

2.3.2 Neogene uplift and subsidence

By the beginning of the Miocene epoch, the northern North Sea had fully developed into a shallow marine basin connected to a deeper central North Sea (Gabrielsen et al., 2010; Faleide et al., 2015) The continental shelf continued to be infilled primarily by prograding successions from Fennoscandia, the East Shetland Platform and the Scottish Highlands (Faleide et al., 2002; Gabrielsen et al., 2010; Anell et al., 2012). Depositional infill continued into the basin during the Miocene and Early Pleistocene, creating a series of prograding sedimentary wedges (Ottesen et al., 2018).

Glaciation initiated in the mountains during Late Pliocene, a contrast to the relatively warm period during Early Pliocene. The dominant prograding thick clastic wedges from Late Pliocene to Early Pleistocene seen in seismostratigraphy, are response to the glacial erosion and uplift. The eastern basin flank experienced substantial uplift during this period. The evident from a Middle Pleistocene angular unconformity, likely caused by tilting of the entire Cenozoic succession (Faleide et al., 2015). As the Early Quaternary commenced, ice sheets advanced over the shelf frequently, bringing poorly sorted glacial debris relatively close to the coast. This change in glacial loading resulted in tectonic tiling of a considerable part of the continental shelf, and consequently tilted reservoir hydrocarbon-water-contacts (HWCs; like in the Troll field) and influenced hydrocarbon migration (Faleide et al., 2015).

The following section describes the period of Quaternary in which the basin experienced many glaciers unloading and loading.

2.4 Quaternary developments

2.4.1 Early to Middle Pleistocene (~ 2.6–0.8 Ma)

A schematic section in Figure 2.4 shows a possible ice sheet margin scenario in the North Sea in the Early Pleistocene, before the Norwegian Channel (also called Norwegian Trench) was formed. The beginning of the this period, ice sheets appears to have reached the West Coast of Norway (Ottesen et al., 2014; Ottesen et al., 2018). Early Pleistocene sediments are mostly interbedded glacigenic with layers of fine-grained tidal marine deposits fluvial-deltaic to shallow marine sandier deposits (Ottesen et al., 2014).

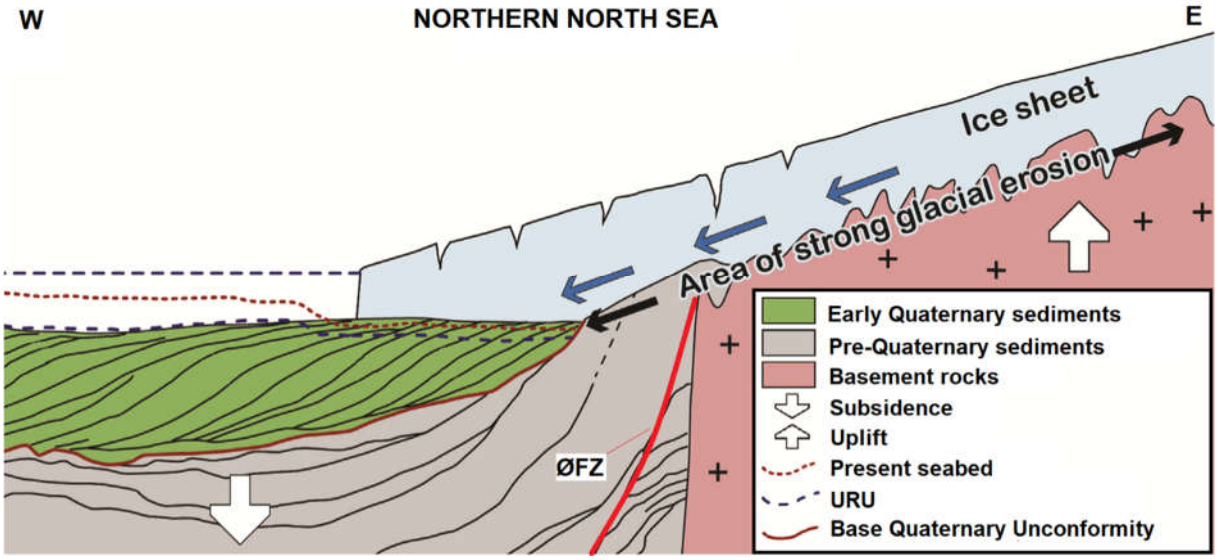

Figure 2.4: Schematic section of the seismic stratigraphy of the North Sea Basin in the Early Pleistocene, before the cutting of the Norwegian Channel by ice-stream activity. The location of the ØFC is approximated. Modified from Ottesen et al. (2014).

Nearly all the basins in the south and higher parts of the northern basin had accumulated sediment by the middle of Early Pleistocene (~1.6–1.7 Ma). Fluvio-deltaic deposits dominated and were delivered from river systems located in Europe and Scandinavia (Ottesen et al., 2018). However, glacigenic debris-flows interpreted on the paleo-slope surfaces in the northern North Sea provide evidence that the Fennoscandia Ice Sheet advanced towards the paleo-shelf episodically during stages of glaciations (Ottesen et al., 2014). In the central North Sea Basin, mega-scale glacial lineations (MSGL) provide evidence for ice sheet grounding during Early Pleistocene (Ottesen et al., 2018). The presence of MSGL indicate fast-flowing ice streams, and the lineations are oriented in the direction of the past ice flow (Ottesen & Dowdeswell, 2009; Ottesen et al., 2014). MSGL are formed during full-glacial conditions

when ice advances (see the model in Figure 2.5; Ottesen & Dowdeswell, 2009). Dating in the southern North Sea shows the oldest age for the MSGL formed at about 1.87 Ma, but uncertainty about their formation (Ottesen et al., 2018).

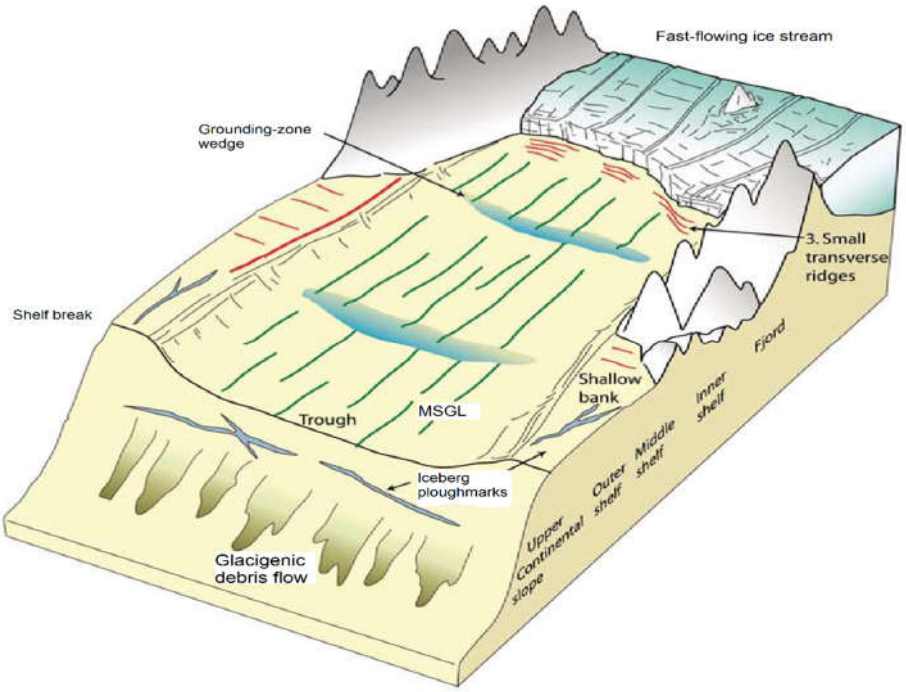

Figure 2.5: Schematic model of submarine landforms produced on continental margins by ice. This model shows an ice-stream–glacial landform assemblage, where fast-flowing ice was fed from a large interior drainage basin. Modified from *Ottesen & Dowdeswell (2009)*.

2.4.2 Middle to Late Pleistocene (~ 0.8–0.12 Ma)

Middle to Late Pleistocene sediments have been traced back to both the Fennoscandia and British ice sheets (Stoker et al., 2005). Sediment core data from the Troll field reveal lithologies from normal to glaciomarine and till in the Quaternary interval (Sejrup et al. (1995). These deposits were interpreted as the result of repeated expansion of the Fennoscandian Ice Sheet towards the shelf edge and noted that every till unit exhibits a sharp erosional boundary or Glacial Erosion Surface (GES) at its base (Sejrup et al. (1995).

On the eastern side of the northern North Sea Basin, there is a prominent Upper Regional Unconformity (URU) has been associated with the formation of the Norwegian Channel by the Norwegian Channel Ice Stream (Ottesen et al., 2018). This unconformity formed during repeated episodes of glacial erosion (Ottesen et al., 2018). The age of the URU is disputed as the event has been dated to approximately 1.1 Ma in Sejrup et al. (1995) based on amino acids, micropaleontological and palaeomagnetic analysis of sediments from the Norwegian Channel. The studies by Ottesen et al., (2018) and Løseth & Nygård (2019) utilized extensive 2D and 3D seismic data to correlate major Quaternary seismo-stratigraphic surfaces and sequences across different sectors of the North Sea Basin, and both suggest the URU is around 0.5 Ma. The Norwegian Channel follows the Norwegian coastline from Skagerrak and up north to the continental margin of the northern North Sea, including the massive North Sea fan to the northwest(see map in Figure 2.7; Sejrup et al., 2003; Nygård et al., 2005). In the Middle-Late Pleistocene the Norwegian Channel Ice Stream advanced and encountered shallow water, it is associated with a significant erosive period in the Middle-Late Pleistocene (Ottesen et al., 2014). Evidence of this event includes dropstones or ice-rafted debris (IRD), and buried linear to curvilinear depressions on the sea floor known as iceberg ploughmarks (Dowdeswell & Ottesen, 2013).

The diagram in Figure 2.6 illustrates the prevalence of the Fennoscandian Ice Sheet throughout south-western Norway (Hjelstuen et al., 2005; Mangerud et al., 2011). Glacial events are connected to their marine isotope stage (MIS), which were developed using deep-sea core and their oxygen-18 isotope analysis of planktonic foraminifera and pollen, as a proxy for paleo-temperatures (Emiliani, 1955, 1966, 1970). The last time stage associated

with glacial influence on the Norwegian Channel and the region of Smeaheia is known as the Weichselian and dates from ~126 Ka to 11.7 Ka.

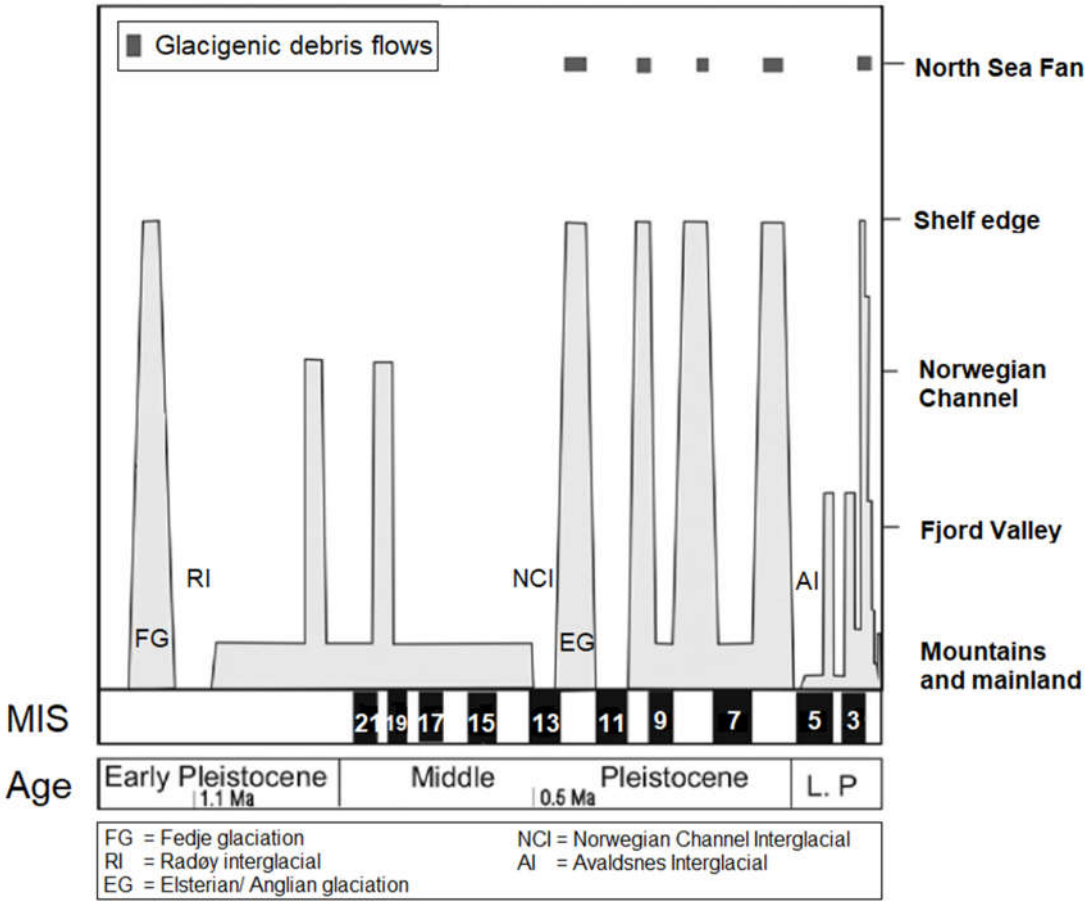

Figure 2.6: Diagram of the Fennoscandian Ice Sheet throughout the Quaternary. Odd numbers for MIS represent warm climate while cold temperatures have even numbers. Modified from Hjelstuen et al. (2005); Mangerud et al. (2011).

2.4.3 Late Pleistocene - Weichselian (~ 126–11.7 Ka)

The Weichselian glaciation is defined as sub-stages of MIS 5e to the end of MIS 2 (~ 121 ka – 14 ka). Most interesting for the Smeaheia area is perhaps the MIS 2, where a decrease in temperature initiated the Last Glacial Maximum (LGM) from ~30 ka –14 ka (Gibbard & Cohen, 2008; Mangerud et al., 2011). The glacial history of the Late Weichselian have seen several fluctuations of ice margins during the period of 30–18 ka (Mangerud et al., 2011).

Studies of other ice sheets around the globe show similar fluctuations. Regional variations from the West Antarctic Ice Sheet to the ice sheets at mid- and northern latitude, indicate that these ice sheets had attained their last local glacial maximum around 33–29 ka. The Laurentide Ice Sheet in North America also continued to extend 26 ka, when most other ice sheets had reached their maximum, and corresponding to a global eustatic sea level fall (Clark et al., 2009).

During the last phase of the LGM, the Norwegian Channel Ice Stream was active but according to King et al. (1998) and Nygard et al. (2007) deposition of glacial sediments at the mouth of the Norwegian Channel, came to a halt approximately 19 ka. Sejrup et al. (2009) dated the Norwegian Channel to 18.5 ka and correlated it to the disintegration of the Norwegian Channel Ice Stream from the Norwegian Channel to this age. Ages were derived from radiocarbon dating. Svendsen et al. (2015) suggest the Norwegian Channel Ice Stream ice front had withdrew 20.5 ka. This age was attained by using cosmogenic radionuclide dating of erratics on the islands of Utsira and Karmøy, offshore Stavanger. Dating of moraines at Blomvåg (west of Bergen) revealed ages of 14.6 ka, implying the Fennoscandian Ice Sheet must have been calving outside the west coast of Blomvåg for several thousands of years (Mangerud et al., 2011). In Figure 2.7**Feil! Fant ikke referansekilden.** two maps show the reconstruction of possible ice margins at the end of LGM. Figure 2.7A is the reconstruction in Svendsen et al. (2015), and map in Figure 2.7B is the latest reconstruction derived from radiocarbon dating of several glaciomarine cores in the Norwegian Channel in Morén et al., (2018) including those in Sejrup et al. (2009) and the results from Svendsen et al. (2015).

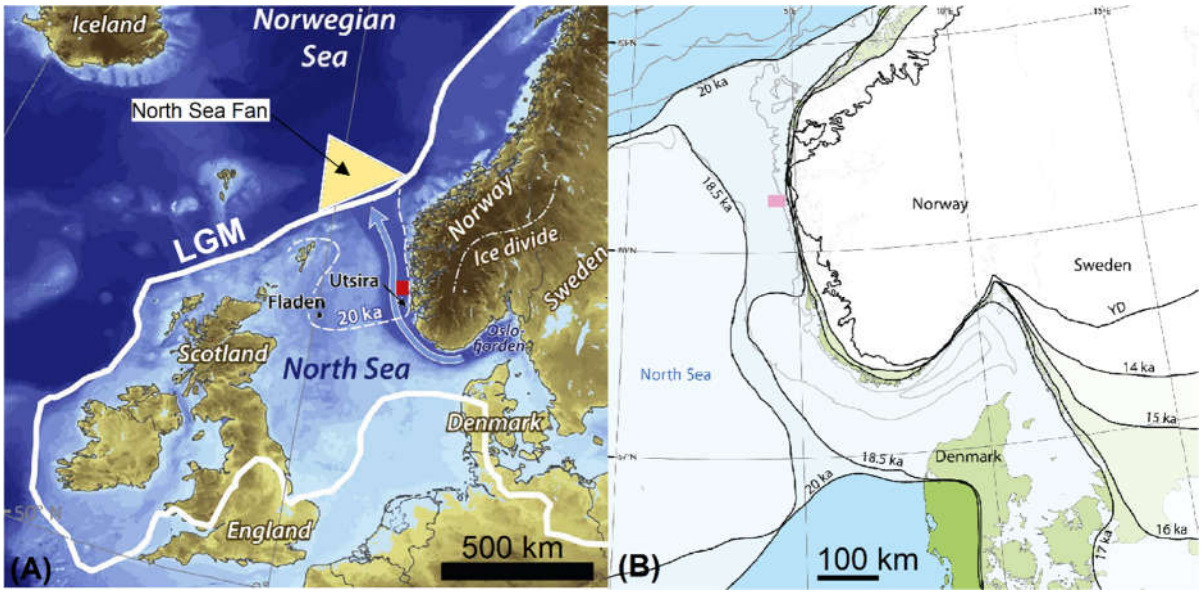

Figure 2.7: Maps of possible ice margins at the end of LGM. (A): The pathway of the Norwegian Channel Ice Stream is marked with an arrow along the Norwegian Channel. Smeaheia area is situated in the red square. The white dashed lines show a possible reconstruction of the as suggested in Svendsen et al., (2015). The North Sea Fan up in the northwest marked by the yellow triangle. (B): Latest reconstruction of the ice margin as suggested by Morén et al., (2018). Reconstruction derived from radiocarbon dating of several glaciomarine cores in the Norwegian Channel.

The deglaciation of ice sheets in the Northern Hemisphere provided source for a rise in sea-level about 14.5 ka which could correlate to the retreat of the West Antarctic Ice Sheet 15.2-13.9 ka (Clark et al., 2009). A sea-level rise would prevent the Fennoscandian Ice Sheet margins on to the West Coast due to the water depth. Thus, forcing calving and preventing the ice margin from growing into deep open water (Mangerud et al., 2011). This principle and evidence imply that the Smeaheia area may have been ice-free during the last 20–18.5 ka, experiencing sea-level rise, drifting icebergs, and glacigenic sedimentation.

At the end of Weichselian, a short near-glacial period called the Younger Dryas Stadial was initiated by a temperature decrease of 7°C at about 12.8 – 11.6 ka (Boulton et al., 2004). Moraines from the Younger Dryas are traceable through the whole West Coast of Norway.

Rise and Rokoengen (1984) studied the surficial geology (sea floor photographs and seabed sediments) between 60° 30′ and 62° N in the North Sea. Investigations suggest the last movement of the ice stream moved mainly in a north-northwest direction and deposited the upper till unit (L2 in Figure 2.9). Rise and Rokoengen (1984) also found a stratified sequence of glaciomarine clays, which likely formed as a result of floating ice sheets in the central part of the Norwegian Channel. Extensive erosion and deposition of eroded material on the Western Slope and the bottom of the Norwegian Channel from before about 12.5–10.0 ka

implies a long period of shallow sea-level. In the following Holocene period (11.7 Ma – present), the area (between 60° 30′ and 62° N in the North Sea) probably experienced a rapid sea-level rise with moderate influx of warmer Atlantic water. Seabed sediments are likely to have been stable since then as little erosion and deposition is evident from this last period. Moreover, although storms and currents may transport small amounts of fine-grained sediments, it is suggested that the present-day seabed reflects the most-recent depositional process (Rise & Rokoengen, 1984).

2.5 Stratigraphy of Smeaheia area

The lithostratigraphic chart in Figure 2.8 is a representation of the stratigraphy in the northern part of the Smeaheia area, based on information from wellbore 32/2-1 and 32/4-1 (see

Figure 1.2).

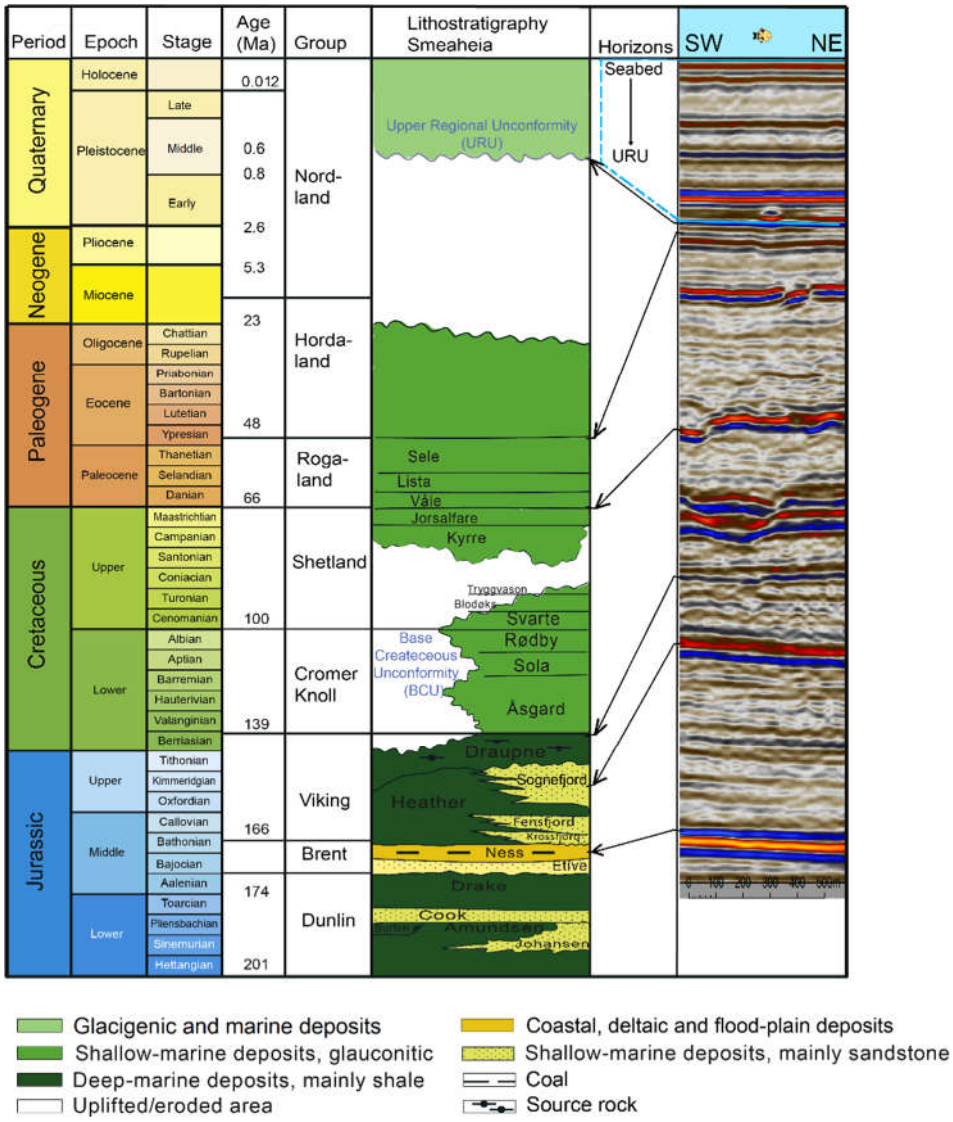

Figure 2.8: Stratigraphic chart of the Horda Platform and the Smeaheia area. Modified from Gradstein & Ogg (2012) and NPD (2014). For detailed Quaternary part see Figure 2.9.

2.5.1 Stratigraphical groups and formations at the Smeaheia area

2.5.1.1 Precambrian-Palaeozoic

The basement of the Horda Platform comprises of Caledonized Precambrian gneiss, based on a core sample from well 31/6-1 at Troll East (Færseth et al., 1995). No other formations are

have been encountered in wells below the Triassic age, although, seismic-stratigraphic analysis infer Devonian sediments under the Triassic Groups in the Vette fault block (Whipp et al., 2014; Duffy et al., 2015).

2.5.1.2 Triassic groups

This period consists of the **Hegre Group** with interbedded sandstone, claystone, mudstones of Scythian (Induan/Olenekian) to Rhaetian ages, and the **Statfjord Group** which comprises of massive sandstones interbedded with silty, lignite mudstones (Lervik, 2006).

2.5.1.3 Jurassic groups and formations

There are three groups in the Jurassic: The Dunlin Gp, Brent Gp, and the Viking Gp.

The Dunlin Gp was deposited between the Hettangian and Bajocian and represent a major marine transgressive sequence that can be subdivided into five formations: The Amundsen, Johansen, Burton, Cook, and the Drake Formations. The Amundsen, Burton and Drake formations consist of primarily of silt and marine mudstones, whereas the Johansen and Cook formations are marine to marginal marine sandstones (Vollset & Doré, 1984; NPD, 2011).

The Brent Gp was deposited between the Bajocian and Bathonian and represent a major deltaic sequence that can be subdivided into five formations, but at Smeaheia, only two have been identified in the well logs (wellbore 32/4-1): The Etive and Ness formations. The Etive, Formation consists of sandstones whereas the overlying Ness Formation consists of coals, mudstones, and siltstones and sandstones (Vollset & Doré, 1984; NPD, 2011).

The Viking Gp was deposited between the Bathonian to Ryazanian (Berriasian) and can be subdivided into five formations: The Heather, Krossfjord, Fensfjord, Sognefjord and Draupne formations. The Heather Formations consists mainly of silty claystones deposited in open marine environment and interfingers with coastal-shallow marine sandstones of the Krossfjord, Fensfjord, and Sognefjord formations. The overlying Draupne Formation consists of black mudstone with very high organic content. The formation was deposited in a marine environment, with limited bottom circulation and anaerobic conditions, and is an excellent source rock in the northern North Sea (Vollset & Doré, 1984; NPD, 2011). T

2.5.1.4 Cretaceous Groups and Formations

There Cretaceous succession in the northern North Sea consists of two groups: The Cromer Knoll Group, and the Shetland Group.

The Cromer Knoll Group was deposited between the Ryazanian (Berriasian) and Albian and can be subdivided into six formations, but only three are identified in the well logs at Smeaheia: The Åsgard, Sola, and Rødby Formations. The Åsgard Formation rests on the Viking Group and is dominated by claystones, often calcareous, and passes into marlstones with limestone stringers. The formation was deposited in an open marine environment with low energy shelf and well-oxygenated bottom water. The overlying Sola Formation consists of shales, often pyritic, interbedded with marlstone and limestone stringers. It was deposited in a marine environment with alternating anoxic and oxic bottom conditions. The Sola Formation is overlain by the Rødby Formation. It consists of marlstone with occasionally sandstones and siltstones. The formation was deposited in an open marine and oxygenated conditions with a limited supply of clastics (Isaksen & Tonstad, 1989).

The Shetland Group which was deposited during the Cenomanian to Maastrichtian has different formation names across the North Sea. The group can be subdivided into five formations at Smeaheia using well logs as guidance: The Svarte, Blodøks, Tryggvason, Kyrre, and Jorsalfare formations. The Svarte Formations rests on the Cromer Knoll Gp and consists of mudstones with interbedded limestones. The mudstones are often calcareous. The Blodøks Formation consists of mudstones with variable calcareous content. The depositional environment was anoxic sea bottom conditions. The presence of carbonates may indicate periods of oxic conditions or the allochthonous supply of chalks and limestones. The Tryggvason Formation and the Kyrre Formation consists of were deposited in similar conditions as the Blodøks Formation, with similar sediments. The Jorsalfare Formation consists of mudstones with interbedded thin limestone beds. Mudstones are often calcareous, and limestone fine-grained with some sand and dolomite. Depositional environment is open marine (Isaksen & Tonstad, 1989).

2.5.1.5 Paleogene Groups and Formations

There are two groups in the Paleogene: The Rogaland Gp, and the Hordaland Gp.

The Rogaland Group ranges in age from the Danian to the Thanetian and is widely distributed in the northern North Sea and usually subdivided into twelve formations. Again, using well log from wellbore 31/4-1, only three formations are present at Smeaheia: The Våle,

Lista, and Sele formations. The Våle Formation rests on the Shetland Group and consists of marls and claystones interbedded with limestone beds and sandstone and siltstone stringers. It was deposited in a marine environment. The younger Lista Formation consists of shales with occasional stringers of limestone and dolomite. The depositional environment of the Lista Formation has been interpreted as deep marine with low-energy conditions. The overlying Sele Formation consists of tuffaceous montmorillonite rich shales and siltstone. These fine-grained sediments are finely laminated and carbonaceous indicating deposition in a deep marine environment (Isaksen & Tonstad, 1989).

The Hordaland Group represents Eocene to Early Miocene deposition. At Smeaheia the group is found to the northeast of the Top Sele Formation subcrop, which is located approximately above the VFZ lineation in the subsurface. The group consists of marine claystones with minor sandstones deposited in an open marine environment (Isaksen & Tonstad, 1989).

2.5.1.6 Neogene Groups and Formations

The Neogene interval is missing at Smeaheia. The URU surface overlies the Rogaland Gp, and this is of Late to Middle Pleistocene of age. This unconformity suggests the Base Quaternary has also been eroded. An estimated 22 M. yrs. of the stratigraphic record us missing in this part of the Norwegian Channel.

2.5.1.7 Quaternary units

The Quaternary interval consists of the Nordland Group. No shallow cores have been obtained from the wells at Smeaheia. Therefore, we extrapolate Quaternary stratigraphy from the Troll East area, as seen in Figure 2.9 (Sejrup et al., 1995; Forsberg et al., 2007).

The Quaternary interval from core 8903 has been interpreted to consist of seven lithological zones (Sejrup et al., 1995):

L1 consists of mostly pelitic unconsolidated sediments with high water content (about 70%). The unit represents the last deglaciation in the Holocene.

L2 consists of massive diamicton with a change in the lower part to sandy sediments. It is a very homogenous unit. Water content changes significantly from unit L1. The unit is envisaged to represent deposition at the base of a glacier (till sediments).

L3 consists of a series of bedded sediments with significant variations of sorted and poorly sorted sand and gravel.

L4 consists of massive matrix-supported diamicton with small variations in grain-sizes, and very similar to unit L2.

L5 consists of well-sorted, fine-grained sediments. Normal marine sedimentation is inferred, perhaps deposited over one period.

L6 consists of matrix-supported diamicts interbedded with thin beds of sorted sand. The depositional environment has been interpreted to be glacigenic, where most sediments are till, but others could represent proximal glacial marine sediments. Sejrup et al., (1995) credited this unit to the Fedje Glaciation.

L7 consists of homogenous hard pelite with some thin laminae of fine sand. The deposits have been interpreted to represent an inner shelf, lagoonal environment.

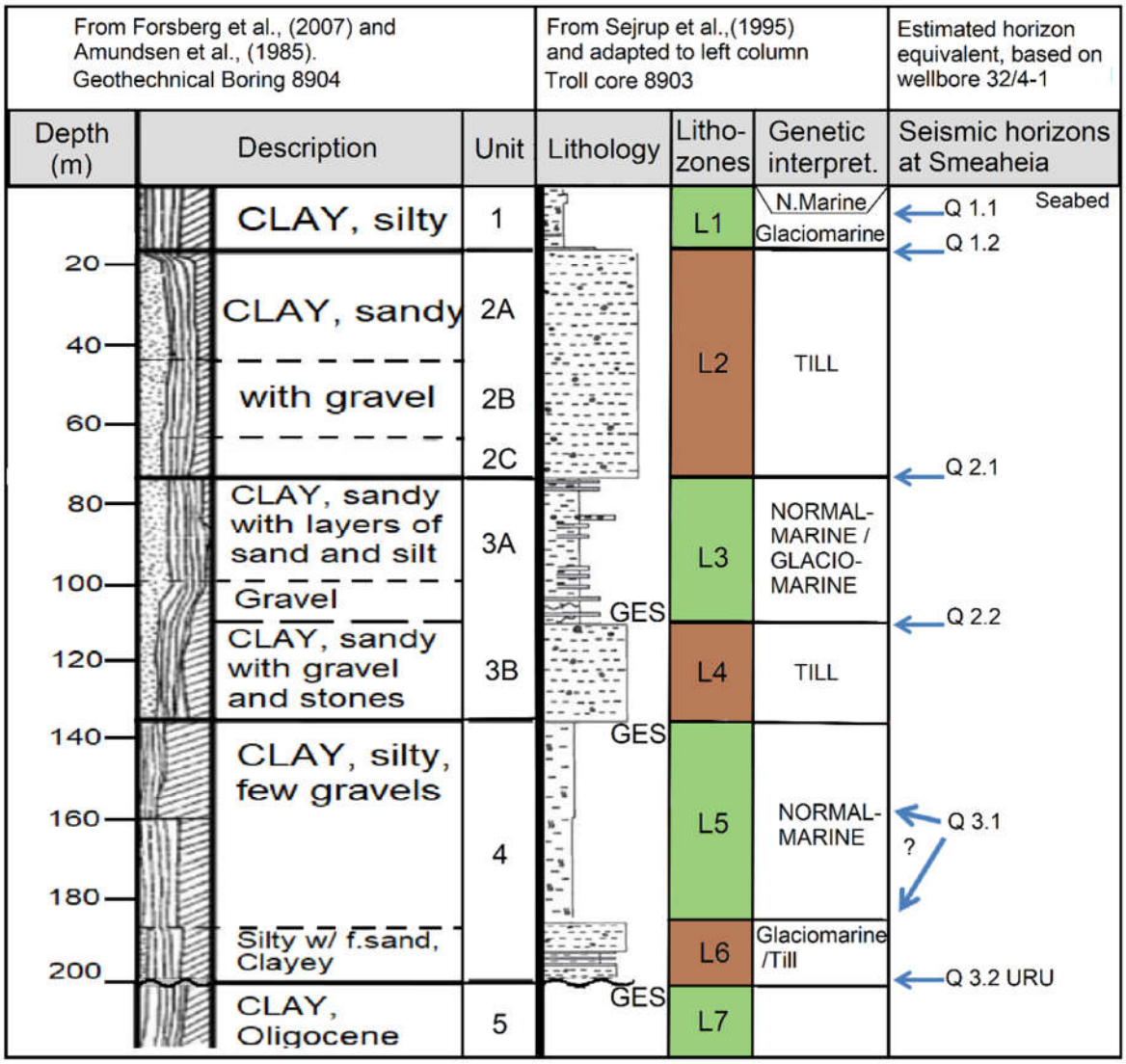

Figure 2.9: Stratigraphic chart for the Quaternary interval. The section on the left is presented in *Forsberg et al., (2007)* based on geotechnical work under the Troll A Platform and originally from Amundsen et al., (1985). Middle section is stratigraphy presented in Sejrup et al., (1995) based on Troll core 8903. This core was 219 m, therefore adapted to the result of Boring 8904 (200 m). The right section is an estimation of what the selected horizon in this thesis may represent, based on data from wellbore 32/4-1. This wellbore is close to the Troll field and is reported to be about 200 m from the seabed to unconformity. GES is a Glacial Erosion Surface identified in Sejrup et al., (1995).

Chapter 3

3 Data set and methodology

This section details the methods used to gather pockmark data and analyse them in order to map their morphology and distribution. Statistical analysis and pockmark distribution are supplementary to the seismic analysis, which can potentially define migration pathways of subsurface fluids. The limitations of the methods are also documented.

3.1 Data set and seismic theory

The following section introduces the seismic data and some theory connected to seismic signalling and resolution limits.

3.1.1 3D seismic data

The provided industry GN1101 3D seismic survey GN1101 aquired by Gassnova SF covers 394 km² of the Smeaheia (see **Feil! Fant ikke referansekilden.**). The seismic data consists of ENE-WSW oriented inlines (25m spacing), and NNW-SSE oriented cross-lines (12.5 m spacing) and contains vertical information down to 5000 ms. Petrel E&P Software Platform was used for seismic interpretation. A frequency decomposition of the GN1101 survey was extracted through the Petrel software to construct a frequency range graph (Figure 4.1). Peak frequencies at ~1 Hz, ~19 Hz and 80 Hz show the multispectral properties of seismic reflections, but most frequencies were in the range of 17-53 Hz.

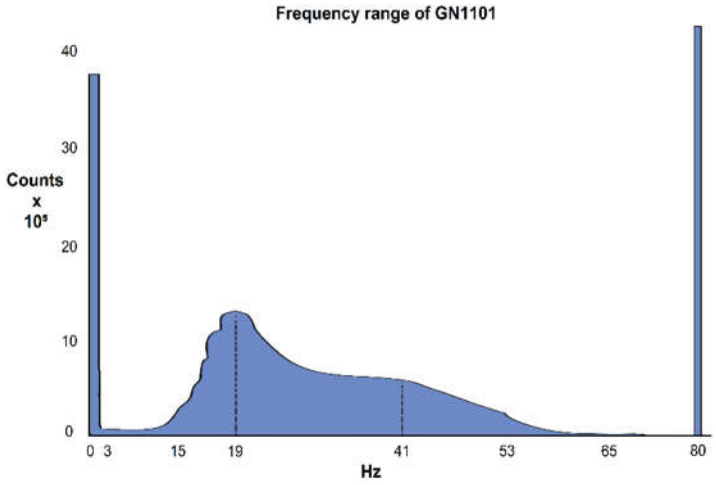

Figure 3.1: Frequency range of seismic survey GN1101. Raw data was extracted through Petrel software program and rearranged in Excel to present this graph of frequencies.

3.1.1.1 Seismic polarity and phase

The convention on seismic polarity governed by the Society of Exploration Geophysicists (SEG) states that positive amplitude (peak) occurs when acoustic impedance increases and

negative amplitude (trough) occurs when acoustic impedance decreases (Brown, 2004). An assessment of the phase and polarity of the survey (GN1101) indicates a normal zero-phase polarity (seen in Figure 3.3). This choice of polarity means the seismic signal can be represented as a Ricker wavelet (seen in Figure 3.2) when propagating through the subsurface. There are several advantages when using zero-phase data. Most important is that the wavelet becomes symmetrical with the majority of the seismic energy in the central lobe, and resolution is improved compared to other wavelets with the same frequency (Brown, 2004).

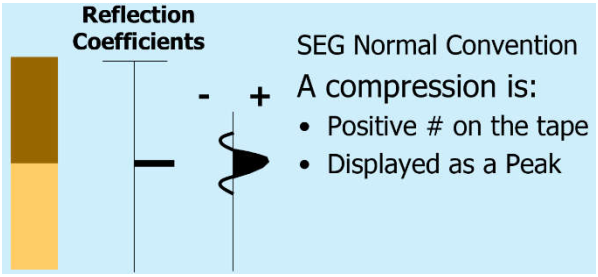

Figure 3.2: Seismic normal polarity convention by SEG. The brown and yellow column to the left, represent two strata with different densities. Velocities increase from the brown to the yellow, giving a positive amplitude. To the far right, a Ricker wavelet representing the increase in acoustic impedance. Image from Schroeder (2017).

3.1.2 Seismic resolution

The threshold of seismic resolution plays a vital role in the investigation of pockmarks w where features below the threshold will not be visible. Different factors affect seismic resolution. In general, both acquisition bandwidth and attenuation of the noise will directly affect resolution. Also, there are factors limiting resolution both in the vertical and horizontal plane (Brown, 2004).

3.1.2.1 Vertical resolution

Resolving power is the ability to distinguish between properties of two or more elements, and is always measured in terms of the seismic wavelength (Brown, 2004; Widess, 1973). The relationship between wavelength velocity and frequency is a quotient of the latter two variables (see Equation 3.3). As seismic waves propagate with depth, the velocities decrease due to compaction of the rocks, while the dominant frequency decreases due to attenuation of the higher frequencies. Both these factors result in lower wavelength and poorer seismic resolution (Brown, 2004).

Furthermore, the vertical resolution has different limits to consider due to interactions of wavelets from other reflected interfaces. The *limit of separability* is set to one-quarter of the wavelength and is the bed thickness corresponding to the closest separation of two wavelets in the seismic signal (Brown, 2004). In Widess (1973) this limit was set to about one-eighth of the dominant frequency-based wavelength. Beyond these wavelength limits, the amplitude will gradually be attenuated and shadowed by surrounding noise signals, also called the *limit of visibility* (Brown, 2004).

For calculating dominant frequencies ($F_{dominant}$) of the seismic horizons, equations 3.1 to 3.3 are used (see results in Table 3.1). These equations, used in Schroeder (2017) originated from empirical methods used to extract wavelet frequency information on isolated reflections. A wave cycle (#cycle) is measured from trough to peak, and the time interval is just the two-way travel time difference between start to end cycles (Schroeder, 2017). A control segment of the seismic signal was used to estimate the wave cycles as shown in Figure 3.3. This image also shows the Ricker wavelet along with the coloured seismic signals. Velocities used in **Feil! Fant ikke referansekilden.**Table 3.1 is based on the sound velocity of water for the seabed horizon, and velocities for glacigenic sediments as presented in Ottesen et al. (2014) and Rafaelsen et al. (2002).

F is for the frequency. # cycle is for the numbers of wave cycles. ΔT is the time interval, and the Greek letter lambda (λ) is the wavelength.

$$F_{apparent} = \#\,cycle / \Delta T \qquad \text{Equation (3.1)}$$

$$F_{dominant} = (2 \times F_{apparent}) / \pi \qquad \text{Equation (3.2)}$$

$$\lambda = Velocity / F_{dominant} \qquad \text{Equation (3.3)}$$

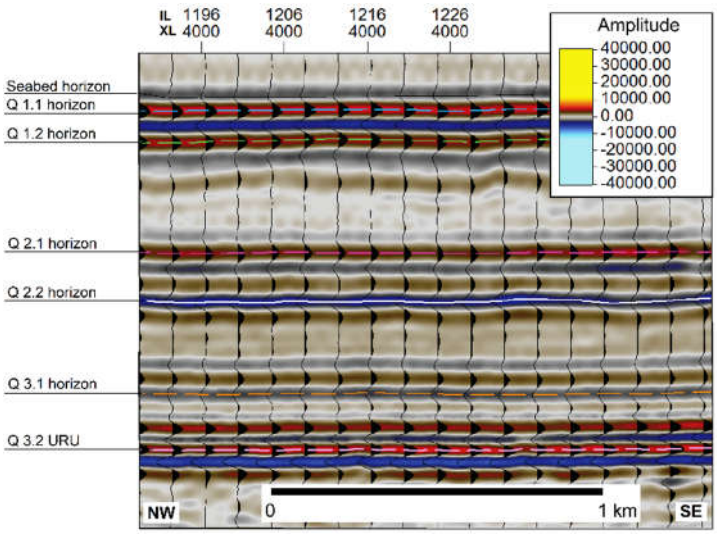

Figure 3.3: Seismic horizons in a small cross-section from x-line 4000. Temporal distance from this section was used to calculate the wavelength in Table 3.1. The amplitude wiggle lines in black shows the peaks and troughs in the seismic image. These were used to count the wave cycles from seabed (in grey colour) down to the URU horizon (peak has red colour amplitude).

Table 3.1: Frequency and wavelength estimation table.These are frequency and wavelength calculations for an estimated resolution. F_{app} is the apparent frequency based on Equation (3.1), F_{dom} is the dominant frequency based on Equation 4.1Equation (3.2)., while Equation 4.3 calculated the wavelength lambda. Two-way-time (TwT) measured from the zero-crossing of the wave seen in Figure 3.3. The baseline for measurements is the seabed.

Horizons	TwT	Cycles	F_{app} (Hz)	F_{dom} (Hz)	V (m/s)	λ (m)
Q1.1	0,013	0,5	38,5	24,5	1500	61,3
Q1.2	0,035	1,5	42,9	27,3	1750	64,1
Q2.1	0,114	5,0	43,9	27,9	1750	62,7
Q2.2	0,148	6,5	43,9	28,0	1750	62,6
Q3.1	0,212	8,5	40,1	25,5	1750	68,6
Q3.2 URU	0,252	11,0	43,7	27,8	1750	63,0

Table 3.2: Estimated vertical and horizontal resolutions. The threshold of vertical resolution is one-fourth of the wavelength. The fact that the seismic signal is composed of many frequencies may give better resolution at shallow levels. Based on the definitions in Widess (1973), the limit can be estimated to one-eighth of the wavelength. The radius of the first Fresnel zone indicates the limit of the horizontal resolution based on Equation 3.4. It also shows that larger radius at depth will give a poorer horizontal resolution.

Horizons	Vertical res. λ/4 (m)	Vertical res. λ/8 (m)	Radius Fresnel zone (m)
Q1.1	15,3	7,7	17,3
Q1.2	16,0	8,0	31,3
Q2.1	15,7	7,8	55,9
Q2.2	15,6	7,8	63,7
Q3.1	17,1	8,6	79,7
Q3.2 URU	15,7	7,9	83,3

3.1.2.2 Horizontal resolution

The horizontal resolution is the threshold to separate features on the subsurface horizon due to seismic waves limitations in an area outside the Fresnel zone. When seismic waves are reflected from a subsurface reflector, some interfere constructively forming the first Fresnel Zone or just Fresnel zone. Beyond this region, the waves will alternate between destructive and constructive interference. Thus, the only clear surface reflector will be the one from within the Fresnel zone (Sheriff, 1996).

In 2D, the Fresnel zone is reduced to an ellipse perpendicular to a line and with improved resolution only along the line, but in the 3D migration, the zone reduces to a small circle, in three dimensions this is a sphere (Brown, 2004). Given the density grid in the survey (GN1101) with inlines every 25m and cross-line every 12.5m, the total horizontal resolution is improved (Rafaelsen et al., 2002). For calculating the radius of the Fresnel zone the following equation was used (Denham & Sheriff, 1981; Brown, 2004):

R is the radius of the Fresnel zone. V is velocity. T is the two-way-time in seconds, and F_{dom} is the dominant frequency.

$$R_f = \frac{\mathrm{V}}{2}\sqrt{\frac{\mathrm{T}}{\mathrm{F_{dom}}}} \qquad \text{Equation (3.4)}$$

3.2 Seismic data interpretation

This section presents the criteria for horizons signals and the identification of pockmarks on the horizons. Also, to uncover geological features and properties, some surface and volume attributes were applied. All horizons show artefacts aligned parallel to the ENE-WSW inlines. These artefacts were the results of movement during acquisition and should not be assessed as geological features (Rafaelsen et al., 2002). The volume attribute *variance* was used to highlight pockmark morphology.

3.2.1 Seismic interpretation

3.2.1.1 Seismic horizon selection

Interpreted seismic horizon have not been smoothened in order to preserve small geological features. Seismic horizons have been tied to wellbores 32/2-1 and 32/4-1 (see cross-section in Figure 4.1, Chapter 4- Results).

Seabed horizon

The seabed corresponds to a prominent trough in the seismic signal. Initially, the Seabed horizon was selected based on signal strength and the SEG convention which corresponded to a peak signal (now Q1.1). Calculating the offset between signal through and peak showed a difference of about 5.5 ms one-way time (OwT). Depth conversion using a velocity of 1500 m/s gave a depth of about 8-9 m, the peak signal maps below the actual seabed. As such, the seismic horizon represents by a trough was chosen as the seabed.

Q 1.1 horizon

The Quaternary 1.1 (Q1.1) horizon is the first strong peak signal marking the reflection coefficient and the middle of the Ricker wavelet, as shown in Figure 3.2. The seismic amplitude is strong and continuous throughout the survey.

Q 1.2 horizon

The Quaternary 1.2 (Q1.2) horizon has a strong seismic amplitude and is the second peak from the seabed. The horizon is eroded on the N-NE part of the map and where it is overlapped in by the overlying Q1.1 horizon. Q1.2 may represent the top of the till unit seen in Figure 2.9.

Q 2.1 horizon

The Quaternary 2.1 (Q2.1) horizon has a strong to normal continuous peak amplitude located deeper in the Quaternary interval. The trough signal mixes with another trough signal above, and this overlapping of signals can be seen in Figure 4.7, as a magenta to purple coloured surface in the Q2.1 horizon time structure map. It is heavily eroded and truncated about one km northeast of the Øygarden Fault Complex, making horizon interpretation difficult past this

region. It may represent the base of the till unit or top of the normal to glacio-marine unit seen in Figure 2.9.

Q2.2 horizon

The Quaternary 2.2 (Q2.2) horizon has a strong continuous trough amplitude signal under the Q2.1 horizon. The surface is considered erosional. It exhibits many glacial marks and is associated with the top of a till unit representing a GES (see Figure 2.9). No pockmarks were identified on this horizon.

Q 3.1 horizon

The Quaternary 3.1 (Q3.1) horizon has a normal continuous trough amplitude signal located near the Base of the Quaternary interval. There are some dimmed and weak signal section in the north, which is orange coloured on the time structure coloured map (Figure 4.6). It is eroded and truncated northeast of the Øygarden Fault Complex, making horizon interpretation difficult past this region. Placing this horizon in the stratigraphy of Figure 2.9 is difficult. This unit may be the top of glaciomarine unit L6 due to the sedimentation thickness between Q3.2 URU and lack of glacial marks.

Q 3.2 URU horizon

The Upper Regional Unconformity (Q3.2 URU) horizon has a strong continuous peak amplitude at the base of the Quaternary interval. It is heavily truncated past northeast of the Øygarden Fault Complex.

3.2.1.2 Pockmark selection

Identification of depression features as pockmarks consisted of several steps in Petrel by flattening horizons and increasing the vertical exaggeration (z-axis) to x 10-15. The colour map, on the time depth horizons, where changed in order to increase the contrast between pockmarks and surrounding topography. Colour maps with many different colours were preferable. Pockmarks were mapped manually by placing a point object in the deepest part of the depression, and by constructing polygons around the rim of the feature. On relatively flat areas, without any erosional features and little topography, horizons were inverted to highlight the pockmarks as peaks. Maximum measured depth has been calculated by the maximum height of the pockmark rim minus the deepest point (object). The intention was to measure the

pockmark depth and use this parameter for comparison with other horizons. However, later observations of pockmarks on seismic cross-sections has shown several pockmarks reach deeper than the horizon. Thus, making depth measurements uncertain. It has therefore only been used for relative depth comparison to neighbouring pockmarks affecting the same horizon. Point objects and polygons were exported to ArcMap® as shapefile objects for calculation of width, length, surface area, depth and directionality (see Figure 3.4 for parameter measurements).

The assembled parameters were later exported to Microsoft Excel® for sorting and the creation of a pockmark database in a comma-separated values (CSV) format for use in the R programming environment, where all the statistical analysis was performed.

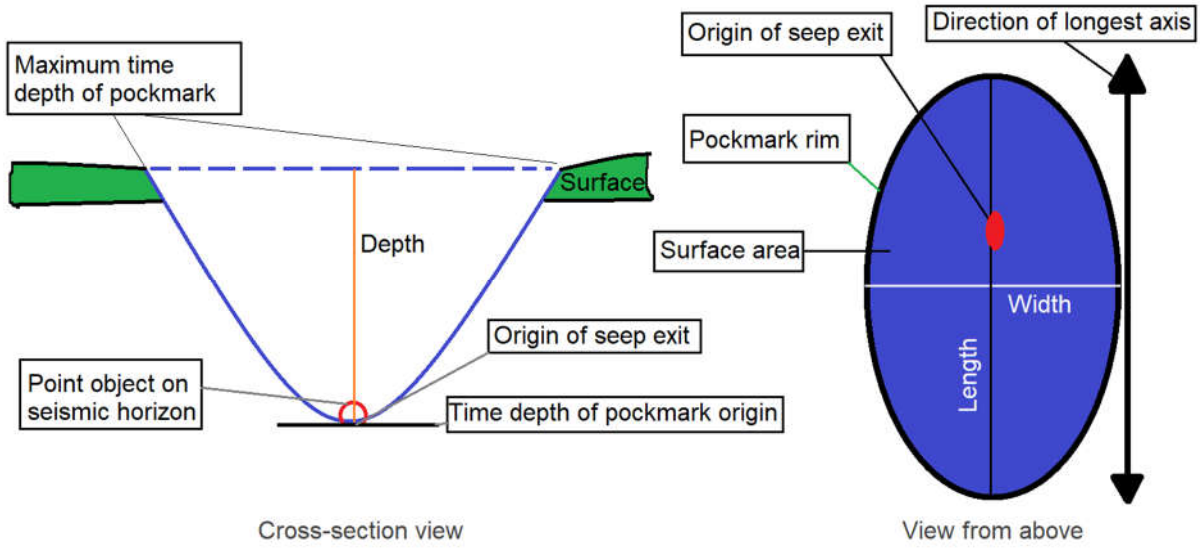

Figure 3.4: Parameters of pockmark measurement. Sketch showing where on the pockmarks and horizon surface parameters as width, length, surface area, depth and directionality were measured.

3.2.2 Seismic attributes

For practical reasons, the primary use of attributes in the analysis were volume attributes, as surface attributes provided little useful information on patterns and features in the Quaternary interval.

3.2.2.1 RMS amplitude

The RMS amplitude volume attribute computes the Root Mean Squares (RMS) on instantaneous trace samples over a specified window of the seismic signal. It is used to analyse differences between two seismic traces and quantify the RMS ratio (Schlumberger Limited, 2018). It has been applied to areas for mapping potential gas or fluid traces, which can show a higher reflective signal (RMS ratio) than surrounding areas.

3.2.2.2 Variance

This volume attribute estimates local variance in the signal, i.e. can visualise discontinuities in the horizontal continuity of amplitude, e.g. faults, fracture corridors and large sedimentary structures such as channels (Schlumberger Limited, 2018). The variance amplitude has been applied to visualise fault traces and pockmarks.

3.2.2.3 3D curvature

Curvature describes how much a surface at a point curves or deviates from a straight line. It is related to the second derivative of the curve defining the surface. 3D curvature volumes can highlight areas that are not readily discernible on variance attribute maps (Schlumberger Limited, 2018). The 3D curvature attribute has been applied to emphasise stratigraphic features and structural discontinuities as the variance volume attribute showed poor structural definitions in some areas below the Q3.2 URU horizon

3.3 Statistical analysis and theory

The statistical analysis herein consists of tests and a collection of data in the pursuit of a significant correlation between the measured parameters. Presentation of pockmarks parameters as descriptive statistics with histograms and scatterplots is a way to describe their features quantitatively which can give insight to their temporal and spatial evolution (Panik, 2012). This thesis also explores inferential statistic as part of the spatial analysis on the shallow Quaternary horizons, which aims to sample data and predict population characteristics such as clustering based on an underlying Poisson probability distribution in the area (Panik, 2012; Diggle, 2014). R Foundation for Statistical Computing software has been used in the statistical analysis (Team, 2018). All computer snippets are available in Appendix 2.

3.3.1 Spatial point pattern

The deepest part of each pockmark is a reference point in the spatial distribution analysis (see Figure 3.4). By mapping the pockmarks this way, it will give the emerging marks a point pattern for evaluation. A spatial point pattern analysis will use all point to point distances to describe a 2D distribution pattern within a region and involve summary statistics with sums and distances. In a point pattern, a *mean centre* is computed over average X and Y coordinate values, a *standard distance* is a measure of variance between the average distances of the features to the *mean centre*, and a *standard deviational ellipse* is a measure of separate standard distances for each axis (see Figure 3.5) (see Appendix 3 for equations) (Gimond, 2019). Point pattern analysis introduces stochastic distribution in the model, and by that, it infers inherent randomness and assumes that all points are distributed independently (Diggle, 2014). Stochastic processes are standard in geographical data, where the outcome is indeterministic. Therefore, along with the analysis, comes a statement of a null hypothesis of Complete Spatial Randomness (CSR) and testing.

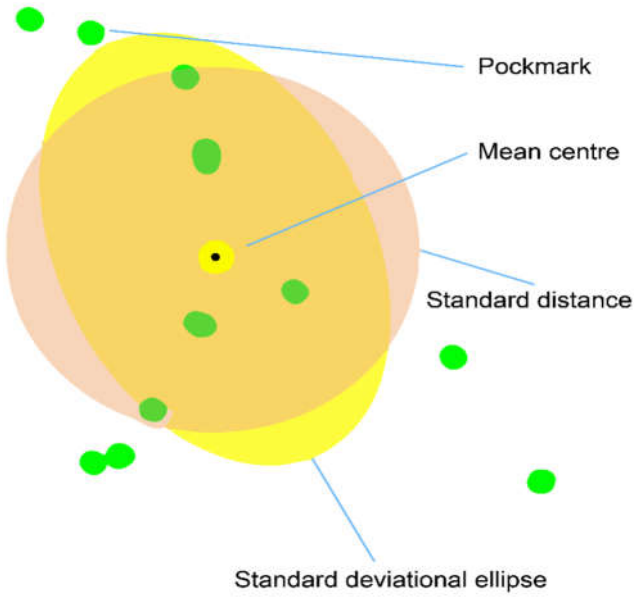

Figure 3.5: Spatial point pattern measurements around the pockmarks. Modified from Gimond (2019).

In this thesis, the point pattern methods serve just as a model to the idea of an existing mechanism generating random spatial point patterns on the seabed. The type of geological information this methodology can give is of more importance. Either the patterns confirm the null hypothesis, meaning the pockmarks are generated randomly by processes evenly distributed over the whole study area, or they have point sources, where clusters of pockmark events are likely to form.

Furthermore, the statistics of pockmark distribution patterns can be analysed by two different approaches: density or distance methods, or both. In the density-based approach, the Quadrat and Kernel density analysis are used. These density methods are part of a *first-order analysis.* Likewise, the use of distance measurement methods like Average Nearest Neighbour (ANN) and the K-function are part of the *second order analysis* (Aldstadt, 2010; Gimond, 2019). It is through these methods that we seek a better understanding of the pockmark pattern.

It has been stated in point pattern analysis that density-based analysis is part of the first-order and distance-based methods are part of the second-order analysis. Distinguishing the two methods is essential to clarify. The first-order analysis is interpreted as changes caused by underlying properties (Gimond, 2019). Here, such changes can be the pockmark source origins, but also additional effects from sediment composition, i.e. sand to silt, to clay ratios. The second-order analysis comes from an interaction between the points (Gimond, 2019).

Pockmarks generated at the seabed surface may not necessarily have been generated through a vertical line and linear conduit from source to the seabed. Unless there is a clear pathway, like an established chimney up to the surface, fluids are more likely to pass through the sediment in a complex network.

3.3.2 Quadrat and Kernel density analysis

In point pattern analysis densities are divided into global and local groups. The global is just the ratio of the observed number of points to the surface area being investigated. The local involves partitioning of the study area into subsets of regions. Such distribution of regions helps to represent the count of points as ratios and avoid forming bias pattern in the data (Aldstadt, 2010; Gimond, 2019). There are several methods for measuring local densities, but this thesis uses the quadrat and the kernel density method.

3.3.2.1 Quadrat density

The quadrat density method uses subsets of regions called quadrats. The calculated density is a partitioning of the study area into some scattered or adjacent equal sized quadrats (Aldstadt, 2010), developed by Greig-Smith (1952). For the Smeaheia, we divide the area into squares or rectangular shaped regions in order to apply a pockmark count every square kilometre. An excess number of high and low cell counts suggests a clustered pattern, while average density suggests a dispersed pattern (Aldstadt, 2010). The method can in a simple way show the count of events spread out through the quadrats, but the choice of the quadrat surface area could also influence the result. Quadrat density is programmed in R with the *quadratcount* command under tool package *spatstat* (Baddeley, Rubak, & Turner, 2015; Baddeley & Turner, 2005).

For a geology analogy: the quadrat count is the equivalent to mapping fractures with scanlines in a damage zone. The method is counting incidents and visualising the frequencies on a map.

3.3.2.2 Kernel density

Where the quadrat delineates the pockmarks into the quadrats, the kernel method calculates regions of localised density, and subregions overlap one another allowing a moving window. It is this moving window that is the kernel. A kernel process introduces a grid of values with smaller cells than the kernel window, and the cell receives the density value from the centred kernel window. The Kernel functions assigned in the analysis are *gaussian* type, for a smooth density map (Gimond, 2019). Kernel density is programmed in R with the *density* command under tool package *spatstat* (Baddeley et al., 2015; Baddeley & Turner, 2005).

3.3.3 Average nearest neighbour analysis (ANN)

The average nearest neighbour (ANN) analysis is part of the second-order analysis and based on the distance between each pockmark point and its neighbour. Clark and Evans (1954) derived the expected value and variance of the average nearest neighbour distance in a CSR pattern (Aldstadt, 2010). The average distance is compared to an expected distance for a random pattern. ANN analysis has been programmed in R with the *nndist* command under tool package *spatstat* (Baddeley et al., 2015; Baddeley & Turner, 2005).

3.3.4 Ripley's K-function and, L-function

The quadrat and nearest neighbour analysis can examine only one scale of interaction at a time, while the distance-based Ripley's K-function can summarise distances between all pair of points within a pre-specified distance *d* (Aldstadt, 2010; Getis, 2005; Ripley, 1977). The K-function is adapted to take into the account distances closer to the boundary of the investigated area, which is essential so that points near the boundary are given more considerable weight in the analysis. In the necessity to stabilise variance, Besag (1977) modified the function into the new L-function (as cited in Getis (2005); Aldstadt (2010)).

The Ripley K-function (K-function) and L-function have been programmed in R with the *Kest* and *Lest* command under tool package *spatstat* (Baddeley et al., 2015; Baddeley & Turner, 2005). Computer snippet is available in Appendix 2 and the equations in Appendix 4.

3.3.5 P-values

Statistical tests start by identifying a null hypothesis for CSR. P-values returned will indicate whether to reject the chosen null hypothesis or not. If some random process created the observed spatial pattern, the p-values would show how probable that is. When the null hypothesis is a random pattern, then a small p-value will indicate that the tested pattern is the opposite of the null hypothesis. In general, the null hypothesis is rejected when a p-value is higher than 0.05 (see Table 3.3).

Table 3.3: Critical p-values.
These scores are confidence levels for tests done in the R program.

p-value (Probability)	Confidence level
< 0.10	90 %
< 0.05	95 %
< 0.01	99 %

3.3.6 Monte Carlo simulation

Several of the method tools in the R program uses the Monte Carlo simulation, which in principle generates random objects using the computer. Such objects are used to model real-life systems or problems, but in many cases, the Monte Carlo techniques introduce random object artificially for problem-solving. Regardless of the techniques used, the idea is to be able to repeat experiments many times and obtain interesting quantities using the Law of Large Numbers and other statistical inference methods. The Monte Carlo method remains one of the most useful approaches to scientific computing due to general applicability and simplicity (Kroese et al., 2014).

For comparison reasons, the Seabed horizon has been simulated with a “true” random pockmark pattern by use of a Monte Carlo simulation. The results from this simulation compute the expected distance for use in the ANN analysis.

3.3.7 Descriptive statistics

Width, length, surface area and temporal depth have been measured for all pockmarks and are presented as box whiskers plots, histogram and scatterplots. The box an whiskers plots are especially useful for showing multiple characteristics of the data and to compare the Interquartile range (IQR), i.e. the spread of the data points showing the weighted mean. The IRQ test is a robust method, which means it is insensitive to outliers.

3.3.7.1 Central limit theorem

The fundamental theorem of statistics, the central limit theorem, states that; The sum of a sufficiently large number of independent and identically distributed random variables, will approximately follow a normal distribution (Charpentier, 2018). The term "sufficiently large" means empirical a sample of $n \geq 30$ (LaMorte, 2016).

All the samples of pockmarks on each horizon has more than 200 pockmarks, sufficient be considered as a normal distribution. Nevertheless, the use of statistical tests has been implemented to investigate the possibility of other distribution features and the degree of normality (in distribution).

3.3.7.2 Shapiro-Wilk test

The Shapiro-Wilk is a normality test that inspects whether vector data comes from a normal distribution (Shapiro & Wilk, 1965). It has a null hypothesis that states that the population sample is normally distributed. A large p-value means there is no convincing evidence to reject the null hypothesis (Crawley, 2012). The W values are distributed in the interval of $0 < W \leq 1$, for $n \geq 3$, and where a value closer to 1 indicates that the distribution is close to normal. W has a simple approximation of straightness measure of the normal quantile-quantile (Q-Q) probability plot (visual normality test) and is similar to the correlation coefficient of a normal probability plot (J. P. Royston, 1982; P. Royston, 1995). The null hypothesis is rejected if W is less than p-value limit of 0.05. The test is executed in R with the command *shapiro.test*.

3.3.7.3 Outlier evaluation

Outliers are detected by using the rule of thumb of setting an upper and lower limit, by multiplying the IQR above the third quartile or below the first quartile by 1.5. The upper limit

is the 75% quartile + 1.5*IQR, and the lower limit is the 25 % quartile – 1.5*IQR (Crawley, 2012). Any data points outside these limits are numerically defined as outliers.

The horizon data sets have been analysed by these methods in order to detect outliers, correct and adjust, and finally reject those data points that violate the normal distribution assumption. After separation of the outliers, a final review of the data set is done with a Grubbs' test, alongside a Q-Q probability plot for normality (Grubbs, 1950).

The IRQ, Grubbs' test, Q-Q plot is executed in R with in order of commands: *summary*(), *grubbs.test*(data, type=11), *qqnorm*(). The installed packages for this in R software are called "outliers" and "e1071".

3.4 Data uncertainty

The descriptions herein are always subject to uncertainty, and while working with seismic interpretations, we cannot avoid observational errors, artefacts and resolution related misinterpretations. Awareness of these possible errors are considered when discussing the outcome (see section 5.X).

3.4.1 Seismic horizons

The selection of horizons in the Quaternary interval is a natural selection of the strongest amplitude signals. Uncertainty occurs when the trace enters the eroded and truncated part of the Smeaheia, and the surface becomes discontinuous. Also, "pixel errors" may occur on the horizon maps. Pixel errors occur where the interpreter has selected portions of the horizon, just below the rest of the horizon, or where local interference may force the software to pick a signal above or below the intended path (during generation of surfaces). These pixel errors may later be mistaken for small pockmarks

3.4.2 Errors in pockmark selection

The best area to map pockmarks in 3D seismic is a relatively flat horizon section, where these features stand out as distinctive sharp pits. When pockmarks appear on slopes, they need to be selected with caution. The same consideration goes for visible eroded areas or pockmarks inside ice carved troughs. Both geological features are part of the topology, and to avoid

mapping more than necessary, the interpreter must envisage the natural shape of the pockmark and what it may have eroded.

Not all selected depressions are real pockmarks. A critical factor that should distinguish a pockmark from other morphological similar features is that pockmarks are erosive, and originate below the seabed (Judd & Hovland, 2007). To distinguish this in a 3D seismic horizon can be harder than compared to a higher-resolution survey made by a multi-beam echo sounder, especially on the buried pockmarks. As such, statistics are used to eliminate the selections of outliers outside a normal distribution. Still, there remains uncertainty in this approach and is accepted to have some spurious pockmarks in the data set.

Chapter 4

4 Results

The results of mapping and subsequent statistical data collection are presented in this chapter. The first subsections will present the important stratigraphic horizons and structures mapped in the Smeaheia area using the GN1101 3D seismic volume. Particularly within the Quaternary interval. A section of distributions and statistics then follow with numerical information about the mapped pockmarks. In addition to the pockmarks, glacier marks evident from the Quaternary horizons, are mapped. Th chapter closes with a summary of key qualitative seismic observations that are useful for understanding pockmarks development in the area of interest.

4.1 Horizon mapping

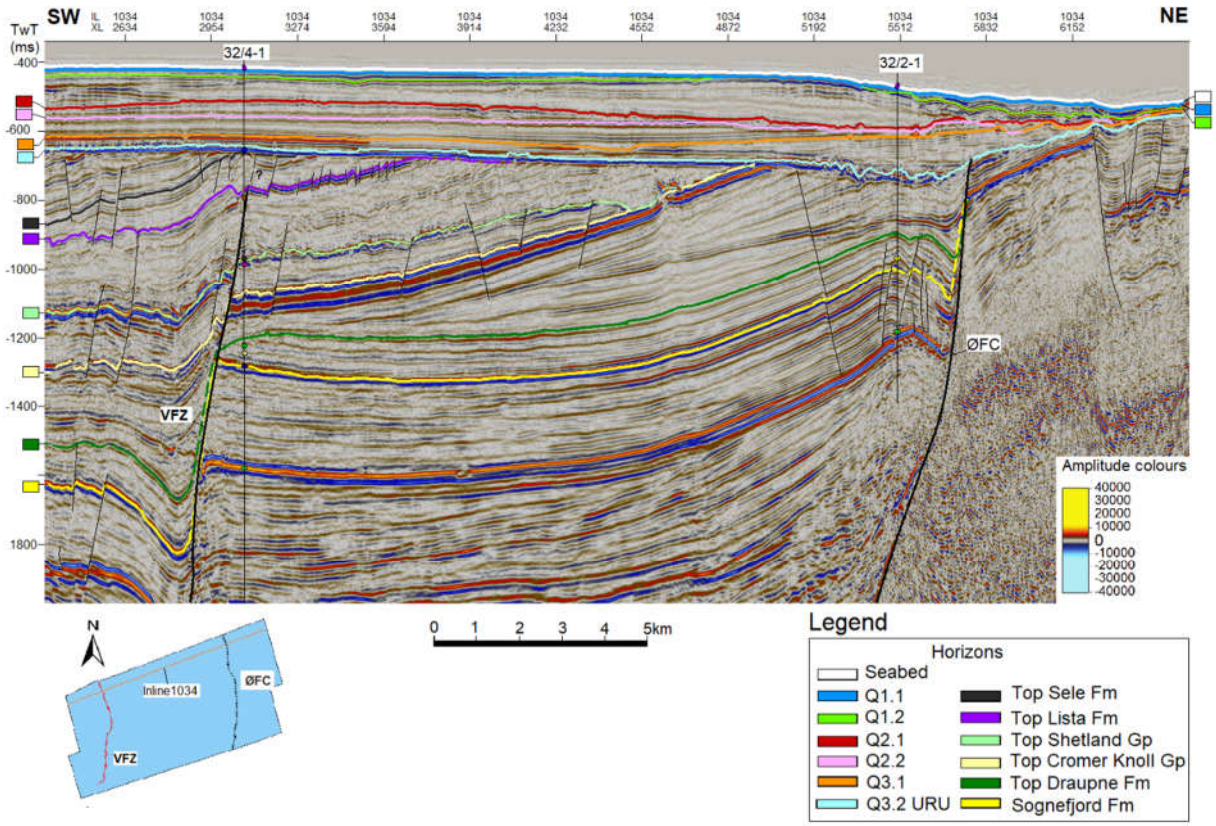

Figure 4.1: Seismic cross-section from SW-NE (inline 1034) with wellbore 32/2-1 and 32/4-1. Quaternary horizons are presented from seabed down to the highlighted light blue Q 3.2-URU horizon. The remaining of the horizons sub-URU are pre-Quaternary. Master faults of VFZ and ØFC are the dominant faults, while faults northeast of the ØFC have no official names and are part of the Øygarden Fault Complex. Z-axis has been exaggerated with 8 times.

The dip-oriented seismic cross-section in Figure 4.1 shows the interpreted stratigraphy and faults from GN1101 inline 1034 in a SW-NE direction. Below is a summary of their geometries.

Horizon 3.2 URU represents the erosional surface, and the oldest horizon in the Quaternary interval. The surface has a small inclination (1°-2°) towards the northeast and before the ØFC footwall high. It also has an extensive eroded region around wellbore 32/2-1. The upper tip of the ØFC appears to be truncated by the URU horizon at this location.

Horizons Q3.1 and **Q3.2** represent the first sedimentary development after the carving out of the Norwegian Channel. The Q3.1 horizon is inclined by less than 1°

Horizon Q2.2 is an erosional surface with multiple indentations and is subhorizontal.

Horizon Q2.1 is partly eroded to the northeast. The layers between Q2.1 and Q2.2 displays apperas to be swollen or inflated in the centre.

Horizon Q1.2 is close to the seabed and partly eroded and subhorizontal. The layers between Q1.2 and Q2.1 also appear to be swelling towards the northeast-east and near the ØFC footwall.

Horizon Q1.1 and Seabed have similar geometries as Q2.1. The difference is that horizon 1.1 has less eroded areas to the northeast-east, and Seabed is the normal marine sedimentation draped over the Q1.1.

The seismic cross-section Figure 4.2 gives a perspective parallel to depositional strike of the interpreted stratigraphy and structures imaged by the GN1101 survey, including the ØFC and the eroded areas from another angle.

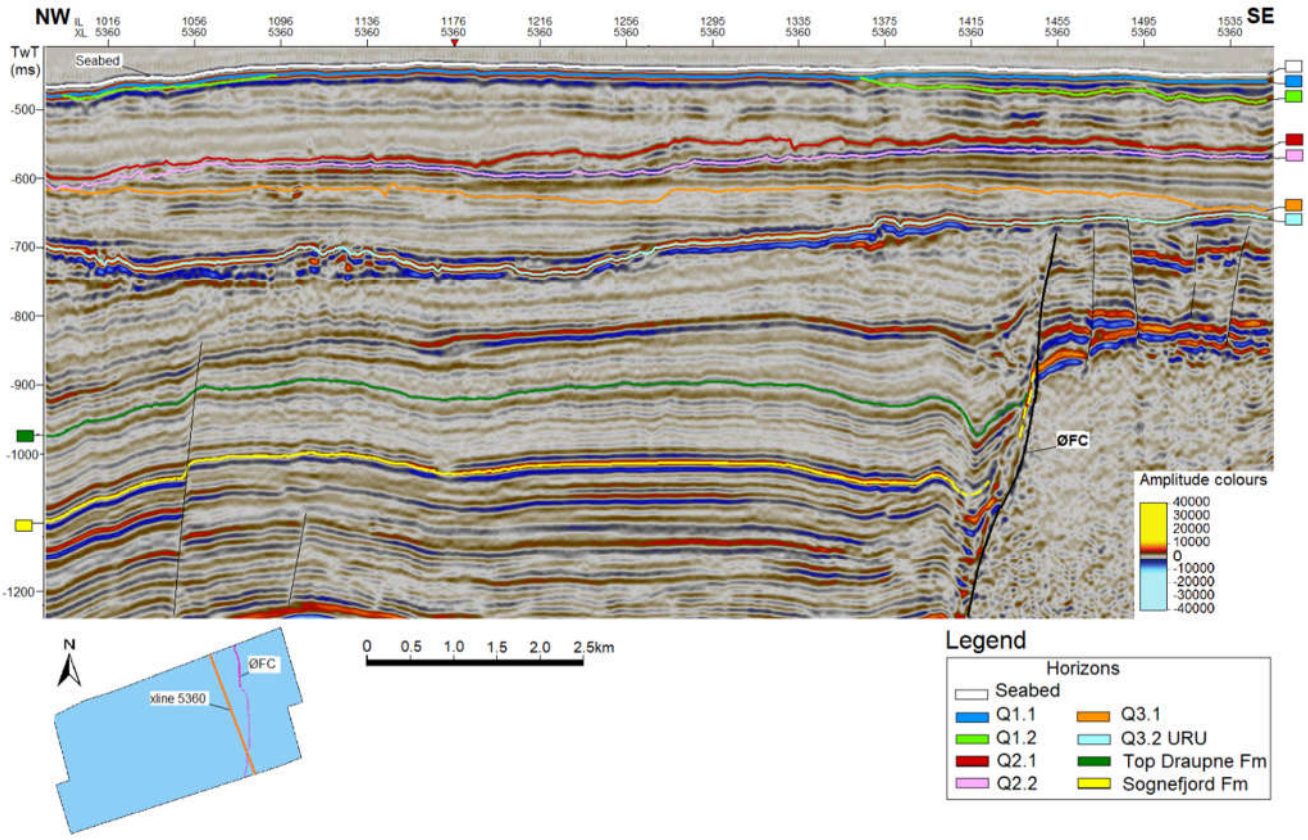

Figure 4.2: Seismic cross-section from NW-SE (x-line 5360). Quaternary horizons are presented down to the highlighted light blue URU horizon at about -700 ms depth. Z-axis has been exaggerated five time.

The horizons of Sognefjord and Draupne formations used in the seismic cross-sections Figures 4.1 and 4.2 are seismic work from Jonassen (2015) master thesis.

4.2 Pockmark, structure, and thickness maps

This section presents the interpreted pockmarks and other important geologic features mapped within the GN1101 seismic volume. They are overlain on structure and isochron thickness maps generated from the interpreted horizons. Mapping of geologic features below the URU surface has been carried out using both amplitude and extracted seismic attribute (3D Curvature) volumes. Pockmarks were mapped primarily from horizon time structure maps

4.2.1 Fault and subcrop structures under the Quaternary sediments

4.2.1.1 Fault and subcrop map

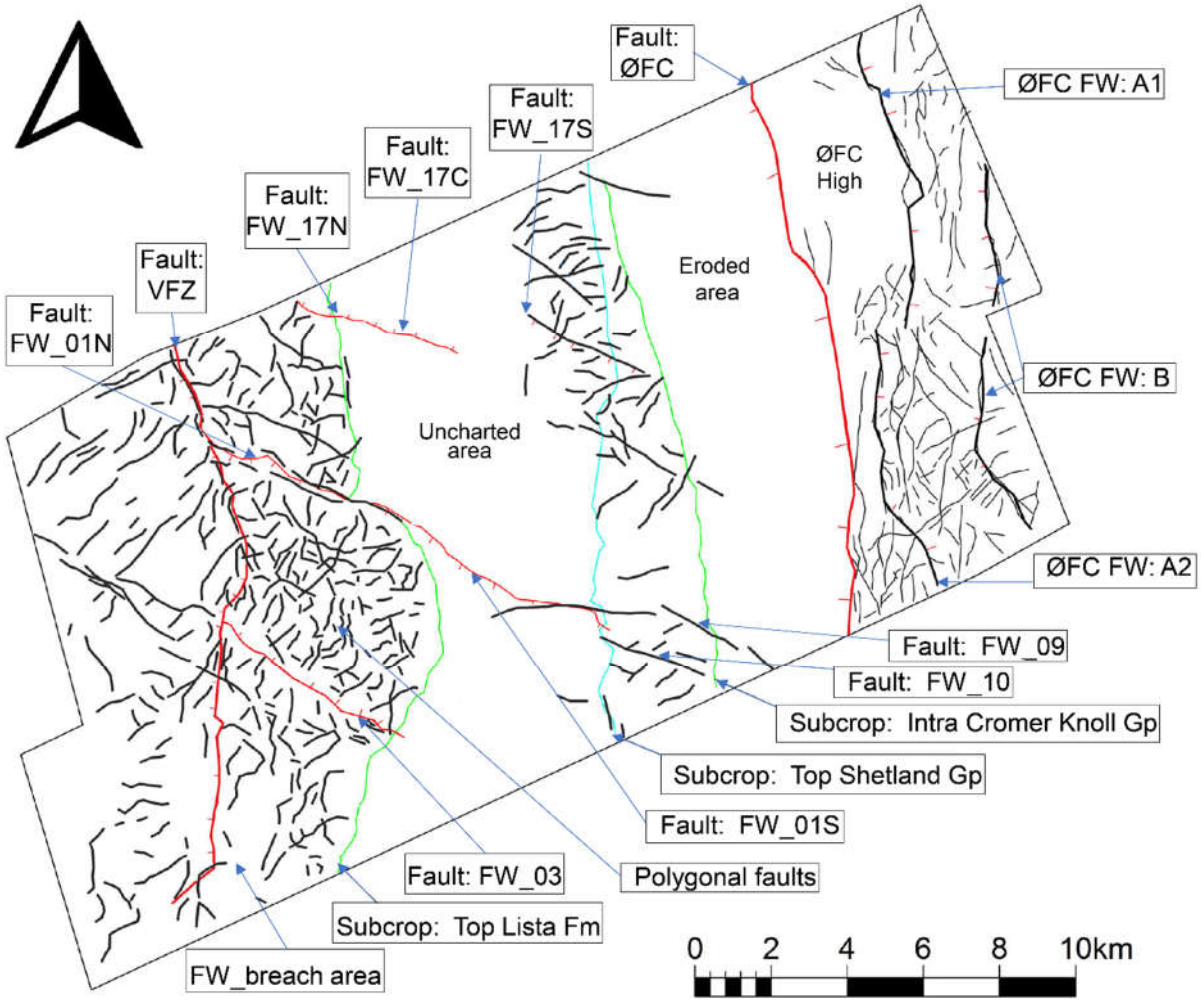

Figure 4.3: Faults and subcrops lineations projected from below the Q3.2 URU horizon. The VFZ is projected from approximately -1100 to -800 ms, while the other faults and lineations from -752 to -740 ms.

The map in Figure 5.3 shows the faults and subcrops found under the URU and are projected from time slices at depth -740 ms. These features are later projected onto the Quaternary maps in sections 4.3.3 and onwards to visualise where pockmarks have formed relative to the faults and boundaries.

4.2.1.2 **3D Curvature map**

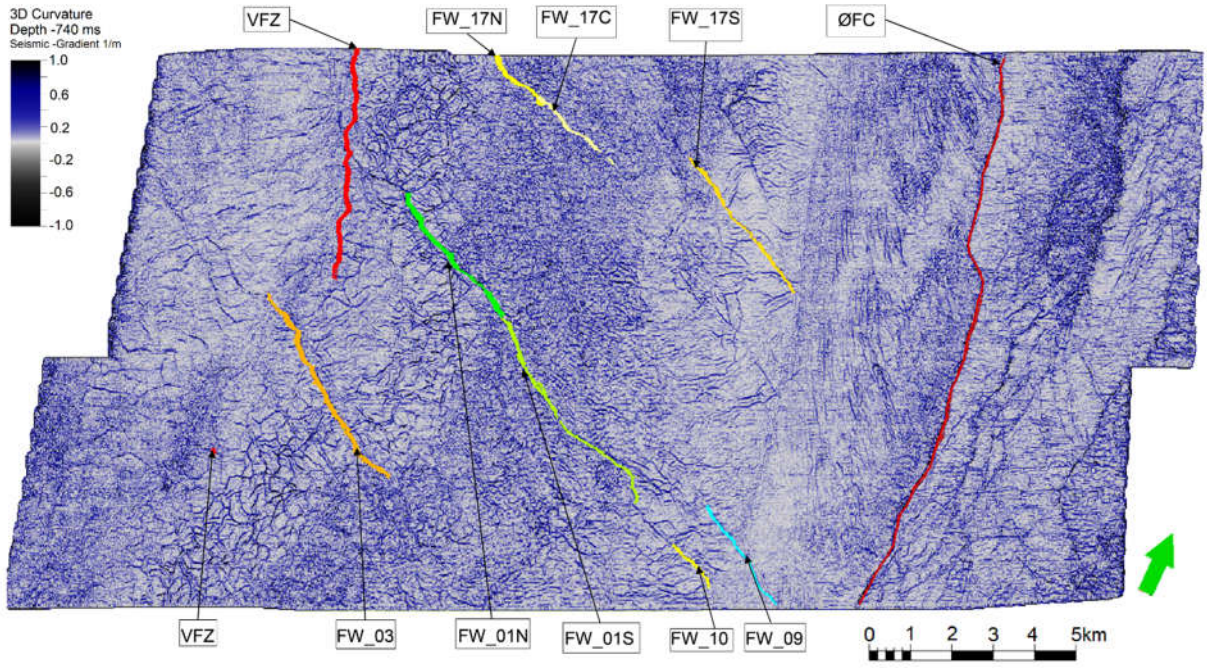

Figure 4.4: Time slice at depth -740 ms using the 3D Curvature attribute. This map was used further map Structures under the angular unconformity are visualised more clearly using the Curvature attribute. The interpreted faults possess fault tips close to Q3.2 URU horizon except the VFZ.

In the uncharted area in Figure 4.3, the polygonal faults are cryptic and difficult to map. The curvature map in Figure 4.4 provides more information about the presence of these faults in the uncharted area.

Prominent through-going faults have been superimposed on to the curvature map. Most of these faults have fault tips close to the URU and can be mapped downsection through the Cenozoic strata. An exception is this fault segment of the VFZ which reaches the Top Lista Formation horizon in the northen part of the GN1101 survey, but only appears to displace the older Top Shetland Group horizon indicating a lower VFZ displacement gradient moving southward.

4.2.2 Pockmark and time structure maps

Time structure maps here show geometry and depth of given Quaternary horizon surface. Pockmarks were interpreted at anomalous point depressions along each horizon surface and are highlighted in each map. The underlying faults and subcrops are superimposed to help envisage how pockmarks may be linked to older geological features. For more detailed information about the pockmark populations and residuals, see section 4.3.5.

4.2.2.1 Time structure of the Q3.2 URU horizon

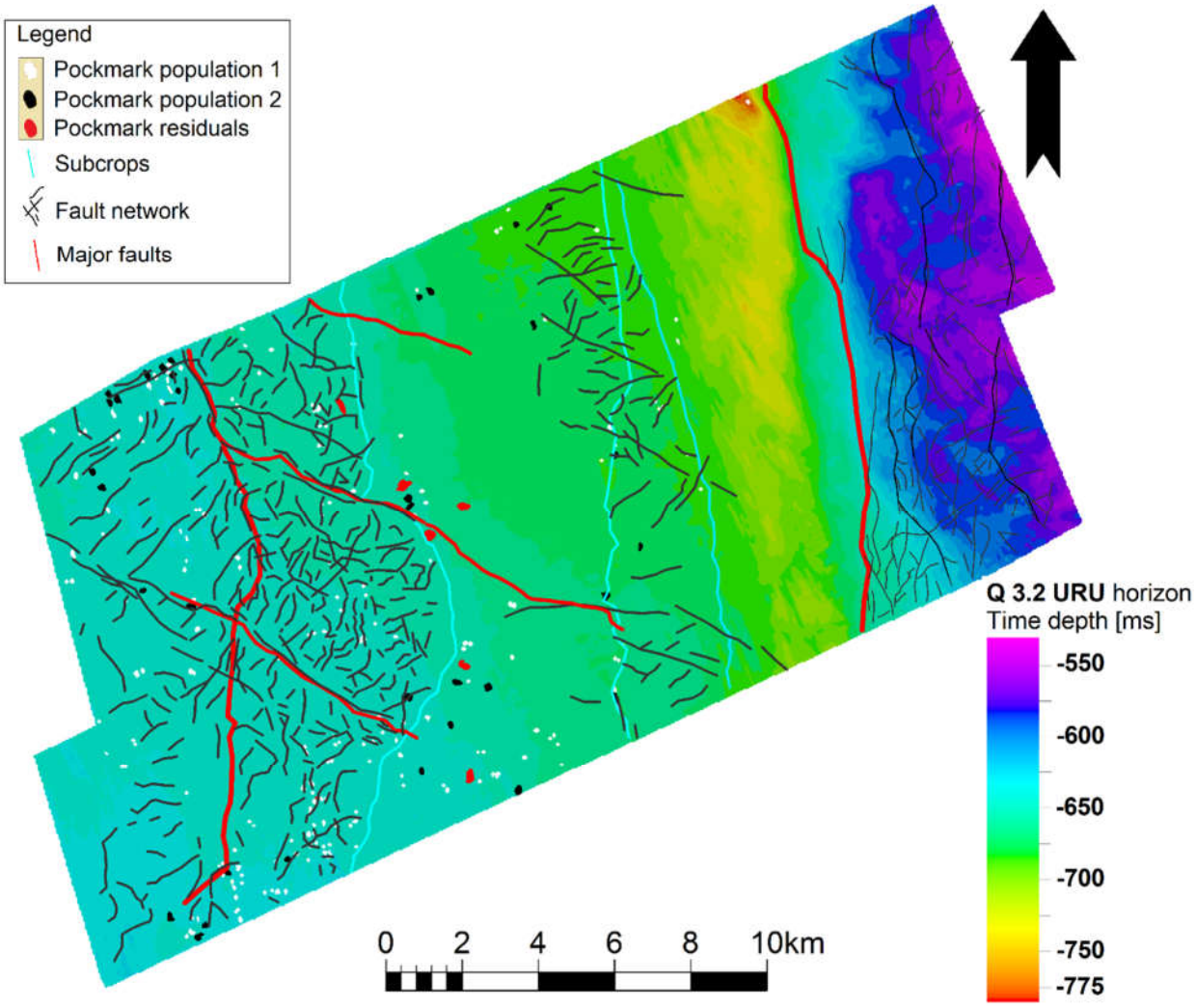

Figure 4.5: Time structure map of Q3.2 URU horizon with pockmark populations.

4.2.2.2 Time structure of the Q3.1 horizon

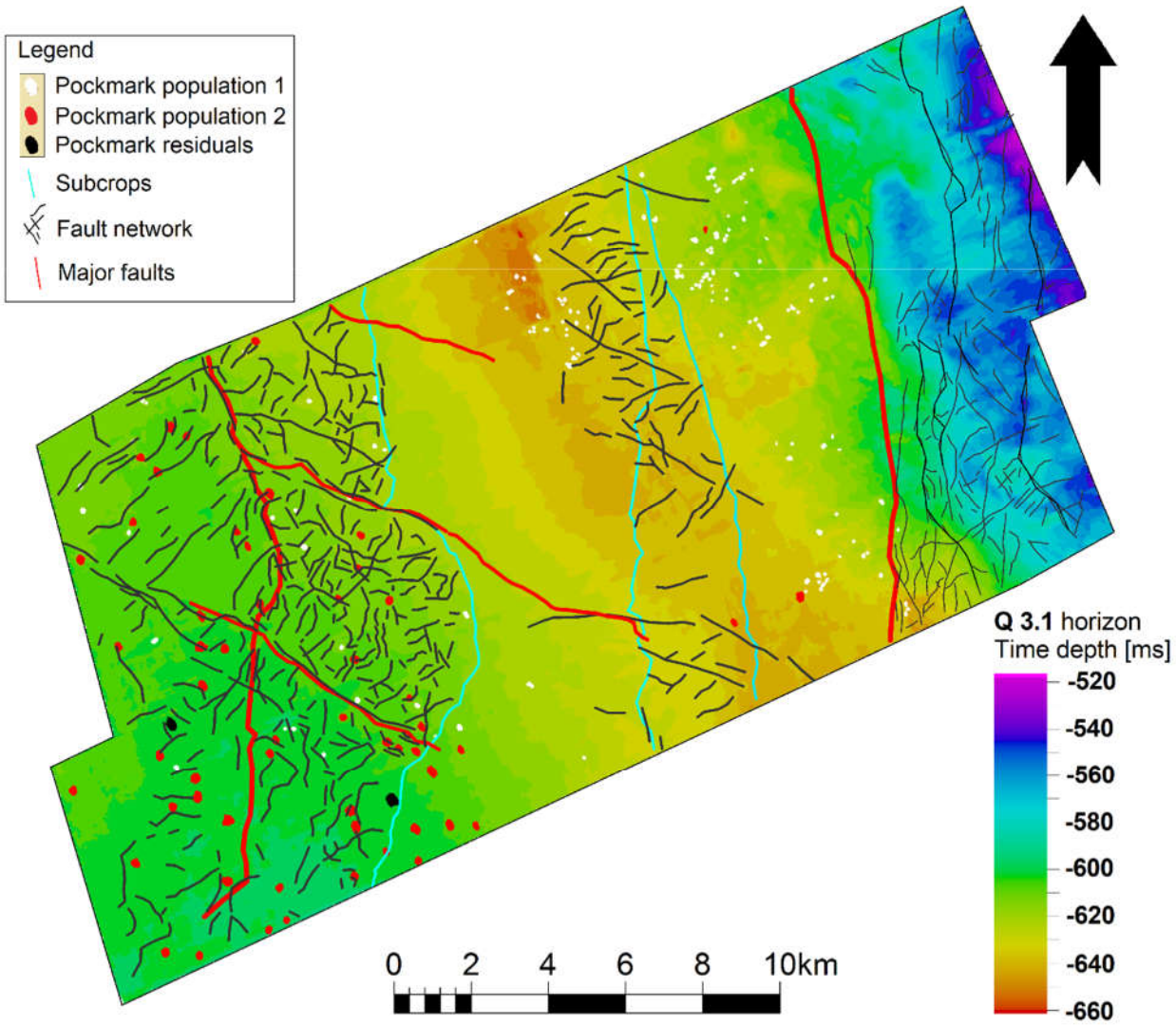

Figure 4.6: Time structure map of Q 3.1 horizon with pockmark populations.

4.2.2.3 Time structure of the Q2.1 horizon

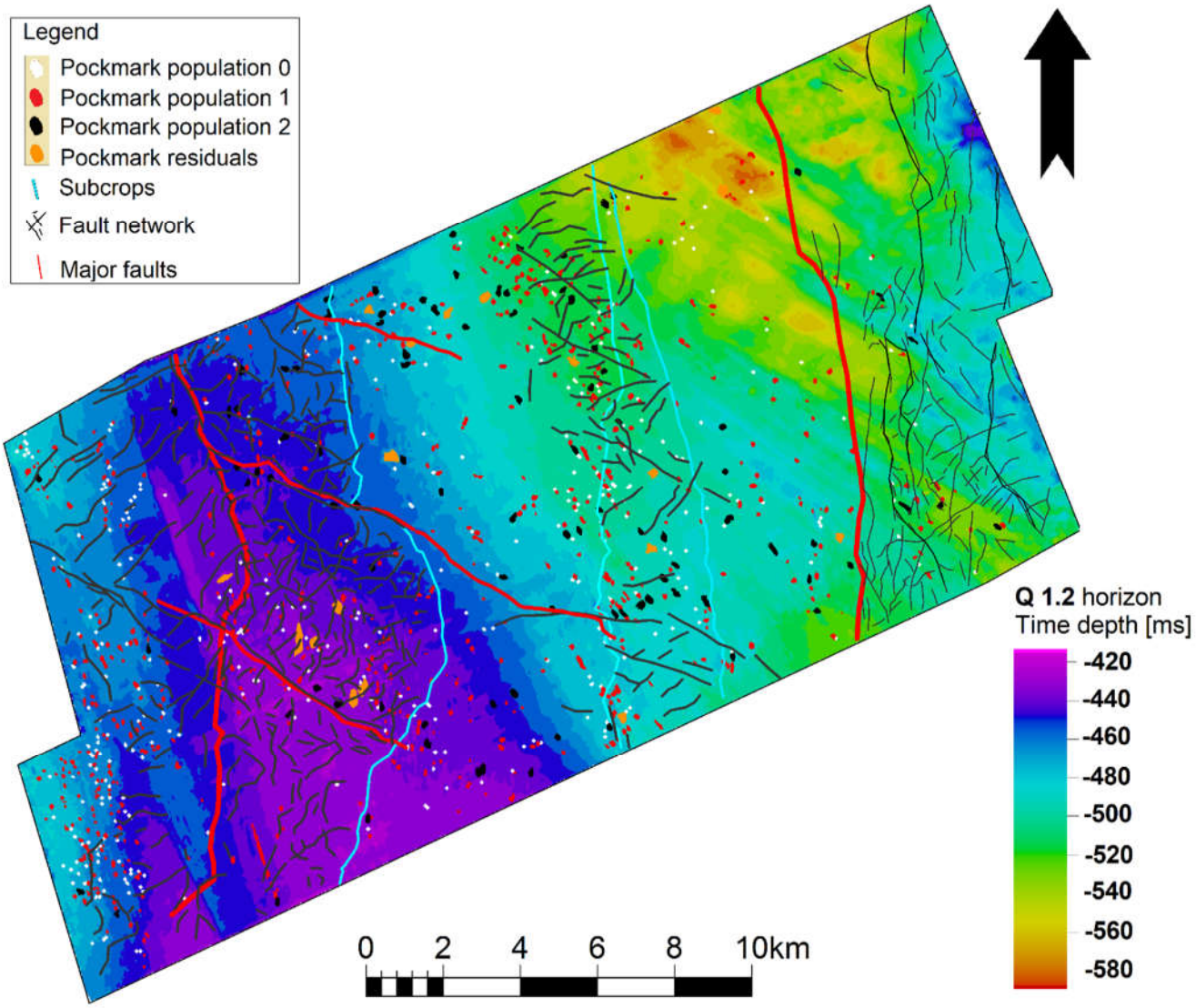

Figure 4.7: Time structure map of Q 2.1 horizon with pockmark populations.

4.2.2.4 Time structure of the Q1.2 horizon

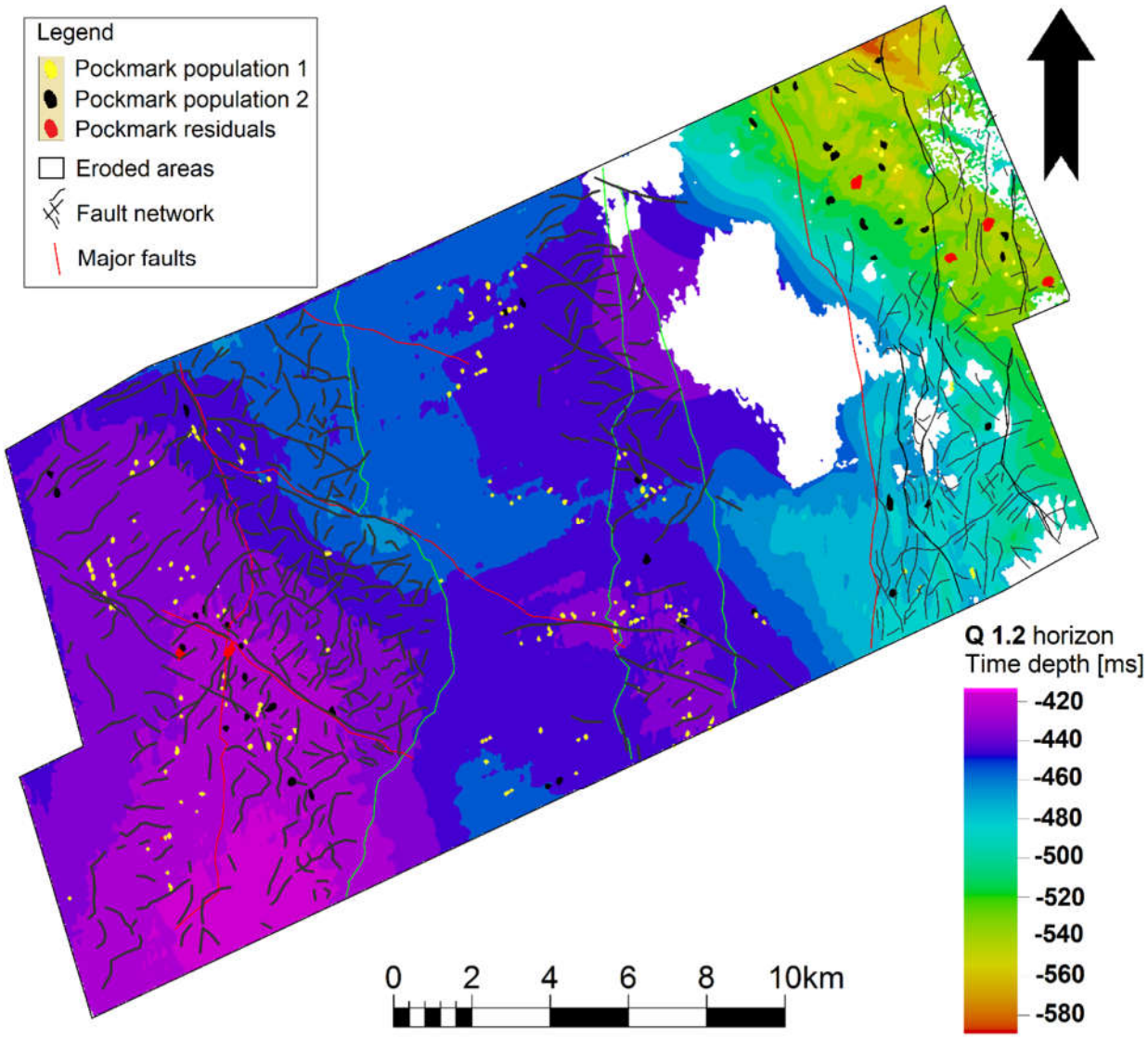

Figure 4.8: Time structure map of horizon Q 1.2 with pockmark populations.

4.2.2.5 Time structure of the Q1.1 horizon

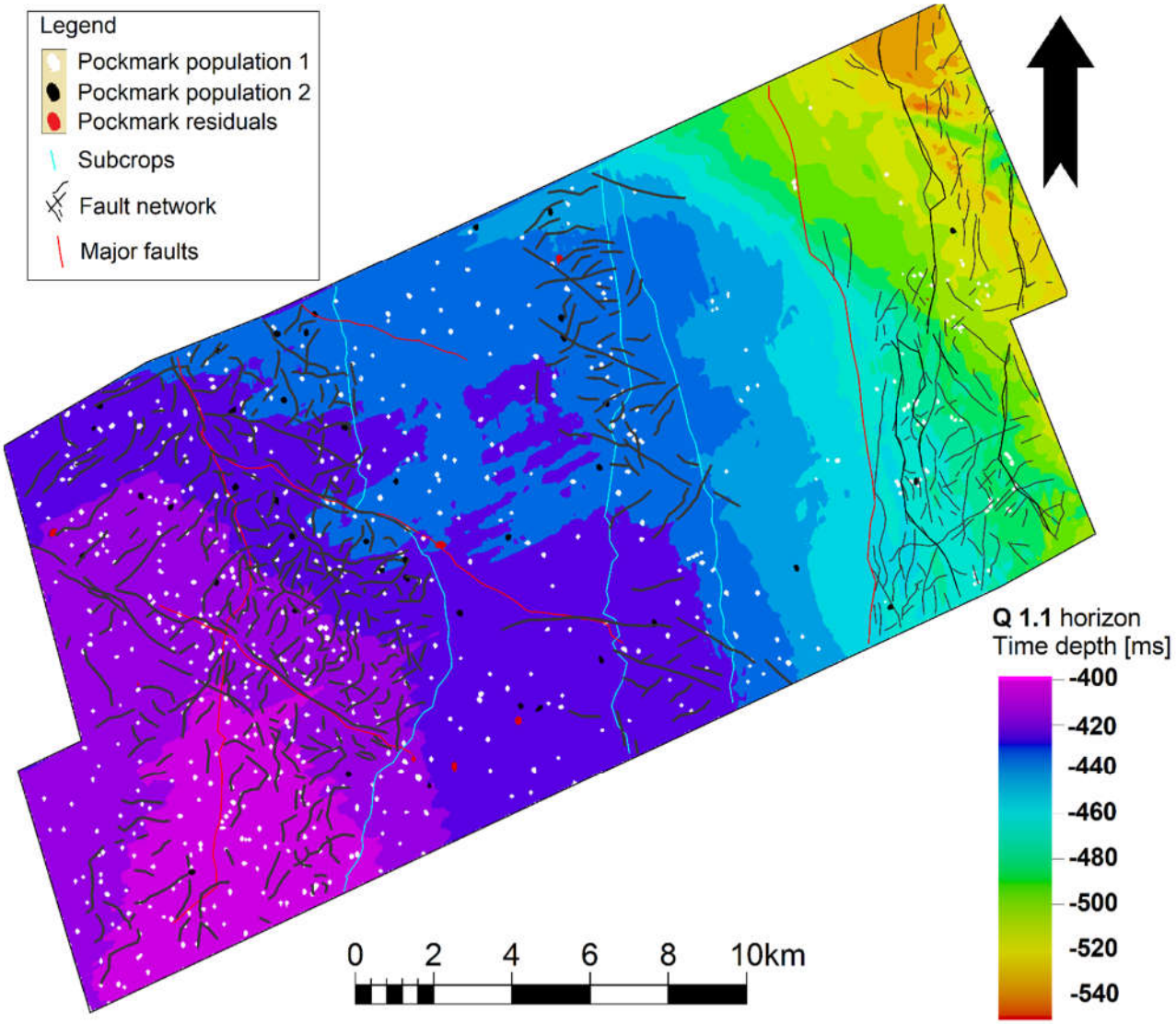

Figure 4.9: Time structure map of horizon Q1.1 with pockmark populations.

4.2.2.6 Time structure of the Seabed horizon

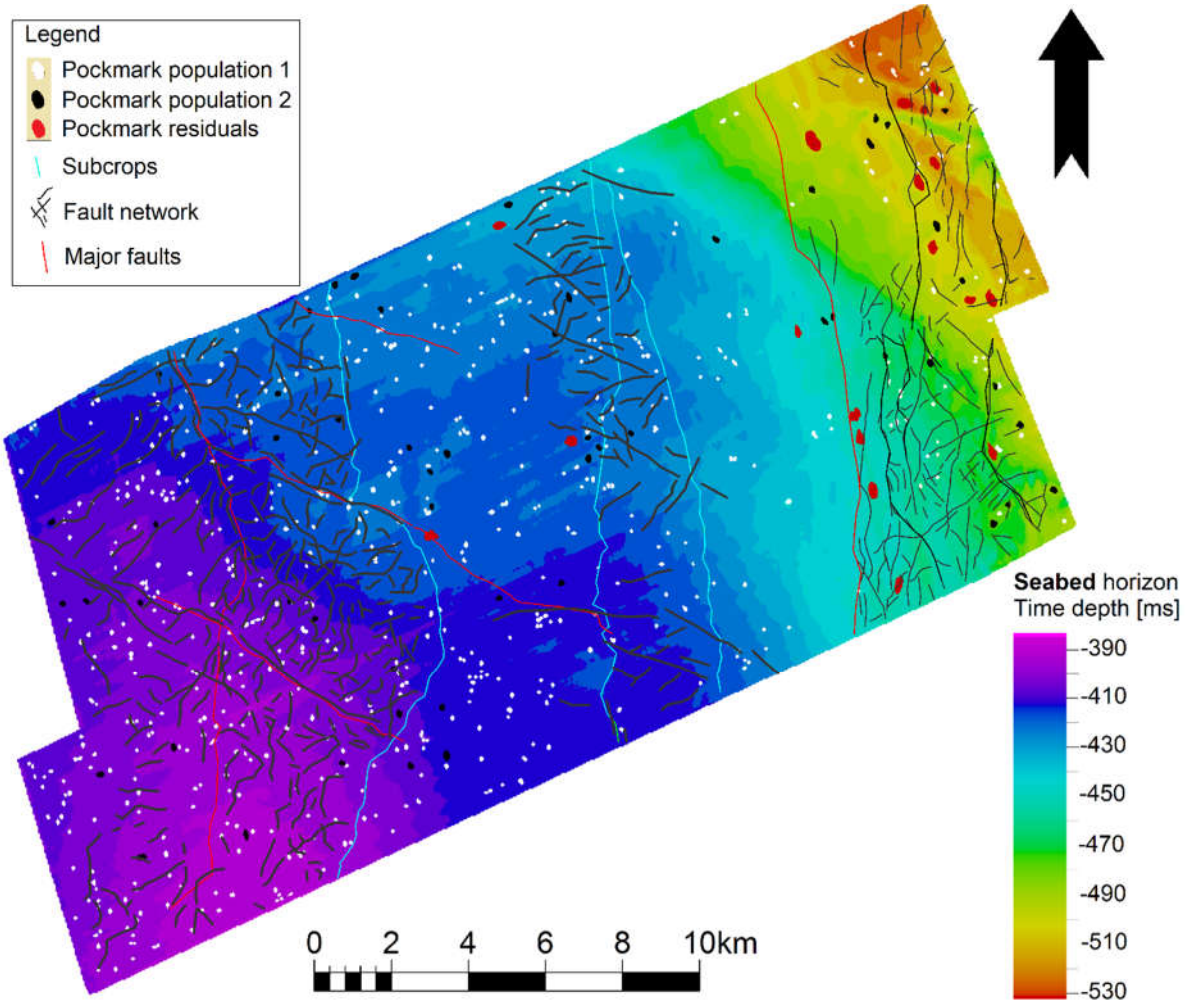

Figure 4.10: Time structure map of the Seabed horizon with pockmark populations.

4.2.3 Pockmark and isochron maps

4.2.3.1 Isochron map between the Q3.2 URU and Draupne Formation horizon

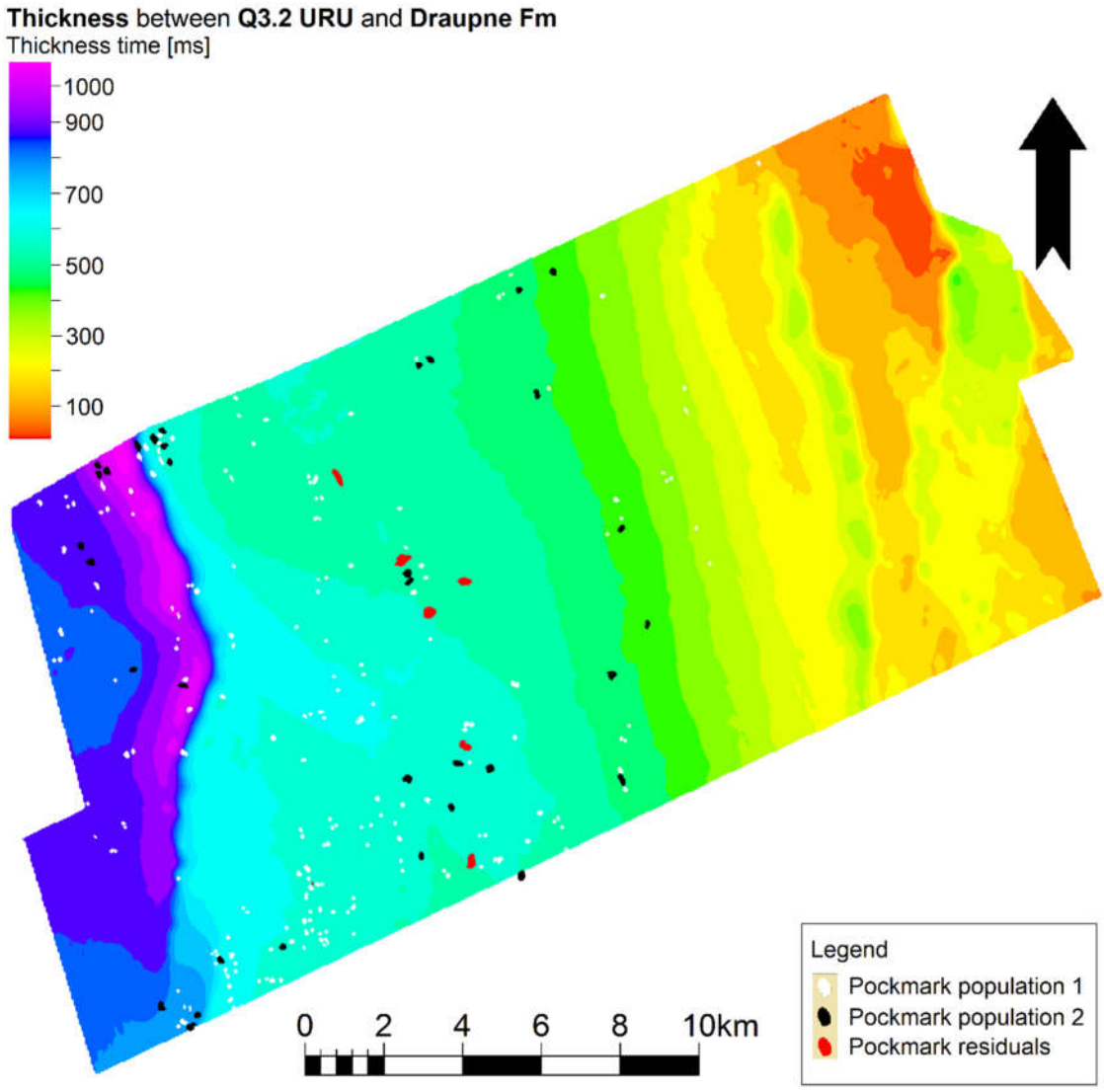

Figure 4.11: Isochron thickness between the Q3.2 URU and Draupne Fm horizons. Pockmarks from the Q3.2 URU horizon have been superimposed.

Figure 4.11 shows the thickness of the sedimentary overburden above the potential Jurassic CO_2 storage foramtion (Sogneford Fm) and seal (Draupne Fm) without the Quaternary interval. The thickness decreases towards the northeast,

The horizon of Draupne Fm used for this map is seismic work from Jonassen (2015) master thesis.

4.2.3.2 Isochron map between the Q3.1 and Q3.2 URU horizons

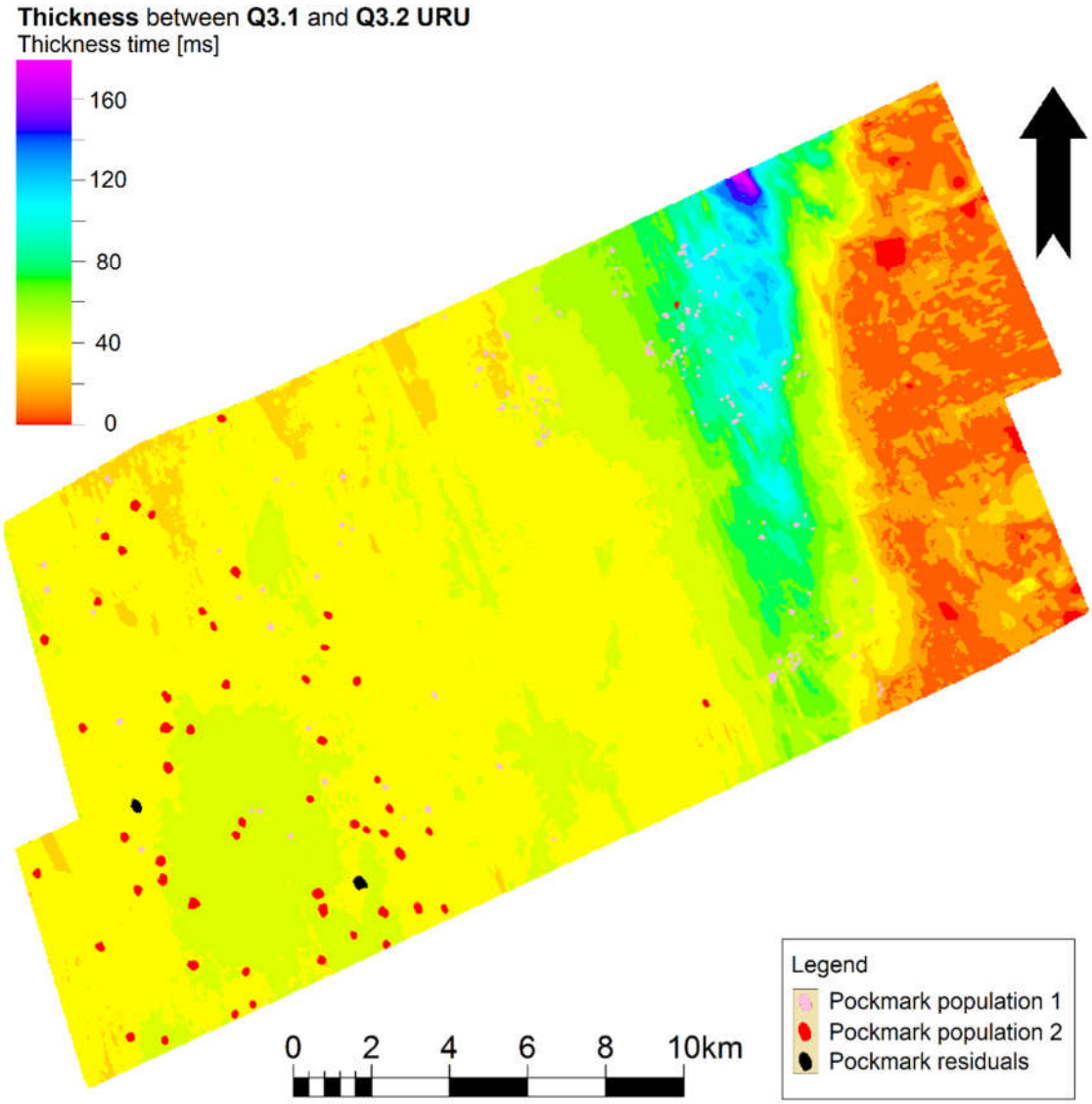

Figure 4.12: Isochron thickness between Q3.1 and Q3.2 URU horizons. Pockmarks from the Q3.1 URU horizon have been superimposed.

The isochron map in Figure 4.12 shows an average thickness of approximately 40 ms between the Q3.1 and Q3.2 horizons, while the eroded areas along the ganging wall of the ØFC have an infill thickness of approximately 80 to 100 ms.

4.2.3.3 Isochron map between the Q2.1 and Q3.1 horizons

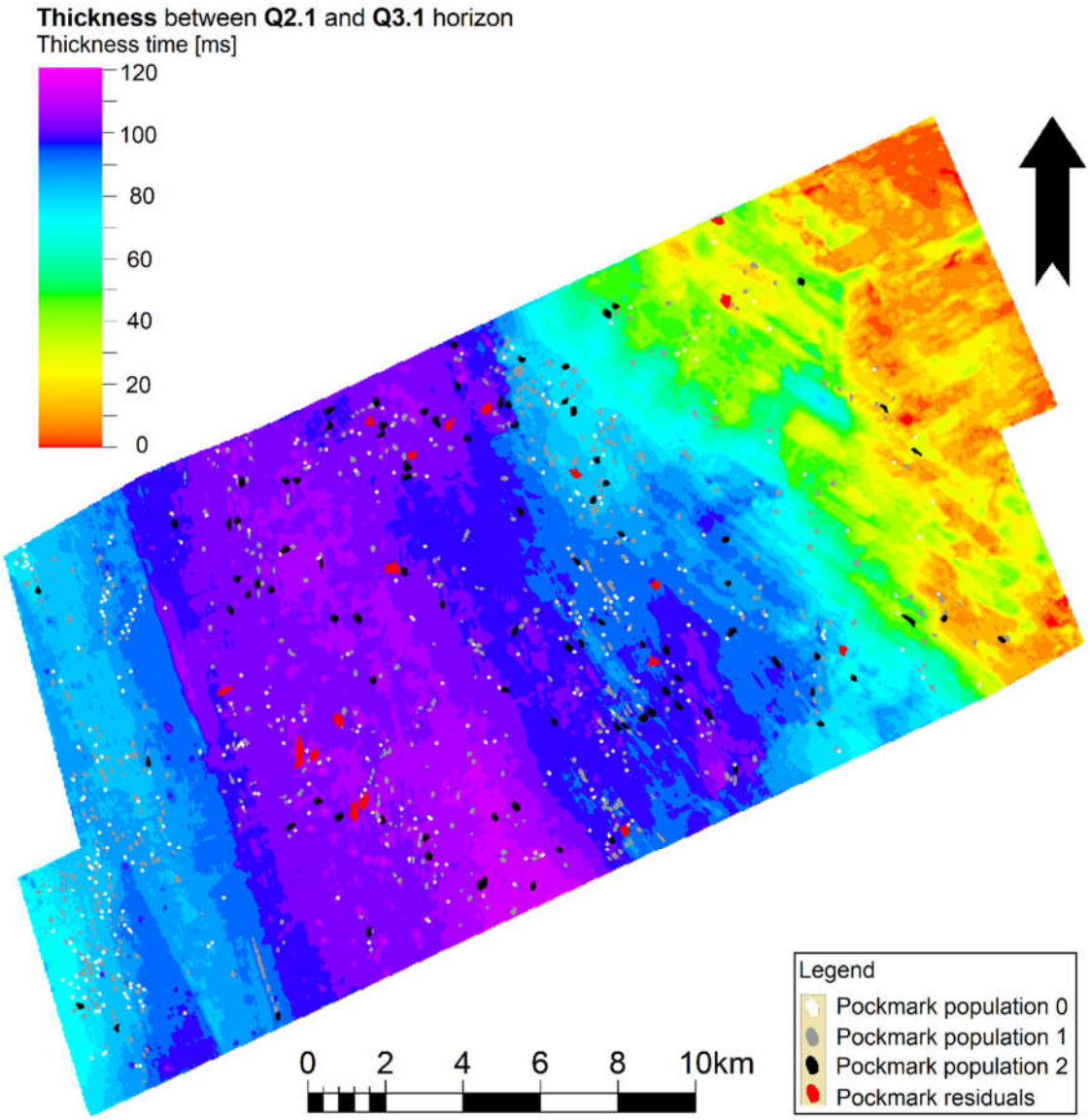

Figure 4.13: Isochron thickness between the Q2.1 and Q3.1 horizons. Pockmarks from the Q2.1 horizon have been superimposed.

The thickness map in Figure 4.13 shows sedimentary package Q1.2 with onlapping the Q2.1 horizon to the east. The thickest area lies further west towards the footwall of the VFZ, and is slightly thicke to the south.

4.2.3.4 Isochron map between the Q1.2 and Q2.1 horizons

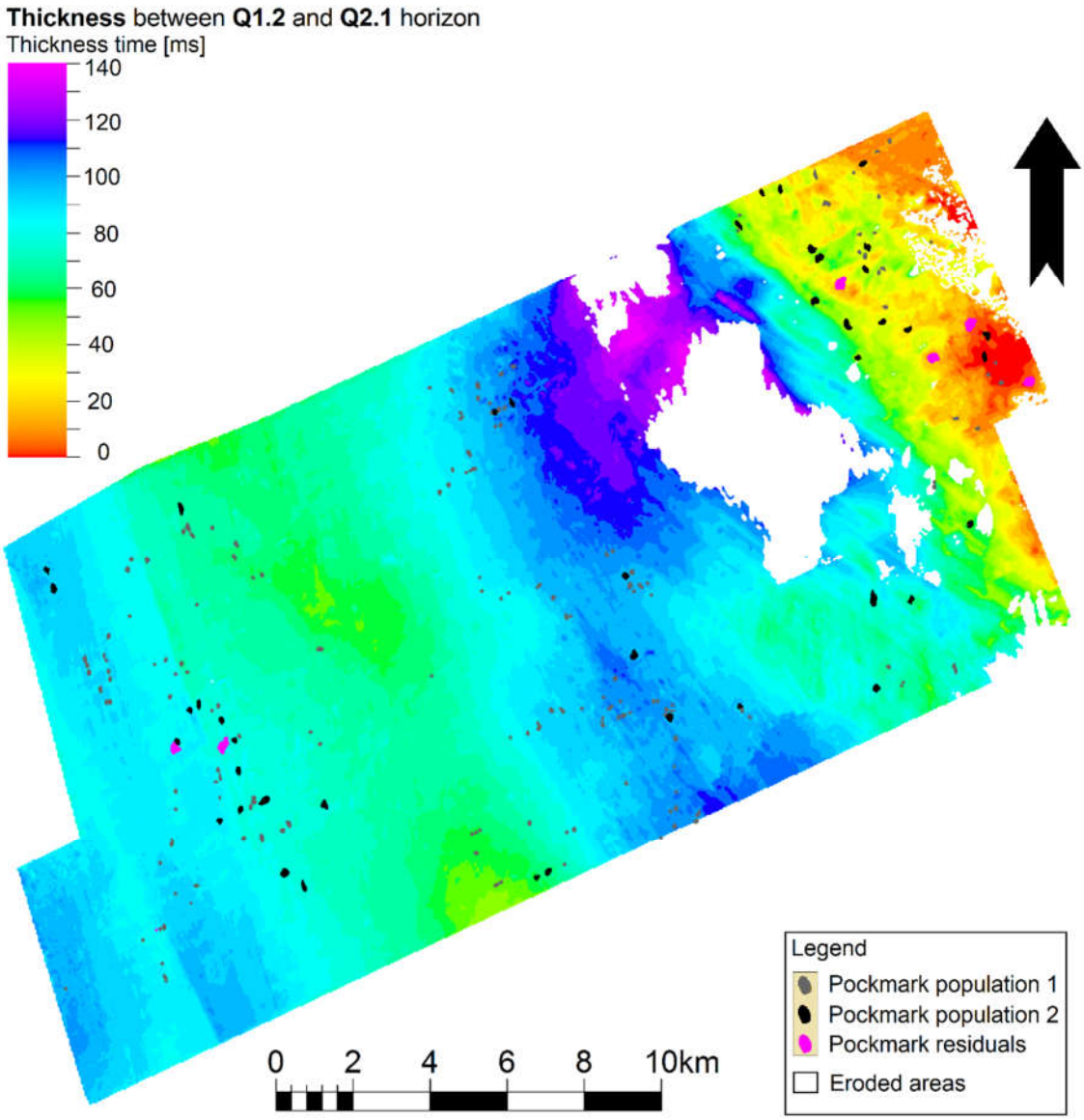

Figure 4.14: Isochron thickness between the Q1.2 and Q2.1 horizons. Pockmarks from the Q1.2 horizon have been superimposed.

The thickness between Q1.2 and Q2.1 in Figure 4.14 is 70 to 80 ms, on average. Maximum thickness 120 to 140 ms is observed east of the eroded areas in the eastern part of the survey.

4.2.3.5 Isochron map between the Q1.1 and Q1.2 horizons

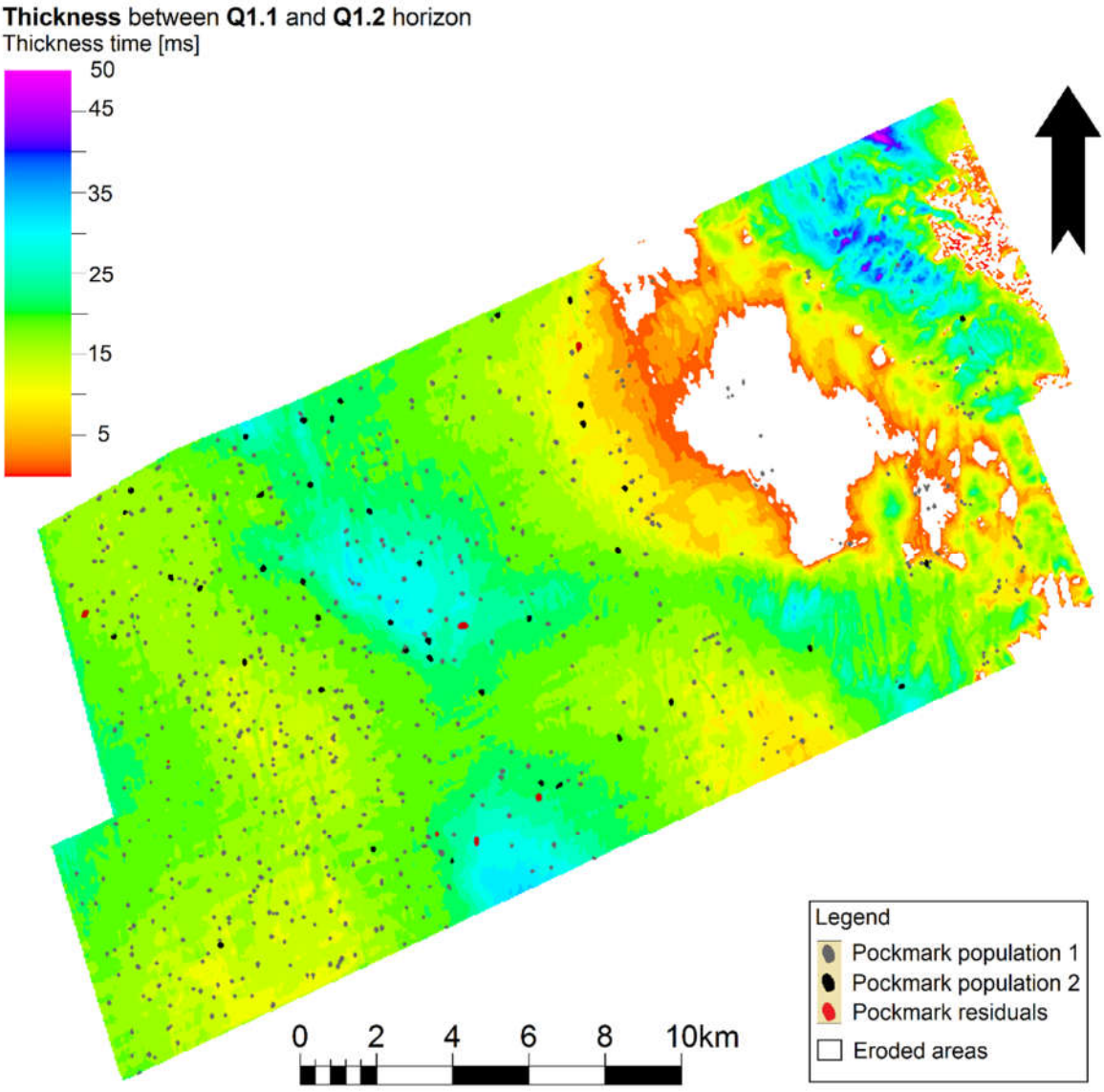

Figure 4.15: Isochron thickness between the Q1.1 and Q1.2 horizons. Pockmarks from the Q1.1 horizon have been superimposed.

The isochron map in Figure 4.15 indicates an average thickness of approximately 15 ms for the Q1.1 package.

4.2.3.6 Isochron map between the Seabed and Q1.1 horizons

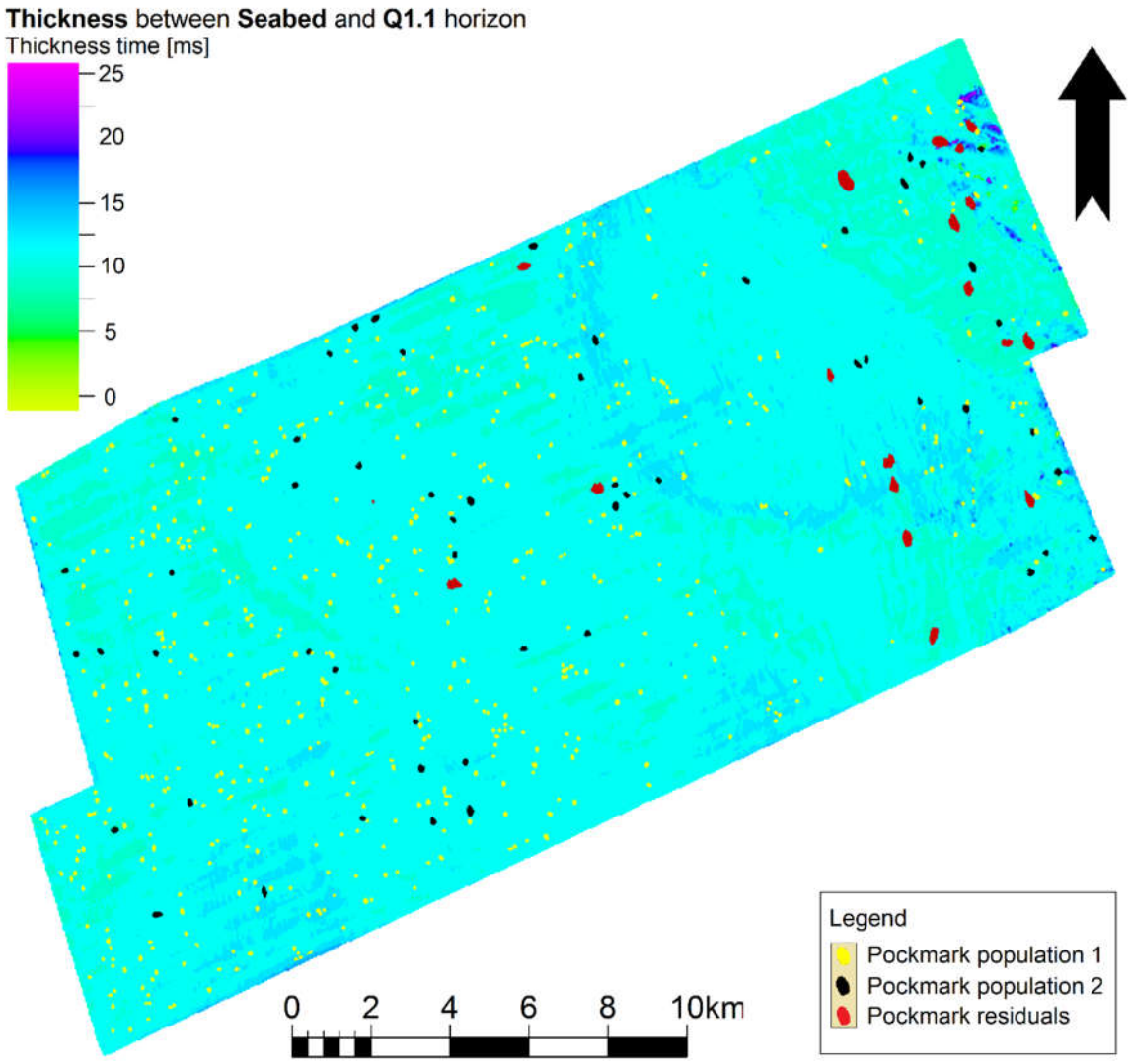

Figure 4.16: Isochron thickness between the Seabed and Q1.1 horizons. Pockmarks from the Seabed horizon has been superimposed.

Figure 4.16 shows the time thickness of the youngest sedimentary unit within the study area.

The average thickness of the interval is approximately 12.5 ms.

4.3 Pockmark distributions and statistics

4.3.1 Pockmark cluster analysis

The reason to only use the Seabed and Q1.1 horizons for cluster analyses is that they present pockmark information for the whole survey area, while other horizons lack information in the eroded eras and the ØFC footwall. Previously studies have conducted such analyses only on the seabed surface.

4.3.1.1 Average nearest neighbour analysis

The results of the average nearest neighbour (ANN) analysis in Table 4.1 show observed mean distance to nearest neighbour points and the expected mean distance. Observed distances shorter than an expected CSR pattern is clustered and, conversely, dispersed if the observed distance is longer. Both horizons possess clustered pockmark point patterns.

Table 4.1: ANN analysis results of Seabed and Q1.1 horizon. Observed distances shorter than an expected CSR pattern are considered clustered and dispersed if the observed distance is longer.

ANN results	***Observed distance***	***Expected distance***	***Pattern***
Seabed horizon 1st nearest	317,36 m	383,35 m	Clustered
Seabed horizon 2st nearest	516,94 m	602,48 m	Clustered
Q1.1 horizon 1st nearest	335,79 m	396,33 m	Clustered
Q1.1 horizon 2st nearest	517,60 m	614,02 m	Clustered

4.3.1.2 K-function and L-function analyses of the Seabed and Q1.1 horizons

Results from the K-function and L-function analysis can be seen in Appendix 5. A field of randomly distributed pockmarks at Smeaheia generated for the calculation of expected point distance in a random pattern is also moved to Appendix 5. Both analyses show the Seabed, and the Q1.1 horizon point distribution as clustered. There is slightly more clustering in the Q1.1 horizon than the Seabed horizon. The result with the L-function has a border edge correction method (L_boarder). This calculation shows that the pattern becomes random and possibly turns to a dispersed pattern after point distances over 6 km (Figure 6.2). This type of result suggests the points patterns cluster and can affect each other within an approximately 6 km radius.

4.3.2 Pockmark quadrat count and intensity maps

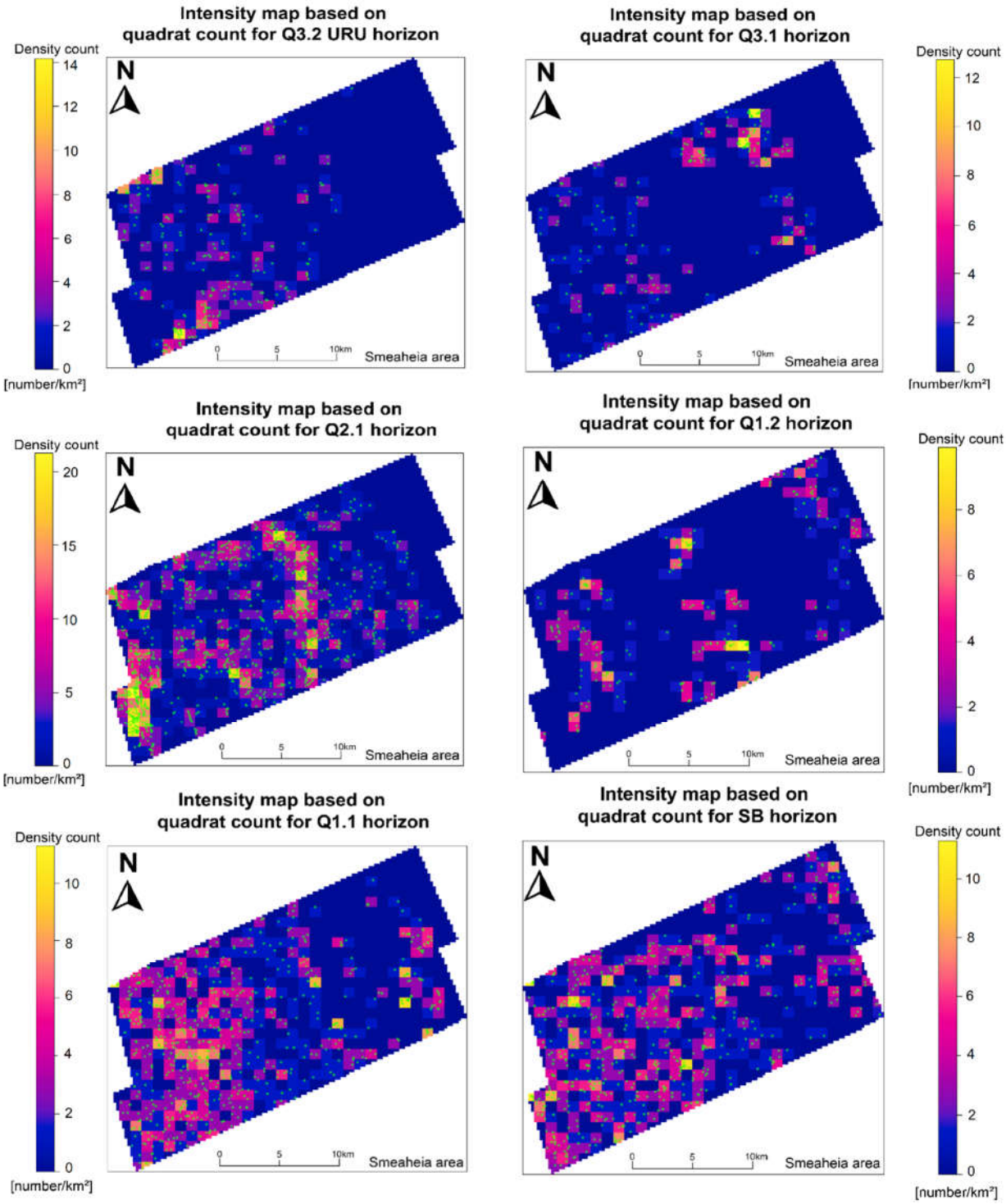

Figure 4.17: Intensity maps for all pockmark mapped horizons. Density is counted for each quadrat of approximately one square kilometre. Green dots indicate pockmark positions.

The intensity maps are the basis for the kernel density maps in the next subsection.

4.3.3 Pockmark kernel density maps

These maps use the same density count from quadrat count, but the count is spread over a normal distribution, and contour lines added. All kernel density maps are presented with sigma equal 0.5 for better visualisation of clusters. A sigma equal to 1 is one standard deviation from the mean.

4.3.3.1 Kernel density for horizon the Q3.2 URU

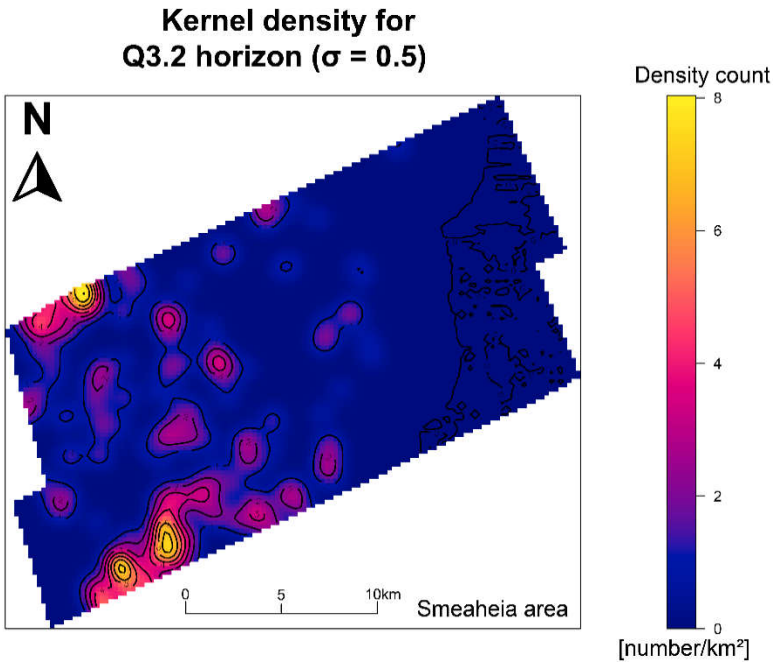

Figure 4.18: Kernel density map for the Q3.2 URU horizon.

Figure 4.18 shows clustering in the southwest and northwest of the Q3.2 horizon.

4.3.3.2 Kernel density for horizon the Q3.1

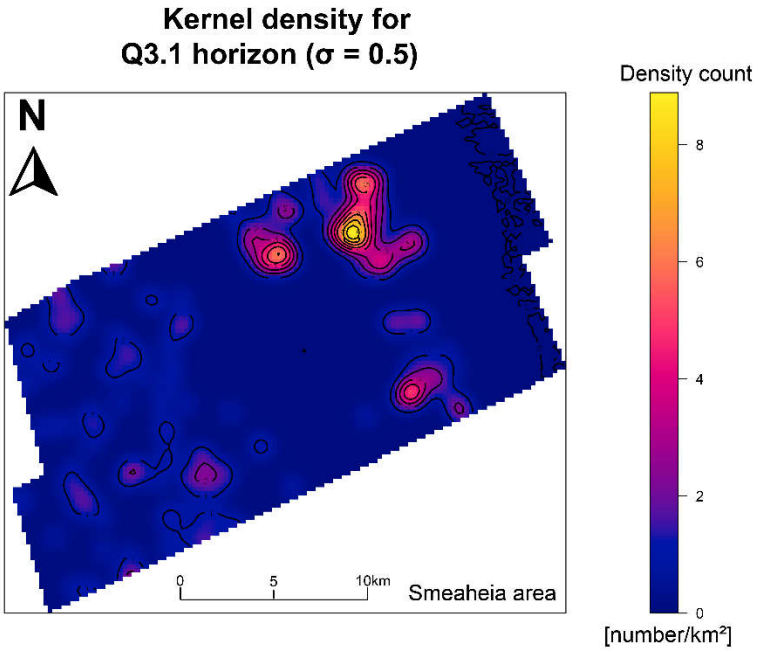

Figure 4.19: Kernel-density map for the Q3.1 horizon.

Cluster patterns in Figure 4.19 show densities in the eroded areas of the Q3.1 horizon. Larger significant pockmarks to the west have lower density count

4.3.3.3 Kernel density for horizon the Q2.1

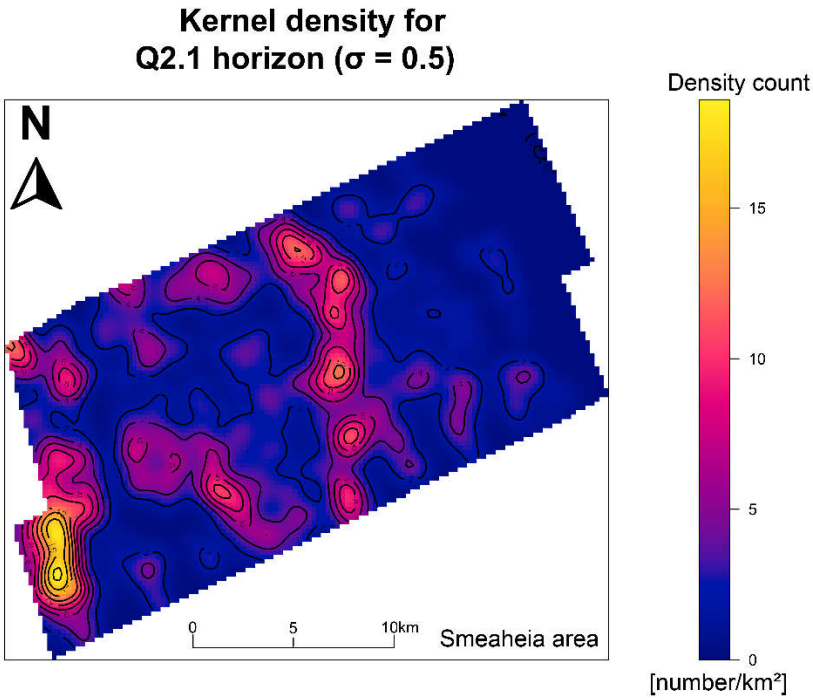

Figure 4.20: Kernel-density map for the Q2.1 horizon.

Cluster patterns in for the Q2.1 horizon (Figure 4.20) show densities along the subcrop of the Top Shetland Group boundary, and in the polygon fault area. There is a high-count cluster down the southwest.

4.3.3.4 Kernel density for horizon the Q1.1

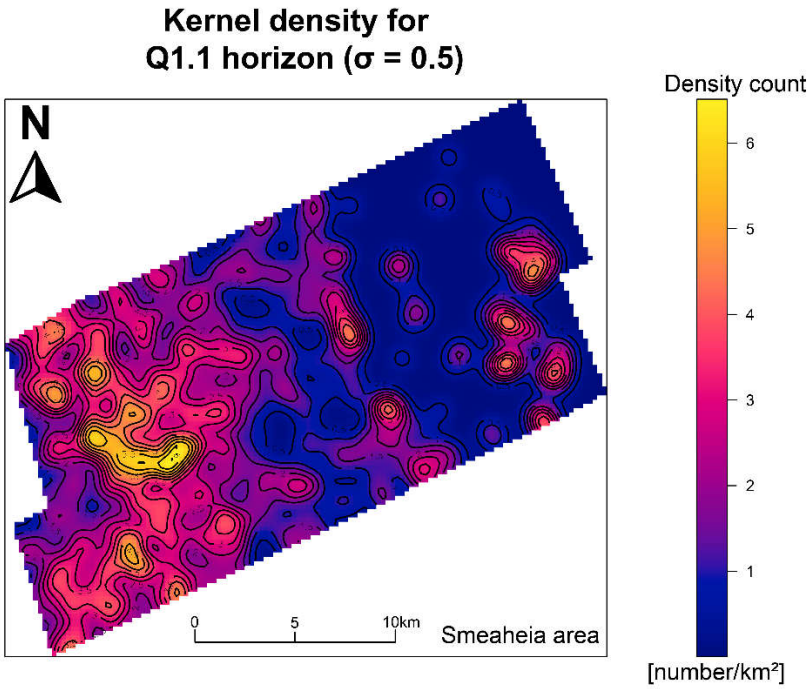

Figure 4.21: Kernel density map for the Q1.1 horizon.

The Q1.2 horizon is not presented as it is partly eroded. Cluster patterns on the Q1.1 horizon indicate a vast variety of density high (Figure 4.21). The significant highs are located over the polygonally faulted area, over the area around fault FW_03, but also over the subcrop of the Top Shetland Group horizon. On the ØFC footwall, densities are found approximately over the faults ØFC FW_A1 and ØFC FW_B (see Figure 4.3).

4.3.3.5 Kernel density for horizon the Seabed

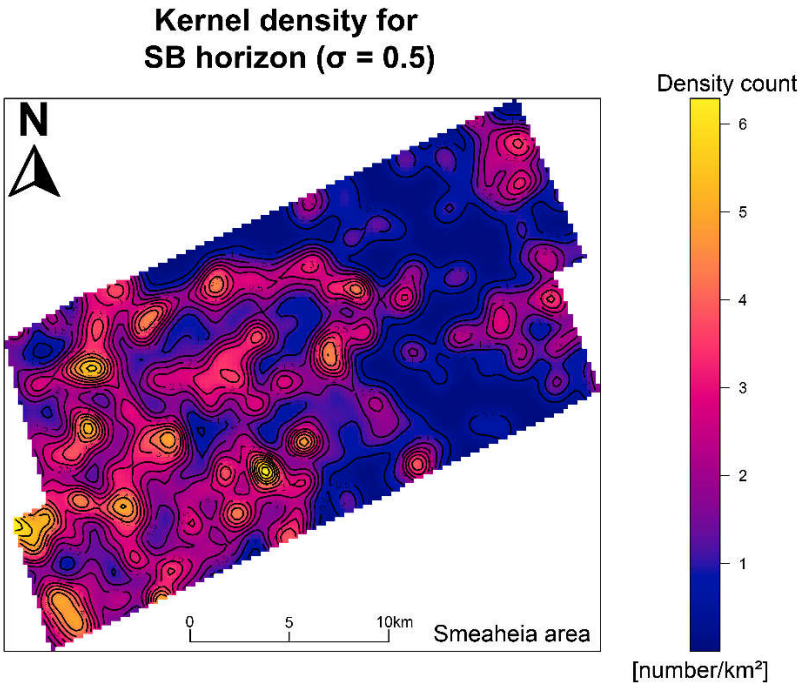

Figure 4.22: Kernel density map for the Seabed horizon.

Pockmark densities along the Seabed horizon in Figure 4.22 illustrates high concentrations over the polygonally faulted area, the subcrop of Top Shetland Group boundary, and three FW_17 faults (17N, 17C and 17 S). Higher densities are observed in the southwest corner of the GN1101 survey. On the ØFC footwall, densities are concentrated over faults ØFC FW_A1 and FW_ A2, and along ØFC FW_B.

4.3.4 Pockmark shapes in 3D seismic

The pockmark shapes are categorized based on terminology used by Judd & Hovland (2007), and the shape of the pockmarks found on the seabed and buried Quaternary horizons are depicted in Figure 4.23. The shapes vary from being symmetrical, to asymmetrical, having minor geometry irregularities.

Pockmark facies

Pockmark facies are categorized as follows:

Pockmarks with elongated shapes are marked with the letter **E** in pockmark tables (see Appendix 1). Elongated pockmarks have one wider side and a narrow tail on the opposite side in the map view, and are the most common pockmark facies.

Pockmark with an elliptical shape are marked with **EL** in pockmark tables (Appendix 1). They resemble a hull shape of a boat, however, it is difficult to interpret if the shape is more asymmetrical resembling an E shape.

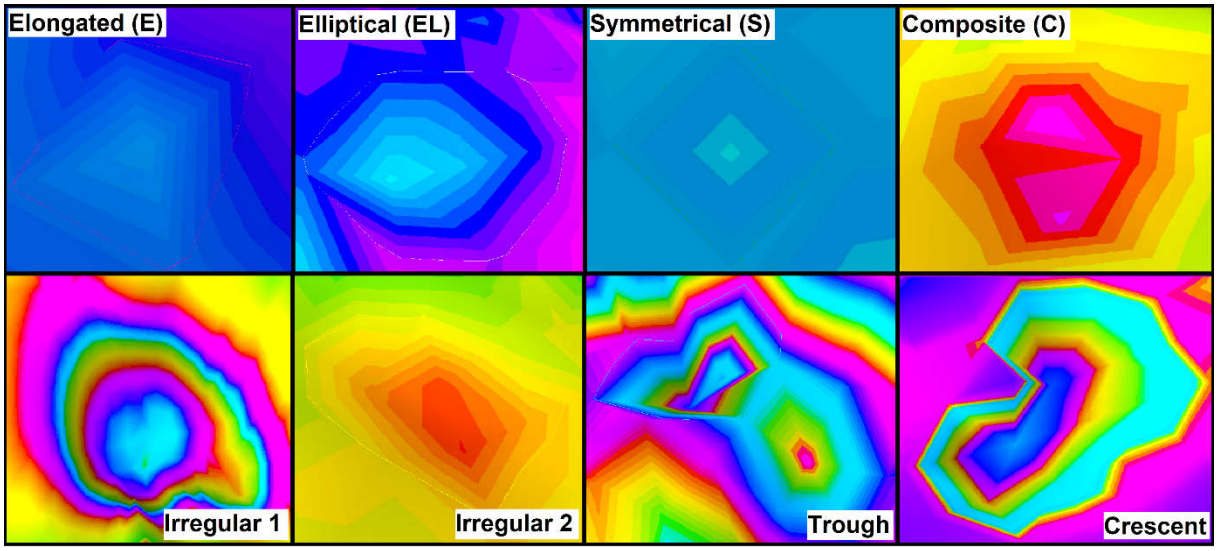

Figure 4.23: Pockmark shapes (facies) as seen in 3D seismic. Most of the smaller and medium-sized pockmarks mapped are (**E**) elongated or the (**EL**) elliptical. Larger pockmarks tend have the irregular 1 **(I1)** and 2 **(I2)** shape**.** The symmetrical (**S**) and composite (**C**) are less common, and the trough (**T**) and crescent (**CR**) shapes are rare.

Interpreted pockmarks with a symmetrical shape are marked with the letter **S** in pockmark tables (Appendix 1). These smaller-sized pockmarks are probably round shaped , but seismic imaging displays them as a nearly perfect square shape due to resolution limits.

The composite pockmark shape is marked with the letter **C** in the pockmarks tables (Appendix 1). These pockmarks appears to be two or more pockmarks amalgamated into a larger pockmark shape.

I1 represents pockmarks with one type of irregular shape (irregular-one). They are generally large round-shaped, and often bowl-shaped pockmarks with no jagged rims — the emerging variations of these types of shapes is the reason to categorise them as irregular.

The irregular-two shape is marked with **I2** in pockmarks tables. These are large pockmarks that do not fit the I1 category. They can resemble the I1 pockmarks sometimes but have jagged edged rims, and often have a longer axis in one direction.

T in the pockmarks tables (Appendix 1) indicates pockmarks with a trough shape and greater pockmark depth than most other shapes.

Pockmarks with crescent shapes are marked with **CR** in pockmarks tables. These are rare and are often located near mounds along the older horizons.

4.3.5 Pockmark statistics

This section presents statistical data, histograms, box plots and rose plots for interpreted pockmarks. In rose plots, the count number is on the x-axis, and all plots have a bin size of 10. Global pockmarks densities are calculated based on the seismic survey area of 394 km²

The first histograms plots of width and surface area of the pockmark data showed data with apparent outliers, including signs of bimodality. Outlier analysis is used as a tool in the statistical analysis of data, but the initiation of proceeding with outlier detection came from the assumption that pockmarks size is normal distributed. Thus, outliers had to be removed as they affect the mean, standard deviation and the whole distribution of the pockmark samples. In the process of detecting statistical outliers in the pockmarks data, outliers were gathered and kept for retesting. Such data selection separated the primary data into two different normal distributed populations, while the remaining pockmarks were gathered as residuals instead of discarding them. Residuals pockmarks do not comply with the central limit theorem to be treated as normally distributed.

4.3.5.1 Statistics for Q3.2 URU horizon pockmarks

Table 4.2: Descriptive statistics for pockmarks on the Q3.2 URU horizon. Presented are the quartiles with mean and standard deviation data. Measured parameter is width (m).

Width	***Min.***	***1st Qu.***	***Median***	***Mean***	***3rd Qu.***	***Max.***	***Stand.dev***	***N***
Population 1	35,0	68,0	74,0	79,8	92,0	126,0	17,0	205
Population 2	114,0	127,5	147,0	148,7	161,0	209,0	25,7	34
Residuals	30,0	171,0	197,0	187,3	233,0	276,0		7

Table 4.3: Descriptive statistics for pockmarks on the Q3.2 URU horizon. Presented are the quartiles with mean and standard deviation data. Measured parameter is surface area (m²).

Area	***Min.***	***1st Qu.***	***Median***	***Mean***	***3rd Qu.***	***Max.***	***Stand.dev***	***N***
Population 1	3525	5464	7285	9248	12684	23023	4456	205
Population 2	23573	26232	28891	32661	38964	47487	7890	34
Residuals	1867	64802	69515	69437	84199	116677		7

Table 4.4: Statistics of pockmark shapes on the Q3.2 URU horizon. Names of the shape have been abbreviated to fit the table. They follow the names presented in Figure 4.23. E is elongated, EL is elliptical, T is for trough like, CR is for crescent, C is for composite, S is for symmetrical, I1 is for irregular one, and I2 is for irregular 2.

Shapes	**E (%)**	**EL (%)**	**T (%)**	**CR (%)**	**C (%)**	**S (%)**	**I1 (%)**	**I2 (%)**
Population 1	69,8	10,7	8,3		0,5	7,3	2,4	1,0
Population 2	23,5	17,6	14,7	2,9	2,9		23,5	14,7
Residuals	14,3	14,3	14,3				42,9	14,3

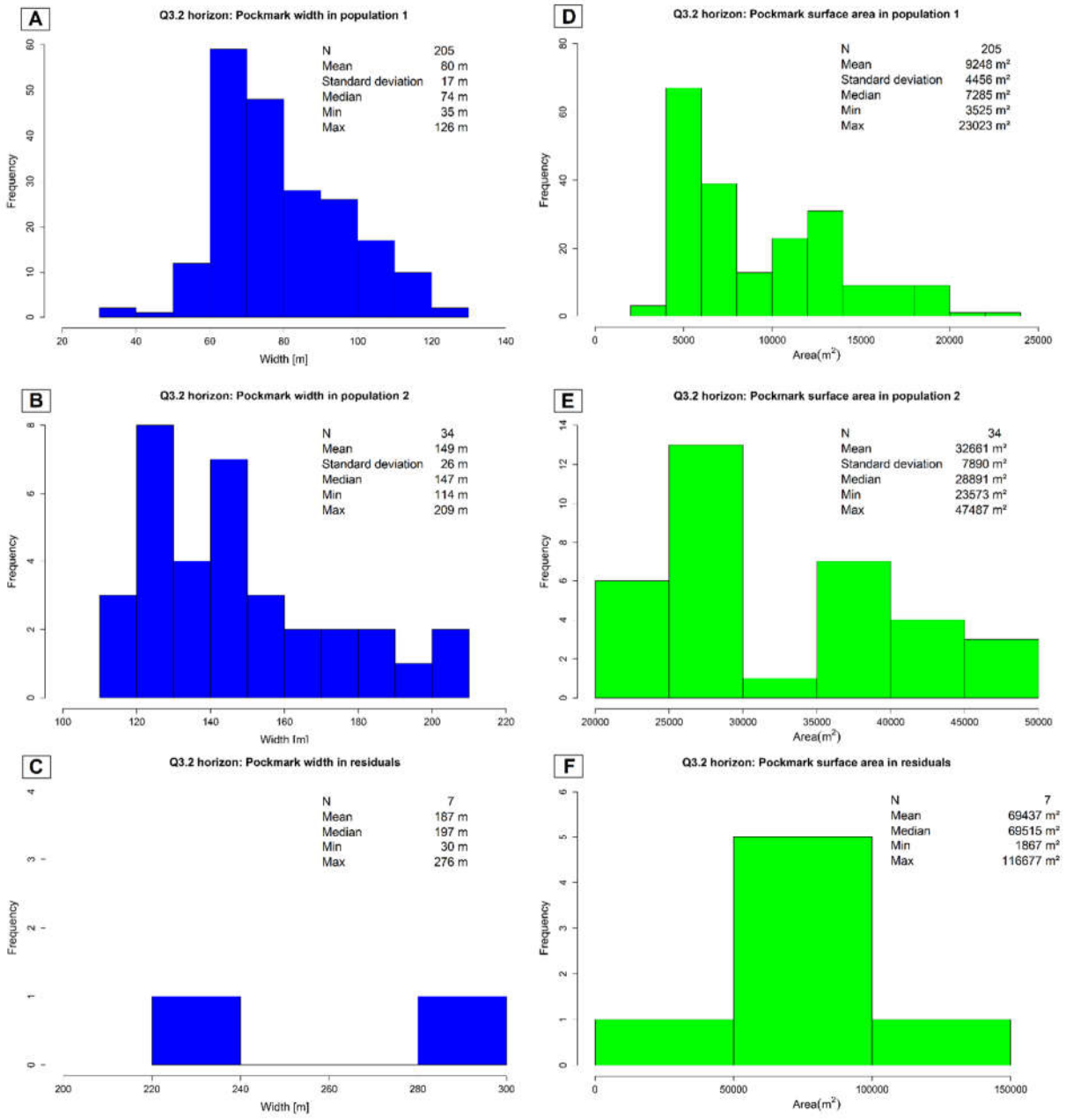

Figure 4.24: Histogram for the Q3.2 horizon. The blue graph shows the parameter width, and green is the surface area data.

Key statistics to notice for the Q3.2 horizon

Population 1 has a mean of 79.8 m in width and 9248 m² in surface area, and most pockmarks are elongate (E) shaped.

Population 2 has a mean of 148.7 m in width and 32661 m² in surface area, and most pockmarks are elongate (E), and irregular-one (I1) shaped.

The residual pockmark are few but has a mean of 187.3 m in width and 69437 m² in surface area, and most pockmarks are irregular-one (I1) shaped.

Q3.2 URU has a total of 246 pockmarks mapped and a global pockmark density of ~ 0.62 pockmarks per km².

4.3.5.1.1 Rose plot for pockmark directions

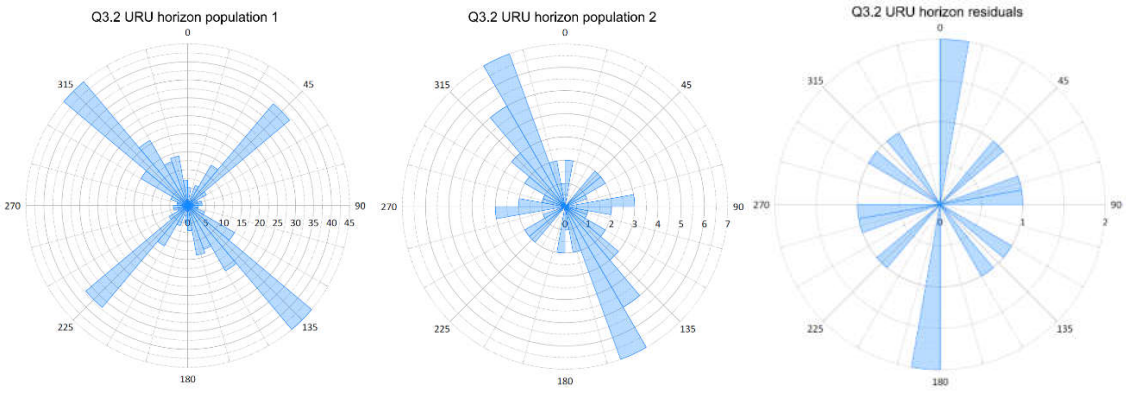

Figure 4.25: Rose plots of populations 1 and 2, and residuals on the Q3.2 URU horizon.

The rose plots in Figure 4.25 show dominant pockmark directions for different groups on Q3.2 URU horizon.

Population 1: NW-SE and NE-SW.

Population 2: NNW-SSE

Residual group: N-S

4.3.5.2 Statistics for Q3.1 horizon pockmarks

Table 4.5: Descriptive statistics for pockmarks on the Q3.1 horizon. Presented are the quartiles with mean and standard deviation data. Measured parameter is width (m).

Width	***Min.***	***1st Qu.***	***Median***	***Mean***	***3rd Qu.***	***Max.***	***Stand.dev***	***N***
Population 1	29,0	69,0	71,0	81,1	98,5	138,0	22,1	155
Population 2	135,0	168,0	193,0	191,1	211,0	275,0	33,7	55
Residuals	235,0	246,8	258,5	258,5	270,2	282,0		2

Table 4.6: Descriptive statistics for pockmarks on the Q3.1 horizon. Presented are the quartiles with mean and standard deviation data. Measured parameter is surface area (m²).

Area	***Min.***	***1st Qu.***	***Median***	***Mean***	***3rd Qu.***	***Max.***	***Stand.dev***	***N***
Population 1	1128	4979	7241	9457	13343	24715	5588	155
Population 2	25448	35701	46883	48403	58244	90462	15189	55
Residuals	94106	97864	101623	101623	105381	109139		2

Table 4.7: Statistics of pockmark shapes on the Q3.1 horizon. They follow the names presented in Figure 4.23. E is elongated, EL is elliptical, S is for symmetrical, I1 is for irregular one, and I2 is for irregular 2.

Shapes	**E (%)**	**EL (%)**	**S (%)**	**I1 (%)**	**I2 (%)**
Population 1	80,0	9,0	3,9	4,5	1,3
Population 2	3,6	21,8		70,9	3,6
Residuals		50,0		50,0	

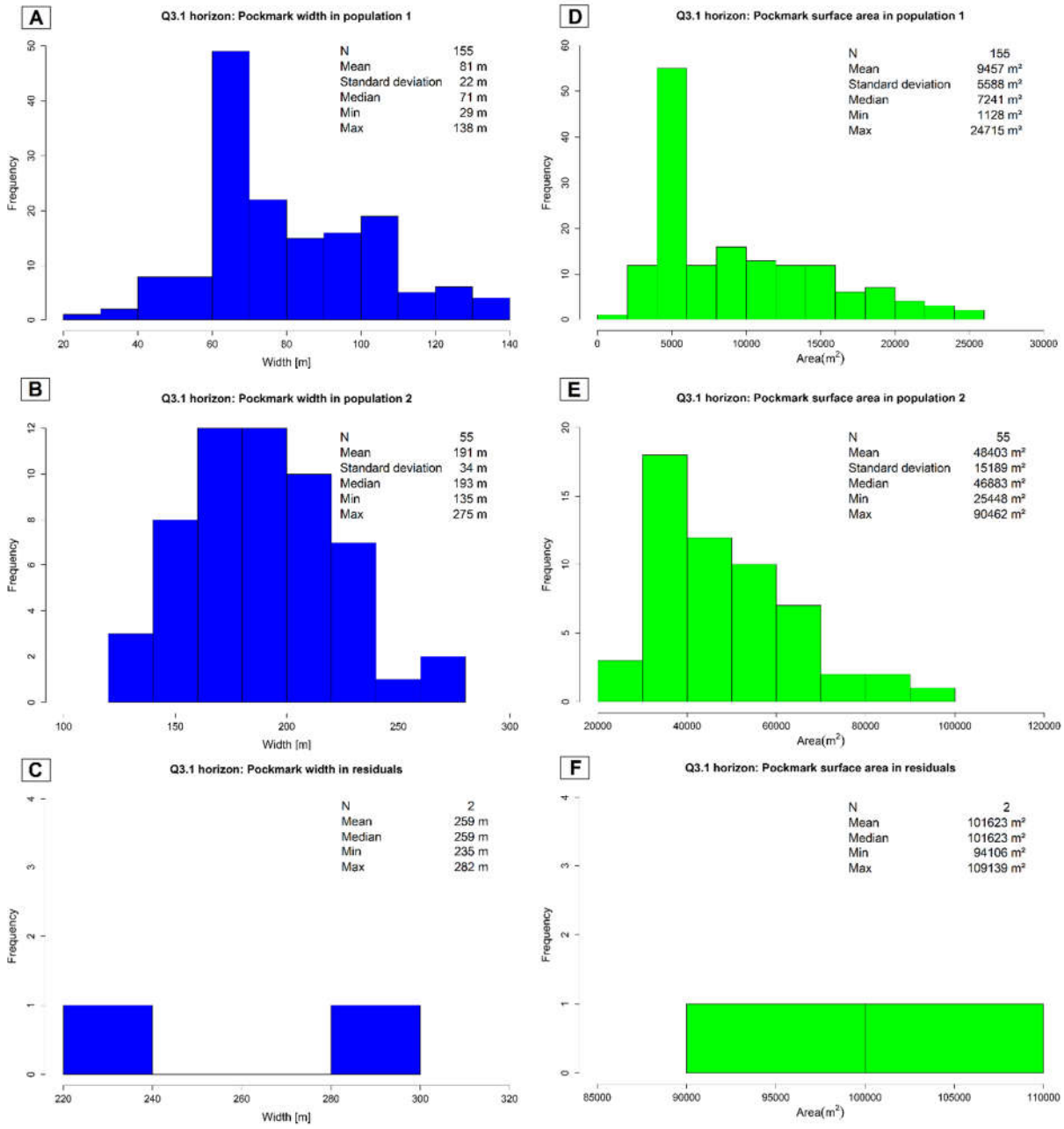

Figure 4.26: Histogram for the Q3.1 horizon. The blue graph shows the parameter width, and green is the surface area data.

Key statistics for the Q3.1 horizon

Population 1 has a mean of 81.1 m in width and 9457 m² in surface area, and most pockmarks are elongated (E).

Population 2 has a mean of 191.1 m in width and 48403 m² in surface area, and most pockmarks are irregular-one (I1) shaped.

There are only two pockmarks in residual group. They have a mean of 258.5 m in width and 101623 m² in surface area, and the pockmarks are irregular-one (I1) and elliptical (EL) shaped.

Q3.1 has a total of 212 pockmarks mapped and a global pockmark density of ~ 0.54 pockmarks per km².

4.3.5.2.1 Rose plot for pockmark directions

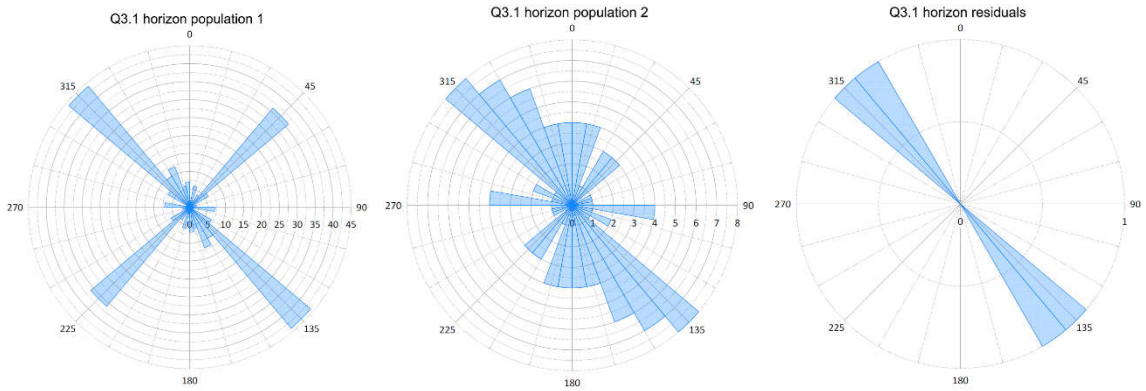

Figure 4.27: Rose plots of populations 1 and 2, and residuals on the Q3.1 horizon.

The rose plots in Figure 4.27 show dominant pockmark directions for different groups on Q3.1 horizon.

Population 1: NW-SE and NE-SW.

Population 2: NW-SE

Residual group: NW-SE

4.3.5.3 Statistics for Q2.1 horizon pockmarks

Table 4.8: Descriptive statistics for pockmarks at on the Q2.1 horizon. Presented are the quartiles with mean and standard deviation data. Measured parameter is width (m).

Width	***Min.***	***1st Qu.***	***Median***	***Mean***	***3rd Qu.***	***Max.***	***Stand.dev***	***N***
Population 0	64,0	68,0	70,0	69,4	71,0	75,0	2,3	342
Population 1	18,0	59,0	76,0	75,6	92,0	138,0	22,7	679
Population 2	89,0	124,8	141,0	140,4	155,0	193,0	22,1	96
Residuals	153,0	200,5	212,0	220,1	231,8	305,0		18

Table 4.9: Descriptive statistics for pockmarks on the Q2.1 horizon. Presented are the quartiles with mean and standard deviation data. Measured parameter is surface area (m²).

Area	***Min.***	***1st Qu.***	***Median***	***Mean***	***3rd Qu.***	***Max.***	***Stand.dev***	***N***
Population 0	4066	4578	4829	4800	4972	5599	319	342
Population 1	378	3733	6506	6882	9230	17130	3754	679
Population 2	14656	19257	21260	23284	26653	36146	5507	96
Residuals	36073	39528	43922	54019	61932	115896		18

Table 4.10: Statistics of pockmark shapes on the Q2.1 horizon. Names of the shape have been abbreviated to fit the table. They follow the names presented in Figure 4.23. E is elongated, EL is elliptical, CR is for crescent, T is for trough like, C is for composite, S is for symmetrical, I1 is for irregular one, and I2 is for irregular 2.

Shapes	**E (%)**	**EL (%)**	**CR (%)**	**T (%)**	**C (%)**	**S (%)**	**I1 (%)**	**I2 (%)**
Population 0	88,9	1,8				8,8	0,6	
Population 1	72,3	17,7	0,1	1,8	0,3	0,4	4,1	3,2
Population 2	14,6	28,1	2,1	7,3	2,1		27,1	18,8
Residuals	5,6	11,1					33,3	50,0

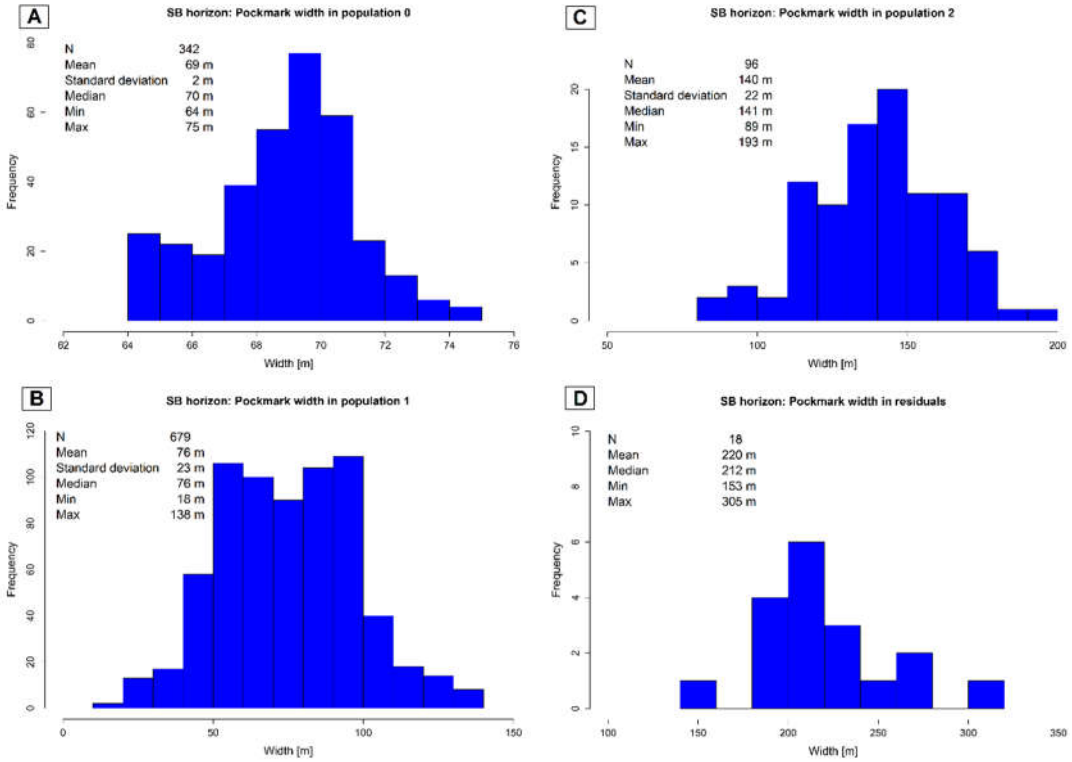

Figure 4.28: Histogram for the Q2.1 horizon. The graph shows the parameter width (m).

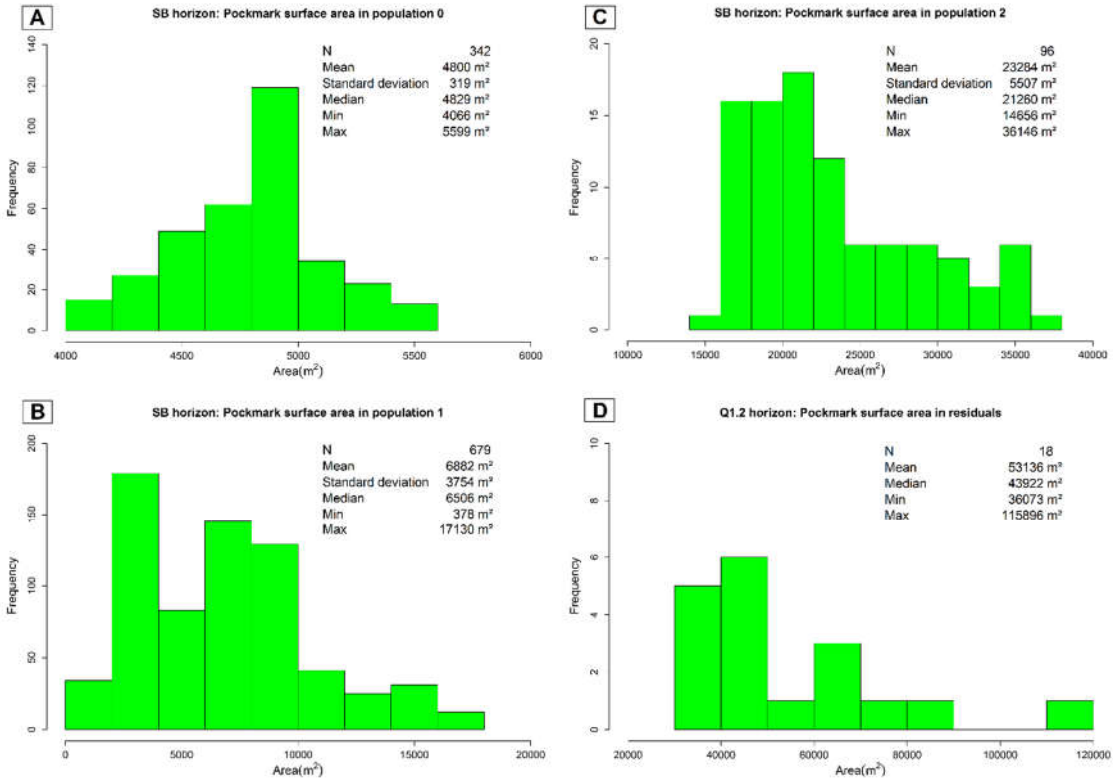

Figure 4.29: Histogram for the Q2.1 horizon. The green graph shows the parameter surface area (m²).

Key statistics for the Q2.1 horizon

Population 0 has a mean of 69.4 m in width and 4800m² in surface area, and most pockmarks are elongate (E) shaped.

Population 1 has a mean of 75.6 m in width and 6882 m² in surface area, and most pockmarks are elongate (E) shaped.

Population 2 has a mean of 140.4 m in width and 23284 m² in surface area, and most pockmarks are elliptical (EL) and irregular-one (I1) shaped.

The residual group are few but has a mean of 220.1 m in width and 54019 m² in surface area, and the pockmarks are irregular-one (I1) and irregular-two (I2) shaped.

Q2.1 has a total of 1135 pockmarks mapped and a global pockmark density of ~ 2.88 pockmarks per km².

4.3.5.3.1 Rose plot for pockmark directions

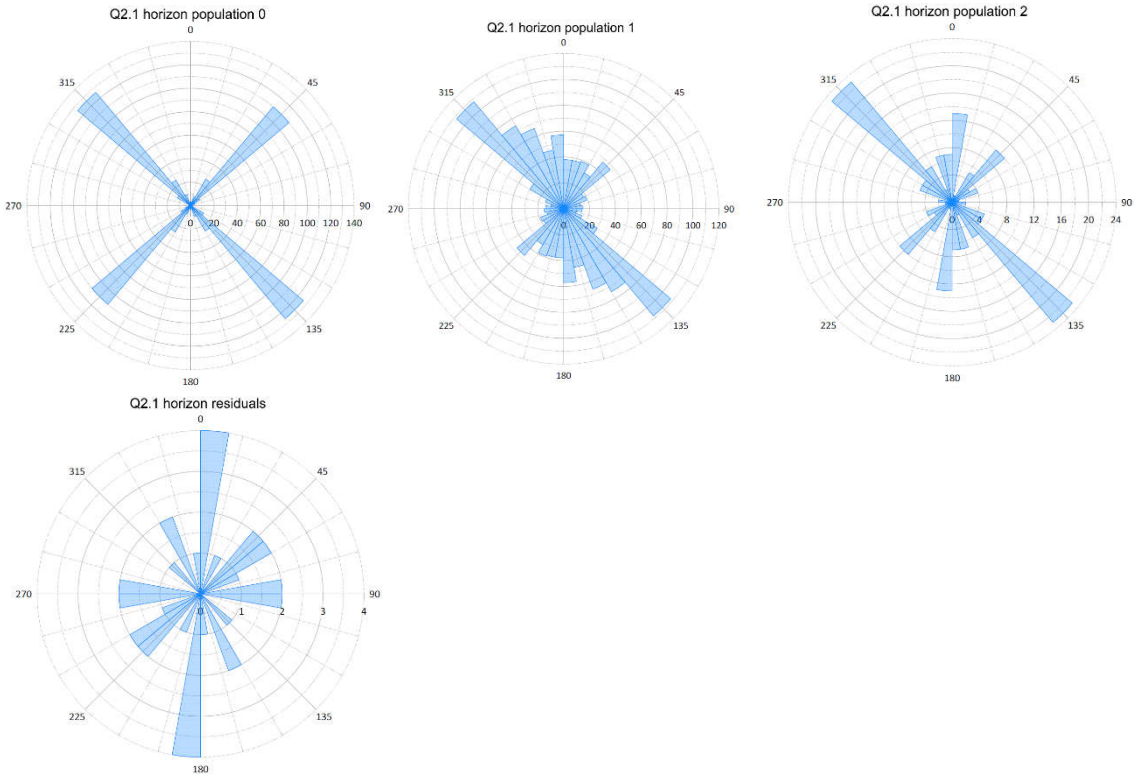

Figure 4.30: Rose plots of populations 0, 1 and 2, and residuals on the Q2.1 horizon.

The rose plots in Figure 4.30 show dominant pockmark directions for different groups on Q2.1 horizon.

Population 0: NW-SE and NE-SW.

Population 1: NE-SW.

Population 2: NE-SW.

Residual group: N-S

4.3.5.4 Statistics for Q1.2 horizon pockmarks

Table 4.11: Descriptive statistics for pockmarks on the Q1.2 horizon. Presented are the quartiles with mean and standard deviation data. Measured parameter is width (m).

Width	***Min.***	***1st Qu.***	***Median***	***Mean***	***3rd Qu.***	***Max.***	***Stand.dev***	***N***
Population 1	48,0	69,0	75,0	80,0	91,0	122,0	14,5	184
Population 2	95,0	125,2	134,0	141,9	161,5	191,0	26,5	42
Residuals	42,0	232,5	240,0	214,0	247,0	257,0		

Table 4.12: Descriptive statistics for pockmarks on the Q1.2 horizon. Presented are the quartiles with mean and standard deviation data. Measured parameter is surface area (m²).

Area	***Min.***	***1st Qu.***	***Median***	***Mean***	***3rd Qu.***	***Max.***	***Stand.dev***	***N***
Population 1	2169	4763	6681	7613	9796	17162	3388	184
Population 2	12897	19472	26737	26630	32469	49986	9389	42
Residuals	2642	59642	69406	65665	84163	101705		7

Table 4.13: Statistics of pockmark shapes on the Q1.2 horizon. Names of the shape have been abbreviated to fit the table. They follow the names presented in Figure 4.23. E is elongated, EL is elliptical, T is for trough like, C is for composite, S is for symmetrical, I1 is for irregular one, and I2 is for irregular 2.

Shapes	**E (%)**	**EL (%)**	**T (%)**	**C (%)**	**S (%)**	**I1 (%)**	**I2 (%)**
Population 1	69,8	10,7	8,3	0,5	7,3	2,4	1,0
Population 2	23,5	17,6	14,7	2,9		23,5	14,7
Residuals	14,3	14,3	14,3			42,9	14,3

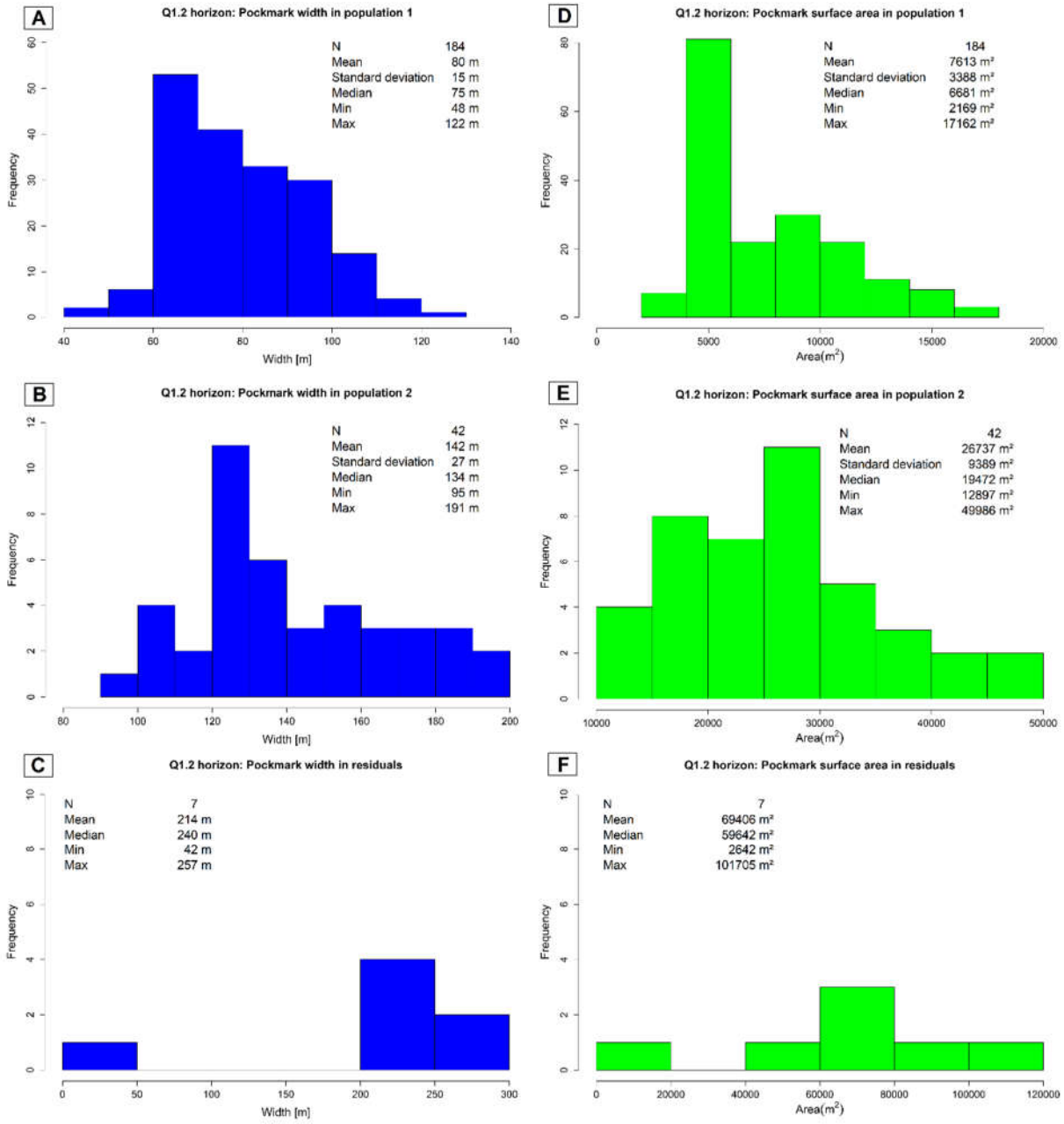

Figure 4.31: Histogram for the Q1.2 horizon. The blue graph shows the parameter width, and green is the surface area data.

Key statistics for the Q1.2 horizon

Population 1 has a mean of 80 m in width and 7613 m² in surface area, and most pockmarks are elongate (E) shaped.

Population 2 has a mean of 141.9 m in width and 26630 m² in surface area, and most pockmarks are elongate (E), and irregular-one (I1) shaped.

The residual group are few but has a mean of 214 m in width and 65665 m² in surface area, and the pockmarks are irregular-one (I1), and irregular-two (I2) shaped.

Q1.2 has a total of 233 pockmarks mapped and a global pockmark density of ~ 0.59 pockmarks per km².

4.3.5.4.1 Rose plot for pockmark directions

Figure 4.32: Rose plots of populations 1 and 2, and residuals on the Q1.2 horizon.

The rose plots in Figure 4.32 show dominant pockmark directions for different groups on Q1.2 horizon.

Population 1: NW-SE and NE-SW.

Population 2: NW-SE and NNW-SSE.

Residual group: NE-SW

4.3.5.5 Statistics for Q1.1 horizon pockmarks

Table 4.14: Descriptive statistics for pockmarks on the Q1.1 horizon. Presented are the quartiles with mean and standard deviation data. Measured parameter is width (m).

Width	***Min.***	***1st Qu.***	***Median***	***Mean***	***3rd Qu.***	***Max.***	***Stand.dev***	***N***
Population 1	40,0	69,0	75,0	79,4	92,0	120,0	14,7	599
Population 2	98,0	110,0	125,0	122,4	133,0	151,0	14,2	43
Residuals	34,0	77,8	124,5	108,8	144,8	165,0		8

Table 4.15: Descriptive statistics for pockmarks on the Q1.1 horizon. Presented are the quartiles with mean and standard deviation data. Measured parameter is surface area (m²).

Area	***Min.***	***1st Qu.***	***Median***	***Mean***	***3rd Qu.***	***Max.***	***Stand.dev***	***N***
Population 1	1609	4767	5445	6434	8347	13591	2387	599
Population 2	13014	14174	14808	15488	16819	20010	1924	43
Residuals	1513	6944	22189	17508	24000	35187	12139	8

Table 4.16: Statistics of pockmark shapes on the Q1.1 horizon. Names of the shape have been abbreviated to fit the table. They follow the names presented in Figure 4.23. E is elongated, EL is elliptical, T is for trough like, C is for composite, S is for symmetrical, I1 is for irregular one, and I2 is for irregular 2.

Shapes	**E (%)**	**EL (%)**	**T (%)**	**C (%)**	**S (%)**	**I1 (%)**	**I2 (%)**
Population 1	63,4	20,0	0,8		9,2	5,7	0,8
Population 2	18,6	41,9	7,0	2,3	4,7	25,6	
Residuals	25,0	62,5	12,5				

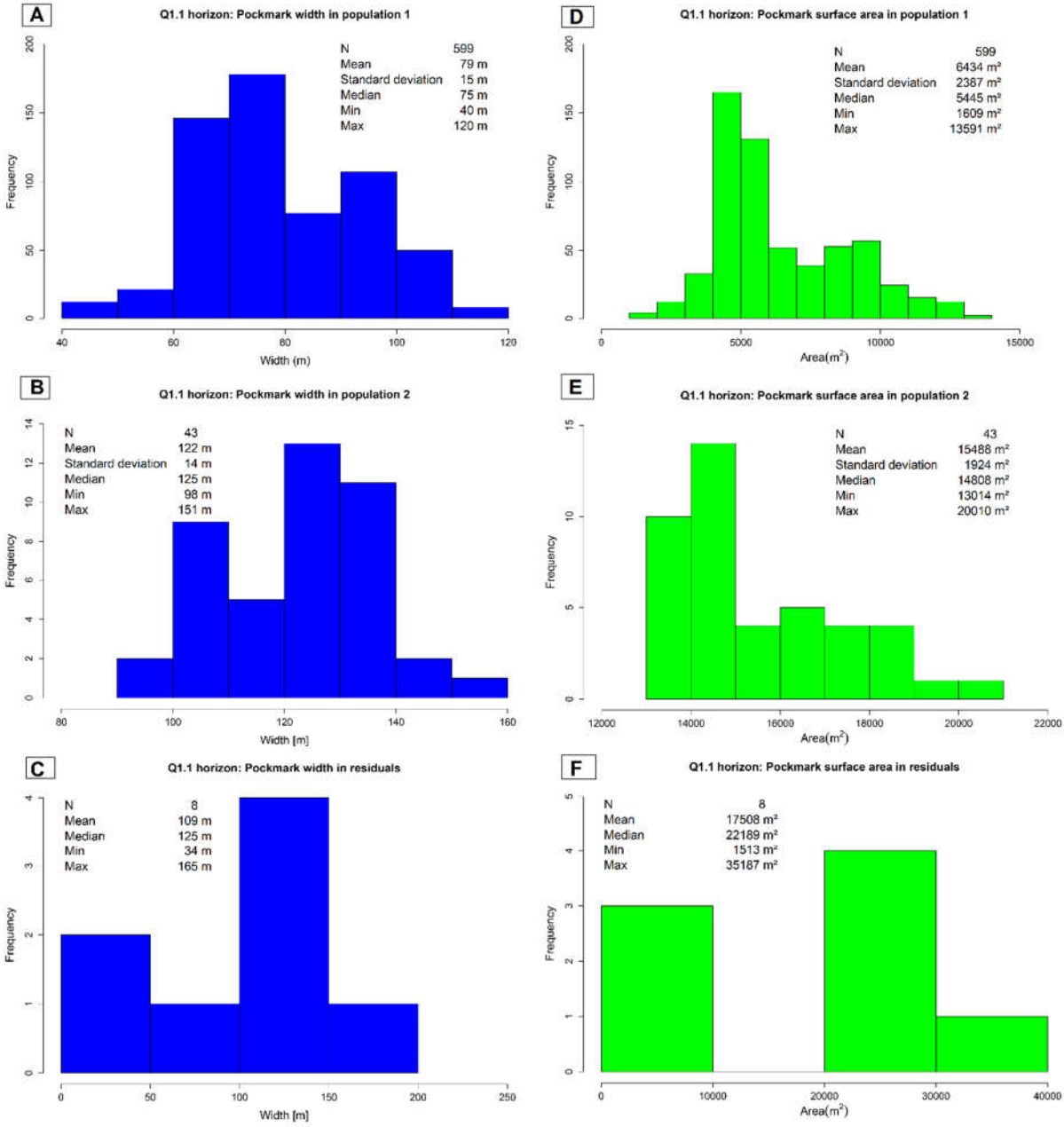

Figure 4.33: Histogram for the Q1.1 horizon. The blue graph shows the parameter width, and green is the surface area data.

Key statistics for the Q1.1 horizon

Population 1 has a mean of 79.4 m in width and 6434 m² in surface area, and most pockmarks are elongate (E) shaped.

Population 2 has a mean of 122.4 m in width and 15488 m² in surface area, and most pockmarks are elliptical (EL) and irregular-one (I1) shaped.

The residual group are few and has a mean of 108.8 m in width and 17508 m² in surface area, and the pockmarks are elliptical (EL) and elongate (E) shaped.

Q1.1 has a total of 650 pockmarks mapped and a global pockmark density of ~ 1.65 pockmarks per km².

4.3.5.5.1 Rose plot for pockmark directions

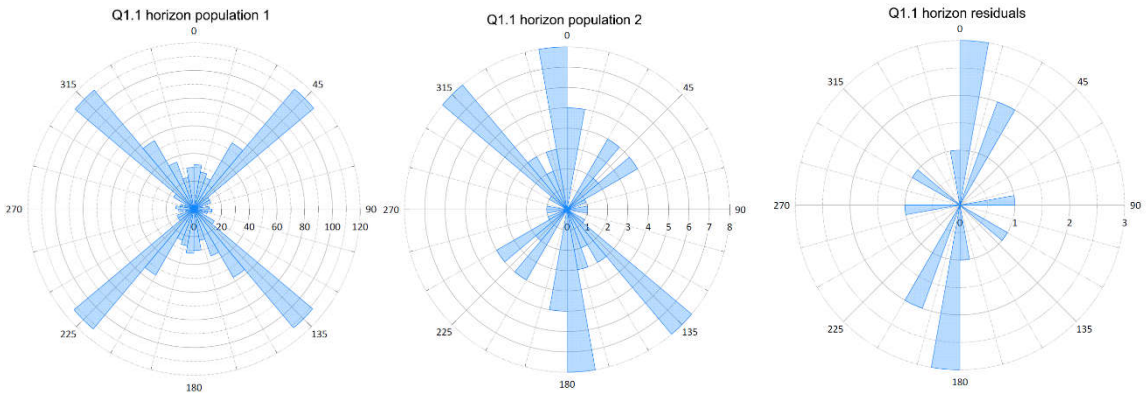

Figure 4.34: Rose plots of populations 1 and 2, and residuals on the Q1.1 horizon.

The rose plots in Figure 4.34 show dominant pockmark directions for different groups on Q1.1 horizon.

Population 1: NW-SE and NE-SW.

Population 2: NW-SE and N-S.

Residual group: N-S

4.3.5.6 Statistics for Seabed horizon pockmarks

Table 4.17: Descriptive statistics for pockmarks on the Seabed horizon. Presented are the quartiles with mean and standard deviation data. Measured parameter is width (m).

Width	***Min.***	***1st Qu.***	***Median***	***Mean***	***3rd Qu.***	***Max.***	***Stand.dev***	***N***
Population 1	41	68	73	77	87	114	13	604
Population 2	97	116	127	129	141	171	18	56
Residuals	36	197	218	214	246	318		19

Table 4.18: Descriptive statistics for pockmarks on the Seabed horizon. Presented are the quartiles with mean and standard deviation data. Measured parameter is surface area (m²).

Area	***Min.***	***1st Qu.***	***Median***	***Mean***	***3rd Qu.***	***Max.***	***Stand.dev***	***N***
Population 1	1882	4648	5279	6213	7870	12675	2183	604
Population 2	12003	14026	16127	18400	21773	32649	5365	56
Residuals	2561	50071	58429	60192	69379	139681		19

Table 4.19: Statistics of pockmark shapes on the Seabed horizon. Names of the shape have been abbreviated to fit the table. They follow the names presented in Figure 4.23. E is elongated, EL is elliptical, C is for composite, S is for symmetrical, I1 is for irregular one, and I2 is for irregular 2.

Shapes	**E (%)**	**EL (%)**	**C (%)**	**S (%)**	**I1 (%)**	**I2 (%)**
Population 1	79,3	10,3	2,0	4,3	3,8	0,3
Population 2	30,4	10,7	3,6		42,9	12,5
Residuals	5,3		5,3		47,4	42,1

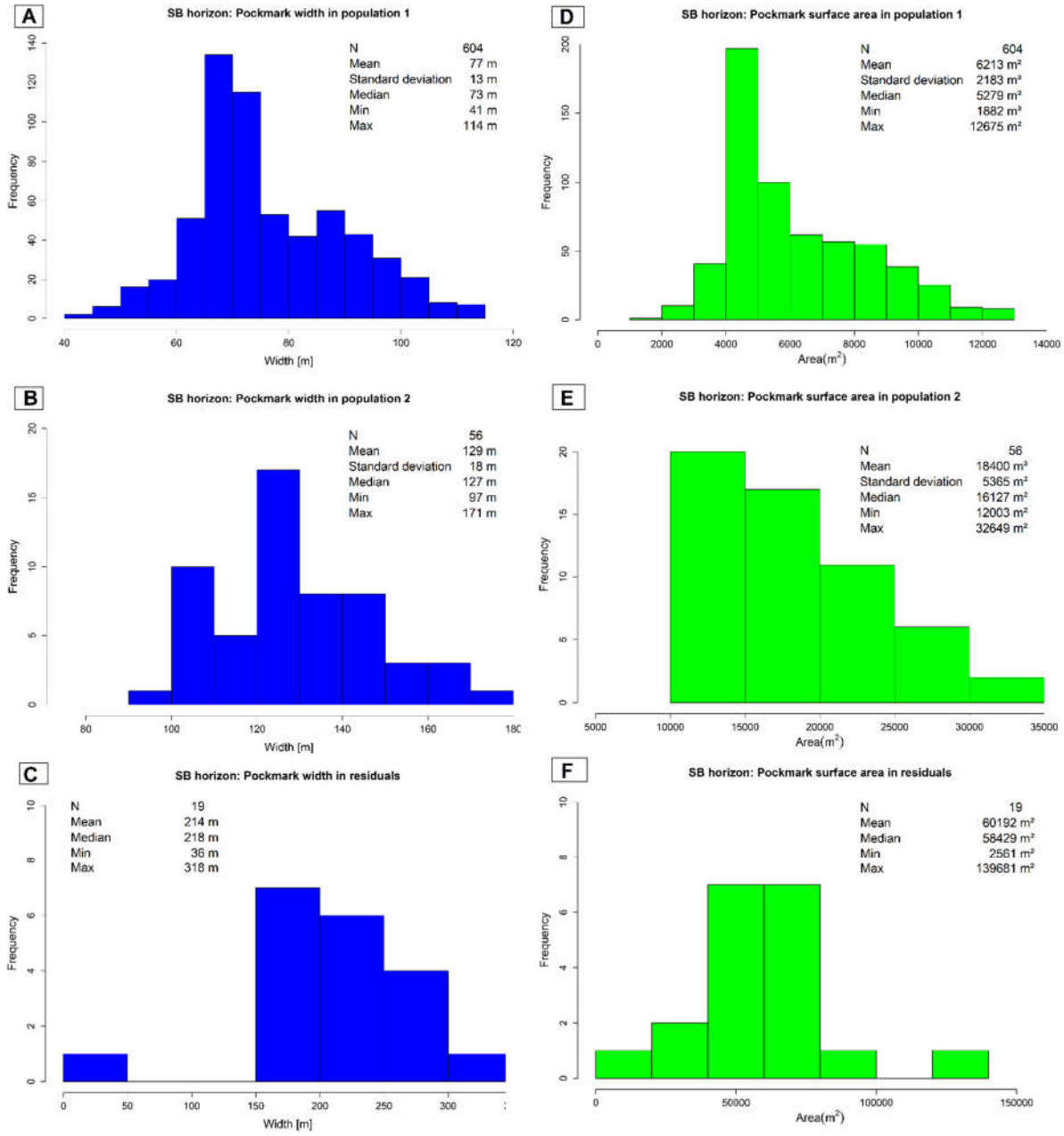

Figure 4.35: Histogram for the Seabed horizon. The blue graph shows the parameter width, and green is the surface area data.

Key statistics for the Seabed horizon

Population 1 has a mean of 77 m in width and 6213 m² in surface area, and most pockmarks are elongate (E) shaped.

Population 2 has a mean of 129 m in width and 18400 m² in surface area, and most pockmarks are elongate (E) and irregular-one (I1) shaped.

There are a few pockmarks in the residual group with a mean of 214 m in width and 60192 m² in surface area. The pockmarks are irregular-one (I1) and irregular-two (I2) shaped.

The Seabed has a total of 679 pockmarks mapped and a global pockmark density of ~ 1.72 pockmarks per km².

4.3.5.6.1 Rose plot for pockmark directions

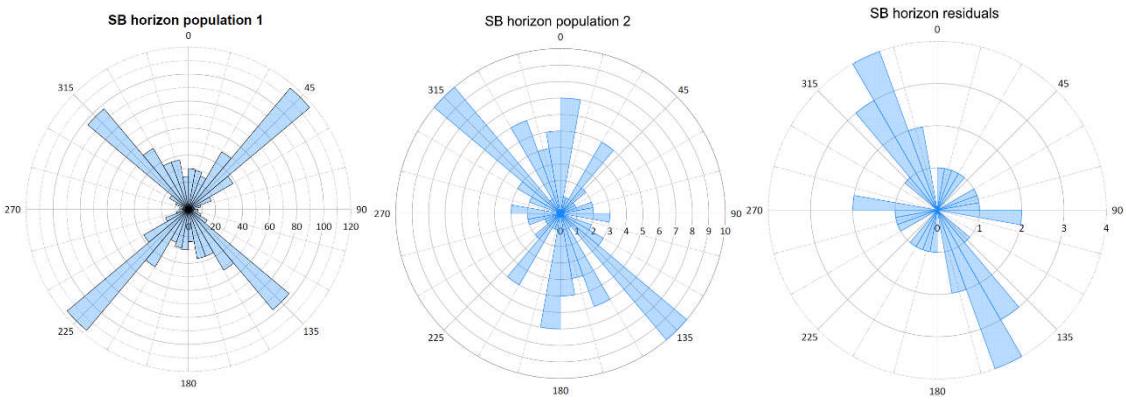

Figure 4.36: Rose plots of populations 1 and 2, and residuals on the Seabed horizon.

The rose plots in Figure 4.36 show dominant pockmark directions for different groups on the Seabed horizon.

Population 1: NW-SE and NE-SW.

Population 2: NW-SE and N-S.

Residual group: NNW-SSE

4.3.5.7 Collective box and whiskers plots for all horizons

4.3.5.7.1 Population 1

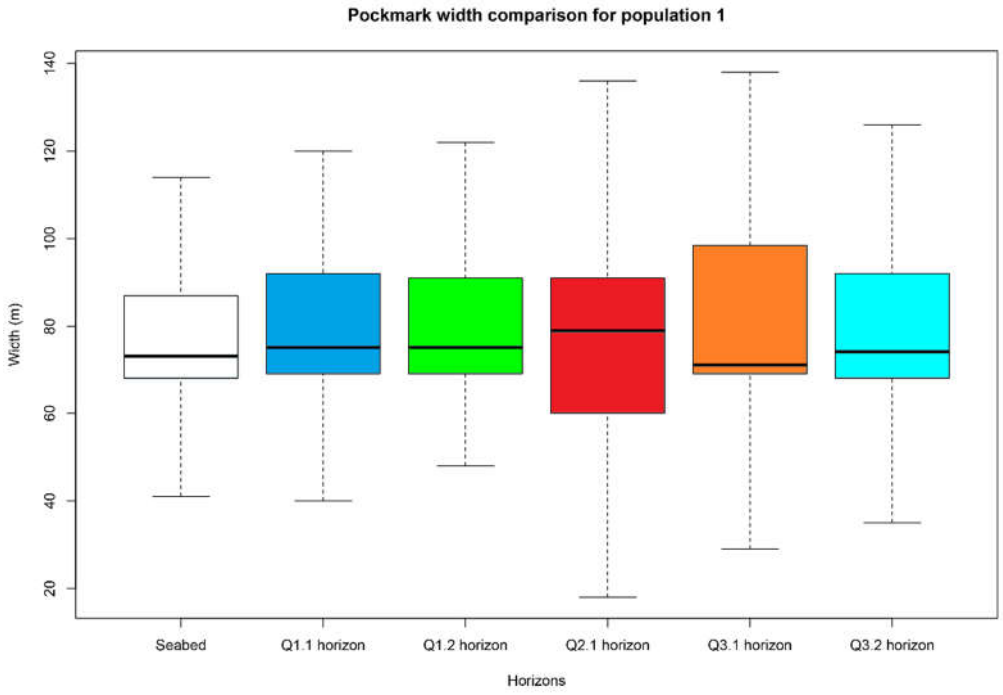

Figure 4.37: Box and whiskers plots for pockmark width in population 1. Black line inside the box is the median.

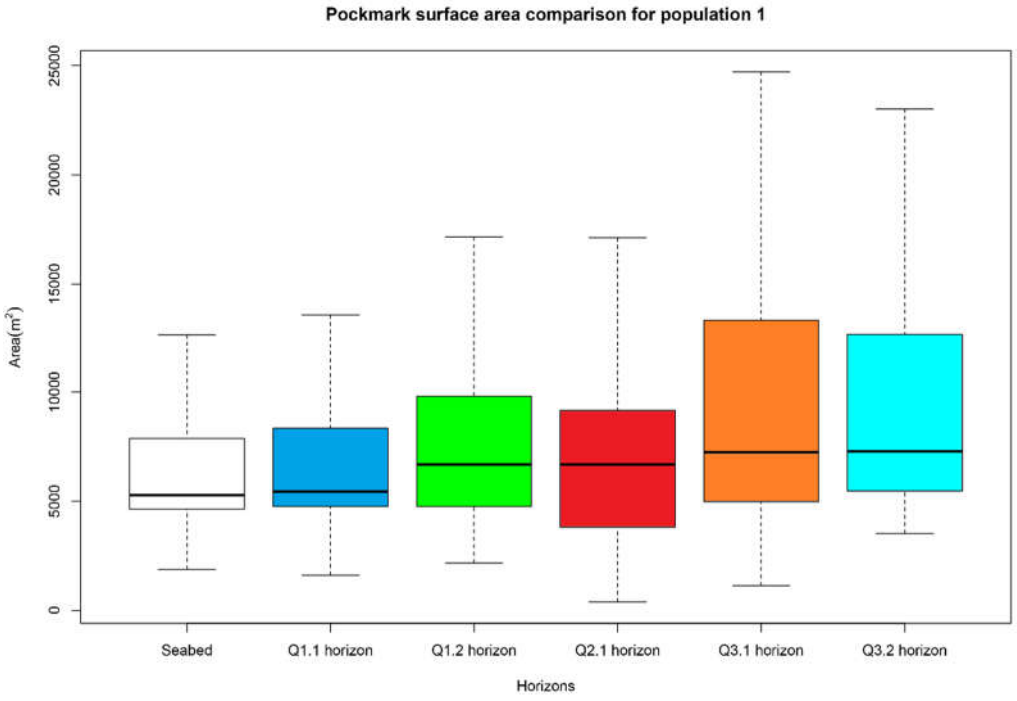

Figure 4.38: Box and whiskers plots for pockmark surface area in population 1. Black line inside the box is the median.

4.3.5.7.2 Population 2

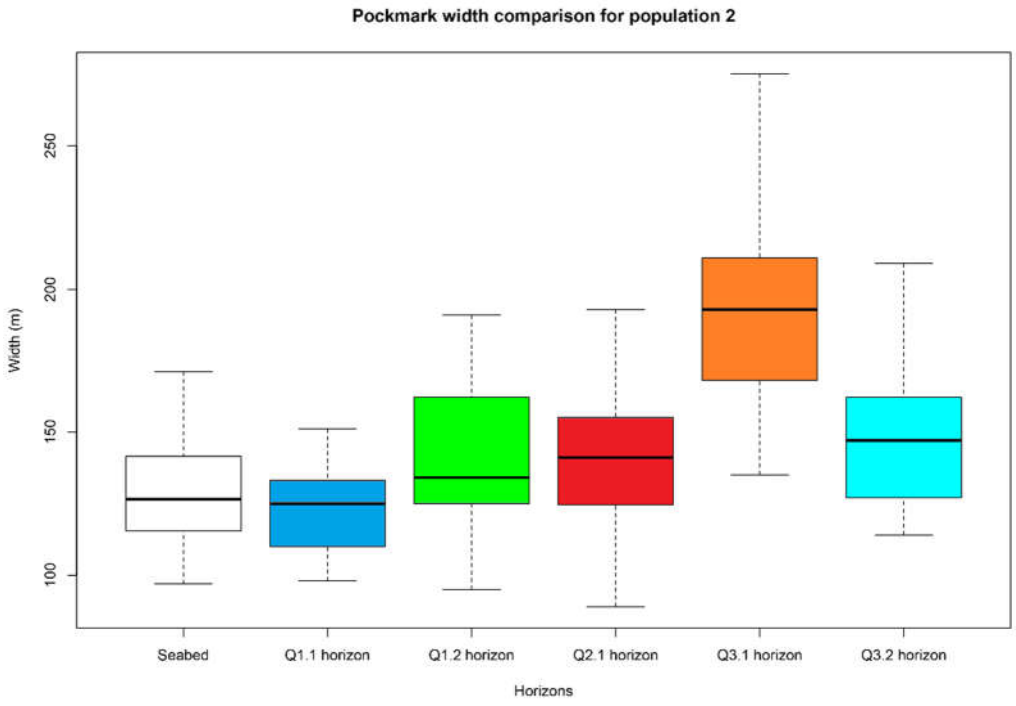

Figure 4.39: Box and whiskers plots for pockmark width in population 2. Black line inside the box is the median.

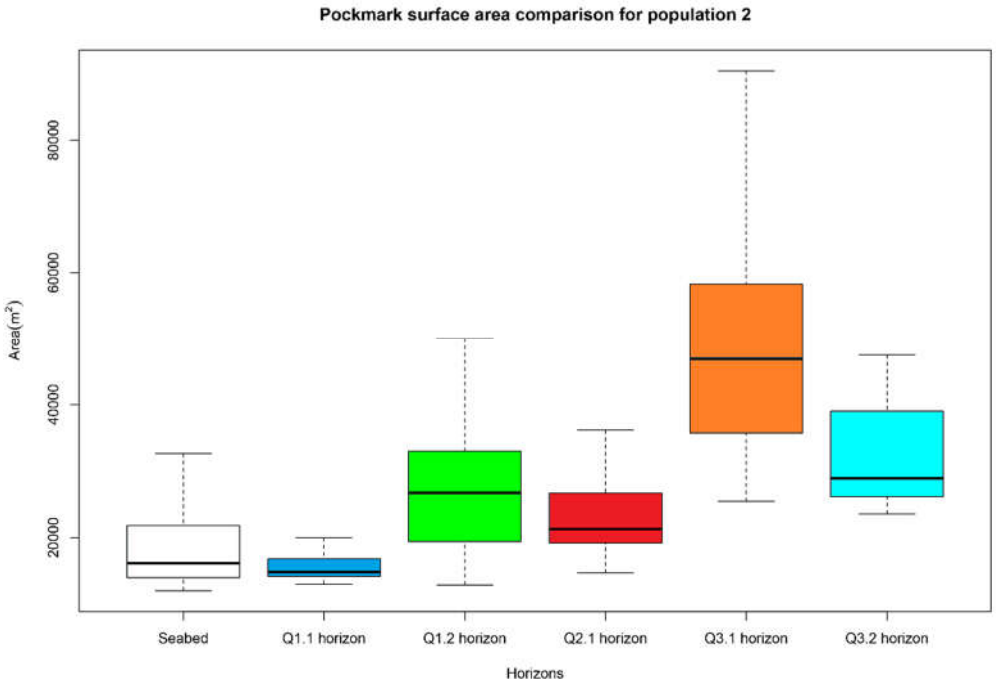

Figure 4.40: Box and whiskers plots for pockmark surface area in population 2. Black line inside the box is the median.

4.3.5.7.3 Residual groups

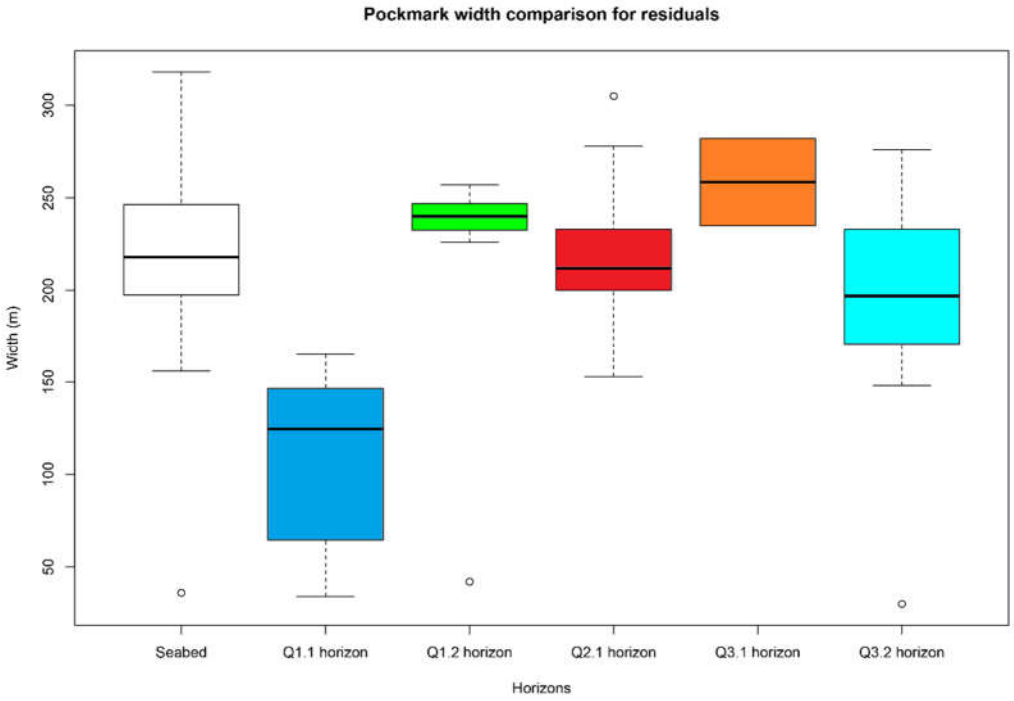

Figure 4.41: Box and whiskers plots for pockmark width in residual group. Black line inside the box is the median.

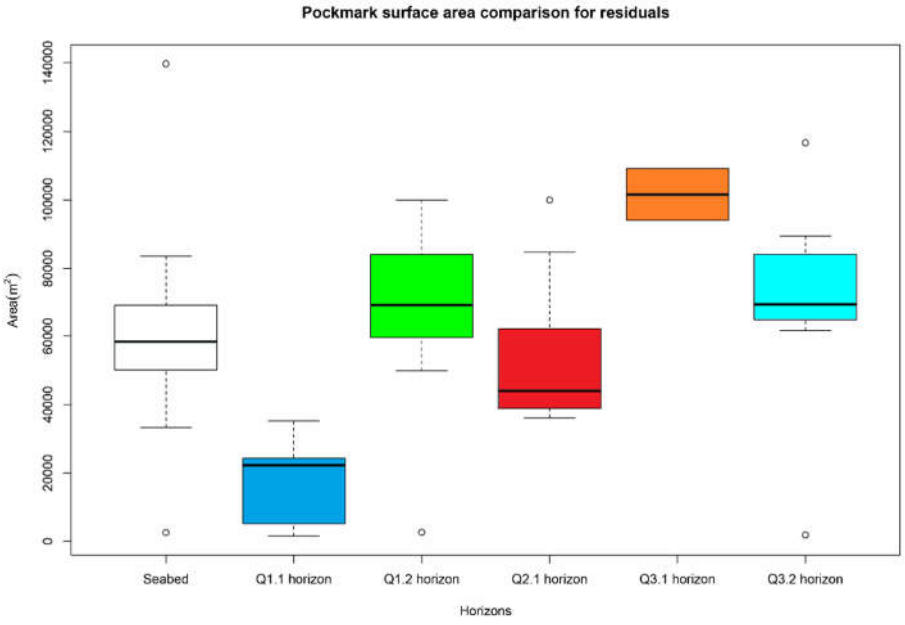

Figure 4.42: Box and whiskers plots for pockmark surface area in residual group. Black line inside the box is the median.

4.3.5.8 Comments on the collective box plots and horizon statistics

Collective box plots of population 1 in Figure 4.37 and Figure 4.38 show pockmark sizes are similar. Population 0 on horizon Q2.1 is not taken into consideration for this overview as their pockmarks deviate from the rest of the samples. The middle 50 % of the data, in the box of the plot, show pockmarks sizes are in the range of:

1 60-95 m in width and have 5000-13000 m² of surface area. The statistics results show they have a mean between 75-81 m in width and a mean surface area between 6200-9400 m².

Collective box plots of population 2 in Figure 4.39 and Figure 4.40 show that pockmark sizes have differences and some similarities. Horizons are grouped by box plot observations. Data ranges are:

2 **Seabed and Q1.1 horizon**: Have pockmarks sizes in the range of 110-140 m in width and have 14000-21000 m² of surface area. The statistics results show they have a mean between 122-129 m in width and a mean surface area between 17500-18000 m².

3 **Q1.2 and Q2.1 horizon**: Have pockmarks sizes in the range of 125-161 m in width and have 19000-32000 m² of surface area. The statistics results show they have a mean between 140-142 m in width and a mean surface area between 23000-26500 m².

4 **Q3.1 and Q3.2 horizon**: Have pockmarks sizes in the range of 127-211 m in width and have 26000-58000 m² of surface area. The statistics results show they have a mean between 149-191 m in width and a mean surface area between 32000-48000 m². The Q3.1 horizon has larger pockmarks and is on the upper end of these ranges.

Residual groups are pockmarks that are not part of any population. These groups have few pockmarks and are the largest pockmarks mapped. Small pockmarks under 50 m in width, appearing as outliers.

4.3.5.9 Results from normality and outlier tests

The pockmark data from each horizon has been subjected to separation of outliers by the IQR rule of thumb. It is in this process that the different populations are distributed, and the remaining pockmarks are grouped as residuals. All normality test results are in Appendix 6 (Shapiro-Wilk test) and Appendix 7 the Q-Q plots (visual normality test).

The results from the Shapiro-Wilk test confirm population 2 as normal distributed, except for horizon Q3.2. All test reject population 1 as being normally distributed. Visual normality evaluation with the Q-Q plots in Appendix 7 allow for population 1 to be interpreted as at least bimodal, and possibly multimodal. The best samples showing normal distribution are width population 2 of Q2.1 and Q3.1 horizon (Figure 6.5 and Figure 6.6). Most of the plots exhibit long distribution tails.

The Grubbs test results for outliers is in Appendix 6 and table 6.8. It shows that all sample groups have no outlier points. Residuals were not tested. The G-value produced from the test shows that the sample distributions are 3 to 5.5 standard deviations from the mean and imply fat-tailed distributions.

4.4 Glacial erosion marks on Quaternary horizons

The Quaternary glaciers have left erosive marks on several horizons, and most of the marks identified are streamlined and interpreted as MSGL. Glaciation marks that vary in direction within the direction pattern are interpreted as ploughmarks. The Seabed and the Q3.1 horizon have no visible glaciation marks.

The glacial lineations on the Q3.2 URU horizon follow a northeast and north-northwest direction in Figure 4.43. Magenta marks are interpreted as MSGL, and white as iceberg plough marks.

The Q2.2 horizon has recorded marks in several directions in Figure 4.44. Moreover, glaciation marks in blue have a front that is interpreted as paleo grounding lines. This kind of lineation signifies a part of the ice sheet rested on the old seabed behind up to this line. The blue marks are then interpreted as subglacial lineations. Glaciation marks in magenta and turquoise are interpreted as MSGL, and the whites as a combination with plough marks and MSGL.

The glacial lineations of Q2.1 horizon in Figure 4.45 are interpreted as MSGL marks.

The Q1.2 horizon is closer to the seabed, and the last glaciation. Glaciation marks are interpreted as plough marks in Figure 4.46.

The Q1.1 is the last horizon with glaciation marks before the seabed. The lineations in Figure 4.47 of magenta colour are interpreted as plough marks, while the white marks may be a combination of are MSGL and plough marks.

Directions and measurements of glaciation marks found on mapped horizon are further presented in Table 4.20. In Table 4.21 the general glacial directions are combined with pockmark direction for comparison.

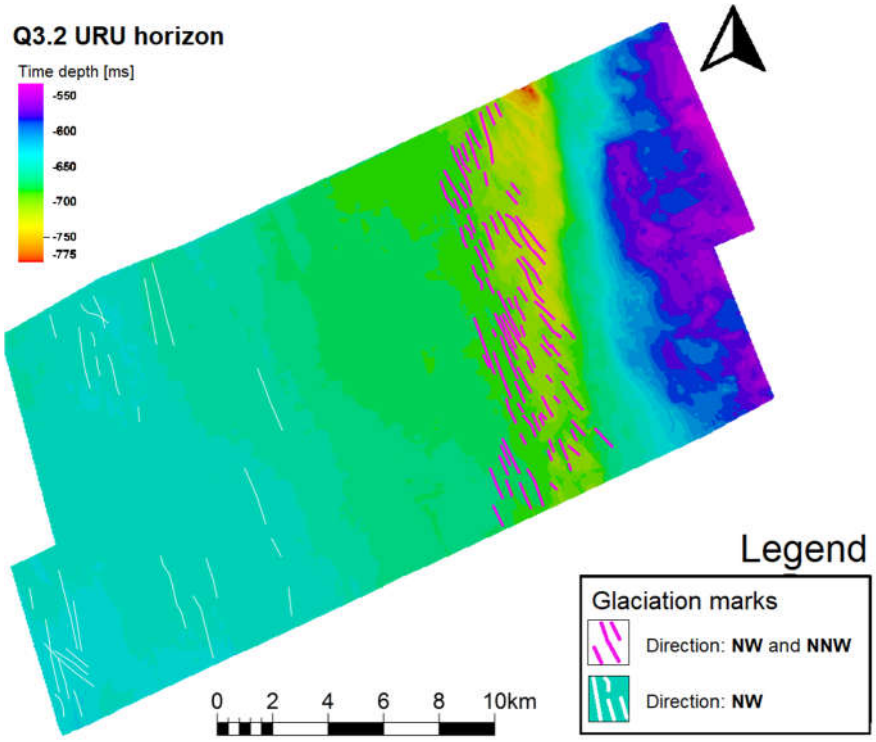

Figure 4.43: Glaciation marks on the Q3.2 URU horizon.

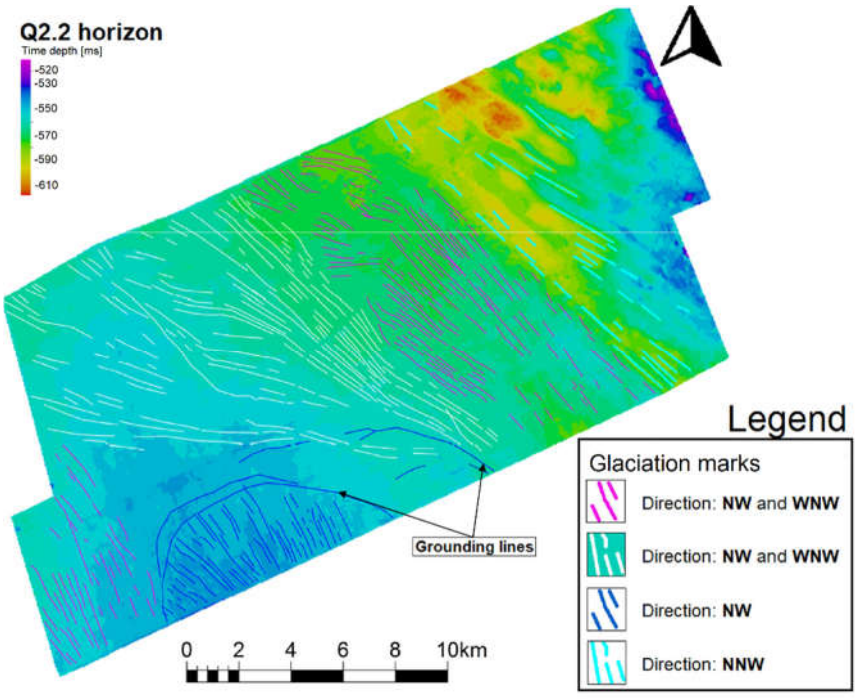

Figure 4.44: Glaciation marks on the Q2.2 horizon. This surface has recorded lineations several directions and other groove marks that are interpreted as paleo grounding lines.

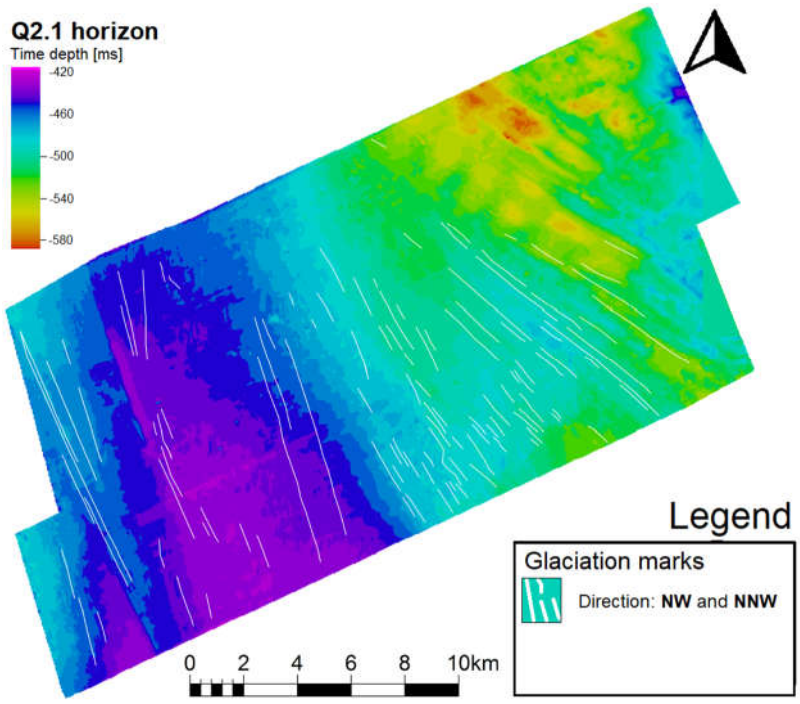

Figure 4.45: Glaciation marks on the Q2.1 horizon.

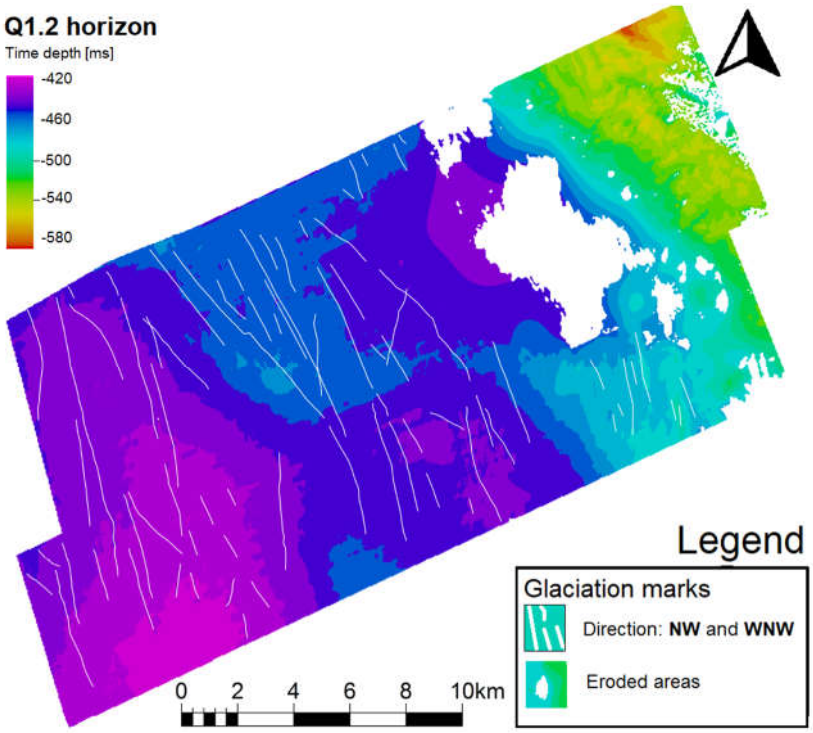

Figure 4.46: Glaciation marks on the Q1.2 horizon.

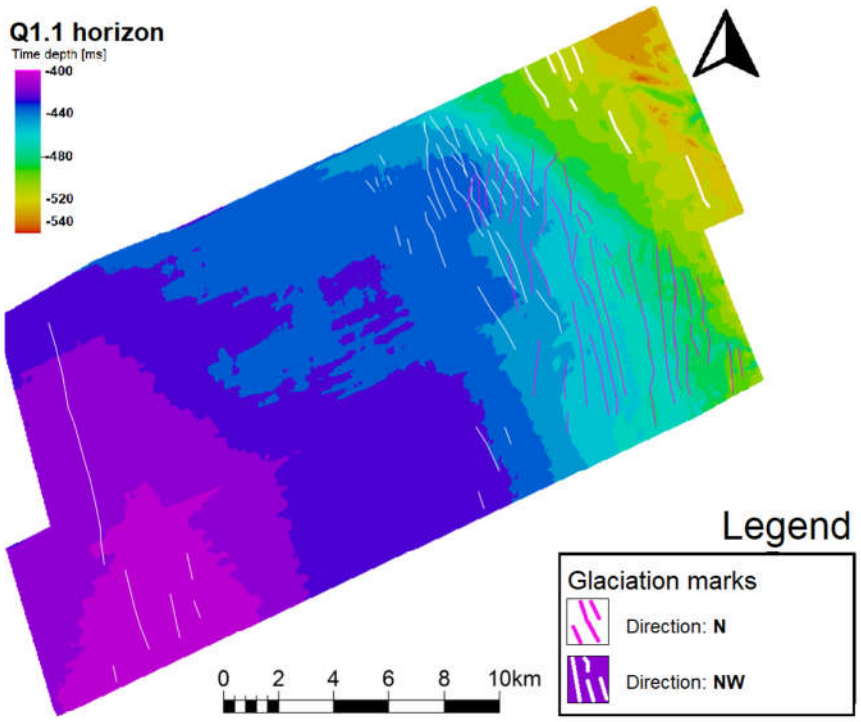

Figure 4.47: Glaciation marks on the Q1.1 horizon.

Table 4.20: Measurements of glacier lineations on the mapped horizons. Measurements are approximately width and length.

Marks on horizon	Min. width	Max. width	Min. length	Max. length	Directions	Glacial marks
Q3.2 (White)	130 m	190 m	0,5 km	2,8 km	NNW, NW	Plough
Q3.2 (Magenta)	140 m	440 m	0,8 km	2,0 km	NNW	MSGL
Q2.2 (Turquoise)	140 m	800 m	0,3 km	3,6 km	NNW	MSGL
Q2.2 (Magenta)	85 m	140 m	0,3 km	3,7 km	NW, WNW	MSGL
Q2.2 (White)	70 m	170 m	0,2 km	8,0 km	NW, WNW	MSGL, Plough
Q2.2 (Blue)	60 m	105 m	0,1 km	3,3 km	NW	Subglacial
Q2.1	45 m	200 m	0,3 km	10 km	NW, NNW	MSGL,Plough
Q1.2	70 m	200 m	0,4 km	10 km	NW, WNW	Plough
Q1.1	40 m	400 m	0,4 km	9,0 km	N(magenta), NW (white)	Plough, MSGL

Table 4.21: Combined glacial direction and pockmarks directions on mapped horizon. Horizon Q2.2 is not included (no mapped pockmarks). Group symbols: P0 = population 0, P1 = population 1, P2 = population 2, R = residuals, G = Glacial.

Groups\Horizon	Seabed	Q1.1	Q1.2	Q2.1	Q3.1	Q3.2
Direction P0				NE-SW		
Direction P0				NW-SE		
Direction P1	NE-SW	NE-SW	NE-SW	NE-SW	NE-SW	NE-SW
Direction P1	NW-SE	NW-SE	NW-SE		NW-SE	NW-SE
Direction P2	NW-SE	NW-SE	NW-SE	NE-SW	NW-SE	NNW-SSE
Direction P2	N-S	N-S	NNW-SSE			
Directions R	NNW-SSE	N-S	NE-SW	N-S	NW-SE	N-S
Directions G		N	NW	NW		NNW
Directions G		NW	WNW	NNW		NW

4.5 Qualitative observations from seismic data

4.5.1 Seismic amplitude anomalies

4.5.1.1 Seismic character around the VFZ

The seismic cross-section in Figure 4.48 was selected to show the general trend of the contact between the layers over Top Lista and Top Sele Formation and the URU.

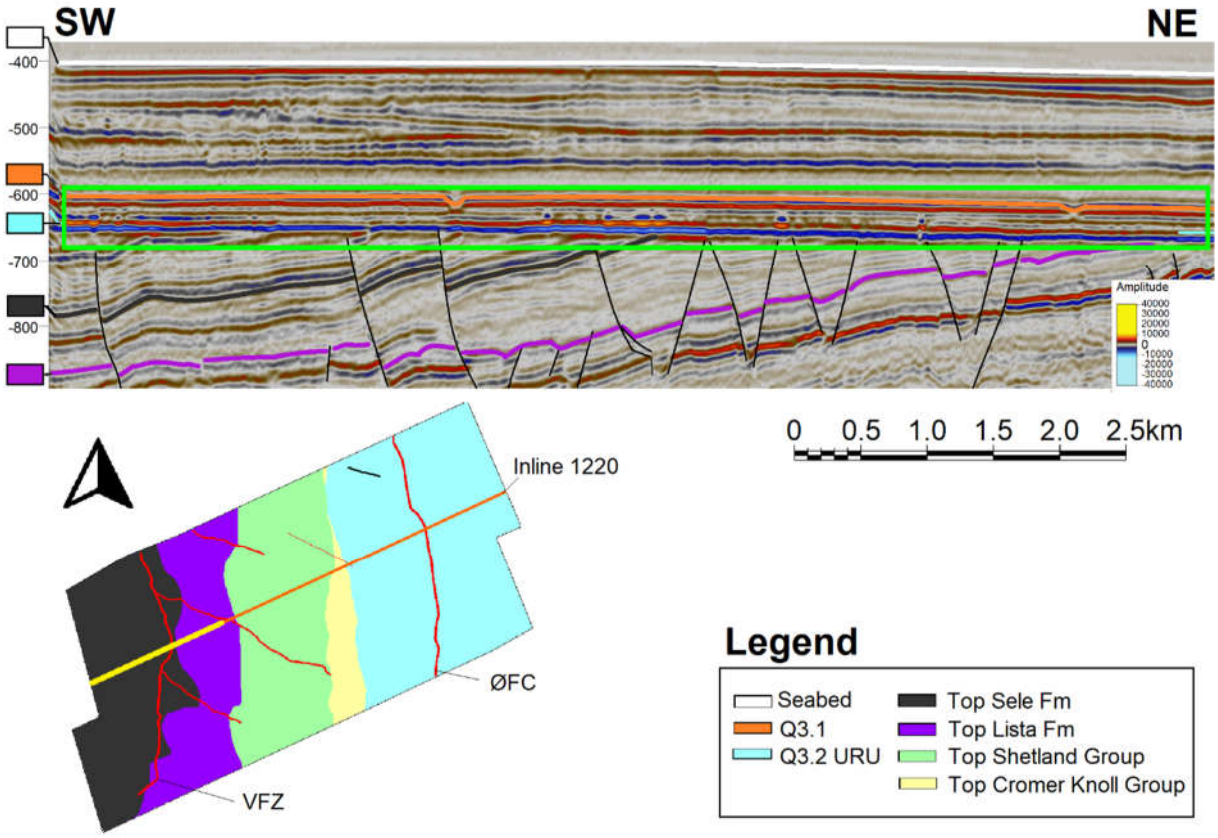

Figure 4.48: A seismic cross-section part of seismic inline 1220 showing amplitude changes along the contact of the URU. The green box points out the affected area between horizons Q3.2 and Q3.1. Horizon Q3.2 is presented without a colour marker to observe the amplitude changes better.

Anomalies between Q3.1 and Q3.2 shows bright spots in combination with dimmed areas. By bright spots, it is meant where the bitmap for large amplitude is changed to brighter colours than surrounding amplitude colours. The bright spots are often seen with fault tips right under them, but there are also sections where brighter amplitudes exist without any visible faults underneath. The amplitude anomalies are seen throughout most of the stratigraphic layers over the Lista Formation in contact with the URU. The anomaly frequency is highest in the upper west corner of the Smeaheia area.

A second interpreted seismic cross-section line, perpendicular to the VFZ is seen in Figure 4.49. Over the Q3.2 horizon, several points of bright negative amplitude are observed. Some of them have narrow dimmed columns above them. These features above the bright spots appears to be seismic pipes (Løseth et al., 2009). Polygon fault tips are observed under most of these points.

Furthermore, on the hanging wall side of the VFZ, the amplitudes are lightly dimmed above the fault. Following the Top Shetland Formation horizon, which is not coloured for clarity, there are two locations with brighter amplitudes. The one highlighted with a magenta box appears to have a slightly dimmed section below.

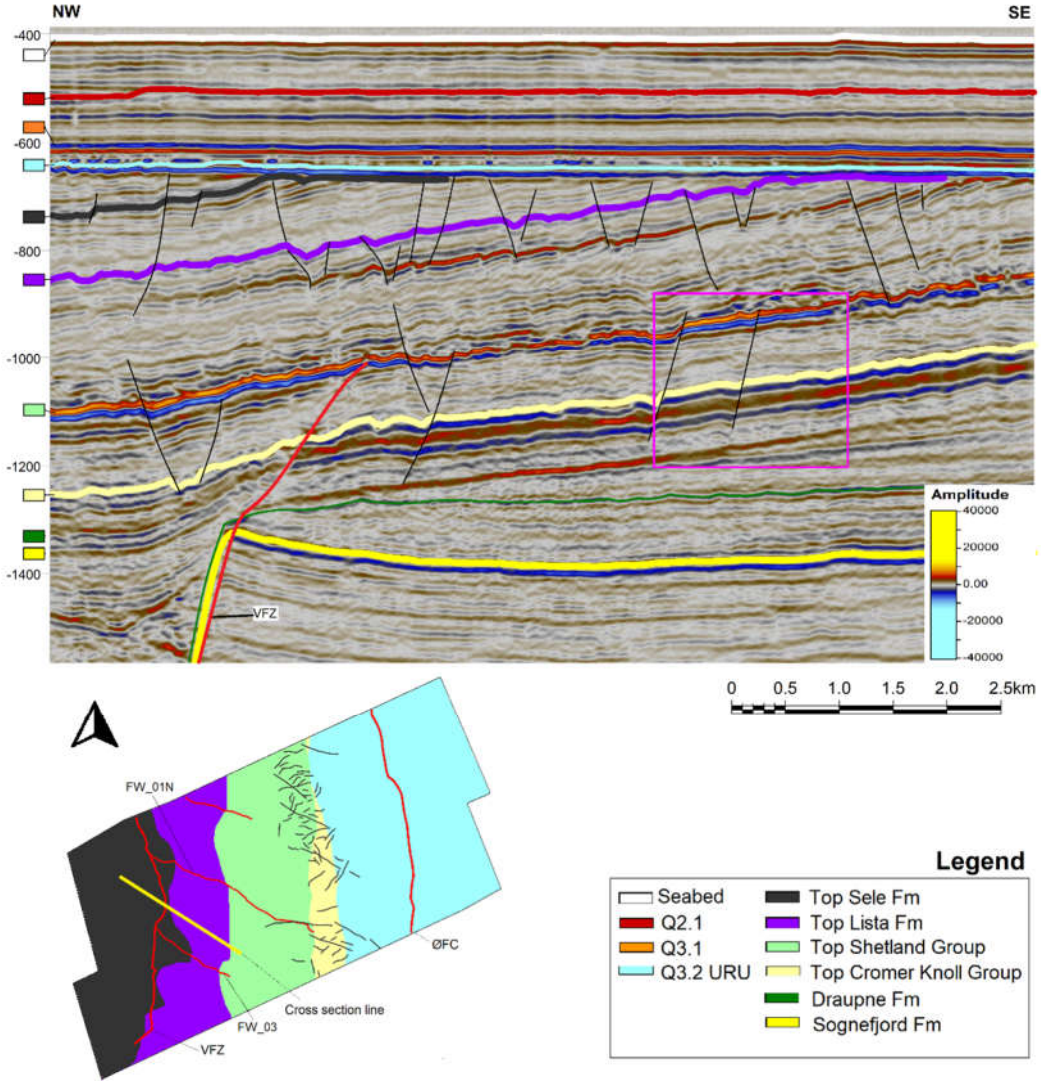

Figure 4.49: A cross section perpendicular to the VFZ and between FW_01N and FW_03.

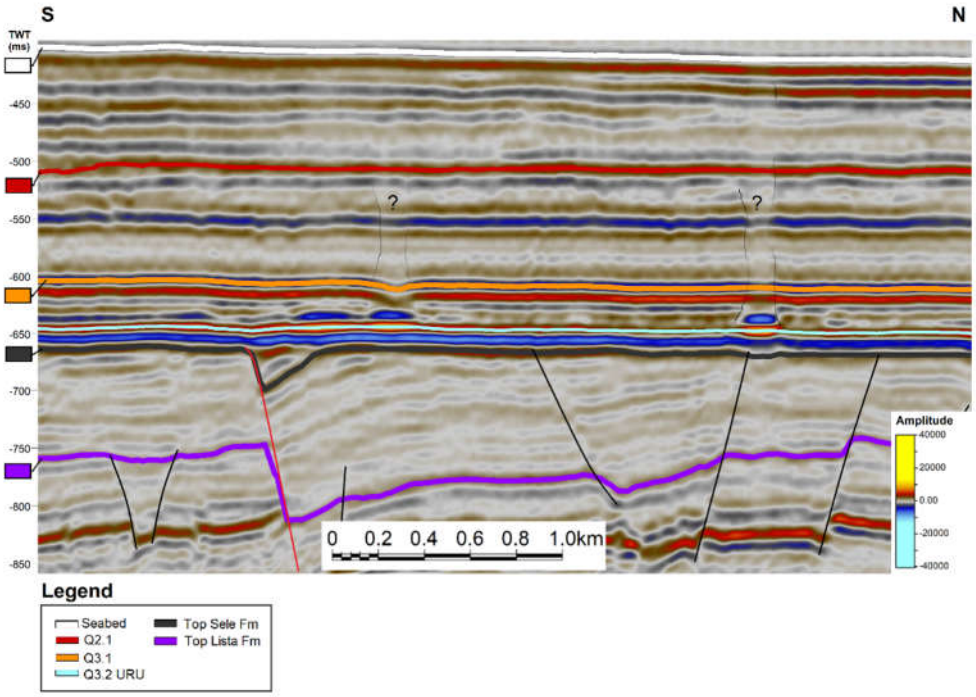

Figure 4.50: N-S seismic cross-section near the VFZ shows the zoomed in part of the polygonal faults and the Quaternary interval. The seismic anomalies observed in the previous cross-section is also seen here. Two of the major bright spots have a dimmed column above them, probably traces of paleo-seepage.

In Figure 4.50, traces of paleo-seepage are dimmed columns (seismic pipes) over two bright amplitude spots. The column in the south rises over a mapped pockmark in the Q3.1 horizon and is one of the larger pockmarks. The column to the north is a buried pockmark with dimmed amplitude trace.

4.5.1.2 Seismic character southwest and centre of Smeaheia

A seismic cross-section perpendicular to fault FW_01 and FW_03 has been studied in Figure 4.51. The Top Shetland Group horizon shows brighter amplitudes to the southwest in the cross-section with dimmed sediment sections below in the Cromer Knoll Group. In the zoomed picture, a small wipe-out zone with a chaotic reflector top. The brighten Shetland amplitudes coupled with dimmed reflectors below are also observed around faults FW_01S and FW_01N. The latter two faults form a fault relay zone near the Top Shetland Group horizon. The highlighted section in magenta shows dimmed amplitude at the base of the Quaternary interval. This prominent feature is observed on several cross-sections east of the Top Lista Formation horizon subcrop.

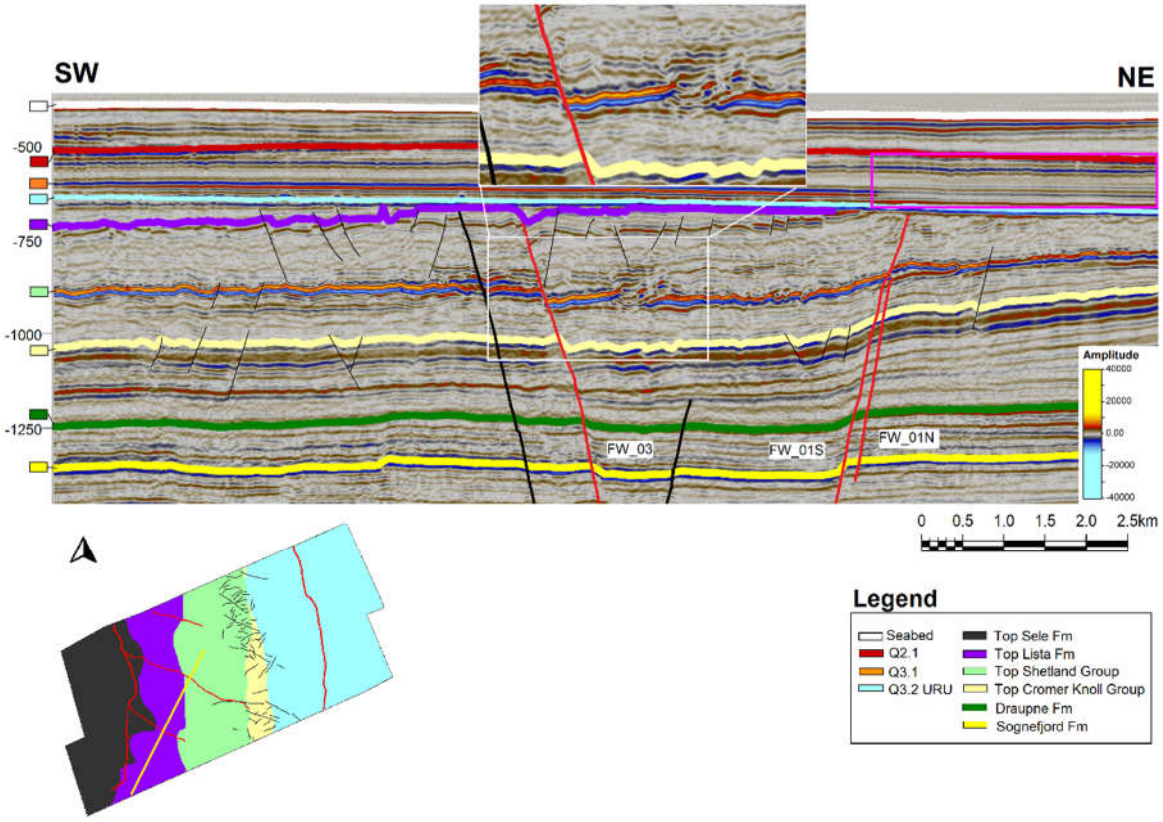

Figure 4.51: Seismic cross-section line perpendicular to faults FW_01N / FW_01S and FW_03. The top Shetland Group and the Q3.1 horizon is not drawn for the observational purpose of the amplitude changes.

4.5.1.3 Seismic character in the centre of Smeaheia

The seismic cross-section presented in Figure 4.52 shows data near the centre of the Smeaheia area. Observations in the green box again show bright Shetland reflector amplitudes with dimmed and disturbed sections below the Cromer Knoll Group horizon. The magenta box shows the fault tip of fault FW_17S truncated by the URU. A pockmark is seen south of the fault tip with disturbances in the sediments around the fault termination. In the black box, a buried pockmark is seen. A time slice at the top of the pockmark shows it has a width of 400-500 m. The bottom of the buried pockmark has a strong amplitude and disturbed sediment area below it.

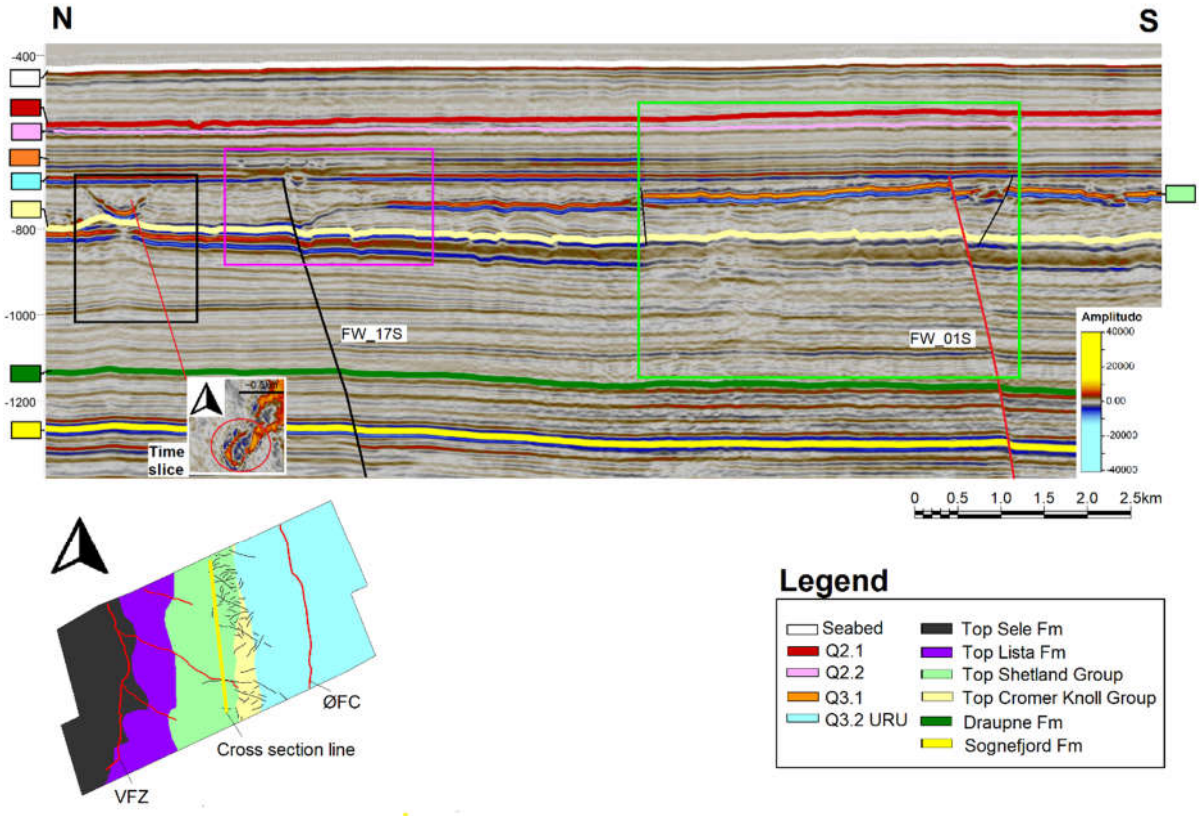

Figure 4.52: N-S seismic cross-section line in the centre part of Smeaheia. Colour boxes are anomalies observed.

4.5.1.4 Seismic character in the eroded areas

In Figure 4.53, another cross-section was set to examine the seismic stratigraphy under the eroded areas. The green and magenta boxes show areas of a higher amplitude on the Q3.2 URU horizon. In the green box section, the layers below show dimmed and slightly distorted, while in the magenta box the horizon is elevated. Anomalies in further up north have some buried pockmarks. A smaller cross-section was set in a SW-NE direction to study one of them (seen in the smaller image). Disturbance and dimmed sediment layers can be observed almost down to the Draupne Formation horizon. The specific pockmark appears on the Q2.1 horizon but has been mapped only partially as there are disturbances in the seismic signal.

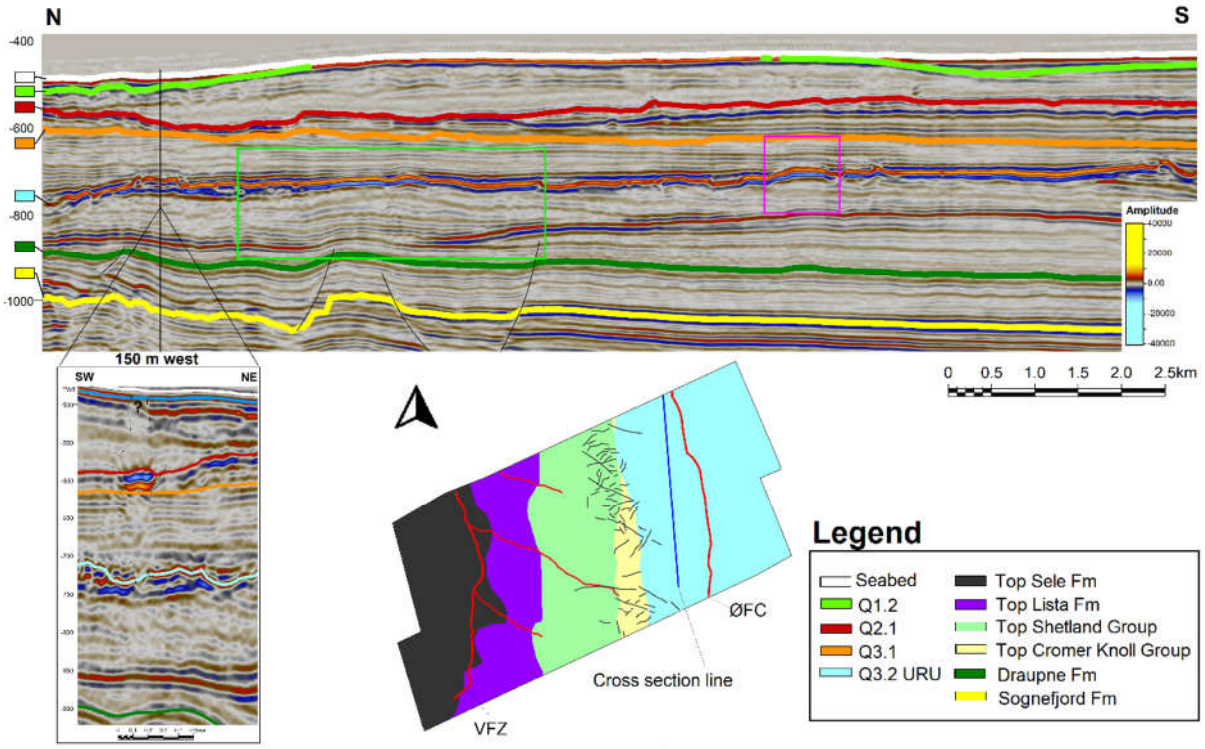

Figure 4.53: N-S seismic cross-section in eroded areas. A smaller SW-NE cross-section was set in the northern area, approximately 150 m west of the original line, to investigate some of the buried pockmarks.

4.5.1.5 Map view of the seismic amplitudes under the URU

A series of amplitude time slices were studied to understand the seismic signal over the area where major stratigraphic horizons subcrop the URU. The blue negative amplitude seen in the

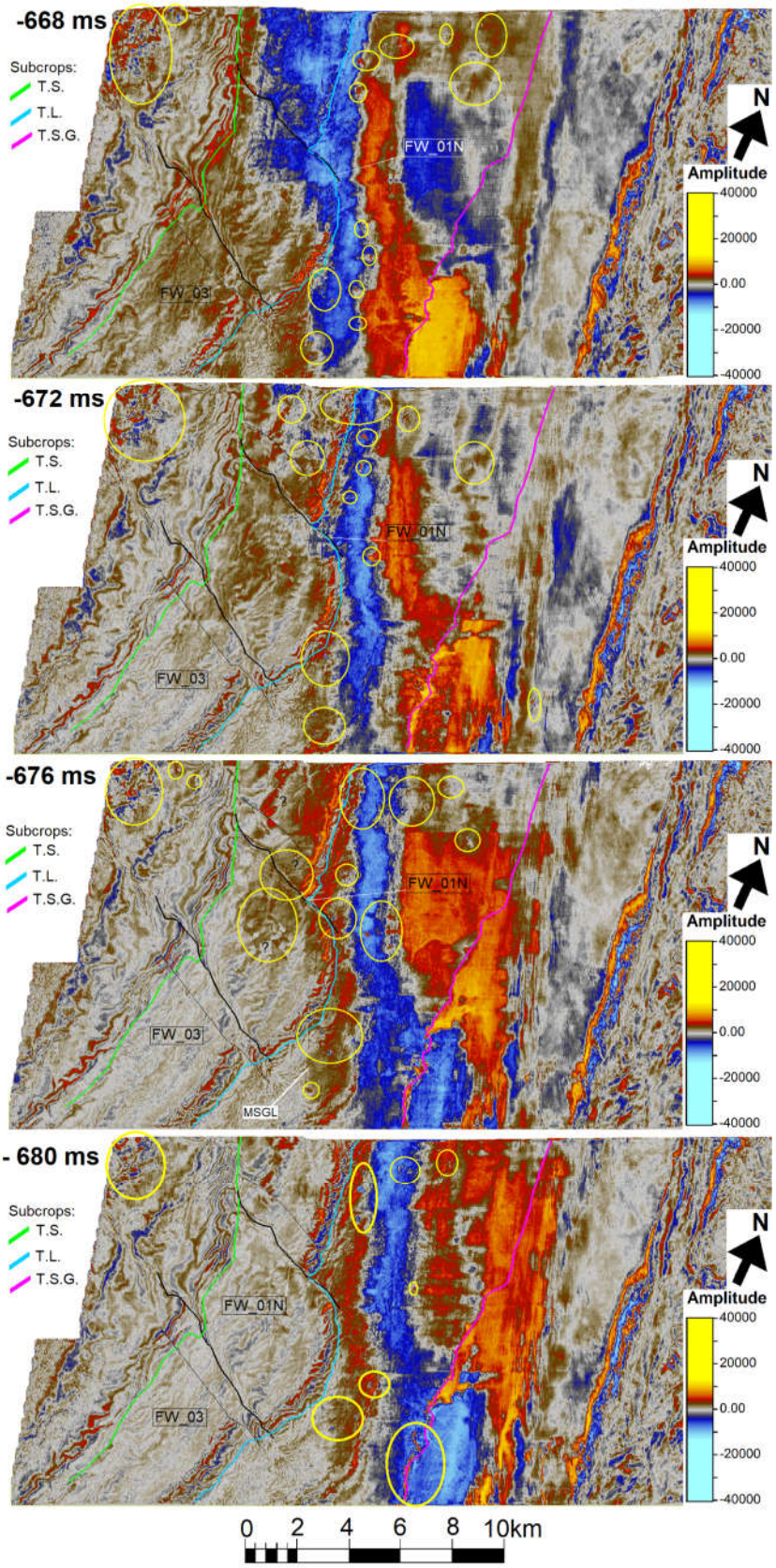

Figure 4.54: Four seismic time slices of the seismic amplitude below the URU from -680 to 668 ms. The unconformity surface has a north-eastern tilt, so the light blue signal represents the surface underneath the Q3.2 URU horizon as slices are moving up. The yellow circles are points of interest or pockmarks through the subsurface. T.S = Top Sele Fm., T.L = Top Lista Fm., and T.S.G. = Top Shetland Group.

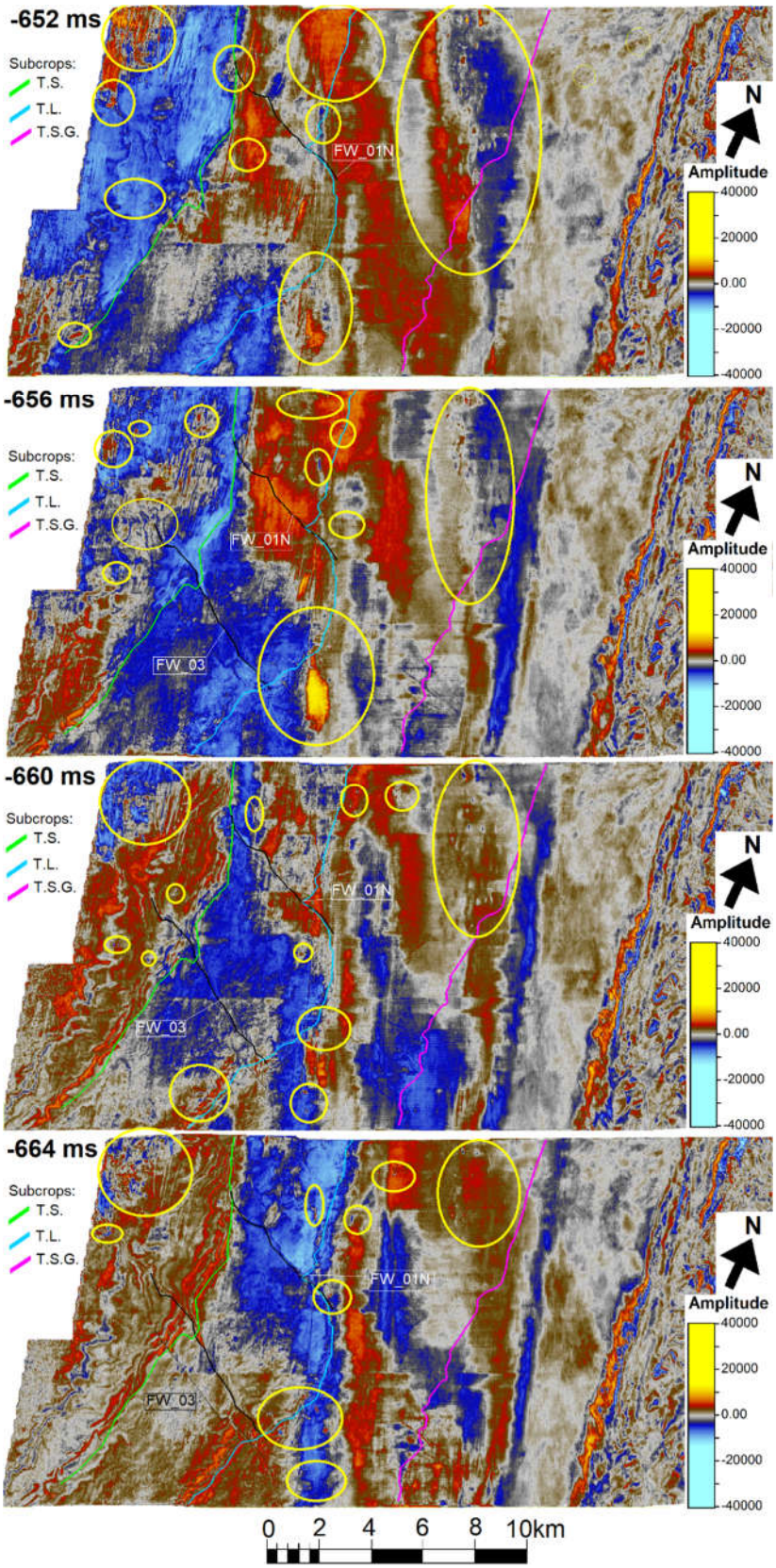

Figure 4.55: Four seismic time slices of the seismic amplitude below the URU from -664 to 652 ms and a continuation of Figure 4.54. The light blue negative signal represents the surface underneath the Q3.2 URU horizon, and yellow circles are points of interest or pockmarks through the subsurface. T.S = Top Sele Fm., T.L = Top Lista Fm., and T.S.G. = Top Shetland Group.

centre area is the contact with the URU. Horizon Q3.2 URU is mapped on the positive amplitude above it.

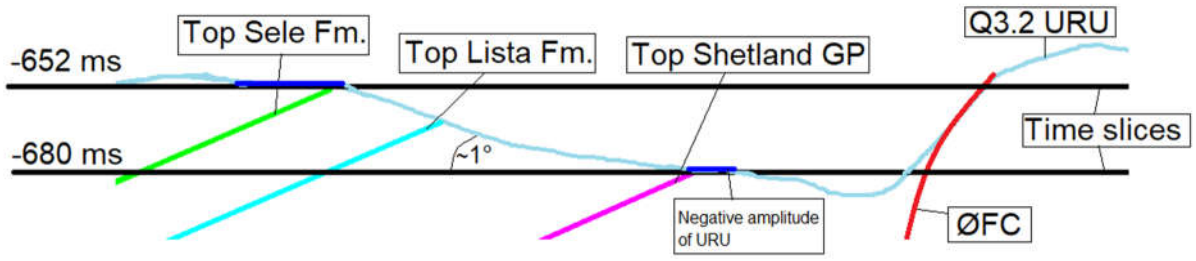

Figure 4.56: Schematic cross-section depicting information from the seismic time slices in Figure 4.54 and Figure 4.55. Moving slices up in time will shift the amplitude signal to the right due to tilt in the area. The diagram is not to scale, and dip is exaggerated.

All areas to the left of the blue amplitude are under the URU, and all areas to the right are on or above the Q3.2 horizon (except ØFC footwall). The time slices in Figure 4.54 show there are high amplitudes where Top Shetland Group subcrops, and several pockmarks emerge to the left of the blue amplitude. In general, observations show that pockmarks are present along the Top Lista Formation subcrop (T.L. on map), and to the southeast between subcrops and faults FW_01N and FW_03. In the northwest corner of the GN1101survey, the amplitude anomalies shown previously in seismic cross-sections are observed as a variegated pattern. Sediments appear disturbed there. Time slice -668 ms shows new pockmarks have emerged in the neutral part of the amplitude, to the right of the blue. Pockmarks are also present at the junction between faults FW_01N and FW_01S. The junction has a fault relay zone as, seen in Figure 4.51, at the Top Shetland Group horizon level.

In Figure 4.55, time slices -664 ms and -660 ms show more pockmarks are emerging on the southeast tip of fault FW_03. These pockmarks may originate from the fluids migrating up the fault itself, or the subcrops further south outside the Smeaheia area. From time slice -660 ms to -652 ms more pockmarks emerge to the northwest of the Top Sele Formation lineation (T.S. on map). The pockmark group situated in the centre-north develops as time slices progress up the Quaternary interval.

4.5.2 RMS amplitude

The Root Mean Square (RMS) seismic amplitude volume time slices were used to study the overall variations in the acoustic signature. The attribute has limited use as the signal can represent many geological features. It has better application in combination with other attributes, or regular seismic amplitude to detect pockmarks and traces of shallow gas. An RMS amplitude seismic time slice between Q3.2 and Q3.1 horizons is shown in Figure 4.57. Pockmarks are observed on what appears to be a bed of high positive amplitude sediments. The red signal in the northwest areas correlates to where most of the pockmarks has been observed. A wavy boundary is observed in contrast to the blue amplitude. The wavy pattern reflects a wave-dominated front. To the northwest of the ØFC, red spots of high amplitudes emerge in the eroded areas. Some of them have been verified to be pockmarks and can be linked to the observations in Figure 4.53. The amplitudes on the ØFC footwall are more challenging to interpret because of the truncation and erosion.

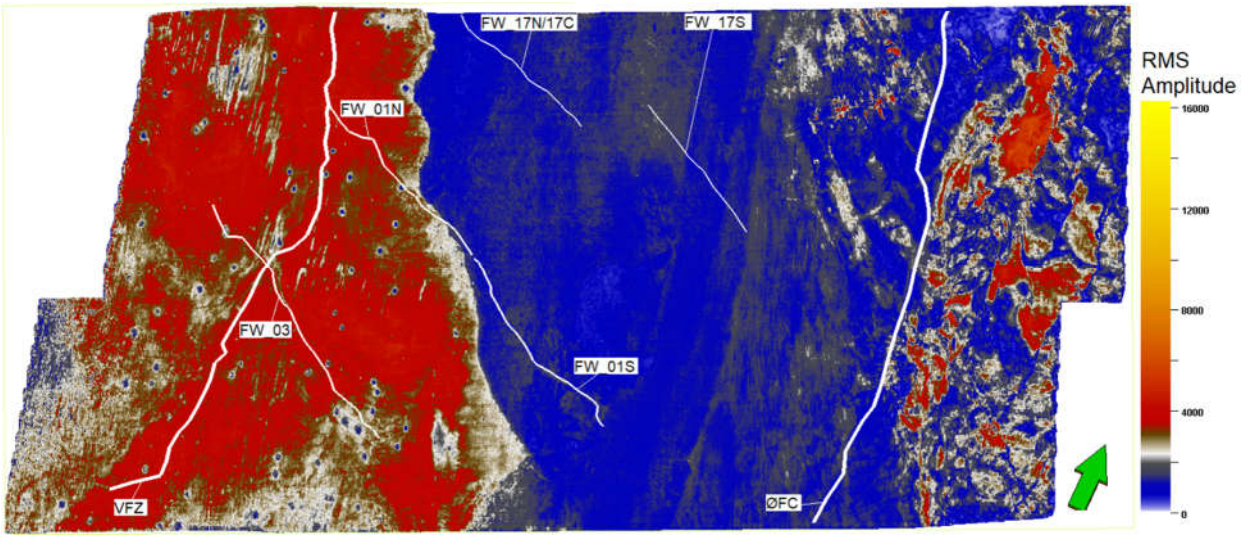

Figure 4.57: RMS amplitude seismic time slice at -616ms, between Q3.2 and Q3.1 horizons. Major faults from deeper levels have been projected up. A wavy pattern is observed in contrast to the blue amplitude.

Chapter 5

5 Discussion

This study aims to analyse the distribution of pockmarks on the seabed and within the subsurface in order to identify the possible connections to deeper geological features. Since the pockmarks are indicators of fluid seepage, the understanding of where seepage has occurred in the past is also essential in the risk assessment of a deeper CO_2 storage reservoir in the future.

In the next sections, results are gathered and discussed before a model of the paleo-seepage is proposed.

5.1 Discussion of results

5.1.1 Quaternary horizons

The seismic horizons interpreted in this study represent different time stages during the Quaternary in the Smeaheia area of the North Sea and can be broken up into three intervals; 1) Q3.2-Q3.1, 2) Q2.2-Q2.1, and 3) Q1.2-Seabed intervals. The horizons will be discussed in order in which they appear in stratigraphic chart in Figure 2.9, which was extrapolated from Quaternary stratigraphy in the Troll field and based on work by Sejrup et al., (1995) and Forsberg et al., (2007).

Q3.2 -Q3.1

There are two horizons in the Smeaheia area that represent stratigraphic surfaces in the lower part of the Quaternary interval; 1) the Q3.2 URU horizon, which is the surface of the Upper Regional Unconformity (URU) and 2) the Q3.1 horizon. In Chapter 4.1, a calculation using the schematic cross-sections indicates that the URU is tilted with a northeast dip of approximately 1°or 2°. A characteristic likely inherited from the uplift of the Norwegian mainland and tilting of the Horda Platform and in the northern North Sea in the Quaternary (Rise and Rokoengen, 1984; Faleide et al., 2015). Based on the stratigraphic chart in Figure 2.9, most of the sediments between the Q3 layers are glacial marine or till in unit L6.

The presence of a till unit L6 with normal marine sediments deposited above it in L5 (see Figure 2.9) indicates the end of an ice age. Sejrup et al., (1995) credited this till to the Fedje glaciation 1,1 Myr ago with the corresponding warm event of the Radøy interglacial (see Figure 2.6), but as explained in chapter 2 the age of URU remains disputed, with suggestion of age around 0.5 Ma (Ottesen et al., 2018; Løseth & Nygård, 2019). The latter age suggestion corresponds to the Elsterian stage glaciation from 430-450 ka (see Figure 2.6). Hence, the till and normal marine unit above the URU can be correlated to the infill of the North Sea Basin after the Elsterian glaciation period. Regardless of the age of the URU, both studies suggest a subsequent warmer period.

Q2.2 -Q2.1

The stratigraphic column in Figure 2.9 suggests that the middle portion of the Quaternary interval at Smeaheia is comprised of a glacial till deposit below horizon Q2.2 with another deposit of normal marine sediments up to the Q2.1 horizon. These Q2 layers may represent the bottom (Q2.2) and top (Q2.1) of the L3 unit. The L3 unit represents a wide range of environments strongly glacial influenced to normal marine deposits, while the unit L4 below is the till (Sejrup et al., 1995). Hence, this thesis suggests the Q2.2 horizon served as a transition to a period of glacier fluctuations in the history of the Quaternary interval.

Forsberg et al., (2007) used reconstructions of the pressure and temperature history based on sedimentation history and sea-level in the Troll area and suggested the L3 unit was deposited during the penultimate glaciation (interpreted as the Weichselian glaciation). The timing complies with Sejrup et al., (1995), but Forsberg et al., (2007) appears to suggest L4 and L3 (called unit 3B and 3A in the study) as a type of till. Their interpretation suggest that glacial erosion surfaces are over-consolidated due to glacial compaction (Forsberg et al., 2007). The pockmark formation model in Forsberg et al., (2007) also suggested high-pressure water under the glacier during formation of L3 and L2. The model is based on pressure and temperature calculations, it rendered the possibility of gas hydrates under the L3 unit as sediment samples showed high gas concentrations under the till unit and low gas concentrations above (L4 and L3 in Figure 2.9). The model is reasonable and will later be adapted to present a pockmark formation model at the Smeaheia area.

Q1.2 to Seabed

The upper portion of the Quaternary interval at Smeaheia consists of Q1.2, Q1.1 and the Seabed horizons. The stratigraphic chart in Figure 2.9 shows Q1.2 as the top of till unit L2. According to Forsberg et al., (2007) and Amundsen et al., (1985), units L2 and L1 are normally consolidated, and Sejrup et al., (1995) dated the surface to ~15 ka BP with geochronological amino acid analysis. The Q1.2 horizon represents the deposition from the end of the Last Glaciation Maximum (LGM). Recent reconstruction of the ice margins in the Norwegian Channel by Svendsen et al., (2015) and Morén et al., (2018) suggests the Troll and the Smeaheia areas were ice-free around 20-18.5 kyr BP. The ice margin models in Figure 2.7 show the areas in the Norwegian Channel, south of Utsira, were still covered by ice and probably funneled icebergs north up through the channel.

Forsberg et al., (2007) reported buried pockmarks found just below the seabed, which corresponds to the Q1.1 horizon. This horizon was radiocarbon dated to maximum 13 kyr at the Troll field, and methane-derived authigenic carbonates (MDAC) in pockmarks at the seabed were dated by U/Th to ~11 kyr BP and formation at the end of the last glaciation (Younger Dryas glaciation). Forsberg and colleagues (2007) also suggested that seabed pockmarks at Troll field formed during the removal of top sediments as no net sedimentation inside the pockmarks has occurred since then. One possible interpretation of this event could be that buoyant fluids used the established distribution channels and pockmarks to migrate through the top of the Quaternary interval at the time. This concept may also be useful for explaining the formation of pockmarks in the Seabed horizon within the nearby Smeaheia area.

5.1.2 Pockmarks in the Quaternary interval

5.1.2.1 Q3.2 to Q3.1

Time structure maps of Q3.2 and Q3.1 horizons (Figure 4.5 and Figure 4.6) show the superimposed faults and subcrops within the strata underlying the URU surface. They indicate that buried pockmarks are present along boundaries where Top Sele Formation, Top Lista Formation and Top Shetland Group subcrop, the polygonal faults, north of the faults FW_17C and FW_17S, and in the north side of the eroded areas. The general impression is that the

combination of polygonal faults, the WNW-SSE deeper faults and subcrops have been favourable as fluid pathways.

Isochron map of Q3.2 in Figure 4.11 shows the thickness of the overburden under the URU. Since the underlying sedimentary layers appear to dip to the west, any fluids originating from greater depths likely migrated in an eastward path towards the URU. This applies only to slow-moving and stationary migrations as high-pressure seepage would choose a vertical path to the above stratum. The thickness between the Q3.1 and Q3.2 horizons (Figure 4.12) shows that accommodation for Q3.1 deposition was relatively uniform, and that larger pockmarks are concentrated past the northeast of the Top Lista Formation subcrop (red pockmarks). Still, the horizons only retain a partial insight into the paleo fluid flow as gas seepage can also occur without the formation of pockmarks (Judd & Hovland, 2007).

The kernel density map in Figure 4.18 and Figure 4.19 indicates a local pockmark density of eight pockmarks per km² in the upper northeast corner, the southwest corner and the eroded areas west of the ØFC. The local densities in the corners may indicate that seepage is migrating from the outside of the survey area, while seepage in the eroded areas is above the north side of injection prospect Beta. The largest more significant pockmarks are poorly represented in the maps, which demonstrates the limitations of presenting densities based on distances. Such methods may be weighted with pockmarks sizes in the future to illustrate better paleo-seepage throughput. The most cogent argument for using these methods is still the point mentioned in section 1.2.4.2. , where Hovland & Judd (1988) explains the first pockmarks through a surface as gas-drainage cells, and that both pockmark density and cell sizes depend on the established migration path. This gas-drainage cell principle may have been the mechanism on how the Troll field and the Smeaheia seabed pockmarks emerged (section 5.2.1 and Forsberg et al., 2007)

Pockmark statistics derived from the interpretations show that sizes can be subdivided into at least three groups. A comparison of population 1 pockmarks on all horizons in Figure 4.37 and 4.38, and the fact that population 1 has the most numerous pockmarks of the groups imply these are more probable to emerge than population 2 and perhaps also the residual grouped pockmarks. Results in section 4.3.4.8 showed that population 1 was in the range of 60-95 m in width and with 5000-13000 m² in surface area. A comparison with other studies is not available for buried pockmarks, but population 1 are present on all horizons throughout

the Quaternary interval. In Judd & Hovland (2007) a collection of studies from the North Sea and the Norwegian Trench shows the general pockmark size was 50-100 m in diameter, which correlates with the general size trend of population 1 in this study. Normality test assumed all population 1 groups not to be from a normal distribution, but the reason for this is probably the at least bimodal distribution. Observing the population 2 pockmarks, they are larger and those from horizon Q3.1 are the largest among these population (seen in Figure 4.39 and Figure 4.40). To account for the size discrepancy, either a geological event created an eruption and directly allowed seepage from below the URU or fluids were temporary stored between horizon Q3.1 and Q3.2, and the event triggered the eruption of the confined fluids. The residual group pockmarks are either rare event pockmarks, or could be a precursor to some population 2 pockmarks

Glacial effects on Q3.2 show two sets in Figure 4.43. The magenta set, interpreted as MSGL, is probably inherited from the carving of the URU and the Norwegian Channel as they only are found in the eroded area, while the white lineations are interpreted as plough marks from drifting icebergs. These plough marks are also seen just below Q3.1, but not on the surface. These sporadic traces of icebergs can be interpreted as the end of a glacier period and the retreat of the Fennoscandian Ice Sheet. Comparing glacial direction with the direction of the longest axis on pockmarks in table 4.21 shows there may be a correlation between pockmark formation of population 1 and 2 with the glacial marks on Q3.2. The pockmarks direction marked with blue (NE-SW) has no connection with glacier movement but could be pockmark alignment to local ocean currents (Judd & Hovland, 2007).

5.1.2.2 Q2.2 to Q2.1

Time structure maps of Q2.1 (Figure 4.7) show the superimposed faults and subcrops within the strata underlying the URU surface. The surface likely represents the upper boundary of succession of till followed by normal marine deposits. This Q2.1 horizon is the surface with most mapped pockmarks, which may relate to the glacier influence as glacial marks are ubiquitous throughout the horizon. The largest pockmarks are from the residual group (orange colours), which appears to cluster above polygonally faulted areas between faults FW_03 and FW_01N. Pockmarks from population 2 (black colour) are dispersed between the subcrops of Top Lista Formation and Top Shetland Group.

The isochron thickness map in Figure 4.13 shows the thickness of the sediments between Q2.1 and Q3.1. The cool colours show the thickest regions within the interval, which thins out towards the ØFC footwall.

The kernel density map in Figure 4.20 indicates a local pockmark density of 15-18 pockmarks per km² in the lower southwest corner. Densities of 10-12 pockmarks per km² are observed along the Top Shetland Group subcrop. There is an intriguing absence of pockmarks just east the lower southwest corner of the GN1101 survey. The shape formed by the absence of pockmark resembles the grounding line zone seen in glacial mark map Figure 4.44. The pattern could be coincidental, but if an ice sheet was grounded, then it could have compacted the sediments locally, and lowering the permeability and porosity.

Pockmark statistics show the Q2.1 horizon has three populations and one residual group of pockmarks. Table 4.8 and Table 4.9 show a distribution where the largest pockmarks have been grouped in the residuals. The surface areas in Table 4.9 suggest that these pockmarks disturbed a substantial amount of sediment from the seabed when they formed. The size statistics of population 2 from Q2.1 horizon are similar to population 2 pockmarks on Q1.2 horizon, which may infer that a similar amount of fluids were expelled at the time these two horizon surfaces formed. Forsberg et al., (2007) proposed methane hydrates had accumulated within unit (L3) and below Q2.1 horizon and were responsible for the pockmark formation of Q1.1 horizon through the Q1.2 (top unit L2). In this scenario, the pockmarks of the residual and population 2 groups could be interpreted as ones formed during significant geological events. There is, however, no need to imply gas hydrates in L4-L3 to explain pockmark formation at Smeaheia. Tertiary subcrops and numerous shallow polygonal faults below the URU could provide fluid pathways into a temporary reservoir under the Q2.2 horizon (L4 unit). While the smaller pockmarks in population 1 are formed in the wake the significant events, population 0 pockmarks are only ones observed on the Q2.1 horizon, and they are not normally distributed. Plots in Figure 6.6A and the Q-Q plots suggest that the outliers biased the population, or they are features from other geological processes, for example dropstones from glaciers (Judd & Hovland, 2007).

Glacial marks show trends in the northwest and north-northwest directions, which indicate glacial movements towards the North Sea Fan (see Figure 2.7). Marks to the northeast of the GN1101 survey appear to be MSGL in Figure 4.45, while those in centre and southwest could be plough marks. Table 4.21 shows that pockmarks population 0 align with the northwest

glacial movements. The rest of the pockmarks are aligned to northeast-southwest, which was likely the dominant ocean current direction.

1.1.1.1 Q1.2 to Seabed

The pockmarks in time structure maps of Q1.2, Q1.1 and Seabed horizons (figures 4.8, 4.9 and 4.10) are dominated by those of population 1. Population 2 and the residual group are generally observed over the ØFC footwall. Pockmarks in the latter category are also observed west of the ØFC and may be locations with established pathways for buoyant fluid migration. Isochron thickness maps in figures 4.15 and 4.16 show there was little sediment infill, except in the footwall of the ØFC. Cluster analysis in section 4.3.1 conducted on of the Q1.1 and Seabed horizon pockmarks infer a clustered pattern. As comparison to other research in section 1.2.3.4 by Mazzini et al., (2017), ANN results provided a distance of 173 m, compared to an expected value of 152.4 m, and a dispersed pattern. Mazzini and colleagues (2017) conducted their study on an area of 296 km² with 3189 pockmarks. The Smeaheia area is 394 km² and has a total of 679 mapped pockmarks on the Seabed horizon. This result is surprising considered that the Troll region is one of the World's largest pockmark fields (Mazzini et al., 2017). The use of high-resolution bathymetry at Smeaheia area would likely have given a higher pockmark count, but maybe when studying pockmark distribution, the level of details from the seabed surface may be less important. Resolution is essential in the study of pockmark shapes, as seen in section 4.3.4., so the limitations of conventional 3D seismic resolution has advantages and disadvantages. Table 5.1 shows a comparison of different pockmarks densities done with different methods.

Table 5.1: Pockmark densities on seabed surfaces in the North and Barents seas. The study by Ostanin et al., (2013) is the only conducted in the Barents Sea. The others are conducted in the Norwegian Channel, the North Sea.

Research	Density per km²	Pockmark count	Method
Hovland (1981)	40-50		Side-scan sonar, sub bottom prof.
Hovland (1982)	30		Side-scan sonar, deep-towed boomer
Tjelta et al., (2007)	15-25		Bathymetry, ROV
Ostanin et al., (2013)	~3	297	3D seismic survey
Mazzini et al., (2017)	~12	3189	Bathymetry, ROV
This thesis	~1.72	679	3D seismic survey

Density maps in Figure 4.20 to Figure 4.22 show high density counts mainly over the polygonally faulted areas and the Top Lista Fm. and Top Shetland Group subcrops. This areal pockmark distribution suggests that buoyant fluids migrated up through the Quaternary interval in this area once they reach the URU from greater depths. In other words, it could have been the preferred zone of migration, as most buried pockmarks appear to have emerged here over time. Fewer glacial marks are observed on these younger surfaces, which is logical considering they formed at the end of the LGM. Table 4.21 for shows correlation between glacial movement trends and pockmark locations for both Q1.2 and Q1.1 horizons. This correlation may show that glaciers played a vital role in triggering pockmarks formation at Smeaheia.

1.1.1.2 Below the URU

The qualitative observations from seismic data in section 4.5 show there is clear evidence for faults and polygon faults influencing fluid movement or acting as fluid pathways. More research is needed to determine fluid sources because it may be that not all fluid escape features are from the same source. In general, fluids likely utilize westward-dipping porous and permeable Tertiary sediments to accommodate horizonal migration from the west. However, it appears that the WNW-SSE trending faults in combination with subcrops and polygonal faults are the potential leakage pathway that might be risks for future CO_2 storage at Smeaheia there. This applies especially for the Alpha prospect closure, while a clear paleo-seepage over the Beta prospect closure indicates that storage in this reservoir is not recommended.

1.1.1.3 Below the URU

The qualitative observations from seismic data in section 4.5 show there is clear evidence for faults and polygon faults acting as fluid pathways. More research is needed to determine fluid sources because the impression is that not all seepage traces are from the same source. It appears that the WNW-SSE trending faults in combination with subcrops and polygonal faults are the potential leakage pathway that might be risks for future CO_2 storage at Smeaheia there. This applies especially for the Alpha prospect closure, while the clear paleo-seepage over the Beta prospect closure indicates that storage in this reservoir is not recommended.

Given that most of the signs of leakage are linked to the west-dipping strata in the subsurface, from the Top Cromer Knoll Group and over the Top Sele Formation horizon, the primary

source for buoyant fluids must be to the west of the Smeaheia area. There are a few indications of seepage originated from locations outside the GN1101 survey in the north and south. Pockmark formation and seepage on the ØFC footwall are separated from the rest of the Smeaheia area and assumed from the faults east of the ØFC.

Chapter 6

6 Conclusions

This study has investigated pockmarks in the Quaternary sediments above the Smeaheia area in the North Sea with the use of 3D seismic data and statistics. Pockmark distribution on the seabed and within the Quaternary interval tells a story of periodic fluid flow since the formation of the Upper Regional Unconformity. Seven horizons have been studied and form three event units: The lower units comprising of Q3.2 and Q3.1 horizons, the middle units comprising of Q2.2 and Q2.1 horizon, and the top units comprising of Q1.2, Q1.1 and Seabed horizon.

6.1 Summary of results and conclusions

- The Upper Regional Unconformity (URU) is tilted with a northeast dip of approximately 1°or 2°.
- The Q3.2 URU and the Q3.1 horizon above it exhibit buried pockmarks. The pockmark density is higher to the northwest of where Top Lista Formation subcrop. The subsurface, below the URU, is dominated by polygonal faults at this high-density area.
- Bright spots are observed over the Q3.2 URU horizon and linked to polygonal and significant faults in the subsurface. The WNW-SSE trending FW_01N, FW_03, FW_17C and faults in the vicinity have
- Pockmarks on the Q3.1 horizon have in average larger sized pockmarks that the rest of the horizon. A significant event may have triggered these in the period shortly after the formation of the URU
- Q2.1 horizon is affected by glaciers and exhibits the highest frequency of pockmarks. The combination of fluid accumulation below Q2.1 and Q2.2 may have been triggered by the glacial erosion or glacial unloading.
- Pockmarks are distributed in three groups. The two groups with the largest pockmarks may be forming under the significant events, while the last group with smaller pockmarks form in the wake of these events.

- Pockmarks in the top part form probably by fluid storage in a temporary reservoir under Q2.1 horizon
- Pockmarks density on the seabed surface is approximately 1.7 per km². This count is lower than the pockmarks field in the Troll region.

Bibliography

Aldstadt, J. (2010). *Spatial Clustering*. (M. M. Fischer & A. Getis, Eds.). Berlin, Heidelberg: Berlin, Heidelberg: Springer Berlin Heidelberg. https://doi.org/10.1007/978-3-642-03647-7_5

Amundsen, T., Lunne, T., Christophersen, H. P., Bayne, J. M., & Barnwell, C. L. (1985). Advanced deep-water soil investigation at the Troll East Field. In *Offshore Site Investigation* (pp. 165–186). Springer.

Anell, I., Thybo, H., & Rasmussen, E. (2012). A synthesis of Cenozoic sedimentation in the North Sea. *Basin Research*, *24*(2), 154–179. https://doi.org/10.1111/j.1365-2117.2011.00517.x

Baddeley, A., Rubak, E., & Turner, R. (2015). *Spatial point patterns : methodology and applications with R*. Retrieved from https://www.crcpress.com/Spatial-Point-Patterns-Methodology-and-Applications-with-R/Baddeley-Rubak-Turner/p/book/9781482210200

Baddeley, A., & Turner, R. (2005). spatstat : An R Package for Analyzing Spatial Point Patterns. *Journal of Statistical Software*, *12*(6), 1–42. https://doi.org/10.18637/jss.v012.i06

Besag, J. (1977). Discussion following Ripley. Journal of Royal Statistical Society.

Bjørlykke, K. (2015a). Introduction to Petroleum Geology. In K. Bjørlykke (Ed.), *Petroleum Geoscience: From Sedimentary Environments to Rock Physics* (2nd ed., pp. 1–29). Berlin, Heidelberg: Springer Berlin Heidelberg. https://doi.org/10.1007/978-3-642-34132-8_1

Bjørlykke, K. (2015b). Petroleum Migration. In K. Bjørlykke (Ed.), *Petroleum Geoscience: From Sedimentary Environments to Rock Physics* (2nd ed., pp. 373–384). Berlin, Heidelberg: Springer Berlin Heidelberg. https://doi.org/10.1007/978-3-642-34132-8_15

Bondarev, V. N., Rokos, S. I., Kostin, D. A., Dlugach, A. G., & Polyakova, N. A. (2002). Underpermafrost accumulations of gas in the upper part of the sedimentary cover of the Pechora Sea. *Geologiya I Geofizika*, *43*(7), 587–598.

Boulton, G. S., Dongelmans, P., Punkari, M., & Broadgate, M. (2004). Evidence of European ice sheet fluctuation during the last glacial cycle. *Developments in Quaternary Science*, *2*(1), 441–460. https://doi.org/10.1016/S1571-0866(04)80095-2

Brown, A. R. (2004). Interpretation of Three-Dimensional Seismic Data Sixth Edition. *AAPG Memoir 42 SEG Investigations in Geophysics, No. 9*.

Busch, A., & Müller, N. (2011). Determining CO2 /brine relative permeability and capillary threshold pressures for reservoir rocks and caprocks: Recommendations for development of standard laboratory protocols. *Energy Procedia*, *4*(C), 6053–6060. https://doi.org/10.1016/j.egypro.2011.02.610

Cartwright, J., Huuse, M., & Aplin, A. (2007). Seal bypass systems. *AAPG Bulletin*.

https://doi.org/10.1306/04090705181

Charpentier, A. (2018). *The SAGE Encyclopedia of Educational Research, Measurement, and Evaluation*. (B. B. Frey, Ed.). Thousand Oaks, : SAGE Publications, Inc. . https://doi.org/http://dx.doi.org/10.4135/9781506326139

Christiansson, P., Faleide, J. I., & Berge, A. M. (2000). Crustal structure in the northern North Sea: An integrated geophysical study. *Geological Society Special Publication*, *167*(1), 15–40. https://doi.org/10.1144/GSL.SP.2000.167.01.02

Clark, P. J., & Evans, F. C. (1954). Distance to Nearest Neighbor as a Measure of Spatial Relationships in Populations. *Ecology*, *35*(4), 445–453. https://doi.org/10.2307/1931034

Clark, P. U., Dyke, A. S., Shakun, J. D., Cartson, A. E., Clark, J., Wohlfarth, B., … McCabe, A. M. (2009). The last glacial maximum. *Science*, *325*(5941), 710. https://doi.org/10.1126/science.1172873

Clausen, J. A., Gabrielsen, R. H., Reksnes, P. A., & Nysæther, E. (1999). Development of intraformational (Oligocene–Miocene) faults in the northern North Sea: influence of remote stresses and doming of Fennoscandia. *Journal of Structural Geology*, *21*(10), 1457–1475. https://doi.org/10.1016/S0191-8141(99)00083-8

Craig, R. F. (2004). *Craig's soil mechanics* (7th ed.). London: Spon Press.

Crawley, M. J. (2012). *The R Book: Second Edition*. https://doi.org/10.1002/9781118448908

Denham, L. R., & Sheriff, R. E. (1981). What is Horizontal Resolution? *AAPG Bulletin*, *65*(10th Annual Convention Proceedings), 119–134. https://doi.org/10.1306/2F919D4B-16CE-11D7-8645000102C1865D

Diggle, P. (2014). *Statistical analysis of spatial and spatio-temporal point patterns*. *Monographs on statistics and applied probability*. https://doi.org/10.1017/CBO9781107415324.004

Domínguez, R. (2007). Structural evolution of the Penguins Cluster, UK northern North Sea. *Geological Society Special Publication*. https://doi.org/10.1144/SP292.2

Dowdeswell, J. A., & Ottesen, D. (2013). Buried iceberg ploughmarks in the early Quaternary sediments of the central North Sea: A two-million year record of glacial influence from 3D seismic data. *Marine Geology*, *344*(C), 1–9. https://doi.org/10.1016/j.margeo.2013.06.019

Duffy, O. B., Bell, R. E., Jackson, C. A. L., Gawthorpe, R. L., & Whipp, P. S. (2015). Fault growth and interactions in a multiphase rift fault network: Horda Platform, Norwegian North Sea. *Journal of Structural Geology*, *80*, 99–119. https://doi.org/10.1016/j.jsg.2015.08.015

Emiliani, C. (1955). Pleistocene Temperatures. *The Journal of Geology*, *63*(6), 538–578. https://doi.org/10.1086/626295

Emiliani, C. (1966). Paleotemperature Analysis of Caribbean Cores P6304-8 and P6304-9 and

a Generalized Temperature Curve for the past 425,000 Years. *The Journal of Geology*, *74*(2), 109–124. https://doi.org/10.1086/627150

Emiliani, C. (1970). Pleistocene Paleotemperatures. *Science*, *168*(3933), 822–825. https://doi.org/10.1126/science.168.3933.822

Færseth, R. B. (1996). Interaction of Permo-Triassic and Jurassic extensional fault-blocks during the development of the northern North Sea. *Journal of the Geological Society*, *153*(6), 931–944. https://doi.org/10.1144/gsjgs.153.6.0931

Færseth, R. B., Gabrielsen, R. H., & Hurich, C. A. (1995). Influence of basement in structuring of the North Sea Basin, offshore southwest Norway. *Norsk Geologisk Tidsskrift*, *75*(2–3), 105–119.

Faleide, J. I., Bjørlykke, K., & Gabrielsen, R. H. (2015). Geology of the norwegian continental shelf. In K. Bjørlykke (Ed.), *Petroleum Geoscience: From Sedimentary Environments to Rock Physics* (2nd ed., pp. 603–635). Berlin, Heidelberg: Springer Berlin Heidelberg. https://doi.org/10.1007/978-3-642-34132-8_25

Faleide, J. I., Kyrkjebø, R., Kjennerud, T., Gabrielsen, R. H., Jordt, H., Fanavoll, S., & Bjerke, M. D. (2002). Tectonic impact on sedimentary processes during Cenozoic evolution of the northern North Sea and surrounding areas. *Geological Society, London, Special Publications*, *196*(1), 235–269. https://doi.org/10.1144/GSL.SP.2002.196.01.14

Fichler, C., Henriksen, S., Rueslaatten, H., & Hovland, M. (2005). North Sea Quaternary morphology from seismic and magnetic data: indications for gas hydrates during glaciation? *Petroleum Geoscience*, *11*(4), 331–337.

Forsberg, C. F., Plank, S., Tjelta, T. I., Svano, G., Strout, J. M., & Svensen, H. (2007). Formation of pockmarks in the Norwegian Channel. In *OFFSHORE SITE INVESTIGATION AND GEOTECHNICS, Confronting New Challenges and Sharing Knowledge*. Society of Underwater Technology.

Gabrielsen, R. H., Faleide, J. I., Pascal, C., Braathen, A., Nystuen, J. P., Etzelmuller, B., & O'Donnell, S. (2010). Latest Caledonian to Present tectonomorphological development of southern Norway. *Marine and Petroleum Geology*, *27*(3), 709–723. https://doi.org/10.1016/j.marpetgeo.2009.06.004

Gabrielsen, R. H., & Koestler, A. G. (1987). Description and structural implications of fractures in late Jurassic sandstones of the Troll Field, northern North Sea. *Norsk Geologisk Tidsskrift*, *67*, 371–381.

Gassnova. (2015). Mandate and letter of assignment. Retrieved 20 July 2018, from http://www.gassnova.no/en/about-us/mandate

Getis, A. (2005). *Geographical information systems : principles, techniques, management, and applications. Chapter 16 - Spatial statistics*. (P. A. Longley, M. F. Goodchild, D. J. Maguire, & D. W. Rhind, Eds.) (2nd ed., a). Hoboken, N.J: Wiley.

Gibbard, P. L., & Cohen, K. M. (2008). Global chronostratigraphical correlation table for the last 2 . 7 million years. *Episodes*, *31*, 243–247.

https://doi.org/10.1029/2001PA000725.Ding

Gimond, M. (2019). Intro to GIS and Spatial Analysis. In *Intro to GIS and Spatial Analysis* (2019th ed.). Waterville, Maine, USA: Colby College. Retrieved from https://mgimond.github.io/Spatial/index.html

Greig-Smith, P. (1952). The Use of Random and Contiguous Quadrats in the Study of the Structure of Plant Communities. *Annals of Botany*, *16*(62), 293–316.

Grubbs, F. E. (1950). Sample Criteria for Testing Outlying Observations. *The Annals of Mathematical Statistics*, *21*(1), 27–58.

Hellevang, H. (2015). Carbon capture and storage (CCS). In K. Bjørlykke (Ed.), *Petroleum Geoscience: From Sedimentary Environments to Rock Physics* (2nd ed., pp. 591–602). Berlin, Heidelberg: Springer Berlin Heidelberg. https://doi.org/10.1007/978-3-642-34132-8_24

Hillman, J. I. T., Gorman, A. R., & Pecher, I. A. (2015). Geostatistical analysis of seafloor depressions on the southeast margin of New Zealand's South Island — Investigating the impact of dynamic near seafloor processes on geomorphology. *Marine Geology*, *360*, 70–83. https://doi.org/10.1016/j.margeo.2014.11.016

Hjelstuen, B. O., Nygård, A., Sejrup, H. P., & Haflidason, H. (2012). Quaternary denudation of southern Fennoscandia – evidence from the marine realm. *Boreas*, *41*(3), 379–390. https://doi.org/10.1111/j.1502-3885.2011.00239.x

Hjelstuen, B. O., Petter Sejrup, H., Haflidason, H., Nygård, A., Ceramicola, S., & Bryn, P. (2005). Late Cenozoic glacial history and evolution of the Storegga Slide area and adjacent slide flank regions, Norwegian continental margin. *Marine and Petroleum Geology*, *22*(1), 57–69. https://doi.org/10.1016/j.marpetgeo.2004.10.002

Hovland, M. (1981). Characteristics of pockmarks in the Norwegian Trench. *Marine Geology*, *39*(1–2), 103–117. https://doi.org/10.1016/0025-3227(81)90030-X

Hovland, M. (1982). Pockmarks and the Recent geology of the central section of the Norwegian Trench. *Marine Geology*, *47*(3–4), 283–301. https://doi.org/10.1016/0025-3227(82)90073-1

Hovland, M., & Judd, A. (1988). *Seabed pockmarks and seepages : Impact on geology, biology and the marine environment.* London: Graham & Trotman.

Isaksen, D., & Tonstad, K. (1989). A Revised Cretaceous and Tertiary lithostratigraphic nomenclature for the Norwegian North Sea. Stavanger: Oljedirektoratet.

Jonassen, P. (2015). *Fault Analysis Based on 3D Seismic Data from the Northern Horda Platform*.

Judd, A., & Hovland, M. (2007). *Seabed fluid flow : the impact on geology, biology, and the marine environment*. (M. Hovland, Ed.). Cambridge: Cambridge University Press.

King, E. L., Haflidason, H., Sejrup, H. P., & Løvlie, R. (1998). Glacigenic debris flows on the

North Sea Trough Mouth Fan during ice stream maxima. *Marine Geology*, *152*(1), 217–246. https://doi.org/10.1016/S0025-3227(98)00072-3

King, L. H., & MacLean, B. (1970). Pockmarks on the Scotian Shelf. *Bulletin of the Geological Society of America*. https://doi.org/10.1130/0016-7606(1970)81[3141:POTSS]2.0.CO;2

Kinn, S., Foldøy, P., Pettersen, K., Ramstad, H., Hansen, T. H., & Goldsmith, P. J. (1997). *PL 205 Licence Group Well 32/4-1: Final well report*. Retrieved from www.npd.no/engelsk/cwi/pbl/wellbore_documents/2918_32_4_1_COMPLETION_REPORT_AND_COMPLETION_LOG.pdf

Kroese, D. P., Brereton, T., Taimre, T., & Botev, Z. (2014). Why the Monte Carlo method is so important today. *WIREs Comput Stat 2014*, (6), 386–392. https://doi.org/doi: 10.1002/wics.1314

Kvenvolden, K. A., Lilley, M. D., Lorenson, T. D., Barnes, P. W., & McLaughlin, E. (1993). The Beaufort Sea continental shelf as a seasonal source of atmospheric methane. *Geophysical Research Letters*, *20*(22), 2459–2462.

LaMorte, W. W. (2016). Central Limit Theorem. Retrieved 5 March 2019, from http://sphweb.bumc.bu.edu/otlt/MPH-Modules/BS/BS704_Probability/BS704_Probability12.html

Lervik, K. (2006). Triassic lithostratigraphy of the northern North Sea Basin. *Norsk Geologisk Tidsskrift*, *86*(2), 93.

Løseth, H., Gading, M., & Wensaas, L. (2009). Hydrocarbon leakage interpreted on seismic data. *Marine and Petroleum Geology*. [Guildford, Surrey] : https://doi.org/10.1016/j.marpetgeo.2008.09.008

Løseth, H., & Nygård, A. (2019). Geological Society of Norway - Abstracts and Proceedings: In H. A. Nakrem & A. M. Husås (Eds.), *Controversies on ages of Quaternary sediments in the Northern North Sea* (pp. 56–57). Trondheim: Norsk Geologisk Forening c/o Norges Geologiske Undersøkelse. Retrieved from https://www.geologi.no/konferanser/vinterkonferanser/item/984-abstract-vk19

Mangerud, J., Gyllencreutz, R., Lohne, Ø., & Svendsen, J. I. (2011). Glacial history of Norway. *Developments in Quaternary Science*, *15*, 279–298. https://doi.org/10.1016/B978-0-444-53447-7.00022-2

Mazzini, A., Svensen, H. H., Forsberg, C. F., Linge, H., Lauritzen, S. E., Haflidason, H., … Tjelta, T. I. (2017). A climatic trigger for the giant Troll pockmark field in the northern North Sea. *Earth and Planetary Science Letters*. https://doi.org/10.1016/j.epsl.2017.02.014

Mazzini, A., Svensen, H. H., Planke, S., Forsberg, C. F., & Tjelta, T. I. (2016). Pockmarks and methanogenic carbonates above the giant Troll gas field in the Norwegian North Sea. *Marine Geology*, *373*, 26–38. https://doi.org/10.1016/j.margeo.2015.12.012

Ministry of Petroleum and Energy. (2014, December 14). The Government's carbon capture

and storage strategy. Retrieved 20 July 2018, from https://www.regjeringen.no/en/topics/energy/carbon-capture-and-storage/the-governments-carbon-capture-and-storage-strategy/id2353948/

Ministry of Petroleum and Energy. (2016a). *Feasibility study for full-scale CCS in Norway Contents*. Retrieved from https://www.gassnova.no/en/Documents/Feasibilitystudy_fullscale_CCS_Norway_2016.pdf

Ministry of Petroleum and Energy. (2016b, January 4). Initiates feasibility study on subsea CO2 storage. Retrieved 20 July 2018, from https://www.regjeringen.no/en/aktuelt/statoil-skal-utgreie-co2-lager-pa-norsk-kontinentalsokkel/id2469150/

Morén, B. M., Sejrup, H. P., Hjelstuen, B. O., Borge, M. V, & Schäuble, C. (2018). The last deglaciation of the Norwegian Channel–geomorphology, stratigraphy and radiocarbon dating. *Boreas*, *47*(1), 347–366.

NIST. (2013). Grubbs' Test for Outliers. Retrieved 2 March 2019, from https://www.itl.nist.gov/div898/handbook/eda/section3/eda35h1.htm

Nolen-Hoeksema, R. (2014). Defining permeability. *Oilfield Review Autumn*, *26*(no.3.), 63–64. Retrieved from https://www.slb.com/-/media/Files/resources/oilfield_review/ors14/aut14/define_perm.pdf?la=en&hash=E6E27C2A079A615DE5E2CE24503E0AB03C88480B

NPD. (n.d.). Norwegian Petroleum Directorate FactMaps. Retrieved 21 July 2018, from http://gis.npd.no/factmaps/html_21/

NPD. (2011). *CO_2 storage Atlas : Norwegian North Sea*. (E. K. Halland, W. T. Johansen, & F. Riis, Eds.). Stavanger: Norwegian Petroleum Directorate.

NPD. (2014). Norwegian Petroleum Directorate - Geology of the North Sea. Retrieved 28 October 2018, from http://www.npd.no/Global/Norsk/3-Publikasjoner/Rapporter/Samleatlas/Figurer-Figures/Chapter-4/Fig-4-002.pdf

Nygård, A., Sejrup, H. P., Haflidason, H., & Bryn, P. (2005). The glacial North Sea Fan, southern Norwegian Margin: architecture and evolution from the upper continental slope to the deep-sea basin. *Marine and Petroleum Geology*, *22*(1), 71–84. https://doi.org/10.1016/j.marpetgeo.2004.12.001

Nygard, A., Sejrup, H. P., Haflidason, H., Lekens, W. A. H., Clark, C. D., & Bigg, G. R. (2007). Extreme sediment and ice discharge from marine-based ice streams: new evidence from the North Sea.(Author abstract). *Geology*, *35*(5), 395. https://doi.org/10.1130/G23364A.1

Odinsen, T., Christiansson, P., Gabrielsen, R. H., Faleide, J. I., & Berge, A. M. (2000). The geometries and deep structure of the northern North Sea rift system. *Geological Society Special Publication*, *167*(1), 41–57. https://doi.org/10.1144/GSL.SP.2000.167.01.03

Ostanin, I., Anka, Z., di Primio, R., & Bernal, A. (2013). Hydrocarbon plumbing systems

above the Snøhvit gas field: Structural control and implications for thermogenic methane leakage in the Hammerfest Basin, SW Barents Sea. *Marine and Petroleum Geology*, *43*, 127–146. https://doi.org/10.1016/j.marpetgeo.2013.02.012

Ottesen, D., Batchelor, C. L., Dowdeswell, J. A., & LøSeth, H. (2018). Morphology and pattern of Quaternary sedimentation in the North Sea Basin (52–62°N). *Marine and Petroleum Geology*, *98*, 836–859. https://doi.org/10.1016/j.marpetgeo.2018.08.022

Ottesen, D., & Dowdeswell, J. A. (2009). An inter-ice-stream glaciated margin: submarine landforms and a geomorphic model based on marine-geophysical data from Svalbard.(Author abstract). *The Geological Society of America Bulletin*, *121*(11 12), 1647. https://doi.org/10.1130/B26467.1

Ottesen, D., Dowdeswell, J. A., & Bugge, T. (2014). Morphology, sedimentary infill and depositional environments of the Early Quaternary North Sea Basin (56°–62°N). *Marine and Petroleum Geology*, *56*(C), 123–146. https://doi.org/10.1016/j.marpetgeo.2014.04.007

Panik, M. J. (2012). Statistical inference : a short course. Hoboken, N.J.: Wiley.

Rafaelsen, B., Andreassen, K., Kuilman, L. W., Lebesbye, E., Hogstad, K., & Midtbø, M. (2002). Geomorphology of buried glacigenic horizons in the Barents Sea from three-dimensional seismic data. *Geological Society, London, Special Publications*, *203*(1), 259–276. https://doi.org/10.1109/GRID.2010.5697987

Ripley, B. D. (1977). Modelling Spatial Patterns. *Journal of the Royal Statistical Society: Series B (Methodological)*, *39*(2), 172–192. https://doi.org/10.1111/j.2517-6161.1977.tb01615.x

Rise, L., & Rokoengen, K. (1984). Surficial sediments in the Norwegian sector of the North Sea between 60°30′ and 62°N. *Marine Geology*, *58*(3–4), 287–317. https://doi.org/10.1016/0025-3227(84)90206-8

Royston, J. P. (1982). An Extension of Shapiro and Wilk's W Test for Normality to Large Samples. *Journal of the Royal Statistical Society: Series C (Applied Statistics)*, *31*(2), 115–124. https://doi.org/10.2307/2347973

Royston, P. (1995). A remark on algorithm AS 181: the W-test for normality. *Journal of the Royal Statistical Society*, *44*(4), 547–550.

Schlumberger Limited. (2018). Petrel E&P software platform.

Schroeder, F. (2017). Seismic Reflection lectures. Retrieved 1 February 2019, from https://www.iris.edu/hq/inclass/lesson/seismic_reflection#

Sejrup, H. P., Aarseth, I., Haflidason, H., Løvlie, R., Tien, Å. B., Tjøstheim, G., … Ellingsen, K. L. (1995). Quaternary of the Norwegian Channel: glaciation history and palaeoceanography. *Norsk Geologisk Tidsskrift*, *Vol. 75*(2/3), pp.65-87.

Sejrup, H. P., Larsen, E., Haflidason, H., Berstad, I. M., Hjelstuen, B. O., Jonsdottir, H. E., … Stalsberg, K. (2003). Configuration, history and impact of the Norwegian Channel Ice

Stream. *Boreas*, *32*(1), 18–36. https://doi.org/10.1080/03009480310001029

Sejrup, H. P., Nygård, A., Hall, A. M., & Haflidason, H. (2009). Middle and Late Weichselian (Devensian) glaciation history of south-western Norway, North Sea and eastern UK. *Quaternary Science Reviews*, *28*(3), 370–380. https://doi.org/10.1016/j.quascirev.2008.10.019

Shapiro, S. S., & Wilk, M. B. (1965). An Analysis of Variance Test for Normality (Complete Samples). *Biometrika*, *52*(3/4), 591–611. https://doi.org/10.2307/2333709

Sheriff, R. E. (1996). Understanding the Fresnel zone. *AAPG Explorer*, 18–19.

Soper, N. J., Strachan, R. A., Holdsworth, R. E., Gayer, R. A., & Greiling, R. O. (1992). Sinistral transpression and the Silurian closure of Iapetus. *Journal of the Geological Society*, *149*(6), 871–880. https://doi.org/10.1144/gsjgs.149.6.0871

Stoker, M. S., Praeg, D., Hjelstuen, B. O., Laberg, J. S., Nielsen, T., & Shannon, P. M. (2005). Neogene stratigraphy and the sedimentary and oceanographic development of the NW European Atlantic margin. *Marine and Petroleum Geology*, *22*(9), 977–1005. https://doi.org/10.1016/j.marpetgeo.2004.11.007

Svendsen, J. I., Briner, J. P., Mangerud, J., & Young, N. E. (2015). Early break-up of the Norwegian Channel Ice Stream during the Last Glacial Maximum. *Quaternary Science Reviews*, *107*(C), 231–242. https://doi.org/10.1016/j.quascirev.2014.11.001

Team, R. D. C. (2018). R: The R Project for Statistical Computing. Vienna, Austria. Retrieved from https://www.r-project.org/

Thomas, G. S. P., & Connell, R. J. (1985). Iceberg drop, dump, and grounding structures from Pleistocene glacio-lacustrine sediments, Scotland. *Journal of Sedimentary Research*, *55*(2), 243–249.

Tjelta, T. I., Svano, G., Strout, J. M., Forsberg, C. F., Johansen, H., & Plank, S. (2007). Shallow Gas And Its Multiple Impact On A North Sea Production Platform. *OFFSHORE SITE INVESTIGATION AND GEOTECHNICS, Confronting New Challenges and Sharing Knowledge*. London, UK: Society of Underwater Technology. Retrieved from https://doi.org/

Van Weering, T., Jansen, J. H. F., & Eisma, D. (1973). Acoustic reflection profiles of the Norwegian Channel between Oslo and Bergen. *Netherlands Journal of Sea Research*, *6*(1–2), 241–263.

Vollset, J., & Doré, A. G. (1984). *A revised Triassic and Jurassic lithostratigraphic nomenclature for the Norwegian North Sea*. Oljedirektoratet.

Whipp, P. S., Jackson, C. A., Gawthorpe, R. L., Dreyer, T., & Quinn, D. (2014). Normal fault array evolution above a reactivated rift fabric. *Basin Research*, *26*(4), 523–549. https://doi.org/10.1111/bre.12050

Widess, M. B. (1973). HOW THIN IS A THIN BED? *GEOPHYSICS*, *38*(6), 1176–1180. https://doi.org/10.1190/1.1440403

Ziegler, P. A. (1992). North Sea rift system. *Tectonophysics*, *208*(1), 55–75. https://doi.org/10.1016/0040-1951(92)90336-5

Appendices

Appendix 1: Produced pockmark data for analysis

Seabed data

Table 6.1: Collected pockmarks data for Seabed horizon

Pock name	Depth (OWT) (ms)	Width (m)	Length (m)	Direction (degree)	Area (m^2)	Primary shape
GO1	0,4	187	279	93	41904	I1
GO2	0,3	97	147	156	10618	I1
GO3	0,3	129	143	134	14849	I1
GO4	0,3	87	103	140	7049	E
GO5	0,3	70	73	135	4714	E
GO6	0,4	106	140	133	12641	I1
GO7	0,1	70	124	159	5509	E
GO8	0,3	68	72	44	4576	E
GO9	0,3	96	146	1	9360	E
GO10	0,5	92	148	4	9135	E
GO11	0,4	72	73	43	4986	E
GO12	0,2	101	125	81	9843	E
GO13	1,0	99	145	179	9624	E
GO14	0,2	68	91	39	5007	E
GO15	0,3	84	128	159	7601	E
GO16	0,3	89	93	125	6431	E
GO17	0,2	52	67	43	2719	E
GO18	0,1	56	65	25	2708	E
GO19	0,2	67	75	55	4398	E
GO20	0,1	51	89	159	2882	E
GO21	0,3	65	73	47	4458	E
GO22	0,1	59	71	33	3192	E
GO23	0,3	70	74	43	4722	E
GO24	0,2	70	72	134	4832	E
GO25	0,3	98	122	167	7867	E
GO26	0,5	88	140	158	8653	E
GO27	0,4	71	75	138	4569	E
GO28	0,3	82	123	14	6688	E
GO29	0,1	55	78	67	2810	E
GO30	0,4	71	74	138	4853	S
GO31	0,1	87	129	17	7773	EL
GO32	0,3	68	69	135	4557	S
GO33	0,5	81	99	35	5449	E

GO34	0,5	82	107	150	5792	E
GO35	0,6	71	73	134	5047	E
GO36	0,4	91	128	165	7724	E
GO37	0,2	70	123	25	5873	EL
GO38	0,1	78	121	30	6502	E
GO39	0,1	70	86	41	5243	E
GO40	0,2	83	108	22	7240	EL
GO41	0,3	72	75	53	4628	E
GO42	0,2	61	84	136	4156	E
GO43	0,1	72	115	153	6049	E
GO44	0,1	89	154	68	10044	EL
GO45	0,1	70	98	96	4789	E
GO46	0,1	67	81	144	4511	E
GO47	0,4	111	167	140	14771	I2
GO48	0,2	70	88	155	4195	E
GO49	0,2	75	81	41	5018	E
GO50	0,2	68	76	139	4451	E
GO51	0,4	70	73	42	4834	E
GO52	0,4	83	114	31	6929	E
GO53	0,3	79	101	149	6227	E
GO54	0,2	58	113	65	4823	E
GO55	0,3	65	74	42	4375	E
GO56	0,4	70	84	49	4666	E
GO57	0,1	88	94	67	6264	E
GO58	0,1	69	82	139	3240	E
GO59	0,2	86	170	167	9804	EL
GO60	0,2	78	138	165	6800	I1
GO61	0,4	83	115	162	6541	EL
GO62	0,2	101	106	138	9097	I2
GO63	0,4	72	77	138	5020	E
GO64	0,2	87	141	176	8679	EL
GO65	0,3	70	72	134	4620	E
GO66	0,1	51	109	165	3883	E
GO67	0,2	68	156	153	7225	E
GO68	0,2	70	77	39	4740	S
GO69	0,2	69	111	145	5748	E
GO70	0,2	63	72	135	4348	E
GO71	0,3	70	83	145	4647	S
GO72	0,2	68	75	133	4612	S
GO73	0,2	64	74	41	4366	S
GO74	0,1	78	88	152	5018	E
GO75	0,3	67	79	47	4531	E
GO76	0,1	104	116	150	9355	I1
GO77	0,1	75	86	33	5143	E
GO78	0,1	51	95	140	3091	E
GO79	0,4	77	97	142	6264	E

GO80	0,2	69	72	43	4593	E
GO81	0,1	69	91	139	5194	E
GO82	0,2	73	108	167	5426	E
GO83	0,1	66	105	149	5876	E
GO84	0,2	70	74	138	4680	E
GO85	0,4	70	72	42	4662	E
GO86	0,5	75	89	42	5773	E
GO87	0,3	70	74	138	4837	S
GO88	0,4	73	75	137	4825	E
GO89	0,1	95	111	44	8705	EL
GO90	0,2	137	274	170	26777	I1
GO91	0,3	110	120	134	10628	I2
GO92	0,3	124	148	40	14078	E
GO93	0,5	124	176	152	15760	E
GO94	0,2	72	80	140	4711	E
GO95	0,5	99	157	176	10079	E
GO96	0,5	87	112	26	6618	S
GO97	0,4	92	142	174	8700	E
GO98	0,3	110	153	135	13816	I1
GO99	0,2	67	69	137	4448	E
GO100	0,1	61	75	41	4101	E
GO101	0,1	65	71	136	4285	E
GO102	0,3	87	158	167	9575	E
GO103	0,2	87	119	51	8448	I1
GO104	0,5	72	77	42	4959	E
GO105	0,3	68	71	45	4701	E
GO106	0,2	79	126	31	7909	E
GO107	0,2	109	149	71	11720	EL
GO108	0,2	75	100	144	5929	E
GO109	0,5	102	152	1	10044	EL
GO110	0,1	66	113	153	5813	E
GO111	0,1	62	114	162	5213	E
GO112	0,3	73	92	146	5468	E
GO113	0,2	67	75	41	4529	E
GO114	0,4	104	134	135	11244	E
GO115	0,3	82	146	157	8287	EL
GO116	0,2	73	95	56	5213	E
GO117	0,1	73	153	167	7558	E
GO118	0,3	72	76	138	4818	E
GO119	0,2	70	77	153	3936	E
GO120	0,1	60	83	146	4086	E
GO121	0,4	73	75	43	5032	E
GO122	0,1	78	141	156	7880	EL
GO123	0,2	98	155	13	10756	E
GO124	0,1	86	95	133	6289	E
GO125	0,1	75	115	176	5268	E

GO126	0,2	73	93	36	5367	E
GO127	0,2	102	137	149	10436	E
GO128	0,2	95	126	11	8750	E
GO129	0,5	83	109	28	6284	E
GO130	0,4	87	119	26	6673	E
GO131	0,2	136	173	40	17264	I2
GO132	0,2	75	104	33	5641	E
GO133	0,3	132	175	42	15736	E
GO134	0,1	36	93	160	2561	E
GO135	0,2	86	130	174	8006	EL
GO136	0,2	96	143	20	9189	EL
GO137	0,4	116	142	176	12003	I2
GO138	0,3	101	147	166	9503	EL
GO139	0,3	113	133	36	12257	I1
GO140	0,2	66	79	51	4541	S
GO141	0,3	124	154	156	13784	I1
GO142	0,3	88	119	24	7316	E
GO143	0,2	82	133	95	7654	EL
GO144	0,3	102	162	136	13181	I1
GO145	0,3	61	69	136	4017	E
GO146	0,4	161	218	166	27064	I1
GO147	0,2	78	102	58	5936	E
GO148	0,1	71	98	147	5095	E
GO149	0,1	74	98	31	5097	E
GO150	0,3	262	325	82	62547	I2
GO151	0,1	47	73	66	2687	E
GO152	0,3	101	137	131	10657	E
GO153	0,3	78	90	53	5698	E
GO154	0,2	101	131	43	10409	E
GO155	0,3	79	129	164	6514	E
GO156	0,3	104	143	146	12130	I1
GO157	0,3	93	140	175	8740	I1
GO158	0,2	70	77	142	4674	E
GO159	0,4	139	163	48	16768	C
GO160	0,4	95	141	166	8969	E
GO161	0,3	75	80	45	5290	E
GO162	0,3	94	139	156	9181	E
GO163	0,1	81	112	165	6304	E
GO164	0,1	64	89	37	4624	E
GO165	0,4	79	80	45	5938	E
GO166	0,1	87	131	153	8153	EL
GO167	0,3	73	77	44	5094	E
GO168	0,2	73	91	110	4473	E
GO169	0,1	67	74	143	3953	E
GO170	0,1	101	161	176	12902	I1
GO171	0,2	63	84	34	4030	E

GO172	0,2	97	150	65	11491	E
GO173	0,5	254	363	77	61829	C
GO174	0,2	87	108	136	7367	E
GO175	0,5	91	128	20	8086	E
GO176	0,3	68	78	128	4686	E
GO177	0,4	69	75	46	4810	E
GO178	0,2	76	87	58	5258	E
GO179	0,2	66	72	135	4422	E
GO180	0,1	62	102	151	4487	E
GO181	0,2	89	120	2	7745	EL
GO182	0,3	90	161	48	10282	E
GO183	0,2	72	86	40	5538	E
GO184	0,2	102	133	15	9517	E
GO185	0,3	74	108	132	6374	E
GO186	0,4	67	74	131	4390	E
GO187	0,3	105	116	134	9419	E
GO188	0,4	72	74	46	5027	E
GO189	0,3	71	82	139	4993	S
GO190	0,4	68	75	40	4639	E
GO191	0,4	70	73	131	4733	E
GO192	0,1	66	93	20	4121	E
GO193	0,3	82	112	156	6090	E
GO194	0,4	70	76	140	4747	EL
GO195	0,3	90	125	24	7936	E
GO196	0,4	78	113	60	6314	E
GO197	0,3	72	86	38	5146	E
GO198	0,4	108	128	43	10958	E
GO199	0,2	73	103	121	6012	E
GO200	0,2	76	83	132	4877	E
GO201	0,4	69	74	45	4786	E
GO202	0,1	62	87	29	3922	E
GO203	0,2	92	138	166	8110	E
GO204	0,2	136	182	77	18146	I1
GO205	0,3	81	125	18	6470	E
GO206	0,3	72	77	46	5026	E
GO207	0,4	90	134	6	7984	E
GO208	0,2	77	78	134	5158	E
GO209	0,2	85	115	33	6934	E
GO210	0,2	77	99	124	6052	E
GO211	0,3	138	146	81	15489	I1
GO212	0,2	79	87	52	5569	E
GO213	0,3	102	180	133	14536	I2
GO214	0,3	98	156	1	10188	E
GO215	0,2	78	154	162	7797	E
GO216	0,1	71	81	41	4860	E
GO217	0,3	72	81	42	5163	E

GO218	0,1	94	159	155	10537	E
GO219	0,2	97	138	105	8942	EL
GO220	0,4	70	73	135	4518	E
GO221	0,2	66	105	29	5758	E
GO222	0,3	115	174	6	12881	E
GO223	0,1	57	71	43	3204	E
GO224	0,1	58	99	23	3791	EL
GO225	0,2	83	128	175	7420	EL
GO226	0,2	95	112	52	8376	E
GO227	0,1	63	131	20	5476	E
GO228	0,3	90	134	24	8564	E
GO229	0,2	68	75	45	4605	E
GO230	0,2	122	152	128	14466	EL
GO231	0,1	60	69	141	3638	S
GO232	0,1	71	108	167	5335	E
GO233	0,4	100	127	17	9673	E
GO234	0,2	93	123	85	8056	EL
GO235	0,2	87	129	16	8556	E
GO236	0,2	71	73	46	4746	E
GO237	0,3	73	93	145	5196	E
GO238	0,5	98	138	97	9637	E
GO239	0,2	91	132	10	8373	EL
GO240	0,2	68	74	47	4527	E
GO241	0,2	70	86	51	4879	E
GO242	0,2	77	104	33	5694	E
GO243	0,2	85	130	11	7695	EL
GO244	0,3	91	126	86	8032	EL
GO245	0,3	90	117	51	7885	E
GO246	0,2	88	149	180	8882	EL
GO247	0,2	102	119	44	10774	E
GO248	0,2	62	67	140	3328	E
GO249	0,3	104	149	56	11507	I1
GO250	0,2	71	131	58	6948	E
GO251	0,2	58	144	70	6070	E
GO252	0,2	68	105	61	5095	E
GT1	0,3	76	84	142	5040	E
GT2	0,5	96	139	9	9177	EL
GT3	0,2	62	68	42	3978	E
GT4	0,2	70	139	149	6931	E
GT5	0,2	84	138	6	8012	EL
GT6	0,3	126	145	39	14789	E
GT7	0,1	54	72	30	2938	I1
GT8	0,2	59	70	48	3582	E
GT9	0,2	112	128	149	11170	E
GT10	0,1	86	92	18	6142	I1
GT11	0,2	71	106	31	4834	E

GT12	0,3	69	73	41	4507	S
GT13	0,3	60	77	52	3970	E
GT14	0,2	73	83	140	5173	E
GT15	0,2	68	80	38	4489	E
GT16	0,2	72	75	136	4897	E
GT17	0,2	101	138	4	9854	EL
GT18	0,3	70	73	43	4731	E
GT19	0,2	92	114	20	8091	E
GT20	0,3	71	78	49	4876	S
GT21	0,3	68	72	133	4596	S
GT22	0,2	70	74	43	4825	S
GT23	0,2	72	74	46	4875	E
GT24	0,3	69	74	42	4647	E
GT25	0,2	70	85	34	4452	E
GT26	0,2	76	100	146	5932	E
GT27	0,1	68	79	48	4459	E
GT28	0,2	80	138	174	7666	EL
GT29	0,2	76	108	152	6243	E
GT30	0,3	74	86	37	5077	E
GT31	0,2	65	69	137	4017	S
GT32	0,3	91	136	1	8805	EL
GT33	0,4	81	121	154	6558	EL
GT34	0,2	76	82	34	4982	E
GT35	0,1	76	157	179	8645	E
GT36	0,2	82	89	155	5654	E
GT37	0,1	64	70	139	3442	E
GT38	0,1	54	76	147	3245	E
GT39	0,1	64	70	46	4193	E
GT40	0,1	101	110	128	8636	C
GT41	0,3	91	131	19	7975	E
GT42	0,3	87	175	3	10859	EL
GT43	0,3	86	97	139	7275	E
GT44	0,2	63	79	147	3945	E
GT45	0,3	100	153	47	10180	I1
GT46	0,2	70	77	51	4721	E
GT47	0,2	93	106	137	8295	E
GT48	0,2	76	97	40	5917	E
GT49	0,2	87	144	171	8547	EL
GT50	0,2	69	98	120	4790	E
GT51	0,1	70	83	151	4506	S
GT52	0,2	69	70	137	4454	E
GT53	0,2	74	105	147	6386	E
GT54	0,3	71	74	46	4711	E
GT55	0,1	61	110	163	4435	EL
GT56	0,1	64	68	144	3437	E
GT57	0,1	84	85	50	6176	E

GT58	0,3	68	85	37	4584	E
GT59	0,3	94	135	2	8964	E
GT60	0,3	144	199	87	21705	I1
GT61	0,3	71	72	44	4802	S
GT62	0,1	53	79	135	3179	E
GT63	0,2	79	84	129	5728	E
GT64	0,3	73	92	147	5306	E
GT65	0,2	62	70	45	3871	E
GT66	0,3	70	71	45	4848	E
GT67	0,1	63	115	9	4421	E
GT68	0,2	55	110	159	4174	EL
GT69	0,2	70	93	143	5184	E
GT70	0,3	70	115	152	6786	E
GT71	0,3	70	145	165	7072	E
GT72	0,2	85	136	1	8030	EL
GT73	0,2	82	137	174	7511	EL
GT74	0,1	62	80	138	4033	EL
GT75	0,4	101	128	21	9678	E
GT76	0,2	70	79	141	4737	E
GT77	0,1	80	105	74	6001	I1
GT78	0,3	93	106	63	7885	E
GT79	0,2	75	128	28	6808	E
GT80	0,1	64	102	158	4897	E
GT81	0,1	65	120	169	4448	E
GT82	0,2	74	88	38	5200	E
GT83	0,1	41	65	58	1882	E
GT84	0,1	68	102	25	4998	E
GT85	0,2	97	141	29	10177	E
GT86	0,4	65	71	137	4347	E
GT87	0,2	75	108	29	6548	C
GT88	0,2	93	134	4	8794	C
GT89	0,1	77	106	75	6095	E
GT90	0,3	76	126	156	6811	E
GT91	0,2	69	112	152	5846	E
GT92	0,3	76	90	38	5528	E
GT93	0,3	89	134	19	8364	EL
GT94	0,4	69	71	44	4694	E
GT95	0,3	82	166	6	9871	E
GT96	0,3	70	89	53	5040	E
GT97	0,2	61	75	37	3782	E
GT98	0,2	70	80	46	5119	E
GT99	0,3	128	201	168	19375	EL
GT100	0,1	59	114	161	4760	E
GT101	0,2	84	121	69	8037	E
GT102	0,2	72	77	42	4826	E
GT103	0,1	57	96	58	3877	E

GT104	0,2	87	100	25	7071	E
GT105	0,2	68	71	132	4462	S
GT106	0,3	70	74	43	4807	E
GT107	0,2	64	72	139	4248	E
GT108	0,3	71	73	45	4863	EL
GT109	0,1	67	72	144	3375	E
GT110	0,2	90	137	8	8105	EL
GT111	0,3	73	101	30	5026	E
GT112	0,3	122	167	91	15131	I1
GT113	0,3	71	73	45	4805	E
GT114	0,2	132	169	67	16306	E
GT115	0,1	56	90	48	3691	E
GT116	0,3	70	80	138	4810	E
GT117	0,1	89	119	119	7306	E
GT118	0,2	70	85	54	4524	E
GT119	0,2	73	77	43	5068	E
GT120	0,1	61	66	125	2903	E
GT121	0,2	53	79	142	3380	E
GT122	0,3	85	107	24	6141	E
GT123	0,1	72	97	60	5057	E
GT124	0,4	70	73	44	4961	S
GT125	0,5	91	131	166	7727	E
GT126	0,2	71	79	137	4929	S
GT127	0,3	88	128	66	8076	S
GT128	0,2	71	87	44	5108	C
GT129	0,1	73	105	13	5145	C
GT130	0,4	95	111	133	8733	I1
GT131	0,2	68	72	137	4554	E
GT132	0,2	71	89	35	4825	EL
GT133	0,3	65	93	146	4883	E
GT134	0,2	80	154	180	7938	E
GT135	0,2	67	70	41	4330	E
GT136	0,2	68	88	34	4704	E
GT137	0,2	75	96	149	5255	E
GT138	0,2	68	78	46	4786	E
GT139	0,1	53	82	140	3169	E
GT140	0,2	69	172	167	8284	EL
GT141	0,3	94	154	3	9295	E
GT142	0,3	124	133	99	12614	I2
GT143	0,3	100	111	1	8416	I1
GT144	0,2	79	102	108	6231	E
GT145	0,3	75	87	52	5321	E
GT146	0,5	147	192	5	21842	I1
GT147	0,4	77	146	165	7964	E
GT148	0,3	69	86	124	4463	E
GT149	0,3	75	80	130	5258	E

GT150	0,0	47	116	36	3365	E
GT151	0,3	75	87	44	5477	E
GT152	0,3	69	73	43	4726	E
GT153	0,3	85	164	14	9316	E
GT154	0,5	100	146	6	9454	E
GT155	0,2	103	113	174	8843	I1
GT156	0,2	72	74	44	4905	S
GT157	0,0	54	117	139	4196	EL
GT158	0,1	59	120	40	5439	E
GT159	0,1	76	135	91	7473	E
GT160	0,1	75	108	39	5860	E
GT161	0,2	72	106	38	6086	E
GT162	0,2	89	168	166	10499	EL
GT163	0,3	144	255	73	26582	EL
GT164	0,2	70	75	41	4921	E
GT165	0,3	77	100	34	5505	E
GT166	0,1	73	93	150	4998	E
GT167	0,1	58	98	169	3260	E
GT168	0,1	74	79	137	4906	E
GT169	0,2	61	95	33	4898	E
GT170	0,2	66	73	46	4526	E
GT171	0,1	96	151	164	9526	E
GT172	0,5	94	140	173	8566	E
GT173	0,2	84	137	180	7795	E
GT174	0,1	63	91	123	4534	E
GT175	0,2	74	97	78	4857	E
GT176	0,3	72	91	141	5185	E
GT177	0,1	42	90	138	3087	E
GT178	0,3	83	137	15	7844	E
GT179	0,3	88	135	167	7681	E
GT180	0,3	84	106	24	7099	E
GT181	0,2	72	77	47	5103	E
GT182	0,2	65	74	132	4360	S
GT183	0,4	90	104	139	7454	E
GT184	0,2	127	288	159	22889	I2
GT185	0,2	90	104	42	7598	E
GT186	0,3	70	73	43	4779	E
GT187	0,4	69	72	48	4498	E
GT188	0,5	71	74	48	4838	E
GT189	0,3	77	87	142	5210	E
GT190	0,4	71	73	43	4871	E
GT191	0,3	80	122	160	7433	E
GT192	0,4	123	151	120	13869	I1
GT193	0,1	64	93	51	4292	E
GT194	0,2	69	72	135	4800	E
GT195	0,3	74	86	38	5127	E

GT196	0,3	86	116	143	7154	E
GT197	0,5	145	172	132	20377	I1
GT198	0,5	99	159	178	9862	EL
GT199	0,3	72	83	44	5085	E
GT200	0,2	67	73	136	4459	S
GT201	0,1	61	78	58	3547	E
GT202	0,2	79	174	15	9821	EL
GT203	0,3	128	177	2	17151	I1
GT204	0,3	91	142	10	8752	E
GT205	0,4	80	88	47	6062	E
GT206	0,1	46	62	24	2298	E
GT207	0,2	66	72	46	4398	E
GT208	0,1	68	83	42	4609	E
GT209	0,3	67	75	49	4503	E
GT210	0,3	68	71	47	4404	E
GT211	0,4	70	72	45	4797	E
GT212	0,3	93	140	168	8560	EL
GT213	0,2	73	81	44	4756	E
GT214	0,4	79	104	149	5679	E
GT215	0,1	109	133	168	10941	I1
GT216	0,2	114	135	96	10660	C
GT217	0,4	72	81	41	4993	E
GT218	0,2	88	166	136	9931	E
GT219	0,4	69	72	48	4718	E
GT220	0,2	68	77	48	4362	E
GT221	0,4	88	123	19	6885	E
GT222	0,3	71	72	135	4887	S
GT223	0,4	72	73	139	4651	E
GT224	0,4	67	81	62	4202	E
GT225	0,2	64	69	130	3811	E
GT226	0,3	69	72	47	4429	E
GT227	0,3	69	71	136	4515	E
GT228	0,1	90	136	20	9109	I1
GT229	0,2	84	117	139	7195	E
GT230	0,2	79	93	59	5644	E
GR1	0,3	73	77	136	5109	E
GR2	0,2	81	137	159	7568	E
GR3	0,4	113	146	144	12459	C
GR4	0,2	63	74	140	4074	E
GR5	0,3	91	142	10	8970	E
GR6	0,4	94	125	147	9449	E
GR7	0,2	76	80	50	5005	E
GR8	0,3	94	105	134	8433	E
GR9	0,1	71	79	128	4605	E
GR10	0,4	71	75	138	4741	E
GR11	0,4	71	76	40	4731	E

GR12	0,2	96	104	115	7282	E
GR13	0,2	64	73	136	4385	E
GR14	0,2	85	117	153	7274	E
GR15	0,2	80	109	56	6751	E
GR16	0,1	71	81	142	4804	E
GR17	0,3	75	89	126	5007	E
GR18	0,3	83	122	26	6207	E
GR19	0,2	82	129	177	7883	E
GR20	0,2	63	71	49	4131	EL
GR21	0,1	80	118	19	6608	E
GR22	0,4	71	91	137	5579	E
GR23	0,3	88	139	154	7392	E
GR24	0,2	70	87	141	4765	E
GR25	0,2	72	114	55	5818	E
GR26	0,2	69	71	41	4251	E
GR27	0,2	77	121	172	6678	EL
GR28	0,2	72	74	45	4328	E
GR29	0,1	58	89	63	3462	EL
GR30	0,1	58	63	127	2899	E
GR31	0,1	66	118	115	5128	E
GR32	0,1	66	70	135	4102	E
GR33	0,2	96	116	139	9533	E
GR34	0,1	95	116	61	8581	E
GR35	0,4	94	145	168	7877	E
GR36	0,2	54	92	65	3646	E
GR37	0,4	69	79	132	4679	E
GR38	0,1	59	85	47	3735	E
GR39	0,1	53	135	55	4110	E
GR40	0,3	69	75	139	4606	E
GR41	0,3	96	160	173	10354	EL
GR42	0,5	72	84	38	5159	E
GR43	0,3	70	79	140	4586	E
GR44	0,3	66	150	12	6846	E
GR45	0,1	72	88	130	5194	E
GR46	0,2	80	131	139	8209	I1
GR47	0,4	170	279	159	32606	EL
GR48	0,3	93	135	3	8813	E
GR49	0,4	62	74	41	4245	E
GR50	0,2	84	96	65	6210	E
GR51	0,1	62	121	92	4823	EL
GR52	0,2	68	96	45	5076	C
GR53	0,2	85	112	55	6956	C
GR54	0,1	56	93	35	4230	C
GR55	0,3	65	76	50	4443	C
GR56	0,2	70	81	38	4964	E
GR57	0,3	99	130	13	9124	E

GR58	0,2	80	102	36	5752	E
GR59	0,2	70	90	55	5579	E
GR60	0,4	72	81	44	5380	E
GR61	0,2	65	70	135	3813	E
GR62	0,3	71	156	6	7325	E
GR63	0,8	222	432	169	76604	I1
GR64	0,7	218	384	6	58252	I2
GR65	0,6	105	214	2	15633	E
GR66	0,5	110	260	137	20495	EL
GR67	0,6	286	358	32	65125	I2
GR68	0,4	190	450	14	64209	I2
GR69	0,5	70	75	140	4675	E
GR70	0,5	71	75	48	4841	E
GR71	0,2	54	94	19	3293	E
GR72	0,1	48	83	147	2774	E
GR73	0,4	73	81	39	5182	E
GR74	0,4	99	155	3	10273	EL
GR75	0,2	74	86	143	5320	E
GR76	0,3	89	99	37	6875	E
GR77	0,2	91	124	155	8494	EL
GR78	0,2	83	101	136	6822	E
GR79	0,2	48	99	32	3502	E
GR80	0,4	110	179	171	13667	I1
GR81	0,4	111	137	47	12455	E
GR82	0,5	69	73	138	4678	E
GR83	0,2	92	133	158	9090	E
GR84	0,4	66	70	43	4278	E
GR85	0,3	91	133	169	8679	EL
GR86	0,4	156	351	165	35397	I1
GR87	0,4	127	214	137	19228	I2
GR88	0,5	74	113	145	6180	E
GR89	0,4	89	104	173	6644	E
GR90	0,7	112	149	70	12675	E
GR91	0,3	98	160	54	11796	I1
GR92	0,3	87	129	78	7767	E
GR93	0,3	73	107	119	5968	E
GR94	0,2	141	185	164	19881	C
GR95	0,8	198	487	153	58429	I2
GR96	0,3	98	134	98	9267	E
GR97	0,4	90	109	37	7880	E
GR98	0,2	126	140	54	12692	E
GR99	0,2	85	109	87	7350	E
GR100	0,3	171	208	177	25539	I1
GR101	0,5	95	117	10	7638	E
GR102	0,7	142	188	120	22251	I1
GR103	0,5	109	118	37	10253	E

GR104	0,5	160	167	127	21750	E
GR105	0,5	97	185	176	13307	E
GR106	0,3	101	164	160	10967	E
GR107	0,6	67	73	49	4228	E
GR108	0,2	61	64	133	3324	E
GR109	0,4	71	72	45	4935	E
GR110	0,6	77	93	49	5854	E
GR111	0,4	71	81	139	4929	T
GR112	1,5	102	143	168	11024	E
GR113	0,3	97	107	144	8638	E
GR114	0,6	162	200	6	24787	E
GR115	0,4	119	164	154	15948	I1
GR116	0,2	88	158	157	11368	E
GR117	0,5	72	74	45	4963	E
GR118	0,3	88	145	71	8715	E
GR119	0,7	239	449	147	76741	I1
GR120	0,8	149	303	155	32649	I1
GR121	0,4	223	344	159	57277	I2
GR122	0,7	223	468	154	73633	I2
GR123	0,5	53	106	51	4067	EL
GR124	1,0	72	81	49	4490	E
GR125	1,2	97	132	154	9838	E
GR126	0,5	78	159	141	9394	E
GR127	0,5	123	294	144	28825	EL
GR128	0,9	114	222	4	18553	E
GR129	0,7	71	72	46	4648	E
GR130	0,8	69	70	46	4513	E
GR131	1,1	318	571	146	139681	I1
GR132	0,7	71	72	136	4719	E
GR133	0,2	99	129	55	9410	I1
GR134	0,8	126	174	29	15347	E
GR135	0,9	125	159	130	13751	E
GR136	1,1	200	214	28	33223	I1
GR137	1,5	262	416	95	83637	I1
GR138	0,2	65	74	135	4213	E
GR139	0,9	106	141	48	12196	E
GR140	0,2	64	94	119	4866	E
GR141	0,3	66	84	66	3558	E
GR142	0,2	76	103	171	6121	E
GR143	0,2	48	124	131	3847	EL
GR144	0,4	91	131	7	8751	E
GR145	0,3	80	110	164	6414	E
GR146	1,1	63	107	111	4803	E
GR147	1,6	200	354	149	52454	I2
GR148	1,3	71	73	42	4787	E
GR149	0,9	94	103	174	6596	E

GR150	0,3	75	92	56	5375	E
GR151	3,8	95	137	18	9187	I1
GR152	0,3	110	135	102	10615	E
GR153	0,5	82	113	149	6809	E
GR154	0,5	140	232	6	25043	I1
GR155	0,2	102	116	42	9338	E
GR156	0,4	105	140	40	12744	I1
GR157	0,3	96	142	10	9305	E
GR158	0,2	60	72	141	3528	E
GR159	0,1	77	107	113	6501	E
GR160	0,3	92	107	131	7942	E
GR161	1,5	197	324	135	49777	I1
GR162	0,2	68	74	44	4568	E
GR163	0,3	110	169	137	15276	E
GR164	0,2	67	79	144	4140	E
GR165	0,3	91	109	80	7622	E
GR166	0,4	85	110	153	6474	E
GR167	0,3	75	120	75	6736	EL
GR168	0,1	68	70	134	4264	E
GR169	0,2	75	85	44	4966	E
GR170	0,6	70	77	40	4695	E
GR171	0,4	68	78	51	4651	E
GF1	0,2	70	88	49	5160	E
GF2	0,1	62	98	116	4201	E
GF3	0,8	154	202	11	20774	E
GF4	0,2	86	130	162	7997	EL
GF5	0,4	150	237	33	24869	I1
GF6	0,4	73	103	45	6161	E
GF7	0,3	202	333	65	50364	I1
GF8	0,3	157	205	95	24811	I1
GF9	0,2	87	147	1	8796	E
GF10	0,5	68	76	48	4783	E
GF11	0,2	69	71	133	4604	E
GF12	0,2	98	138	140	11444	C
GF13	0,1	72	97	118	4931	E
GF14	0,1	88	109	129	8153	E
GF15	0,2	67	85	36	4709	E
GF16	0,1	83	121	25	7989	E
GF17	0,2	70	85	49	5013	E
GF18	0,2	90	130	74	7799	E
GF19	0,2	75	108	58	5847	E
GF20	0,2	65	81	55	4179	E
GF21	0,1	69	83	141	5071	E
GF22	0,2	89	139	143	9289	I1
GF23	0,2	82	112	18	6558	E
GF24	0,3	106	157	136	13081	E

GF25	0,3	87	129	167	8139	E
GF26	0,2	114	154	170	12259	E

Q 1.1 data

Table 6.2: Collected data of pockmarks at Q 1.1 horizon.

Pock name	Depth (OWT) (ms)	Width (m)	Length (m)	Direction (degree)	Area (m²)	Primary shape
ADD1	0,5	55	72	150	2912	S
ADD2	0,7	67	76	139	4588	E
ADD3	0,4	68	71	135	4490	E
ADD4	0,3	40	57	81	1609	E
ADD5	2,1	70	72	45	4887	E
ADD6	1,9	66	93	151	4287	E
ADD7	0,9	73	91	146	5200	E
ADD8	0,4	59	71	40	3720	E
ADD9	0,3	66	71	136	4297	E
ADD10	0,2	58	95	65	3558	E
ADD11	0,3	56	99	143	4344	I1
ADD12	0,4	64	99	149	4779	I1
ADD13	0,4	67	75	58	4176	E
ADD14	0,3	97	129	143	10368	I1
ADD15	0,3	61	79	126	4132	E
ADD16	0,4	65	90	55	4795	E
ADD17	0,4	85	103	64	6701	EL
ADD18	0,6	71	74	133	4293	E
ADD19	0,4	75	94	111	4874	E
ADD20	0,1	82	102	35	6320	I1
ADD21	0,4	67	72	137	4293	E
ADD22	0,5	66	72	43	4442	E
ADD23	1,7	69	75	50	4605	E
ADD24	0,3	91	98	138	7404	E
ADD25	0,3	65	101	165	3785	E
ADD26	0,1	47	67	157	1999	E
ADD27	0,4	92	191	39	12942	EL
ADD28	0,8	66	71	45	4314	E
ADD29	0,2	71	92	39	5072	E
ADD30	0,2	72	104	165	5355	E
ADD31	0,3	89	123	170	7681	E
ADD32	0,4	83	107	29	6505	E
ADD33	0,3	92	118	19	7544	EL
ADD34	0,8	80	88	143	5755	E
ADD35	0,5	111	129	162	10895	I1
ADD36	0,5	92	141	94	8410	I1
ADD37	0,6	93	127	109	7953	E
ADD38	0,4	78	113	119	6702	E
ADD39	0,5	95	161	40	11845	I1
ADD40	0,3	79	82	133	5383	E
ADD41	0,5	102	140	129	11373	I1

ADD42	0,3	70	71	136	4473	E
ADD43	0,3	84	94	29	5740	E
ADD44	0,4	90	130	11	8393	E
ADD45	0,2	50	61	145	2216	E
ADD46	0,3	95	131	157	8768	EL
ADD47	0,3	58	64	38	3115	E
ADD48	0,2	60	89	67	4197	I1
ADD49	0,2	75	120	34	6450	EL
ADD50	2,4	74	105	160	5195	E
ADD51	0,3	121	162	55	14282	I1
ADD52	1,4	76	88	38	5419	E
ADD53	1	68	75	40	4616	E
ADD54	0,7	69	83	42	4978	E
ADD55	0,8	45	79	168	2310	E
ADD56	1,1	82	144	122	9565	EL
ADD57	0,6	74	79	41	5069	E
ADD58	6	74	78	145	4630	E
ADD59	1,4	52	69	50	2815	E
ADD60	1	62	89	55	4195	E
ADD61	0,1	55	67	147	2838	E
ADD62	0,3	53	73	35	2889	E
ADD63	0,2	45	82	21	2131	E
ADD64	0,2	77	116	47	7040	EL
ADD65	0,1	38	72	24	1775	E
ADD66	0,2	74	120	170	5685	E
ADD67	0,2	71	97	158	4661	E
ADD68	0,1	59	72	141	3497	E
ADD69	0,4	70	81	142	4746	E
ADD70	0,2	94	109	24	7201	E
ADD71	0,2	84	122	166	7150	EL
ADD72	0,2	68	101	101	5414	EL
ADD73	0,2	65	76	149	3983	E
ADD74	0,3	66	76	40	4152	E
ADD75	0,3	68	76	44	4474	E
ADD76	0,3	81	101	27	6503	EL
ADD77	0,8	69	81	123	4237	E
ADD78	0,4	71	75	47	4510	E
ADD79	0,3	60	79	124	3954	E
ADD80	0,2	76	115	11	6225	EL
ADD81	0,2	72	88	37	5062	E
ADD82	0,2	110	142	53	11670	I1
ADD83	0,5	69	92	46	4975	EL
ADD84	0,4	71	81	38	4488	E
ADD85	0,2	90	107	33	7241	I1
ADD86	0,2	87	93	135	6869	E
ADD87	0,1	64	77	36	3992	E
ADD88	0,5	62	88	157	3768	E
ADD89	0,5	88	108	32	6992	E
ADD90	0,6	79	141	144	6971	E
ADD91	1,7	68	69	135	4549	S
ADD92	0,5	66	69	134	4295	E
ADD93	0,4	68	71	41	4497	S
ADD94	0,4	67	101	150	4872	E
ADD95	0,2	56	74	138	3143	E

ADD96	0,4	57	160	167	6198	EL
ADD97	0,1	52	71	32	2524	E
ADD98	0,2	62	75	142	3938	E
ADD99	0,1	54	121	143	4604	EL
ADD100	0,4	89	134	171	7941	EL
ADD101	0,8	48	67	176	2195	EL
ADD102	0,7	53	72	151	3165	E
ADD103	0,4	102	127	65	9950	I1
ADD104	0,8	85	122	154	6883	E
ADD105	0,5	46	76	158	2148	I1
ADD106	0,3	44	80	30	2633	I1
ADD107	1,3	93	138	102	8717	EL
ADD108	1,4	69	103	135	5858	I1
ADD109	0,4	94	147	165	9073	I1
ADD110	2,1	121	143	138	13928	I1
ADD111	0,8	83	111	150	6166	E
ADD112	0,7	71	76	139	4792	E
ADD113	1,3	65	78	152	3646	E
ADD114	0,5	52	98	145	3082	E
ADD115	1,1	61	86	25	3235	EL
ADD116	0,3	67	71	138	4518	E
ADD117	0,4	44	47	51	1647	E
ADD118	0,3	42	66	46	1700	E
ADD119	0,5	34	56	122	1513	EL
ADD120	1,2	65	82	146	4167	EL
ADD121	0,9	44	70	10	2162	E
ADD122	0,5	75	138	156	8060	E
ADD123	0,2	62	73	125	3620	E
ADD124	0,2	80	86	77	5586	EL
ADD125	0,2	88	106	124	6479	I2
ADD126	0,2	101	191	161	14356	EL
ADD127	0,5	93	120	98	8239	EL
ADD128	0,4	79	110	77	6596	EL
ADD129	0,7	74	109	114	5197	EL
ADD130	0,6	91	107	80	6951	EL
ADD131	0,4	64	72	132	4202	EL
ADD132	2,3	78	96	143	5786	EL
ADD133	0,6	85	191	156	11530	EL
ADD134	0,4	64	79	138	3843	E
ADD135	1,2	101	141	89	9786	EL
ADD136	2,2	84	100	56	6572	E
ADD137	1,1	82	105	30	6430	E
ADD138	1,6	70	73	44	4749	E
ADD139	0,8	68	71	134	4513	E
E1	0,4	103	142	96	9604	EL
E2	0,5	126	160	5	15163	EL
E3	0,9	94	144	5	8658	E
E4	0,6	77	86	52	5355	E
E5	0,8	93	145	14	8821	E
E6	0,8	120	191	149	17389	EL
E7	0,5	74	87	143	5172	E
E8	0,5	87	107	107	7210	E
E9	0,4	131	147	85	13014	EL
E10	0,4	66	80	141	3656	E

E11	0,9	148	196	178	19798	EL
E12	1,3	104	142	134	12548	I2
E13	1,1	96	146	1	9348	E
E14	0,9	108	134	103	10313	I1
E15	0,9	70	74	137	4697	E
E16	0,6	99	110	137	8894	EL
E17	1,8	68	74	44	4800	E
E18	0,9	83	113	150	6237	E
E19	0,5	98	148	179	9724	EL
E20	0,5	96	148	178	9489	EL
E21	0,8	85	116	151	6269	E
E22	1,1	76	109	144	6109	E
E23	1,1	84	107	22	6156	E
E24	0,9	69	76	41	4454	E
E25	0,7	125	134	45	13242	E
E26	0,4	113	142	164	11984	I1
E27	0,5	73	96	33	4958	E
E28	0,4	96	128	154	8813	E
E29	1,2	131	136	37	13640	E
E30	0,7	68	78	141	4776	E
E31	0,3	88	119	160	7473	E
E32	0,3	55	91	161	3376	E
E33	0,5	94	130	30	9825	E
E34	0,6	102	119	91	8691	EL
E35	1,1	74	82	140	5314	S
E36	1,3	79	101	146	5863	E
E37	1,2	102	145	175	10045	E
E38	0,4	94	116	142	8204	E
E39	0,8	70	76	44	4953	E
E40	0,9	73	85	139	5530	E
E41	0,2	75	96	102	5395	EL
E42	0,6	107	112	130	9478	E
E43	0,5	91	141	9	8800	EL
E44	0,7	69	95	135	5648	EL
E45	0,7	67	80	43	4678	E
E46	0,7	69	72	43	4643	S
E47	0,4	65	72	142	4055	E
E48	0,8	93	114	136	8691	E
E49	0,8	75	91	37	5368	E
E50	1,1	98	197	179	14319	EL
E51	1	119	142	137	13804	EL
E52	0,7	65	67	44	4287	S
E53	0,5	67	73	47	3893	E
E54	1,3	151	173	96	20010	I1
E55	0,8	126	133	135	13293	EL
E56	1,1	83	92	43	6372	E
E57	1,1	90	141	92	8441	E
E58	0,7	106	112	43	10336	EL
E59	0,7	113	223	51	17752	I1
E60	0,8	99	141	45	12405	I1
E61	1,1	71	77	138	4981	E
E62	1,1	72	74	47	5040	E
E63	0,7	80	123	157	6292	E
E64	1,2	96	147	6	9578	E

E65	0,6	72	99	141	5835	E
E66	0,7	96	116	2	7401	E
E67	1	139	143	135	16756	I1
E68	0,5	69	72	42	4590	E
E69	0,4	85	135	25	7486	E
E70	0,8	73	76	137	5182	E
E71	0,5	83	97	134	6501	E
E72	1,2	133	171	127	17039	E
E73	0,8	69	72	131	4758	E
E74	0,5	63	95	150	4244	E
E75	0,7	91	145	2	9056	E
E76	0,6	73	81	138	4957	E
E77	0,8	96	139	2	9207	EL
E78	0,7	63	79	142	4125	E
E79	0,4	64	84	143	4163	E
E80	0,9	125	191	179	15766	E
E81	1	106	126	45	11168	EL
E82	0,7	81	107	147	7032	E
E83	0,7	71	76	47	4916	E
E84	0,4	81	112	83	6742	E
E85	0,6	135	161	167	16286	EL
E86	0,6	106	124	47	10752	E
E87	0,5	58	93	70	3625	E
E88	0,7	70	82	142	4685	E
E89	0,4	63	73	39	3916	E
E90	0,4	68	73	134	4641	E
E91	0,5	90	115	168	7507	E
E92	1,1	77	89	38	5178	S
E93	1,1	139	144	42	16802	S
E94	0,8	69	80	43	4856	E
E95	1,1	72	79	52	5034	E
E96	0,7	67	75	47	4685	S
E97	1	98	189	168	13591	EL
E98	0,7	71	74	136	5017	E
E99	0,4	72	90	56	4911	S
E100	0,7	79	109	146	6212	E
E101	0,8	68	75	44	4470	E
E102	0,4	133	180	34	18929	EL
E103	0,7	74	75	48	5155	E
E104	0,7	91	144	180	8729	EL
E105	0,5	93	132	8	8416	EL
E106	0,6	66	72	132	4381	E
E107	2,7	106	196	9	14942	EL
E108	1,4	99	142	97	9534	EL
E109	0,6	79	93	148	5132	E
E110	0,6	106	117	144	9268	S
E111	0,5	94	175	171	12349	EL
E112	0,8	78	126	18	7362	EL
E113	0,2	61	77	45	3787	E
E114	0,3	78	131	12	6781	E
E115	0,4	77	104	117	6351	E
E116	0,7	98	142	175	8843	E
E117	0,3	97	105	17	7740	E
E118	0,6	71	73	46	4810	E

E119	0,6	71	82	140	4813	E
E120	0,7	69	75	135	4864	E
E121	0,6	113	135	106	11634	EL
E122	0,6	63	71	134	4381	E
E123	3,2	72	77	137	5171	E
E124	0,7	69	73	137	4764	S
E125	0,4	79	84	42	5469	E
E126	0,6	73	75	47	5210	E
E127	1	71	79	137	5095	E
E128	1	83	109	31	5625	E
E129	1,2	71	74	137	4971	S
E130	0,5	89	93	37	6357	E
E131	0,7	91	125	153	9235	E
E132	0,8	72	72	134	4981	E
E133	0,8	89	134	20	7414	E
E134	1,3	72	81	132	5090	S
E135	0,3	66	70	50	4031	S
E136	1,5	73	77	44	5214	S
E137	0,7	107	125	139	11411	E
E138	0,3	96	131	3	8239	E
E139	0,8	100	113	39	9565	E
E140	0,6	68	76	53	4276	E
E141	1,9	72	74	137	5047	E
E142	0,9	97	124	85	8493	EL
E143	1,8	76	83	40	5129	E
E144	0,6	68	72	47	4582	E
E145	1,1	99	134	0	8883	EL
E146	1,1	133	150	64	15407	E
E147	0,9	100	118	35	8874	E
E148	1,3	72	81	132	5429	S
E149	1	70	91	47	5145	S
E150	0,5	91	110	141	7676	EL
E151	0,5	71	79	46	4928	E
E152	0,6	86	120	163	7539	E
E153	0,9	71	73	45	4925	E
E154	0,6	116	138	0	12272	EL
E155	0,7	93	145	1	9076	EL
E156	0,8	106	143	44	13234	E
E157	1,4	71	73	44	4911	E
E158	0,5	88	131	88	7832	EL
E159	1,4	67	72	42	4351	E
E160	1	68	83	144	4541	E
E161	0,7	91	132	16	6984	I2
E162	0,7	66	71	45	4500	S
E163	0,5	89	153	66	10378	EL
E164	0,7	136	163	135	17157	I1
E165	1,4	109	147	83	10669	EL
E166	0,7	68	68	45	4449	E
E167	0,7	72	74	137	4930	E
E168	0,4	68	75	141	4423	S
E169	1,3	77	95	26	5251	E
E170	1,4	73	76	133	5288	E
E171	0,7	96	136	17	8241	E
E172	0,6	97	138	14	10071	E

E173	0,6	67	74	50	4501	E
E174	1	165	275	81	35187	EL
E175	0,4	104	138	87	10073	E
E176	0,3	98	135	156	9167	E
E177	0,7	99	129	94	8919	E
E178	0,8	102	149	179	9968	EL
E179	0,3	63	86	123	3761	E
E180	1,2	73	82	141	5060	S
E181	0,4	70	90	31	4704	S
E182	0,6	72	80	41	5085	E
E183	0,9	71	74	48	4852	E
E184	1,1	72	74	135	5201	S
E185	0,5	67	74	44	4550	S
E186	0,5	69	82	52	5016	S
E187	1,3	94	143	178	9399	E
E188	0,6	86	146	177	8618	EL
E189	2,1	74	94	30	5909	E
E190	1,4	99	112	142	8762	E
E191	0,7	67	74	37	4242	E
E192	0,6	71	76	45	4966	E
E193	3,5	83	117	99	7182	E
E194	1,5	67	74	46	4627	S
E195	0,3	97	139	10	8922	E
E196	0,3	109	122	35	10286	EL
E197	0,6	60	67	42	3484	E
E198	0,4	64	81	64	4204	E
E199	0,4	62	91	126	3720	E
E200	0,9	93	155	8	9433	EL
E201	0,4	103	111	141	9494	E
E202	0,5	70	88	54	4487	E
E203	0,4	65	81	48	4178	E
E204	0,4	68	78	129	4654	E
E205	0,5	95	110	148	7927	E
E206	0,8	70	74	44	4777	E
E207	0,4	65	72	43	4265	S
E208	1,1	92	144	180	8700	E
E209	0,9	71	78	136	5015	S
E210	0,7	71	76	132	4927	E
E211	0,4	118	182	35	14932	E
E212	0,9	71	73	44	4926	S
E213	1	74	85	39	5093	E
E214	0,6	69	119	167	5729	EL
E215	0,4	72	97	65	5036	EL
E216	0,5	124	168	172	15458	S
E217	0,8	73	82	38	4926	S
E218	0,7	70	71	43	4801	E
E219	0,4	62	70	41	3818	E
E220	0,7	89	91	134	6902	E
E221	0,7	80	87	139	5874	E
E222	0,7	89	147	98	8998	EL
E223	0,5	76	84	138	4986	E
E224	0,8	67	70	45	4393	E
E225	0,3	71	93	19	4614	EL
E226	0,2	91	132	15	8364	EL

E227	0,3	65	82	137	4359	E
E228	0,3	44	104	159	3375	EL
E229	0,6	97	134	9	8854	EL
E230	0,6	124	144	60	13282	E
E231	0,6	94	137	85	8439	EL
E232	0,9	75	79	134	5398	S
E233	0,7	100	147	176	9592	E
E234	0,6	77	91	39	5661	E
E235	0,3	74	97	149	5509	E
E236	0,5	132	216	25	23728	EL
E237	0,8	87	125	39	8901	E
E238	0,1	70	74	138	4729	E
E239	0,6	79	112	28	7553	S
E240	0,9	74	87	132	5450	E
E241	0,6	72	97	134	5722	E
E242	0,9	102	138	169	9448	EL
E243	0,4	125	158	35	14424	I1
E244	1,3	81	114	45	7000	E
E245	0,5	70	74	44	5017	E
E246	0,4	71	82	44	5089	E
E247	0,2	99	144	44	12667	EL
E248	0,4	93	146	177	8904	EL
S1	3,5	99	150	176	9669	E
S2	2,8	71	76	138	5033	E
S3	1,5	80	92	128	5665	E
S4	3,2	73	76	132	5195	E
S5	3,3	101	144	160	9240	E
S6	3	102	197	179	14619	EL
S7	2	95	131	16	8494	E
S8	2,1	72	74	136	5186	S
S9	0,8	68	73	137	4727	E
S10	1,7	106	143	130	10513	E
S11	3	84	134	155	8169	E
S12	1	95	151	179	9892	EL
S13	1,7	99	146	2	9611	E
S14	1,4	111	132	138	12456	EL
S15	1,2	80	115	156	6262	E
S16	0,7	109	167	156	14368	EL
S17	3,8	91	137	157	8728	T
S18	2,8	70	85	45	5445	E
S19	2,2	100	199	2	14069	T
S20	2,5	70	76	40	4844	E
S21	3,2	71	78	40	4762	
S22	3,4	69	71	44	4892	E
S23	4,1	97	148	175	9933	EL
S24	0,1	101	148	1	10401	E
S25	0,4	97	102	135	4990	E
S26	0,7	98	119	72	9151	EL
S27	0,7	72	87	34	4694	E
S28	0,4	103	217	56	14808	EL
S29	0,3	67	86	135	4463	E
S30	1,4	150	195	1	23063	EL
S31	1	108	141	138	13140	EL
S32	1,3	100	148	4	9916	EL

S33	0,6	75	85	38	5310	E
S34	0,9	110	135	132	12407	EL
S35	0,8	120	145	34	12641	EL
S36	0,8	75	87	40	5612	E
S37	0,8	92	97	118	6971	EL
S38	1	102	144	176	9948	EL
S39	1,1	78	92	36	5571	E
S40	0,5	78	89	54	5647	E
S41	1,1	68	73	137	4660	S
S42	0,6	101	155	155	11361	EL
S43	1,1	74	80	130	4947	S
S44	0,9	83	103	28	5976	E
S45	0,7	71	73	46	4838	E
S46	0,4	74	89	138	5671	E
S47	0,9	70	103	3	5103	I1
S48	0,9	117	246	0	21315	EL
S49	0,9	96	98	134	8185	E
S50	0,7	73	81	129	5272	E
S51	0,9	89	136	159	8322	E
S52	0,8	86	146	98	8832	E
S53	1	93	144	173	9060	S
S54	1,1	68	71	47	4515	E
S55	0	91	141	9	8667	E
S56	1,5	99	155	177	9572	I1
S57	0,1	102	150	140	11436	I1
S58	0,5	137	180	142	18213	E
S59	1,7	80	122	31	6075	I1
S60	0,8	63	83	46	4174	I1
S61	1,2	80	97	162	5463	EL
S62	1,2	90	147	178	9116	E
S63	1	73	74	45	5142	EL
S64	0,9	95	150	89	9497	E
S65	1,1	91	144	167	8681	E
S66	0,3	72	76	136	4894	S
S67	0,9	65	75	42	4232	E
S68	1	73	74	44	5217	E
S69	0,9	73	75	49	5082	E
S70	0,6	69	75	44	4757	E
S71	0,6	125	143	6	13461	I1
S72	0,8	71	73	44	4984	S
S73	1,2	87	116	71	6761	E
S74	0,9	76	90	37	5371	E
S75	1	91	125	120	7442	E
S76	1,3	101	152	5	10006	EL
S77	1,3	99	151	179	9798	E
S78	1,8	78	88	50	5968	I1
S79	1	99	149	0	9743	EL
S80	1,1	69	78	38	4773	E
S81	1	89	140	21	7611	E
S82	0,9	71	74	43	4943	E
S83	0,9	84	116	30	6514	E
S84	0,7	77	84	144	5271	E
S85	0,6	75	94	37	5720	E
S86	0,8	72	74	132	4887	E

S87	0,6	68	73	135	4626	E
S88	1,1	71	78	37	4751	E
S89	0,9	81	87	141	5679	E
S90	0,5	73	81	43	4934	E
S91	1,3	72	73	137	5098	S
S92	0,5	97	118	143	8421	I1
S93	1,1	101	146	3	9017	EL
S94	1,3	93	117	166	6873	EL
S95	1,4	107	141	19	10555	EL
S96	0,7	79	106	28	5643	E
S97	0,7	89	144	179	8700	E
S98	0,6	102	156	0	11011	EL
S99	0,5	116	136	12	10927	I1
S100	0,8	85	177	6	10506	E
S101	2,8	85	87	137	5934	E
S102	0,9	95	139	173	8851	EL
S103	0,6	71	72	136	4878	S
S104	0,7	61	68	46	3434	S
S105	1	93	132	13	7965	E
S106	0,6	81	115	23	6066	E
S107	0,7	71	84	129	4993	S
S108	0,5	73	82	141	5271	E
S109	0,6	94	150	172	9835	EL
S110	0,8	88	145	157	6462	E
S111	0,8	84	122	153	5998	E
S112	1	97	110	50	8284	E
S113	1,1	71	76	135	5081	S
S114	1,1	95	97	40	7976	E
S115	0,7	74	76	137	5189	E
S116	0,4	105	120	129	10069	EL
S117	0,6	74	84	139	5421	E
S118	0,7	95	131	13	8973	EL
S119	1,5	103	140	16	9521	E
S120	0,9	73	78	133	5304	E
S121	0,8	74	80	42	5241	E
S122	0,8	96	159	166	9689	E
S123	0,6	69	74	43	4780	S
S124	0,8	95	153	4	10574	EL
S125	0,9	71	77	40	4884	S
S126	0,9	75	84	140	5428	E
S127	1,2	68	74	41	4605	E
S128	0,7	97	154	174	9789	EL
S129	1	88	108	174	5891	E
S130	0,9	79	122	152	6131	E
S131	1,1	99	137	20	8970	E
S132	0,8	69	88	104	4402	E
S133	0,9	73	78	43	5288	S
S134	1	72	74	45	5016	E
S135	0,8	92	116	50	8161	EL
S136	1,2	75	75	45	5473	E
S137	0,9	74	90	61	5169	E
S138	0,8	66	74	138	4299	E
S139	1	85	139	158	6973	E
S140	0,8	72	76	44	5121	E

S141	0,9	102	148	178	10094	EL
S142	0,7	68	72	134	4431	S
S143	1,5	67	111	63	5058	E
S144	1	84	127	155	7197	E
S145	1,2	73	77	41	4931	E
S146	0,7	65	101	44	5403	I1
S147	1	72	76	134	5098	E
S148	1,1	70	72	45	4983	S
S149	0,7	70	81	42	4765	E
S150	0,7	103	115	137	9959	EL
S151	0,7	102	136	77	9383	EL
S152	0,7	76	91	36	5258	E
S153	0,7	72	74	44	4944	E
S154	0,6	62	88	147	3989	EL
S155	0,6	79	98	146	5478	E
S156	0,5	74	80	140	5118	E
S157	0,4	66	70	138	4166	E
S158	0,6	74	83	41	5401	S
S159	1	74	130	168	5886	EL
S160	1	87	112	18	6380	E
S161	0,8	88	131	11	8266	E
S162	0,8	80	104	33	6083	E
S163	1,1	81	99	30	5213	E
S164	0,7	97	102	65	7580	I1
S165	0,6	68	74	43	4789	E
S166	0,4	86	129	19	7530	EL
S167	0,9	63	110	16	5063	E
S168	1	79	113	151	5524	E
S169	0,6	67	73	143	4341	E
S170	0,9	71	76	134	4459	E
S171	0,7	97	106	139	8416	E
S172	0,6	80	103	32	5799	E
S173	0,5	73	98	144	5412	E
S174	0,4	61	73	138	3863	S
S175	0,8	83	108	32	5780	E
S176	0,5	74	110	30	5506	E
S177	0,3	86	103	108	6685	I1
S178	0,5	71	73	136	4977	E
S179	1,2	138	141	134	16836	C
S180	0,2	64	102	156	5109	EL
S181	0,3	75	148	86	7340	EL
S182	0,4	71	72	46	4769	E
S183	0,3	70	84	140	4686	E
S184	0,4	105	129	137	11153	I1
S185	0,6	87	151	161	7493	E
S186	0,5	66	105	138	5518	E
S187	0,4	63	127	156	4916	EL
S188	0,6	74	80	134	5062	E
S189	0,5	80	87	136	5518	E
S190	0,5	93	113	68	7978	EL
S191	0,8	100	169	134	12764	I1
S192	1,9	71	76	42	4886	E
UW1	3,2	102	200	172	14757	T
UW2	2,6	143	255	173	24815	T

UW3	1,3	104	133	140	10949	EL
UW4	2,6	99	152	0	9843	EL
UW5	2,8	92	145	160	8094	I2
UW6	2,3	74	76	44	5237	E
UW7	4,5	90	90	46	6640	E
UW8	3	70	71	135	4855	S
UW9	1,4	102	144	44	11748	E
UW10	1,5	81	92	44	6391	T
UW11	1	68	73	135	4703	E
UW12	1,3	74	85	131	5351	E
UW13	1	70	72	134	4720	E
UW14	0,7	79	120	61	7481	I1
UW15	0,5	69	79	143	4523	E
UW16	1,2	68	73	133	4564	E
UW17	2,8	72	77	135	4916	E
UW18	1,2	75	127	169	6032	EL
UW19	1,3	51	105	45	3836	EL
UW20	0,7	62	86	112	3175	E
UW21	0,9	65	110	7	5295	EL
UW22	2	84	109	32	6194	T
UW23	0,8	77	149	20	8330	T
UW24	1,6	73	80	39	4941	E
UW25	0,9	92	108	142	7434	E
UW26	1,4	70	100	138	5468	T
UW27	1,2	70	71	46	4799	S
UW28	1,6	72	72	136	4870	E
UW29	0,7	71	73	46	4565	E
UW30	1,4	70	75	44	5057	E
UW31	0,9	71	73	45	4695	E
UW32	0,5	119	160	15	12700	E
UW33	2,6	100	145	87	9820	E
UW34	0,6	127	168	151	16235	EL
UW35	0,9	108	149	99	10755	E
UW36	2,4	100	144	1	9216	E
UW37	1,7	101	145	3	9362	E
UW38	1,6	102	148	0	11063	EL
UW39	1,2	70	72	45	4830	E
UW40	0,9	72	82	47	5423	E
UW41	1	98	143	98	9234	EL
UW42	0,6	67	70	44	4492	S
UW43	1,6	111	145	134	13631	I1
UW44	1,6	105	121	138	10123	E
UW45	2,8	103	147	178	9849	E
UW46	2,7	107	138	136	12423	I1
UW47	2,4	144	182	171	18331	EL
UW48	1,1	101	162	135	11200	I2
UW49	1,9	128	185	147	18942	I1
UW50	1,1	82	90	134	5995	E
UW51	0,7	71	75	136	4916	E
UW52	1	97	122	147	8915	E
UW53	1,4	74	80	49	5220	E
UW54	1,3	101	143	95	10053	EL
UW55	0,7	85	183	158	9787	EL
UW56	0,6	81	104	31	6098	EL

UW57	0,5	93	130	47	9636	EL
UW58	1,5	103	149	1	9835	EL
UW59	0,4	71	76	142	4711	E
UW60	0,6	95	142	13	9387	E
UW61	0,4	91	109	172	6628	E
UW62	1	90	110	25	7435	EL
UW63	1,1	127	161	0	14278	I1
UW64	0,4	90	119	109	7991	EL
UW65	0,4	76	105	152	5761	EL
UW66	0,4	71	98	22	5084	EL
UW67	0,4	95	127	136	9735	EL
UW68	0,9	69	84	37	5199	E
UW69	0,7	83	110	28	7095	E

Q 1.2 data

Table 6.3: Collected data of pockmarks at Q 1.2 horizon.

Pock name	Depth (OWT) (ms)	Width (m)	Length (m)	Direction (degree)	Area (m^2)	Primary shape
1	1,3	71	77	135	4739	E
2	0,5	68	69	135	4270	E
3	0,5	65	67	137	3882	S
4	0,5	82	131	28	7555	E
5	0,7	90	167	175	10512	EL
6	0,4	63	95	148	4447	EL
7	0,2	42	68	31	2642	EL
8	0,9	71	71	135	4714	E
9	0,6	83	142	136	7901	I1
10	2,6	69	73	139	4567	E
11	0,8	89	127	122	8660	E
12	0,5	48	58	39	2169	E
13	0,7	101	230	174	17162	EL
14	0,8	105	131	49	11446	EL
15	0,2	69	82	33	4246	S
16	0,6	83	129	155	6665	E
17	0,5	66	127	171	5822	E
18	0,6	88	160	24	11549	I1
19	0,4	82	141	13	6823	I2
20	0,4	102	157	56	11422	E
21	0,3	66	85	127	4232	E
22	0,3	68	85	33	4384	E
23	0,4	81	202	157	11411	EL
24	0,4	57	118	165	4503	EL
25	1	96	90	44	4493	E

26	1	70	102	44	5717	EL
27	0,6	64	73	132	4093	EL
28	0,3	61	101	20	4689	EL
29	0,4	89	111	155	7547	E
30	0,3	67	70	44	4765	E
31	0,6	100	146	145	11493	EL
32	1,3	189	260	25	32960	I1
33	0,8	69	81	42	4988	E
34	0,6	63	130	20	5137	EL
35	1	70	75	138	4724	S
36	0,4	56	141	102	4793	EL
37	1	180	228	178	29406	I1
38	0,9	67	72	47	4256	E
39	0,6	82	132	160	8748	I1
40	0,8	54	73	42	3027	E
41	0,4	80	118	150	6554	E
42	0,8	67	72	46	4387	S
43	0,8	91	152	20	9836	EL
44	1,1	75	78	41	5127	E
45	0,9	108	141	6	9875	E
46	1,3	114	126	88	11194	I1
47	0,7	86	90	27	5587	EL
48	0,9	67	131	26	5485	E
49	1,3	57	70	46	3603	E
50	0,9	100	151	159	10633	E
51	0,4	78	87	47	5258	E
52	0,6	71	79	138	5094	E
53	0,7	78	83	140	5362	E
54	0,3	94	99	142	7928	E
55	0,4	66	76	135	4674	S
56	0,2	72	89	60	4923	E
57	0,6	74	77	139	5177	E
58	0,4	128	160	34	15336	I1
59	1	138	216	40	21091	EL
60	1	67	73	46	4587	E
61	1,1	67	102	49	5208	E
62	1,1	95	146	174	9716	E
63	0,5	84	159	180	9206	EL
64	0,4	102	140	47	11262	EL
65	1,8	97	141	179	9491	I2
66	1,7	133	147	63	12897	E
67	0,6	68	102	140	5483	EL
68	0,4	68	72	136	4569	E
69	1,6	71	74	37	4139	E
70	1,5	59	68	123	2807	E
71	1,6	88	124	120	7806	I1

72	4,7	159	430	1	49305	I1
73	1,6	130	219	27	20738	I2
74	1,5	83	187	164	11220	I2
75	1,2	80	142	19	7041	E
76	0,7	69	100	41	5678	E
77	0,6	103	199	180	14996	EL
78	0,7	79	174	134	10962	EL
79	0,6	68	72	137	4520	S
80	0,5	111	154	3	12195	E
81	0,8	150	193	134	21948	I2
82	0,9	70	137	165	6989	E
83	1,2	72	100	145	5530	E
84	0,6	72	78	136	5107	E
85	0,6	84	167	159	11018	E
86	0,4	80	95	59	5567	EL
87	0,6	66	69	136	4305	E
88	0,4	66	72	44	4443	E
89	0,4	70	84	38	4763	E
90	0,5	68	74	46	4249	E
91	0,8	111	188	90	16041	EL
92	0,6	91	128	156	8328	E
93	0,5	71	95	133	5452	E
94	0,4	84	124	14	7063	E
95	0,4	68	117	20	4888	E
96	0,3	74	82	49	5311	S
97	0,5	69	79	45	4531	E
98	0,4	61	86	161	3409	E
99	0,5	74	76	139	4798	S
100	0,4	67	97	149	4399	EL
101	0,4	73	76	40	4622	EL
102	0,6	94	134	1	9095	EL
103	0,5	70	88	40	4973	EL
104	0,4	75	136	177	7115	EL
105	0,5	95	148	85	10709	EL
106	0,4	72	76	135	4659	E
107	0,3	68	72	138	4306	E
108	0,5	101	138	172	9540	EL
109	0,6	98	136	156	9783	EL
110	1,2	109	194	153	15134	E
111	1	92	139	159	8370	E
112	1	74	76	137	5014	E
113	0,6	74	76	137	5236	E
114	1,1	125	165	161	14974	I1
115	0,9	99	147	4	10830	I2
116	1	88	122	27	7857	E
117	0,7	70	76	45	4785	E

118	0,9	91	111	47	8064	E
119	1,4	122	256	143	21533	I2
120	2	100	149	93	10895	E
121	0,5	93	146	50	10053	EL
122	0,5	72	96	32	4860	E
123	0,6	71	74	44	4381	E
124	3,7	81	278	163	14664	T
126	3,5	181	267	59	35945	T
127	4,9	191	239	118	34139	T
128	0,7	69	71	136	4389	EL
129	0,8	98	180	5	12499	EL
130	0,9	94	149	1	9361	EL
131	0,7	101	201	160	13961	EL
132	0,9	97	155	12	10822	EL
133	0,7	109	161	3	12497	EL
134	0,6	95	147	13	9437	E
135	0,6	103	183	162	14064	E
136	0,5	141	206	134	16656	I2
137	0,7	162	269	175	28747	I1
138	0,7	84	189	170	11751	EL
139	1	70	77	47	4648	EL
140	1,7	115	327	164	27622	T
141	0,9	97	158	172	9610	EL
142	1,3	96	191	11	13222	EL
143	1,5	70	131	29	5943	EL
144	1,5	69	72	138	4762	S
145	0,9	69	100	135	5756	EL
146	1,1	83	117	28	6697	E
147	1,2	83	114	28	7336	E
148	1,4	70	71	135	4650	E
149	0,6	108	313	159	22829	E
150	0,8	122	202	165	15615	I2
151	1,1	110	141	88	10636	I1
152	0,6	72	76	138	4768	E
153	0,7	72	97	46	5914	E
154	0,8	167	256	157	27447	I2
155	1	191	221	35	34905	I1
156	0,7	64	72	138	4278	E
157	0,6	96	214	10	15109	E
158	0,9	88	132	167	7758	E
159	0,6	71	72	44	4574	E
160	0,8	89	129	154	8381	E
161	0,8	128	160	122	15898	I1
162	1,1	123	209	175	18235	EL
163	0,8	65	80	35	4204	E
164	1,5	95	267	2	18972	EL

165	0,6	75	98	33	5343	E
166	0,2	74	78	141	4512	E
167	1	85	146	170	8103	E
168	1,7	226	449	27	69356	I2
169	0,8	127	145	163	14614	I1
170	0,6	72	120	158	6566	EL
171	1,4	239	274	136	49928	E
172	1,1	142	181	136	19381	EL
173	0,9	92	150	0	9366	E
174	0,6	72	84	127	4797	E
175	0,6	74	75	48	5116	S
176	0,3	71	135	25	7570	EL
177	0,5	62	144	166	6144	E
178	0,9	79	144	162	8306	EL
179	0,7	82	167	0	8813	EL
180	0,7	90	142	0	9063	E
181	0,5	82	134	8	7653	EL
182	1,1	172	321	54	38802	EL
183	0,8	88	123	88	7909	E
184	0,4	112	151	87	12545	EL
185	0,6	84	153	14	9212	EL
186	1	126	233	174	20173	I1
187	0,7	126	218	13	17721	EL
188	0,7	135	158	32	14588	E
189	0,6	50	103	165	3555	EL
190	0,8	69	78	137	4682	S
191	0,8	65	210	169	8609	E
192	2,6	171	189	28	26026	I1
193	0,7	103	132	21	10454	E
ADD1	7,5	253	379	31	95815	I1
ADD2	2,4	159	315	155	49986	T
ADD3	1,6	105	196	156	20635	T
ADD4	3,1	106	240	165	25368	T
ADD5	5,4	115	320	161	36920	T
ADD6	4,4	91	175	88	15905	T
ADD7	1,5	89	108	49	9607	E
ADD8	5,8	162	254	147	41179	T
ADD9	3,1	112	278	164	30996	T
ADD10	2,4	241	301	82	72510	I1
ADD11	2,1	87	96	148	8301	I1
ADD12	0,9	102	124	28	12667	I1
ADD13	1,6	65	105	162	6794	E
ADD14	3,2	240	290	62	69406	I1
ADD15	2,6	131	220	67	28911	T
ADD16	4	59	74	134	4333	E
ADD17	1,5	96	128	126	12360	E

ADD18	2,5	139	210	49	29204	I2
ADD19	3,6	73	129	11	9461	T
ADD20	3,2	87	170	113	14721	T
ADD21	5,1	132	227	146	29897	T
ADD22	1,9	97	174	3	16967	E
ADD23	3	160	223	125	35643	T
ADD24	2	75	108	141	8090	E
ADD25	3,3	91	144	178	13054	EL
ADD26	2,4	73	78	43	5629	E
ADD27	4,3	156	215	32	33589	I1
ADD28	3,2	113	281	0	31818	T
ADD29	5,5	124	159	69	19745	T
ADD30	4,4	188	230	66	43303	I1
ADD31	9,7	248	316	136	78111	I1
ADD32	5,6	244	396	50	96665	I2
ADD33	5,3	257	396	18	1E+05	I2
ADD34	4,6	101	290	138	29183	E
ADD35	4,2	64	79	145	5042	E
ADD36	2	70	73	136	5106	E
ADD37	5,4	65	84	59	5451	E
ADD38	5,6	77	121	175	9278	E
ADD39	1,8	91	123	62	11160	T
ADD40	4,2	65	79	146	5120	E
ADD41	5,4	129	216	41	27951	I1
ADD42	2,3	79	142	162	11148	E
ADD43	1,7	72	134	82	9624	I2
ADD44	3,7	83	146	26	12154	T
ADD45	1,8	97	141	141	13680	EL

Q 2.1 data

Table 6.4: Collected data of pockmarks at Q 2.1 horizon

Pockm. Name	Depth (OWT) (ms)	Width (m)	Length (m)	Direction (degree)	Area (m^2)	Primary shape
E_1	1,4	76	101	130	6086	E
E_2	1,7	169	238	28	23130	CR
E_3	2	93	150	175	9043	E
E_4	2,2	73	80	44	5237	E
E_5	0,8	53	91	65	4127	E
E_6	1,3	68	71	44	4650	E
E_7	1	60	88	139	4218	S
E_8	0,5	88	111	80	5619	E
E_9	0,4	130	171	41	15435	E
E_10	0,6	151	257	166	26123	E

E_11	1	66	96	69	4069	E
E_12	4,5	134	217	61	18433	I2
E_13	0,3	66	78	127	4139	S
E_14	0,5	90	113	133	7930	E
E_15	0,5	71	74	132	4829	E
E_16	1,6	134	174	30	16790	E
E_17	1,9	105	142	134	11991	E
E_18	3,4	71	72	135	4922	E
E_19	1,2	88	124	104	7438	EL
E_20	2,7	142	178	135	19650	E
E_21	1,2	120	128	45	11667	E
E_22	2,3	84	109	54	7269	E
E_23	2,8	153	178	161	20513	E
E_24	3,7	106	190	45	15538	E
E_25	3,5	115	146	81	11141	E
E_26	3	94	134	24	9067	E
E_27	2	87	113	70	7312	E
E_28	3,8	70	71	47	4501	E
E_29	1,9	83	100	60	6078	E
E_30	1,6	81	123	161	7223	E
E_31	1,7	71	73	45	4950	E
E_32	1,8	119	230	56	18113	EL
E_33	1,6	98	187	21	10683	EL
E_34	2,4	107	151	134	12407	I1
E_35	0,9	85	152	31	9311	E
E_36	2	72	99	135	6003	E
E_37	0,8	89	151	36	10214	EL
E_38	2,1	143	196	57	20758	I1
E_39	3,1	136	227	153	11834	C
E_40	2,3	70	74	44	4964	E
E_41	0,6	55	85	144	2800	E
E_42	0,4	28	83	7	1429	E
E_43	0,6	39	94	161	2163	E
E_44	1,6	89	137	80	8474	EL
E_45	1,1	89	125	76	7436	E
E_46	1,1	56	75	162	2863	E
E_47	3,4	97	179	131	13226	I1
E_48	1,1	57	109	24	4630	E
E_49	1,3	83	115	159	7181	EL
E_50	3,1	122	228	47	19595	CR
E_51	1,2	89	113	15	6595	E
E_52	2	82	112	56	6174	E
E_53	1,8	57	80	23	2725	E
E_54	2,1	106	126	142	10373	E
E_55	6,1	213	314	46	55270	I1
E_56	6,5	132	300	7	28021	T
E_57	0,6	40	68	159	2230	E
E_58	1,8	75	184	142	10551	EL
E_59	1,2	65	105	145	5061	E
E_60	0,9	65	92	157	3869	E
E_61	3,1	99	144	179	9483	EL
E_62	2,3	70	70	46	4803	E
E_63	2,2	93	146	10	8986	E
E_64	1,2	102	132	153	9613	E

E_65	2,2	80	110	124	6951	EL
E_66	4,2	107	189	35	16137	I1
E_67	2,1	94	117	40	9137	EL
E_68	0,9	54	66	143	2869	E
E_69	0,3	21	46	153	599	E
E_70	1	74	167	59	7469	E
E_71	2,3	125	139	155	12929	I1
E_72	1,5	86	124	60	8832	E
E_73	0,9	87	140	2	8238	E
E_74	1,6	144	206	111	20348	C
E_75	3,3	71	166	142	9109	E
E_76	5,9	144	178	44	19825	I1
E_77	2,8	70	73	45	4893	E
E_78	1,3	90	145	7	7900	E
E_79	1	75	98	35	5776	EL
E_80	0,8	84	106	135	6569	I1
E_81	1,5	84	188	173	11268	EL
E_82	1,3	72	74	44	4902	E
E_83	1,8	92	146	148	9948	E
E_84	2	109	194	155	16564	I1
E_85	0,8	68	153	175	6696	E
E_86	1,8	111	149	134	13142	E
E_87	1,6	74	82	126	4535	E
E_88	0,6	63	69	140	3927	E
E_89	1,1	68	78	35	4457	E
E_90	0,9	67	143	166	7177	E
E_91	0,7	59	79	25	3203	E
E_92	0,5	66	76	142	3820	E
E_93	0,6	54	65	137	2738	E
E_94	1,2	70	150	129	7479	E
E_95	1,3	48	56	56	1935	E
E_96	1	57	66	133	3268	E
E_97	0,9	65	75	126	3948	E
E_98	1,5	100	136	92	9855	EL
E_99	1	81	94	146	5804	E
E_100	0,4	54	100	152	4367	E
E_101	0,4	54	72	118	3239	E
E_102	0,4	62	94	69	3930	E
E_103	1,2	161	246	176	31539	I2
E_104	0,9	68	71	136	4692	E
E_105	0,9	69	73	136	4224	E
E_106	1,7	91	108	79	6966	E
E_107	0,8	85	168	176	9642	E
E_108	1,2	92	140	86	9148	EL
E_109	0,5	83	154	106	7586	E
E_110	0,8	68	73	134	4388	E
E_111	1,5	70	75	43	4955	E
E_112	0,9	79	105	133	6597	E
E_113	0,4	38	104	150	2688	E
E_114	0,4	66	112	131	5394	E
E_115	0,4	66	142	142	7044	E
E_116	0,4	62	71	141	3730	E
E_117	0,1	46	143	140	4152	E
E_118	2,1	135	174	61	17730	E

E_119	1,2	77	111	30	5951	E
E_120	0,6	83	131	37	8739	EL
E_121	0,7	54	89	166	3603	E
E_122	1,8	147	210	34	22380	I1
E_123	1,1	81	124	104	7267	E
E_124	0,5	70	85	135	4893	E
E_125	1	98	114	137	8446	E
E_126	0,9	80	172	134	10887	E
E_127	0,9	79	106	159	6809	E
E_128	0,6	59	78	30	3223	E
E_129	1,3	78	127	154	7382	E
E_130	0,9	62	199	168	7586	EL
E_131	1,2	86	124	147	8625	E
E_132	3,5	124	152	49	15616	I1
E_133	1,3	61	70	136	3621	S
E_134	1,1	59	71	42	3569	E
E_135	0,5	71	78	38	4779	S
E_136	0,8	62	96	158	3784	E
E_137	1,2	69	75	39	4377	S
E_138	0,8	58	68	34	2901	E
E_139	0,4	44	76	137	2244	E
E_140	0,7	78	187	136	9294	E
E_141	1	105	201	135	15921	EL
E_142	2,8	89	107	19	6166	E
E_143	1,5	68	77	139	4753	S
E_144	2,8	192	252	50	38154	I1
E_145	3,5	178	273	136	34532	EL
E_146	1,7	80	120	151	5535	E
E_147	1,4	71	74	47	4787	E
E_148	1,7	131	158	133	15574	I1
E_149	3,1	71	71	135	4993	E
E_150	1,5	105	153	2	10303	EL
E_151	1,3	48	80	67	2882	E
E_152	2,6	155	239	79	27282	I2
E_153	1,4	109	180	139	15898	E
E_154	0,9	101	175	167	12837	E
E_155	1,4	72	72	46	4927	E
E_156	2,3	103	196	89	14934	EL
E_157	0,5	29	79	142	1598	EL
E_158	1,7	138	260	143	25268	EL
E_159	1,3	101	145	90	9903	I1
E_160	1,3	70	73	136	4928	E
E_161	1,3	99	145	2	9500	E
E_162	1,3	71	73	136	5019	S
E_163	0,9	94	117	39	7936	E
E_164	1	72	74	137	5016	E
E_165	0,6	64	90	125	4451	E
E_166	1,3	70	73	44	4887	E
E_167	2,5	98	148	177	9316	E
E_168	2,6	122	279	138	24802	EL
E_169	2,2	69	72	136	4669	E
E_170	2,1	70	72	44	4811	E
E_171	1,4	97	144	95	9144	E
E_172	0,8	67	69	136	4463	E

E_173	0,9	94	123	138	8642	E
E_174	1	68	75	51	4378	E
E_175	0,5	59	90	147	4766	E
E_176	1	69	72	43	4718	E
E_177	3	152	273	44	26299	I2
E_178	1,4	95	136	46	9366	E
E_179	2,1	129	165	45	14400	I2
E_180	0,6	73	112	160	5644	E
E_181	1,5	71	72	134	4983	S
E_182	0,6	48	120	127	3937	E
E_183	0,5	77	118	61	6193	E
E_184	1,9	106	167	65	11984	I2
E_185	2,3	71	102	52	5043	E
E_186	3,2	150	253	175	25749	I2
E_187	0,9	72	117	158	6776	E
E_188	1,1	94	148	178	9075	EL
E_189	1,3	91	137	20	9017	E
E_190	0,4	53	75	135	3102	E
E_191	0,5	45	114	149	3773	E
E_192	1	111	223	180	17889	EL
E_193	1,8	94	139	77	8820	E
E_194	2	71	71	136	4845	E
E_195	2,1	100	143	89	9644	E
E_196	0,9	110	141	110	12589	I1
E_197	1,2	51	72	154	2445	E
E_198	1,7	70	71	136	4800	S
E_199	0,7	69	113	171	5177	E
E_200	1,3	124	225	83	19999	I1
E_201	0,5	83	177	123	9673	EL
E_202	0,6	53	71	127	2929	E
E_203	0,7	72	151	6	7561	E
E_204	0,6	75	116	160	6498	E
E_205	0,8	70	71	135	4781	E
E_206	0,9	110	140	42	13418	E
E_207	3,3	70	72	46	4829	E
E_208	0,3	24	66	158	1167	E
E_209	2,5	70	72	136	4724	E
E_210	1,3	99	145	2	9569	E
E_211	0,4	70	90	121	4939	E
E_212	3	70	72	137	4681	E
E_213	0,9	74	145	155	7938	E
E_214	1	59	71	47	3303	E
E_215	1,4	91	117	159	7969	EL
E_216	1,4	70	78	135	5165	E
E_217	1,2	68	81	146	4205	E
E_218	1,2	71	107	136	6137	E
E_219	0,8	63	106	147	5073	E
E_220	1,1	69	71	134	4743	E
E_221	1,1	106	204	132	17723	E
E_222	0,6	84	94	78	5415	E
E_223	1,1	69	73	44	4881	S
E_224	0,9	74	81	126	4555	E
E_225	0,8	78	132	156	7844	E
E_226	1	87	106	161	6698	E

E_227	0,8	99	202	140	15088	EL
E_228	1,3	55	69	146	2961	E
E_229	1	44	69	68	1914	E
E_230	1,4	71	92	44	5042	E
E_231	1,8	89	103	144	6296	E
E_232	2,8	136	144	48	16438	I1
E_233	1,4	94	159	143	10592	E
E_234	1,3	70	73	47	4806	E
E_235	1	70	77	46	5088	E
E_236	2,4	70	71	45	4878	E
E_237	2,5	93	165	135	12972	EL
E_238	1	71	72	137	4586	E
E_239	0,8	82	117	144	7090	E
E_240	2,3	70	73	43	4595	E
E_241	1,6	71	72	135	4884	E
E_242	1,9	65	184	135	10107	E
E_243	2,6	67	72	134	4545	E
E_244	3,2	69	71	44	4757	E
E_245	5,8	71	73	44	4983	S
E_246	0,7	83	107	146	7486	EL
E_247	2,3	68	73	139	4414	S
E_248	0,4	61	111	10	4002	E
E_249	1,2	56	111	150	4611	E
E_250	0,5	61	89	156	3457	E
ET_1	1,3	68	103	137	5794	E
ET_2	1,5	71	72	45	4922	E
ET_3	1	68	75	41	4563	E
ET_4	1,6	133	171	37	15465	I1
ET_5	1	65	108	63	4384	E
ET_6	3,1	190	142	135	16063	I1
ET_7	2,3	100	138	91	9527	EL
ET_8	0,9	65	84	117	3529	E
ET_9	1,3	69	71	135	4793	S
ET_10	1,6	70	72	134	4895	E
ET_11	2,2	71	71	135	4901	E
ET_12	0,9	86	145	4	7600	E
ET_13	2,1	97	146	175	9604	EL
ET_14	0,9	65	72	138	4393	E
ET_15	5	148	179	60	21596	EL
ET_16	3,9	93	139	161	8870	E
ET_17	1,9	102	137	131	9408	I2
ET_18	3,4	140	144	48	16950	I1
ET_19	1,1	66	74	140	4235	E
ET_20	1,3	73	81	44	5257	E
ET_21	0,8	71	73	46	4927	E
ET_22	2,3	67	87	29	3923	E
ET_23	5	104	134	136	9568	EL
ET_24	0,6	73	169	141	8248	I2
ET_25	1,2	84	100	71	5637	E
ET_26	2,9	128	177	136	18440	E
ET_27	2,5	111	135	143	11307	I2
ET_28	1,9	114	192	147	17130	EL
ET_29	1,6	100	219	152	15479	EL
ET_30	0,8	52	68	84	2593	E

ET_31	1,1	71	102	13	4722	E
ET_32	1,7	72	75	43	5132	E
ET_33	2,8	67	107	52	5396	E
ET_34	1,4	71	73	136	4899	E
ET_35	0,7	65	120	154	5599	E
ET_36	3	145	191	145	20987	I1
ET_37	1,3	67	75	50	4479	E
ET_38	1	68	149	144	6471	EL
ET_39	3,3	111	168	138	16031	I2
ET_40	0,9	64	84	39	4084	E
ET_41	2,6	97	142	139	9910	EL
ET_42	2,4	91	161	126	11851	E
ET_43	2,1	100	119	49	10007	E
ET_44	2,5	131	178	27	15705	I2
ET_45	2,7	98	148	0	9665	EL
ET_46	2,2	100	151	179	10045	EL
ET_47	2,4	70	70	135	4869	E
ET_48	1,6	117	138	137	11972	EL
ET_49	3	87	122	164	7920	EL
ET_50	1	51	108	155	3791	EL
ET_51	3	100	106	136	9190	EL
ET_52	1,9	98	133	4	9220	E
ET_53	2,3	70	71	44	4619	E
ET_54	0,6	69	79	143	4532	E
ET_55	1,9	108	143	130	13423	E
ET_56	2,2	93	143	157	9849	EL
ET_57	0,6	84	309	138	15216	E
ET_58	0,8	85	152	146	9438	E
ET_59	0,8	98	148	141	9409	I2
ET_60	1,1	69	93	136	5449	E
ET_61	1	66	102	40	5334	E
ET_62	2,8	121	164	15	11344	E
ET_63	3,2	124	147	129	15595	E
ET_64	1,6	91	143	164	7928	E
ET_65	0,9	69	136	152	4872	E
ET_66	1,7	90	110	149	7661	E
ET_67	0,5	59	91	150	4023	E
ET_68	1	63	68	47	3867	E
ET_69	0,5	44	70	158	2378	E
ET_70	0,6	39	69	151	2410	E
ET_71	1,4	79	184	133	8300	E
ET_72	5,6	115	259	143	23288	T
ET_73	0,7	48	147	141	5986	E
ET_74	2,2	66	172	145	8623	E
ET_75	3,2	69	71	46	4830	E
ET_76	2,8	100	143	180	9689	E
ET_77	1,3	91	176	84	11004	EL
ET_78	1,6	71	76	43	4985	E
ET_79	1,7	68	69	135	4624	E
ET_80	1,3	70	72	45	4808	E
ET_81	1,8	96	277	137	21198	EL
ET_82	2,9	100	223	139	14464	E
ET_83	1,3	72	97	44	5917	E
ET_84	1,1	67	130	149	5876	EL

ET_85	1,6	70	72	45	4926	E
ET_86	0,8	40	161	147	4929	E
ET_87	2,6	114	212	138	17662	EL
ET_88	0,4	67	83	146	3950	E
ET_89	2,1	149	273	178	27386	I1
ET_90	1,5	71	73	135	4869	E
ET_91	1,7	66	77	142	4192	E
ET_92	3,3	103	235	128	19645	EL
ET_93	1	81	114	135	7379	E
ET_94	5,2	139	246	135	28963	EL
ET_95	2,4	85	117	133	6700	E
ET_96	2,4	87	108	135	7481	E
ET_97	2,8	71	84	44	5489	E
ET_98	2	80	96	47	6274	E
ET_99	0,7	45	119	142	3605	E
ET_100	1	71	94	150	4988	E
ET_101	1,3	96	139	129	9191	E
ET_102	0,5	53	162	134	6410	EL
ET_103	1,5	98	136	175	9431	EL
ET_104	1,2	70	91	46	5477	E
ET_105	1,7	69	71	49	4470	E
ET_106	0,9	31	95	147	1996	E
ET_107	1,9	90	106	135	7956	EL
ET_108	6,3	115	195	157	16351	EL
ET_109	1,7	66	149	7	6969	E
ET_110	2,7	70	71	45	4868	E
ET_111	2,3	90	273	8	16925	EL
ET_112	1,3	120	220	1	18722	EL
ET_113	0,5	44	71	156	2740	E
ET_114	2,2	95	151	92	9774	EL
ET_115	1	69	72	133	4603	E
ET_116	1,8	69	73	138	4577	E
ET_117	0,7	67	78	22	3603	E
ET_118	3,9	161	352	159	36146	EL
ET_119	0,7	71	142	138	7165	E
ET_120	1,1	70	77	133	5039	E
ET_121	1,1	145	299	132	25748	I2
ET_122	1,7	70	71	134	4859	E
ET_123	1,7	70	74	134	4908	E
ET_124	2,9	92	136	109	8603	E
ET_125	2,7	71	74	136	4959	E
ET_126	5,5	141	141	135	17026	I1
ET_127	5,7	131	211	119	17519	I2
ET_128	3,2	69	71	45	4705	E
ET_129	0,8	67	69	133	4354	S
ET_130	2,4	99	203	1	14452	EL
ET_131	1	73	82	41	5252	E
ET_132	0,8	97	118	134	9306	E
ET_133	1,2	69	74	134	4749	E
ET_134	3,7	100	198	91	14704	EL
ET_135	2,2	101	141	7	9702	E
ET_136	4,2	124	176	180	15952	E
ET_137	3,8	140	172	128	17348	E
ET_138	2,7	60	138	151	6616	E

ET_139	2,5	59	78	37	3981	E
ET_140	2,9	85	112	145	7523	E
ET_141	1,5	70	104	31	5155	E
ET_142	1,3	102	146	135	10444	E
ET_143	2,5	113	151	44	12029	E
ET_144	0,9	56	77	76	3279	E
ET_145	0,4	19	45	110	619	E
ET_146	3,4	95	247	0	17276	EL
ET_147	3,7	113	196	180	14787	EL
ET_148	2,2	70	73	45	4877	E
ET_149	1,2	57	74	106	2523	E
ET_150	5,7	132	179	136	19712	EL
ET_151	0,8	43	83	37	2406	E
ET_152	3,1	114	372	142	33685	EL
ET_153	1,4	89	103	82	6457	E
ET_154	2,3	98	147	8	9453	E
ET_155	1,4	69	71	45	4751	S
ET_156	1	48	76	135	2512	E
ET_157	1,9	68	129	12	6041	E
ET_158	3,8	95	149	33	10014	E
ET_159	0,8	37	57	141	1208	E
ET_160	1	48	111	180	2980	E
ET_161	4,7	71	92	23	4718	E
ET_162	3,5	70	91	26	4533	EL
ET_163	5,6	69	72	136	4836	E
ET_164	4,3	96	143	173	9266	EL
ET_165	4,4	200	251	179	36196	I1
ET_166	2,7	102	162	35	11907	E
ET_167	2,1	69	111	145	4826	E
ET_168	1,6	67	98	151	4445	E
ET_169	1,6	56	145	136	5744	E
ET_170	1,6	97	76	58	4805	E
ET_171	1,3	102	243	145	12608	E
ET_172	1,4	132	209	125	17761	EL
ET_173	5,8	72	72	45	4887	E
ET_174	1,9	70	141	12	7116	E
ET_175	1,7	124	232	131	20383	EL
ET_176	2	99	168	143	12875	E
ET_177	4,3	84	136	22	8419	EL
ET_178	4,7	134	186	37	19102	I2
ET_179	2	56	87	125	2491	E
ET_180	2,5	99	105	45	9162	EL
ET_181	3,6	99	145	173	9308	EL
ET_182	6,7	70	71	45	4734	E
ET_183	4,6	106	124	136	9755	E
ET_184	0,8	62	132	114	6342	E
ET_185	9,4	106	209	135	15770	EL
ET_186	6,5	131	451	133	34691	EL
ET_187	3	69	71	46	4794	E
ET_188	2,7	122	138	44	11977	E
ET_189	1,5	72	102	155	5286	E
ET_190	2,8	133	152	129	16406	I1
ET_191	2,2	66	79	36	4114	E
ET_192	1,8	73	129	124	7596	E

ET_193	7,8	107	142	135	12001	I2
ET_194	3,7	108	147	44	13712	EL
ET_195	5,3	92	144	13	8627	EL
ET_196	3,9	117	139	39	12897	E
ET_197	2,6	71	72	44	4925	E
ET_198	0,8	53	86	116	3164	EL
ET_199	1,6	73	103	136	6139	E
ET_200	3,2	97	122	114	8967	EL
ET_201	4,1	70	71	44	4872	E
ET_202	1,5	89	133	71	6365	E
ET_203	1,3	62	137	126	6582	E
ET_204	2,8	112	185	132	15123	E
ET_205	2,1	72	160	113	8308	E
ET_206	3,2	71	72	45	4968	E
ET_207	2,6	43	88	146	3032	E
ET_208	5,1	71	73	44	4821	E
ET_209	2,5	104	166	177	9080	E
ET_210	3,2	84	101	126	6695	E
ET_211	3,1	88	165	103	6950	I2
ET_212	3,4	70	71	135	4864	E
ET_216	1,8	63	93	153	3927	E
ET_217	2,6	79	116	155	6374	E
ET_218	1	60	86	30	3804	E
ET_219	3,4	69	84	153	3852	E
ET_222	3,1	163	198	115	24083	I1
ET_223	2	79	152	131	7729	EL
ET_224	1,5	54	97	102	3199	E
ET_225	2,1	95	187	95	13530	E
ET_226	1,8	72	77	140	4918	E
ET_227	4,5	93	138	167	8561	EL
ET_228	3,3	77	116	13	5841	EL
ET_229	1,5	71	77	38	4746	E
ET_230	2,5	95	108	47	8888	E
ET_231	3,8	126	199	116	15780	CR
ET_232	1,7	84	142	179	6078	EL
ET_233	1,1	41	78	162	2148	E
ET_234	3,8	52	115	120	4164	E
ET_235	5,4	70	73	47	4897	E
ET_236	3,1	68	69	42	4527	S
ET_237	1,5	70	72	44	4898	E
ET_238	1,3	69	70	135	4718	E
ET_239	2,3	71	73	137	4895	E
ET_240	1,8	80	129	47	7484	E
ET_241	3,4	101	154	178	10175	E
ET_242	1,1	49	106	93	3622	EL
ET_243	2,4	89	132	154	8486	E
ET_244	1	96	117	180	9390	I1
ET_245	5,2	92	125	32	7670	E
ET_246	6,7	70	72	46	4904	E
ET_247	0,7	26	86	83	1421	E
ET_248	1,6	140	198	120	17890	I1
ET_249	1,5	70	73	47	4844	E
ET_250	1,2	47	93	19	3048	E
ET_251	4,1	99	143	88	9691	I1

ET_252	2	66	129	112	5171	E
ET_253	5,7	202	309	83	44105	I2
ET_254	3	111	276	137	17334	I2
ET_255	4,6	71	72	46	4894	E
ET_257	1,9	65	115	123	5118	E
ET_258	3,8	90	307	132	17652	E
ET_260	3,4	71	79	44	5212	E
ET_261	1,2	69	78	54	4285	E
ET_262	1,1	69	72	46	4753	E
ET_263	2,3	89	123	63	8175	E
ET_264	2	108	173	138	15208	C
L_1	4,9	153	453	63	43738	EL
L_2	4,4	119	260	0	22437	T
L_3	3,1	178	264	136	31079	I1
L_4	2	145	255	179	26786	I1
L_5	3,3	149	307	0	29205	E
L_6	2,3	221	465	25	68367	I2
L_7	4,8	233	475	9	75424	E
L_8	4,2	173	204	66	25641	I1
L_9	4,5	116	275	42	23668	I2
L_10	2,4	85	108	136	7614	E
L_11	6,2	191	319	6	43289	I1
L_12	4,1	213	875	4	1E+05	EL
L_13	3,5	113	140	45	12302	E
L_14	2,2	106	146	135	13306	I1
L_15	0,5	77	94	66	5267	E
L_16	2,1	89	158	163	9474	E
L_17	5,5	142	289	3	29092	T
L_18	1,8	113	323	2	23911	EL
L_19	6	168	247	47	30003	T
L_20	5	154	174	42	20363	I1
L_21	2,9	155	188	158	22555	I1
L_22	4	244	331	155	62110	I1
L_23	5,5	172	255	137	34364	EL
L_24	3	159	197	114	26608	C
L_25	1,3	75	293	0	15866	EL
L_26	2,3	150	226	127	23275	I1
L_27	5,7	305	409	94	84776	I1
L_28	5,4	173	247	130	33363	I2
L_29	2,4	130	238	1	20300	I2
L_30	1,6	136	181	135	19022	I1
L_31	2,9	156	278	63	30510	I2
L_32	3,4	228	263	92	36073	I2
L_33	3,6	168	226	37	28019	I2
L_34	2,9	169	181	100	22757	I2
L_35	5,1	171	304	161	34709	EL
L_36	4,6	198	331	57	38850	I2
L_37	2	128	230	163	19309	EL
L_38	4,3	209	309	140	42398	I2
L_39	2,3	156	177	177	20320	E
L_40	4,2	154	230	138	29200	I1
L_41	3,7	128	244	170	21117	I1
L_42	3,2	209	236	54	38386	I2
L_43	3,2	78	92	130	5849	E

L_44	4,1	211	275	156	41562	I2
L_45	5,9	261	293	81	46349	I2
L_46	3,8	193	252	35	35550	I2
L_47	3,6	166	270	135	35471	I1
L_48	7,7	278	378	0	61396	I2
L_49	8,8	170	249	131	33199	EL
M_1	0,8	71	129	13	6071	EL
M_2	1,7	93	146	1	8828	EL
M_3	0,7	53	95	154	3599	E
M_4	0,6	82	110	31	6944	E
M_5	0,7	48	79	165	2694	E
M_6	0,8	72	82	45	5305	E
M_7	1,1	70	75	45	4732	E
M_8	1,3	68	73	47	4617	E
M_9	1,5	58	67	50	3270	E
M_10	1	71	82	140	4928	E
M_11	0,6	63	88	58	3973	E
M_12	0,8	79	166	10	9752	EL
M_13	0,8	68	95	25	4408	E
M_14	0,6	59	95	152	4094	E
M_15	0,8	62	92	24	3793	EL
M_16	0,8	75	84	129	5234	E
M_17	1	93	149	174	9084	E
M_18	1	68	71	136	4555	E
M_19	0,2	44	70	161	1957	E
M_20	0,8	121	209	14	16967	I2
M_21	0,5	62	64	50	3379	E
M_22	0,6	64	76	141	4202	E
M_23	0,3	43	56	28	2159	E
M_24	0,1	23	44	73	600	E
M_25	0,5	77	89	124	5639	E
M_26	0,4	112	138	180	9486	I2
M_27	0,5	74	127	135	7901	EL
M_28	1,9	71	105	134	6050	E
M_29	1,2	71	84	44	5155	E
M_30	0,9	66	84	150	3799	E
M_31	1,4	72	95	148	4789	E
M_32	0,4	54	80	27	2848	E
M_33	0,4	44	70	153	2172	E
M_34	0,8	71	71	135	4944	E
M_35	1,8	70	72	137	4827	E
M_36	0,9	65	73	47	4442	E
M_37	0,9	65	84	127	4300	E
M_38	1,7	70	70	135	4818	E
M_39	0,3	47	59	36	1970	E
M_40	0,5	57	98	168	3192	E
M_41	0,2	42	56	139	1636	E
M_42	0,5	76	105	16	5482	E
M_43	1,1	70	72	45	4762	E
M_44	0,7	66	80	35	4014	E
M_45	0,8	73	186	170	9718	E
M_46	1	83	173	20	10418	E
M_47	0,7	125	261	164	20206	E
M_48	0,8	89	197	177	11627	E

M_49	0,6	61	73	47	3739	E
M_50	0,3	50	132	162	4605	E
M_51	0,4	71	90	44	5358	E
M_52	0,2	60	99	136	4658	E
M_53	0,2	63	107	165	4421	E
M_54	0,3	60	69	133	2950	E
M_55	0,3	66	92	62	4371	E
M_56	0,6	66	117	152	4817	E
M_57	0,7	66	177	173	8320	EL
M_58	0,7	92	196	174	13122	E
M_59	0,8	141	194	46	21321	E
M_60	0,2	52	110	7	3784	EL
M_61	0,5	92	129	154	8138	E
M_62	0,6	75	118	32	6367	E
M_63	1	69	103	157	4473	E
M_64	0,9	69	78	135	4916	E
M_65	1,7	71	107	135	6271	E
M_66	1,4	82	124	15	7382	EL
M_67	1,1	70	146	13	7335	E
M_68	1,1	169	243	48	31247	I1
M_69	3,3	70	71	134	4815	E
M_70	1,2	69	71	134	4810	E
M_71	1,8	71	104	135	5977	E
M_72	2,7	70	70	46	4835	E
M_73	0,6	62	120	55	5469	E
M_74	0,3	51	102	174	2987	EL
M_75	0,3	32	54	70	998	E
M_76	0,8	73	100	33	6071	E
M_77	1,9	70	75	135	5020	E
M_78	1,2	52	55	143	2118	E
M_79	0,5	59	68	31	3376	E
M_80	0,7	64	86	34	4117	E
M_81	0,6	72	79	29	4258	E
M_82	0,8	65	82	148	3318	E
M_83	0,7	65	96	23	3936	E
M_84	1,4	67	86	148	4390	E
M_85	0,7	68	71	44	4530	E
M_86	0,9	62	76	28	3031	E
M_87	1,1	68	124	144	6447	E
M_88	0,5	88	286	159	14982	I2
M_89	0,8	69	79	141	4512	S
M_90	0,9	57	83	79	2864	E
M_91	0,4	73	77	136	4568	E
M_92	0,7	67	70	137	4465	S
M_93	0,6	66	84	39	4296	E
M_94	0,4	44	105	149	2829	E
M_95	1,3	79	96	18	5276	EL
M_96	0,8	83	129	66	6556	E
M_97	0,7	69	79	39	4552	E
M_98	0,9	77	136	155	7110	E
M_99	0,3	63	118	39	5095	I2
M_100	0,3	65	100	42	5259	E
M_101	0,4	74	87	143	5182	E
M_102	0,6	87	92	52	6815	E

M_103	0,4	66	130	161	6100	EL
M_104	0,2	67	107	17	4564	E
M_105	0,4	84	97	68	5896	E
M_106	0,3	74	104	171	5585	I1
M_107	0,2	45	92	167	2413	E
M_108	0,3	61	82	155	3297	E
M_109	0,4	68	77	40	4594	E
M_110	0,4	63	72	138	4207	E
M_111	0,9	69	74	133	4828	E
M_112	0,9	70	77	135	4948	E
M_113	0,4	56	132	173	4245	E
M_114	0,8	45	126	117	3773	I2
M_115	0,8	71	81	44	5288	S
M_116	0,5	77	103	47	6935	E
M_117	0,8	71	71	134	4905	E
M_118	0,7	71	73	135	4864	E
M_119	0,2	46	53	136	2008	E
M_120	0,3	66	74	30	3860	E
M_121	0,5	70	80	140	4914	E
M_122	0,5	90	105	47	7366	E
M_123	0,6	92	157	154	9994	E
M_124	1,6	69	77	125	4183	E
M_125	0,6	54	106	167	3848	EL
M_126	0,3	66	96	25	4110	E
M_127	0,3	48	64	63	2106	E
M_128	0,8	141	241	3	23934	E
M_129	0,8	71	77	45	5115	E
M_130	0,2	58	92	171	2967	E
M_131	0,7	65	216	2	9231	E
M_132	0,2	25	59	164	911	E
M_133	0,7	50	73	24	2203	E
M_134	0,4	48	86	19	3227	EL
M_135	0,3	22	65	16	771	E
M_136	0,5	68	86	35	4501	E
M_137	0,2	44	73	84	2034	E
M_138	1,5	90	143	164	9047	E
M_139	0,9	77	144	176	7099	E
M_140	0,3	55	97	142	3757	E
M_141	0,6	67	121	163	6317	E
M_142	2,5	71	71	45	4922	E
M_143	1,1	49	171	173	5670	EL
M_144	1,5	97	144	179	9412	E
M_145	1,1	72	89	52	4976	E
M_146	0,6	93	96	137	7700	E
M_147	0,5	86	137	171	8654	I1
M_148	6,9	140	156	45	20083	E
M_149	2,2	77	171	164	9814	E
M_150	1,6	69	113	18	5547	E
M_151	1,3	62	138	15	5143	E
M_152	2,2	116	129	128	11562	EL
M_153	2,8	73	100	22	4566	E
M_154	2,7	105	132	134	11210	E
M_155	1,2	84	178	180	9506	EL
M_156	1	80	202	163	11053	E

M_157	0,8	81	118	48	7966	E
M_158	1,2	70	105	133	5989	E
M_159	1,9	161	197	31	20670	EL
M_160	2,6	143	249	2	23661	I1
M_161	1,9	99	149	2	8973	E
M_162	0,5	74	176	173	8191	EL
M_163	0,8	54	201	174	7752	EL
M_164	2	119	222	20	17231	EL
M_165	3	78	93	37	5736	E
M_166	2,8	124	235	146	21829	EL
M_167	0,6	93	125	70	8916	E
M_168	2,2	85	119	28	6586	E
M_169	0,8	62	88	17	3772	E
M_170	0,9	70	76	134	4947	E
M_171	1,8	76	86	143	5134	E
M_172	1,4	92	181	172	11956	EL
M_173	4,1	95	98	46	7276	E
M_174	2,7	125	213	17	16929	I2
M_175	1,2	85	111	146	7333	E
M_176	1,9	67	77	51	4184	E
M_177	0,6	38	54	146	1495	E
M_178	1,1	69	72	43	4757	E
M_179	0,3	32	91	92	2042	E
M_180	0,3	45	76	66	2391	E
M_181	1,8	66	72	133	4507	E
M_182	0,4	45	59	138	1932	E
M_183	1,4	95	204	14	12625	E
M_184	0,5	58	67	132	2655	E
M_185	1	88	186	33	10954	EL
M_186	1,5	82	118	11	6885	E
M_187	2	75	119	80	6299	T
M_188	4,4	96	143	175	8819	E
M_189	0,9	75	119	87	6682	EL
M_190	0,4	30	55	19	1295	E
M_191	1,9	126	166	46	15274	I1
M_192	1,7	98	145	91	9947	I1
M_193	1,8	68	160	13	7076	T
M_194	2,4	89	277	179	18233	T
M_195	1,3	68	111	96	5250	E
M_196	1,6	155	179	136	20223	I1
M_197	2,9	70	72	46	4885	E
M_198	1,3	66	70	134	4511	S
M_199	1,8	96	144	89	9124	EL
M_200	1,1	88	131	29	7610	E
M_201	2,5	70	74	43	4286	E
M_202	1,3	69	73	137	4720	E
M_203	0,5	47	92	38	3032	E
M_204	1	79	104	36	6741	E
M_205	0,8	64	96	148	4975	E
M_206	1,4	92	136	170	8291	E
M_207	1,2	117	166	160	14636	E
M_208	0,8	70	78	134	4851	E
M_209	0,5	68	74	143	4284	E
M_210	1,3	72	77	42	4979	E

M_211	0,4	50	83	124	3271	E
M_212	1	68	74	49	4473	S
M_213	1	46	107	143	3662	EL
M_214	0,4	66	74	135	3428	E
M_215	1,1	70	71	136	4783	E
M_216	1,2	70	101	158	5352	E
M_217	3,4	100	137	2	9030	E
M_218	0,9	70	71	44	4724	S
M_219	0,5	82	82	45	5414	E
M_220	0,8	93	149	18	8526	E
M_221	1,9	87	112	33	7569	E
M_222	1	57	77	136	3482	E
M_223	1,1	71	72	47	4582	E
M_224	1,6	82	90	44	5800	E
M_225	0,6	45	60	56	2018	E
M_226	0,5	30	49	116	942	E
M_227	0,3	46	57	117	1658	E
M_228	0,7	82	162	13	9657	E
M_229	1,4	87	148	21	7200	E
M_230	1,9	100	140	179	9546	E
M_231	0,4	53	67	136	2765	E
M_232	3	135	217	147	22476	I1
M_233	1,8	105	158	134	13606	I1
M_234	0,9	130	154	76	15082	I1
M_235	0,5	59	105	10	4378	EL
M_236	0,4	53	56	140	2456	S
M_237	0,4	55	61	128	2657	E
M_238	1,4	70	72	47	4743	E
M_239	1,7	95	148	93	9541	EL
M_240	1,2	70	74	133	4985	E
M_241	1,1	81	131	171	7427	E
M_242	0,6	66	104	43	5512	E
M_243	1,2	58	66	69	2797	E
M_244	1,6	66	77	38	4335	E
M_245	0,7	80	120	163	6506	E
M_246	1	72	166	0	7798	EL
M_247	0,3	48	65	136	2275	E
M_248	0,7	73	91	38	5273	E
M_249	1,6	85	139	119	8092	E
M_250	0,8	69	84	138	4668	E
M_251	0,7	60	96	35	4084	E
W_1	1,4	71	72	135	4942	E
W_2	1,4	54	77	134	3412	E
W_3	1,8	56	63	138	3185	E
W_4	3,4	71	73	134	4981	E
W_5	2,2	70	71	135	4864	E
W_6	1,8	67	70	133	4399	S
W_7	1,4	60	99	130	4466	I1
W_8	2	100	148	173	9696	I1
W_9	0,7	56	68	141	2827	E
W_10	1,5	143	197	6	14656	I2
W_11	0,9	78	106	42	6462	I2
W_12	0,9	83	100	29	6184	E
W_13	1,8	68	88	34	4965	E

W_14	1	65	105	27	4706	E
W_15	1,4	60	71	145	3140	E
W_16	1,6	70	72	136	4850	E
W_17	1,3	79	98	53	6063	E
W_18	0,7	41	89	145	3040	E
W_19	1,9	68	107	150	5436	E
W_20	1,1	71	118	16	5654	E
W_21	2,4	149	209	99	20922	I2
W_22	2	93	104	133	7442	E
W_23	0,8	67	144	147	6037	I2
W_24	1,2	70	108	64	5406	E
W_25	2,2	92	142	151	9005	EL
W_26	1	71	100	98	4903	E
W_27	1	71	72	135	4922	EL
W_28	1	65	107	137	5318	E
W_29	0,9	72	74	137	4788	E
W_30	0,6	64	73	150	3353	E
W_31	2,4	70	71	135	4918	EL
W_32	1,8	71	72	136	4935	E
W_33	1,6	71	77	39	4701	E
W_34	2,1	68	72	44	4655	E
W_35	0,6	112	144	115	10477	I1
W_36	1	65	75	132	4498	E
W_37	0,7	54	77	133	3213	E
W_38	1,6	58	90	138	3926	E
W_39	1,5	97	142	1	9749	E
W_40	2,3	100	199	3	13382	T
W_41	1,6	70	79	143	4453	E
W_42	1,3	88	94	128	7162	E
W_43	1,2	72	86	135	5462	E
W_44	1,3	67	75	144	4128	E
W_45	1,5	66	111	150	4974	E
W_46	1,7	92	148	145	9865	I2
W_47	2,1	86	152	171	8186	E
W_48	4,3	99	147	94	9796	I1
W_49	1,3	76	209	131	9790	EL
W_50	1,1	58	81	138	3473	E
W_51	3,7	70	73	135	4915	E
W_52	2,3	71	75	45	5085	E
W_53	2	104	142	132	11293	E
W_54	1	60	99	147	4553	E
W_55	2	72	72	46	4990	EL
W_56	1,8	70	70	45	4806	E
W_57	2,1	72	74	41	4861	E
W_58	1,8	97	146	3	9450	EL
W_59	1,3	71	74	44	4989	S
W_60	0,6	38	66	143	1684	E
W_61	1,3	86	137	155	7767	E
W_62	1,2	65	85	152	3891	E
W_63	1,2	72	132	105	6990	E
W_64	1,7	71	80	137	5144	E
W_65	0,7	55	76	145	3236	E
W_66	0,8	72	88	36	4959	E
W_67	0,8	70	107	137	6370	EL

W_68	1	70	74	136	4741	E
W_69	1	73	83	134	4883	E
W_70	1,3	67	79	55	4392	E
W_71	1,4	64	78	53	3969	E
W_72	1,6	68	78	143	4224	E
W_73	1,2	54	85	30	3084	E
W_74	0,6	63	86	26	3557	E
W_75	0,7	66	88	61	3926	E
W_76	0,9	60	91	20	3234	E
W_77	1	74	81	56	5027	E
W_78	0,6	52	73	43	2539	E
W_79	0,6	52	74	132	2781	E
W_80	1,3	87	122	134	8205	E
W_81	1,7	68	70	134	4461	E
W_82	1,3	67	99	148	4876	E
W_83	1,4	71	72	136	4942	S
W_84	1,5	63	73	128	3943	E
W_85	0,6	39	57	88	1754	EL
W_86	1	75	90	144	5471	E
W_87	0,9	54	107	44	4207	E
W_88	0,6	62	97	14	3299	E
W_89	1,1	62	71	45	3952	E
W_90	2,1	69	71	134	4787	E
W_91	1,6	73	84	134	5292	S
W_92	2	71	72	45	4947	E
W_93	0,8	81	129	175	6749	E
W_94	2,1	71	72	136	4921	S
W_95	2,3	74	133	135	7508	E
W_96	1,5	64	91	158	3966	E
W_97	1,9	72	81	130	4928	E
W_98	1	55	61	139	2957	E
W_99	0,8	41	81	165	2320	EL
W_100	1,4	83	85	123	5297	E
W_101	0,9	38	87	93	2113	E
W_102	1,8	94	136	14	8660	E
W_103	0,6	57	92	126	4173	E
W_104	1,1	68	69	134	4552	E
W_105	1,3	63	72	45	4214	E
W_106	1,4	60	126	165	5794	EL
W_107	2,5	67	77	53	4295	E
W_108	2,2	97	110	42	8877	E
W_109	1,6	58	82	58	3520	E
W_110	2,1	60	70	135	3514	E
W_111	1,3	55	64	136	2864	E
W_112	1,6	80	99	158	5615	E
W_113	0,7	49	69	117	2469	E
W_114	1,8	67	74	129	4009	E
W_115	0,9	61	113	157	5268	E
W_116	1,1	40	121	13	3175	EL
W_117	1,6	102	125	136	10147	E
W_118	1,4	45	82	97	2255	E
W_119	1,1	62	65	135	3291	E
W_120	0,9	45	57	146	1983	I1
W_121	0,7	82	122	50	7656	E

W_122	0,9	69	81	148	4094	E
W_123	0,6	67	103	174	3810	EL
W_124	1	60	92	24	3796	E
W_125	0,9	69	77	40	4526	E
W_126	1,8	83	84	45	6301	E
W_127	1,5	65	83	29	3775	E
W_128	1,8	64	77	46	4066	E
W_129	1,3	60	78	56	3455	E
W_130	1,1	47	74	160	2442	E
W_131	0,8	49	82	161	2709	I1
W_132	1,1	60	71	47	3735	E
W_133	1,3	84	128	5	7844	EL
W_134	0,9	66	138	156	6585	EL
W_135	0,6	62	90	29	3884	E
W_136	3,2	68	72	137	4690	E
W_137	1,3	69	72	138	4675	E
W_138	1,3	70	100	46	5935	E
W_139	1,2	68	108	54	5639	E
W_140	2,7	70	72	44	4879	E
W_141	2,7	69	71	45	4778	E
W_142	1,4	68	71	136	4743	E
W_143	0,9	62	149	18	5574	E
W_144	1,2	65	107	150	5003	E
W_145	0,2	47	69	145	2366	E
W_146	0,7	68	72	42	4551	E
W_147	1,2	66	93	43	5050	E
W_148	1,1	69	108	153	5073	E
W_149	1	66	85	153	3718	E
W_150	0,9	72	80	49	5047	E
W_151	1,6	71	72	135	4867	E
W_152	0,7	60	70	152	2984	E
W_153	0,5	75	114	151	6370	E
W_154	1,1	70	72	132	4751	S
W_155	0,7	68	103	162	5056	I1
W_156	0,9	70	87	136	4975	E
W_157	1,4	72	76	44	4906	E
W_158	1,3	75	134	7	6777	E
W_159	2	70	76	134	4929	E
W_160	6	121	189	146	15579	I2
W_161	1,4	69	72	42	4784	E
W_162	1,4	93	102	41	7781	E
W_163	0,6	66	74	39	4361	E
W_164	0,4	62	77	24	3400	E
W_165	0,5	65	115	61	5727	E
W_166	0,6	61	69	133	3613	E
W_167	0,5	102	115	36	9543	EL
W_168	1	94	143	177	9283	E
W_169	0,6	83	167	170	9660	E
W_170	0,5	60	122	154	4521	E
W_171	0,9	67	75	40	4478	E
W_172	0,3	63	78	154	3184	E
W_173	0,8	83	146	167	7809	E
W_174	1	64	76	143	3920	E
W_175	1,1	69	70	135	4750	EL

W_176	1,3	67	80	35	4218	E
W_177	1	88	103	160	6223	E
W_178	1	72	133	155	6930	E
W_179	1,3	70	108	133	6091	E
W_180	0,5	42	56	30	1619	E
W_181	1,3	76	152	175	7319	T
W_182	1	75	78	115	4742	E
W_183	0,9	84	135	159	7245	E
W_184	0,8	65	100	134	5425	E
W_185	1,2	98	144	1	9283	E
W_186	0,7	68	118	124	5597	E
W_187	1,1	97	140	93	8997	EL
W_188	1,1	110	162	133	13738	I2
W_189	0,7	71	85	137	5199	E
W_190	0,6	72	103	45	6015	E
W_191	0,3	56	94	156	3709	E
W_192	1,3	77	101	142	5698	E
W_193	1	41	139	169	2851	T
W_194	1,1	87	146	172	9052	EL
W_195	1	97	147	0	9495	E
W_196	0,4	63	88	48	4542	E
W_197	0,4	86	199	135	10123	E
W_198	1,2	100	153	171	10564	E
W_199	0,3	69	77	41	4594	E
W_200	0,5	74	113	148	5651	E
W_201	0,7	96	135	5	9225	E
W_202	0,3	61	123	155	5939	E
W_203	0,6	80	124	158	7573	EL
W_204	0,6	73	81	133	5337	E
W_205	2	96	135	23	9127	E
W_206	1,6	70	71	136	4797	S
W_207	1,6	69	79	36	4413	E
W_208	0,4	64	78	126	4036	EL
W_209	0,4	75	135	20	6114	E
W_210	0,6	70	74	44	4702	S
W_211	0,5	76	88	36	5387	E
W_212	0,4	75	79	131	5212	E
W_213	0,5	68	90	138	5172	E
W_214	0,6	63	70	137	3802	E
W_215	1,1	74	84	41	5042	E
W_216	2	98	150	1	9757	EL
W_217	0,7	65	110	150	6248	E
W_218	0,5	80	148	177	7950	EL
W_219	0,8	66	122	152	5853	EL
W_220	0,7	61	85	138	4474	E
W_221	1,1	89	143	173	8702	E
W_222	0,9	66	96	157	4700	E
W_223	0,7	67	81	137	4818	E
W_224	2	70	71	135	4868	E
W_225	0,6	72	79	139	4743	E
W_226	0,3	55	80	28	3121	E
W_227	2,1	105	178	136	14055	I2
W_228	0,9	45	65	148	2130	E
W_229	1,9	57	62	127	2809	E

W_230	0,5	24	59	165	882	E
W_231	0,8	43	56	146	1651	E
W_232	0,6	34	43	145	1060	E
W_233	3,8	132	200	162	17277	I1
W_234	2,1	131	211	45	16423	I1
W_235	1,3	57	86	149	3450	EL
W_236	0,4	36	56	140	1267	E
W_237	0,4	27	33	52	612	E
W_238	0,3	18	36	23	378	E
W_239	0,6	66	80	23	3672	E
W_240	1,4	69	79	144	4271	E
W_241	2,9	71	72	135	4978	EL
W_242	3,9	73	83	44	5297	E
W_243	1,3	79	105	148	5944	E
W_244	1,3	68	91	43	5079	E
W_245	1,3	69	70	45	4719	E
W_246	0,9	65	67	136	4114	E
W_247	1,7	73	99	124	5390	E
W_248	1,2	68	88	39	4867	E
W_249	0,3	43	53	127	1759	E
W_250	1,3	99	144	82	9618	EL
W_251	2	87	120	152	7586	E
W_252	0,5	60	76	27	2879	E
W_253	0,7	69	71	46	4647	E
W_254	0,6	69	76	140	4499	E
W_255	0,8	60	76	149	3177	E
W_256	0,6	112	133	49	11151	EL
W_257	0,6	78	143	14	6585	E
W_258	1	71	131	33	7892	E
W_259	1,2	69	84	30	4555	E
W_260	1,1	71	73	136	4861	E
W_261	0,6	70	75	133	4901	E
W_262	1,1	69	73	134	4767	E
W_263	1,1	65	105	149	4857	E
W_264	0,2	29	70	18	1356	E
W_265	0,6	58	104	46	4664	E
W_266	0,4	57	102	53	4188	E
W_267	0,4	74	107	152	6173	EL
W_268	1,4	72	141	170	6826	E
W_269	1,5	87	140	168	9228	E
W_270	2,7	56	139	135	5668	T
W_271	1,7	70	73	133	4833	E
W_272	1,1	70	72	46	4823	E
W_273	0,5	63	75	39	3986	E
W_274	0,6	66	104	140	5113	E
W_275	0,5	56	98	163	3727	E
W_276	0,8	80	101	136	6307	EL
W_277	0,6	84	143	177	8237	E
W_278	0,7	59	109	63	3731	E
W_279	0,3	65	74	128	4198	E
W_280	0,7	68	104	175	4445	E
W_281	2	115	257	3	19720	T
W_282	1,3	93	135	22	9189	E
W_283	0,4	57	72	137	3019	E

W_284	0,5	90	143	9	8829	EL
W_285	0,6	70	93	33	4894	E
W_286	0,9	72	74	44	4822	E
W_287	0,3	57	92	176	3033	E
W_288	0,4	69	72	44	4465	E
W_289	0,4	67	69	46	4230	E
W_290	0,3	63	71	134	4043	E
W_291	0,5	66	101	139	4902	E
W_292	0,4	64	69	43	4138	S
W_293	0,4	68	83	132	5030	E
W_294	0,5	69	75	138	4801	E
W_295	0,6	73	86	41	5202	E
W_296	0,3	64	89	141	4705	E
W_297	0,5	88	122	20	7419	E
W_298	0,6	83	122	28	6490	E
W_299	0,7	73	74	139	5140	E
W_300	0,7	91	139	21	9065	E
W_301	0,4	64	115	37	5138	E
W_302	0,5	91	132	6	8383	E
W_303	0,4	57	60	138	2859	E
W_304	0,3	53	63	133	2745	E
W_305	1	68	72	42	4495	E
W_306	0,9	69	72	135	4799	S
W_307	3,1	101	195	179	14309	E
W_308	2,1	71	72	44	4754	E
W_309	1,5	72	75	136	5045	E
W_310	1,1	58	97	160	3932	E
W_311	0,6	46	75	135	2695	E
W_312	0,7	68	111	156	4998	E
W_313	3,9	99	252	1	19811	EL
W_314	3	101	181	169	12702	EL
W_315	1,2	53	74	175	2574	E
W_316	1,5	54	140	161	5119	T
W_317	1,8	64	170	164	7947	T
W_318	3	76	192	174	10884	T
W_319	3,6	86	191	170	12194	T
W_320	2,4	79	197	176	10728	T
W_321	1,7	79	157	165	9465	T
W_322	0,7	48	168	171	5517	EL
W_323	0,4	37	98	3	2574	EL
W_324	0,5	63	67	172	3206	E
W_325	0,6	42	93	118	2766	E
W_326	0,9	68	71	46	4691	E
W_327	0,8	76	148	169	8034	EL
W_328	1,2	90	140	17	8912	E

Q 3.1 data

Table 6.5: Collected data of pockmarks at Q 3.1 horizon

Pock name	Depth (OWT) (ms)	Width (m)	Length (m)	Direction (degree)	Area (m^2)	Primary shape

1	7,4	203	231	173	46904	I1
2	5,6	168	230	12	38604	I1
3	11,8	200	252	146	50391	I1
4	5,2	196	239	175	46883	I1
5	7,1	211	253	144	53361	I1
6	1,3	107	143	135	15357	E
7	2,6	238	275	47	65365	I1
8	6,8	237	282	23	66815	I1
9	7,4	211	279	169	58647	I1
10	2	275	300	93	82423	I1
11	3,1	233	301	98	70191	I1
12	5,5	162	221	9	35676	I1
13	4,1	164	195	8	32008	I1
14	1,5	174	211	42	36774	I1
15	5,6	201	231	2	46423	I1
16	3,7	157	213	169	33353	I1
17	3,5	175	190	43	33335	I1
18	3,4	186	285	157	53094	I1
19	6,3	221	277	125	61148	EL
20	5,7	282	387	140	109139	I1
21	2,7	145	245	155	35548	EL
22	2,8	212	320	135	67967	I1
23	5,2	153	233	151	35726	EL
24	2,5	130	184	146	23903	I1
25	1,1	69	74	43	5132	E
26	2,2	168	254	142	42685	I1
27	6,6	176	268	140	47171	EL
28	5,6	143	205	132	29269	EL
29	5,9	214	242	134	51653	I1
30	5,9	233	351	177	81870	I1
31	7,3	259	283	69	73371	I1
32	2,4	105	155	134	16187	E
33	6	146	174	151	25448	E
34	6,1	178	192	109	34209	I1
35	4,9	136	156	19	21205	I1
36	1	100	149	1	14880	E
37	2,2	180	266	169	48082	E
38	6	181	226	138	40806	I1
39	1	71	72	134	5138	E
40	1,3	101	144	91	14608	E
41	6,8	194	257	117	49873	I1
42	2	101	125	37	12609	E
43	5,7	195	236	12	46053	I1
44	4,3	150	225	131	33799	EL
45	3,8	145	218	96	31595	EL
46	4,4	210	227	31	47715	I1

47	2,2	211	261	17	55127	I1
48	6,1	232	298	146	69157	I1
49	4,3	264	342	74	90462	I1
50	2,3	191	232	148	44269	I1
51	0,8	113	194	52	21852	I1
52	3,3	235	401	146	94106	EL
53	6,4	200	295	140	59094	EL
54	3,2	208	256	11	53403	I1
55	2,5	136	175	165	23820	I1
56	1,7	122	162	16	19791	E
57	1,7	98	151	175	14703	EL
58	5,1	180	215	3	38626	I1
59	4	193	261	151	50278	I1
60	4,8	199	208	94	41510	I2
61	1	67	89	152	5975	EL
62	1,9	69	71	45	4938	E
63	2	105	147	175	15457	E
64	4,1	240	276	37	66039	I1
65	5,1	168	222	33	37285	I1
66	1,7	135	263	156	35572	EL
67	2,8	158	211	139	33392	I1
68	0,9	97	106	138	10293	E
69	2,4	210	292	141	61342	I1
70	0,9	101	116	34	11696	E
71	1,3	106	131	146	13905	I1
72	3,3	138	176	143	24241	I1
73	5,6	172	219	117	37750	EL
74	1,9	103	146	85	15015	EL
75	0,6	68	71	44	4861	E
76	0,4	75	95	95	7146	E
77	2	110	136	157	14976	E
78	5,5	103	112	134	11523	E
79	0,4	47	72	161	3363	E
80	1,6	114	147	147	16783	E
81	3,9	183	215	87	39359	I1
82	1,2	68	108	134	7320	E
83	1,1	99	199	152	19712	EL
84	1,4	89	138	75	12335	E
85	0,8	71	79	131	5641	E
86	4,3	139	217	142	30053	EL
87	1,9	54	122	132	5062	E
88	1,3	124	193	129	17619	C
89	1,1	124	137	128	12484	E
90	1,6	71	72	45	4910	E
92	2,8	69	72	135	4942	E
93	1,4	70	73	43	5122	E

94	1,2	69	71	135	4877	E
95	0,6	65	141	148	9242	E
96	0,8	70	72	135	5033	E
97	1,2	90	126	11	11412	E
98	1	66	70	138	4670	S
99	0,6	61	65	43	3951	E
100	7	70	71	45	4970	E
101	4	82	103	54	8481	E
102	4,6	70	104	135	7241	E
103	1,5	97	145	7	14117	E
104	1	77	119	154	9170	E
105	2,6	107	223	136	23813	EL
106	1,9	70	71	45	4976	S
107	0,7	61	80	25	4860	E
108	1,3	59	66	139	3910	E
109	0,4	29	39	58	1128	E
110	1,5	70	72	135	5063	E
111	0,6	81	105	153	8495	E
112	1,2	102	143	178	14600	S
113	0,9	69	71	135	4922	E
114	1,5	116	157	46	18253	E
115	1,5	96	146	14	13908	E
116	2,9	104	139	43	14371	E
117	0,6	70	95	42	6622	E
118	4,6	103	176	46	18089	EL
119	4,6	100	109	135	10865	E
120	8	71	72	135	5097	S
121	3,1	69	71	136	4939	E
122	2,8	70	71	135	5018	E
123	1,9	71	89	134	6364	E
124	1,9	69	73	132	5030	E
125	2,9	102	149	91	15218	E
126	2,5	70	71	45	4977	E
127	1,4	73	105	46	7684	E
128	1,1	74	76	41	5598	E
129	0,7	40	84	61	3387	E
130	1,1	46	70	42	3222	E
131	4,2	74	132	158	9750	E
132	0,2	52	70	129	3666	E
133	1,7	70	91	145	6402	E
134	2,7	137	200	163	27371	I2
135	1,6	95	191	12	18184	E
136	2,7	70	71	134	4981	E
137	1	87	130	177	11254	E
138	1,7	44	100	135	4418	E
139	1,7	71	78	140	5543	E

140	1,3	90	109	157	9833	E
141	1,2	68	71	139	4851	E
142	1,2	82	102	44	8349	E
143	5,3	132	188	128	24715	E
144	1,5	84	135	154	11381	E
145	2,2	67	71	134	4769	E
146	1,7	70	74	137	5211	E
147	3	92	143	166	13206	E
148	1	107	116	160	12498	E
149	2,1	69	86	48	5974	E
150	1,8	71	74	45	5233	E
151	1,1	59	86	43	5118	E
152	2,6	78	117	177	9139	E
153	0,8	46	65	39	2979	E
154	1	62	72	140	4446	E
155	0,8	51	65	45	3322	E
156	0,7	43	78	46	3382	E
157	0,5	48	73	43	3476	E
158	1,1	71	74	131	5280	E
159	0,6	69	80	116	5515	E
160	0,7	87	111	47	9630	E
161	1,1	97	139	152	13480	EL
162	3,5	93	136	71	12666	E
163	1	76	93	146	7107	E
164	0,6	60	86	109	5150	E
165	2,3	106	196	45	20808	E
166	2,5	94	129	60	12109	E
167	1	79	123	151	9671	E
168	1,3	83	104	138	8600	E
169	2,4	79	106	43	8353	E
170	2,2	67	95	54	6332	E
171	1,1	96	176	128	16855	E
172	0,9	69	70	135	4829	S
173	2,1	70	72	43	5001	E
174	1,7	70	103	46	7196	E
175	0,9	70	171	44	11970	E
176	2	69	71	134	4875	E
177	0,9	90	116	46	10459	E
178	1,5	69	74	42	5110	E
179	0,8	40	84	25	3381	EL
180	1,1	120	158	100	18979	I1
181	1,1	64	69	42	4419	E
182	5,3	107	141	46	15039	E
183	1	60	116	173	6906	E
184	0,5	47	88	92	4111	E
185	2,3	102	159	140	16285	EL

186	3,8	68	79	144	5388	E
187	4,1	69	71	134	4935	EL
188	1,5	126	167	138	21063	I2
189	1,5	69	70	136	4847	E
190	2,8	70	71	45	4936	E
191	1,8	100	139	178	13972	EL
192	4,1	92	126	163	11602	E
193	2,7	80	142	164	11319	E
194	1,4	75	88	130	6663	E
195	0,8	85	132	156	11193	EL
196	1	46	80	126	3695	E
197	1,6	83	101	146	8459	E
198	1,3	70	74	137	5214	S
199	0,7	70	133	17	9288	E
200	1,1	71	72	136	5059	E
201	0,9	86	128	43	11015	E
202	1	127	152	100	19304	I2
203	1,3	69	77	140	5299	E
204	1,2	113	145	46	16359	I1
205	4,2	199	290	176	57841	EL
Add1	2,3	99	141	93	13993	EL
Add2	1,1	63	69	52	4354	E
Add3	0,9	66	68	40	4544	E
Add4	3,5	71	74	137	5267	E
Add5	0,6	87	104	140	8999	E
Add6	0,6	75	123	162	9288	EL
Add7	1	62	66	136	4093	E
Add8	0,8	59	91	142	5390	E

Q 3.2 URU data

Table 6.6: Collected data of pockmarks at Q 3.2-URU horizon.

Pockm.name	Depth (OWT) (ms)	Width (m)	Length (m)	Direction (degree)	Area (m²)	Primary shape
1	1,6	82	98	42	8008	E
2	3,4	146	173	58	25324	EL
3	1,2	70	105	53	7311	E
4	1,0	73	73	136	5345	S
5	1,9	91	144	178	13052	E
6	1,8	126	156	139	19605	EL
7	0,6	67	78	43	5246	E
8	0,5	127	194	87	24645	I1
9	1,8	116	136	129	15780	E
10	2,4	66	98	34	6492	E

11	1,7	73	82	39	5981	S
12	1,2	55	141	169	7734	E
13	1,4	43	99	161	4209	E
14	1,8	180	248	157	44676	I2
15	2,5	114	186	123	21171	I2
16	1,2	69	107	140	7338	E
17	0,2	38	99	125	3729	EL
18	2,0	69	74	136	5111	E
19	0,6	62	81	142	5051	EL
20	1,0	79	85	136	6717	E
21	1,9	98	137	176	13418	EL
22	1,8	101	194	179	19578	EL
23	2,2	153	188	146	28606	I1
24	1,0	62	72	134	4410	S
25	1,2	58	82	151	4757	E
26	1,1	61	106	140	6518	E
27	0,8	59	184	150	10864	EL
28	1,1	78	86	142	6652	E
29	1,0	67	85	37	5717	E
30	1,3	66	70	43	4651	S
31	0,2	54	76	137	4077	E
32	0,8	86	126	52	10906	E
33	0,8	72	77	129	5519	E
34	0,7	74	80	43	5960	E
35	0,4	58	64	49	3665	E
36	0,6	102	132	137	13536	E
37	0,7	79	139	12	10903	E
38	0,4	120	251	97	30296	I2
39	0,3	111	150	74	16624	E
40	1,0	90	117	29	10558	E
41	0,6	92	147	139	13482	E
42	0,4	112	153	59	17066	I1
43	1,0	91	125	153	11364	E
44	0,6	65	70	49	4532	S
45	0,9	77	84	44	6448	E
46	0,7	67	91	138	6089	E
47	3,7	71	77	45	5467	E
48	1,7	106	182	137	19290	C
49	3,0	103	141	135	14573	T
50	0,6	30	61	7	1867	E
51	1,1	69	70	133	4807	E
52	1,3	88	121	68	10593	E
53	1,0	67	76	139	5066	E
54	1,4	65	78	52	5067	E
55	2,0	109	171	180	18639	E
56	3,3	72	75	137	5409	E
57	2,3	66	70	135	4626	E
58	1,3	77	94	144	7232	E
59	0,8	69	80	126	5551	E
60	1,2	116	137	129	15903	EL
61	1,5	90	133	72	12020	E
62	0,7	69	105	147	7285	E
63	0,8	68	75	130	5080	E
64	0,9	86	127	113	10915	E

65	0,7	68	77	44	5268	S
66	0,5	61	110	122	6723	E
67	1,5	92	118	122	10896	E
68	1,0	118	138	152	16357	E
69	2,3	120	145	134	17487	E
70	1,3	196	222	115	43551	CR
71	1,3	92	127	165	11664	E
72	1,7	94	143	138	13474	E
73	0,7	67	76	141	5136	E
74	0,6	68	73	43	4925	E
75	1,2	66	71	137	4631	S
76	0,5	68	73	43	4931	S
77	1,2	97	131	157	12810	EL
78	0,6	66	105	27	6904	E
79	1,2	73	81	138	5961	E
80	1,2	97	184	47	17788	I2
81	1,1	85	88	143	7477	E
82	2,0	84	128	30	10710	I1
83	2,8	116	166	39	19239	T
84	1,9	181	258	10	46657	I1
85	1,7	210	376	6	78869	I2
86	1,8	80	85	46	6799	E
87	1,6	67	86	35	5759	E
88	3,5	99	141	81	13924	EL
89	0,9	65	73	49	4726	S
90	0,9	68	73	49	4903	S
91	0,8	69	74	48	5155	E
92	1,2	69	73	132	5016	E
93	1,0	70	80	41	5633	E
94	2,3	135	196	154	26423	E
95	1,0	74	96	39	7098	E
96	0,9	73	78	132	5685	E
97	0,8	96	122	8	11738	E
98	2,6	185	205	59	37878	I1
99	1,6	167	263	66	43900	E
100	1,0	70	71	45	5011	S
101	2,3	101	134	46	13550	EL
102	2,9	197	313	123	61609	I1
103	1,9	143	273	96	38991	I1
104	0,5	65	115	160	7429	E
105	1,0	108	138	103	14876	E
106	2,6	103	135	87	13869	EL
107	1,2	94	137	171	12795	E
108	1,5	107	146	6	15577	E
109	1,4	93	142	1	13262	EL
110	3,1	256	456	47	116677	I1
111	2,2	208	218	138	45271	I1
112	1,9	114	236	44	26795	EL
113	2,0	276	325	73	89528	I1
114	1,6	123	147	51	18040	I1
115	1,1	85	111	62	9455	E
116	1,4	94	112	50	10499	E
117	0,6	72	113	107	8129	E
118	1,7	91	143	95	13045	E

119	1,9	148	471	150	69515	T
120	2,2	73	89	142	6518	E
121	1,9	149	169	162	25159	I1
122	3,7	148	251	146	37010	T
123	2,2	194	350	88	67995	EL
124	3,1	96	140	130	13487	T
125	4,9	129	313	152	40403	T
126	2,6	74	91	46	6729	T
127	2,6	89	101	46	9017	T
128	2,3	82	117	154	9552	E
129	0,7	66	73	128	4816	E
130	1,4	68	94	169	6413	E
131	0,9	122	225	3	27346	I1
132	3,7	71	74	42	5259	S
133	1,8	120	201	43	24140	EL
134	0,8	70	74	135	5188	E
135	1,4	148	159	148	23573	I2
136	0,7	64	95	70	6048	EL
137	1,6	93	136	167	12684	E
138	1,1	66	70	47	4628	S
139	1,5	70	73	43	5095	S
140	1,0	68	83	147	5668	S
141	1,1	75	98	38	7342	E
142	1,5	74	141	160	10377	E
143	3,0	85	140	162	11864	E
144	1,0	77	118	150	9111	E
145	1,3	76	83	134	6338	E
146	0,8	80	152	170	12069	E
147	1,6	75	78	48	5849	S
148	0,7	73	90	133	6525	E
149	0,5	82	126	116	10345	E
150	0,9	71	88	131	6242	E
151	0,6	87	95	133	8344	E
152	0,8	125	209	137	26168	EL
153	0,4	73	83	39	6026	E
154	0,2	56	76	119	4248	E
155	0,5	70	74	126	5166	E
156	1,8	120	140	49	16859	E
157	1,2	78	86	46	6715	E
158	1,2	149	179	86	26652	E
159	3,0	75	112	152	8361	T
160	1,5	98	142	98	13916	E
161	2,3	62	88	142	5500	E
162	1,3	53	80	134	4271	E
163	2,4	62	198	153	12271	T
164	1,9	96	128	123	12304	E
165	2,4	74	84	52	6184	E
166	0,9	88	154	173	13585	E
167	0,6	70	86	44	6050	EL
168	0,7	105	157	165	16542	E
169	0,8	83	162	171	13454	EL
170	0,7	65	101	132	6606	E
171	0,7	74	92	32	6781	E
172	2,0	73	75	40	5464	E

173	1,6	71	74	43	5215	E
174	1,0	83	116	136	9612	E
175	1,0	89	130	164	11547	E
176	1,1	82	83	30	6760	E
177	0,9	69	105	27	7236	E
178	1,4	71	83	43	5950	E
179	0,9	129	192	177	24848	C
180	1,2	92	144	9	13226	E
181	1,3	73	79	130	5728	E
182	0,8	63	79	151	5022	E
183	1,7	209	227	160	47487	E
184	1,5	95	131	91	12454	E
185	0,7	74	120	88	8897	E
186	1,8	105	137	138	14299	E
187	1,3	71	74	137	5222	S
188	0,7	73	82	33	5958	E
189	0,9	70	72	43	5067	S
190	0,3	54	82	115	4423	E
191	2,4	66	87	149	5749	T
192	0,7	64	68	47	4353	S
193	0,4	79	81	49	6383	S
194	0,9	67	99	47	6588	EL
195	0,6	67	74	133	4938	S
196	1,3	98	137	79	13440	E
197	1,0	71	73	136	5172	E
198	1,0	101	228	31	23023	EL
199	0,5	71	83	134	5903	E
200	1,0	79	116	161	9169	EL
201	1,3	87	134	77	11618	EL
202	2,3	63	108	117	6765	T
203	2,5	77	119	133	9130	T
204	3,6	103	149	4	15264	E
205	2,5	86	140	106	12043	T
206	2,3	148	193	90	28609	T
207	1,6	134	177	154	23766	E
208	3,1	127	217	123	27417	E
209	3,3	162	241	139	39129	E
210	1,9	58	228	150	13287	T
211	2,1	100	116	129	11625	E
212	1,6	69	171	162	11860	T
213	1,9	107	170	136	18162	E
214	1,8	94	194	150	18269	E
215	3,9	107	131	148	14071	T
216	1,1	35	101	170	3525	EL
217	3,2	136	282	142	38412	T
218	1,9	96	140	147	13344	E
219	4,3	135	185	141	24938	T
220	3,0	155	235	157	36418	I2
221	4,3	127	220	155	28023	EL
222	2,2	88	227	149	19928	T
223	1,5	86	140	162	12129	EL
224	1,1	80	105	135	8428	E
225	1,2	72	76	138	5454	S
226	2,6	81	127	156	10260	E

227	1,2	70	73	138	5059	S
228	1,7	171	227	101	38882	E
229	1,8	84	194	146	16324	T
230	2,6	101	159	137	16016	E
231	1,4	87	129	156	11123	E
232	1,3	87	145	27	12575	E
233	1,2	120	132	145	15845	I1
234	0,8	70	77	137	5335	E
235	1,1	74	81	46	6001	E
236	1,0	51	136	161	6983	E
237	1,2	53	103	153	5451	E
238	1,0	103	134	135	13771	I1
239	1,5	158	189	123	29903	EL
240	1,1	95	139	81	13220	E
241	0,7	60	180	149	10763	T
242	1,0	72	95	37	6884	E
243	1,2	70	75	132	5277	E
244	2,2	70	73	46	5117	S
245	1,1	121	242	162	29173	I2
Add1	2,7	87	122	147	10664	EL

Appendix 2: Computer code for statistical data

Density and clustering code

```
# Point pattern analysis at Smeaheia for thesis work
# April 201, Elias Heimdal Leon

# Install of packages and library
install.packages("spatstat")
install.packages("stats")
install.packages("spdep")
install.packages("ggplot2")
library(spdep)
library(stats)
library(rgdal)
library(maptools)
library(spatstat)
library(ggplot2)

#My working directories to whereever shape files are
work <-'F:\\'
setwd(work)

# Load an GN1101 polygon shapefile as owin=observation window class
# This can be used for any other shapefile with points
```

```
s    <- readOGR(".", "GN1101")
smea    <- as(s, "owin")

# Load Horizon points merge into one shapefile, in ppp=point pattern class
po  <- readOGR(".","Seabed_Points")
SBpocks    <- as(po, "ppp")

p0  <- readOGR(".","Q11_Points")
Q11pocks    <- as(p0, "ppp")

#assign window to my observation window smea
Window(SBpocks) <- smea
Window(Q11pocks) <- smea

# Length between points are in meter, change to km
SBpocks.km <- rescale(SBpocks, 1000, "km")
Q11pocks.km <- rescale(Q11pocks, 1000, "km")
smea.km <- rescale(smea, 1000, "km")

# reassign points
marks(SBpocks)  <- NULL
marks(Q11pocks)  <- NULL
#_____________________________________________________
#Quadrate density
Q <- quadratcount(Q11pocks, nx= 32, ny=32)# nx=length and ny=height of Smeaheia
plot(Q11pocks, pch=16, cols="lightskyblue", main=NULL)  # points
plot(Q, cols="red", add=T)  # Add quadratcount grid and count
title(main = "Quadrat count for Q1.1 horizon ",
     cex.main = 2,   font.main= 4, col.main= "black")
#_____________________________________________________
# Adding my fault/subcrops polylines to the quadrata map
plot(vette,col="red", add=T,lwd=2)
plot(oygarden,col="red",add=TRUE,lwd=2)
plot(fw03,col="magenta",add=TRUE, lwd=2)
plot(fw01n,col="blue",add=TRUE,lwd=2)
plot(fw01s,col="blue",add=TRUE,lwd=2)
plot(shetland,col="green",add=TRUE,lwd=2)
plot(cromerKnoll,col="darkgreen",add=TRUE,lwd=2)
#_____________________________________________

# Compute the intensity/density for each quadrat (in counts per km2)
Q   <- quadratcount(Allpocks.km, nx= 32, ny=32)
plot(intensity(Q, image=TRUE), main=NULL, las=1)  # Plot density raster
plot(Allpocks.km, pch=20, cex=0.7,col=rgb(0,1,0,.5), add=T)  #points
title(main = "Intensity map based on
     quadrat count for all mapped pockmarks ",
     cex.main = 2,   font.main= 4, col.main= "black",
```

```
     xlab="Density count per km")

#Kernel density calc with sigma adjustment, and plot
K <- density(Allpocks.km, sigma=1) # sigma = st.dev
plot(K,las=1, main=NULL)
title(main = "Kernel density for
     SB horizon (sigma=1)",
     xlab="Density count per km",
     cex.main = 2,   font.main= 4, col.main= "black")
contour(K,add=T,lwd=1.5,col="black", nlevels = 10)
#_____________________________________________________________

#Monte Carlo simulation with 1000 points
n     <- 1000  #numb points
for (i in 1:n){
  # Generate random points
  random.p   <- rpoint(n=SBpocks.km$n, win=smea.km)
}

#What if Smeaheia had pockmarks randomly distributed?
#A complete random pockmark field at Smeaheia
plot(rand.p, pch=20, cex=0.7,
    main="Monte Carlo simulation.
    Random pockmark field generated at Smeaheia (points=1000)",
    cols=rgb(1,0,0,0.7))

# Cluster Tests_____________________________

#ANN average first nearest neighbor
# k_th nearest neighbour
mean(nndist(random.p, k=1))
mean(nndist(SBpocks, k=1))

# Edge correction methods:isotropic, translate and border corrections
#K_pois =theoretical K-function or estimated
#K-function estimated under the null hypothesis that the points are completely
#randomly distributed
K <- Kest(Q11pocks.km, correction=c("Ripley")) #"Ripley"
plot(K, main=NULL, las=1, cex.axis=1.5,cex.lab=1.7)
title(main = "Ripley's K-function for Q1.1 horizon",
     cex.main = 2,   font.main= 4, col.main= "black")

#Calculates an estimate of the L-function
#(Besag's transformation of Ripley's K-function)
L1 <- Lest(SBpocks.km)
plot(L1, main=NULL, las=1, cex.axis=1.5,cex.lab=1.7)
title(main = "L-function for Q1.1 horizon",
```

```
    cex.main = 2,   font.main= 4, col.main= "black")
```

Plots and normality test code

```
# Histograms, box plots, Q-Q plots and normality test for Smeaheia data
# April 2019, Elias Heimdal Leon

#load data
Horizon_population1_data<-read.table("F:\\HorizonPop1_Data.csv", header=T, sep=";")
Horizon_population2_data<-read.table("F:\\HorizonPop2_Data.csv", header=T, sep=";")
Horizon_residu<-read.table("F:\\Horizon_residu.csv", header=T, sep=";")

#Attach name to variables in object
attach(Horizon_population1_data)
names(Horizon_population1_data)

# SCATTERPLOTS FOR STATISTICS

# Histogram plots
hist(XX_data$Variable_name, col="whatever_colour", xlab = "Variable_name [m]",
    xlim = c(XX,XX),ylim =c(0,XX),cex.axis=1.3,cex.lab=1.5,
    main="XX horizon: Pockmark XX in population XX", cex.main=1.5)

## Normal Q-Q plot
qqnorm(XX_data$Width,col="blue", lwd=2,cex.axis=1.3,cex.lab=1.5,
      main = "Normal Q-Q plot for XX horizon population 1 - Width",cex.main=1.5)
qqline(XX_data$Width, col="black",lwd=2) # 1-3 percentile

boxplot(XX1_data$Width,XX2_dataOut$Width, XX3_dataOut2$Width,col="lightblue",
       cex.axis=1.2,cex.lab=1.3,names=c("Pop. 1","Pop. 2", "Residuals"),
       ylab ="Width (m)", xlab ="Q3.2 populations")
title("Box and Whisker plot of pockmark width on XX horizon", cex.main=1.5)
#_____________________________________________
# Outlier test
install.packages("magrittr")
```

```
install.packages("outliers")
library(outliers)
library(ggpubr)


#Normality test Shapiro-Wilk test of normality for one variable (univariate):
#the p-value > 0.05 implying that the distribution of the data are
#not significantly different from normal distribution. In other words,
#we can assume the normality.!! Very sensitive to outliers!!
shapiro.test(Dataset$Variable_name)

# Grubbs Test for ouliers, type 11 tests both ends
# G value is standard deviations from mean,
# Additional value U is ratio of sample variances
grubbs.test(Dataset$Variable_name,type = 11)
```

Appendix 3: Spatial point analysis equations

Mean centre: $$\bar{s} = \left[\frac{\sum_{i=1}^{n} x_i}{n}, \frac{\sum_{i=1}^{n} y_i}{n}\right]$$

Standard distance: $$d = \sqrt{\frac{\sum_{i=1}^{n}(x_i - u_x)^2 + (y_i - u_y)^2}{n}}$$

Standard deviational ellipse: $$d_x = \sqrt{\frac{\sum_{i=1}^{n}(x_i - u_x)^2}{n}} \quad , \quad d_y = \sqrt{\frac{\sum_{i=1}^{n}(y_i - u_y)^2}{n}}$$

Equations from Gimond (2019).

Appendix 4: Mathematical equations for the statistical analysis.

K-function (Ripley, 1977)

$$\widehat{K}(d) = \frac{R}{n^2}\sum_{i=1}^{n}\sum_{j=1}^{n} W_{ij} \qquad for \quad \text{i} \neq j$$

Equations from Aldstadt (2010), where ***R*** is the size of the study area, ***W*** is a binary weights matrix equal to one when points ***i*** and ***j*** are within distance ***d***, and zero otherwise.

L-function (Besag, 1977)

$$\hat{L}(d) = \sqrt{\frac{\hat{K}(d)}{\pi}}$$

Equations from Aldstadt (2010). Where K(d) is the original K-function. The expected value of L(d) under CSR is ***d***. Values greater than ***d*** indicates clustering and the lesser value than ***d*** is dispersion.

Letter**s** ***i*** and ***j*** is less than d, otherwise zero. A given edge correction will modify $\mathbf{k_{ij}}$ slightly, just as the original K-function.

Grubb's test (Grubbs, 1950)

Grubbs' test is defined for the hypothesis:

H_null: There are no outliers in the data set

H_ alternative: There is exactly one outlier in the data set

The Grubbs' test statistic is defined as:

$$G = \max |Y_i - \bar{Y}| / s$$

, where $\bar{Y}$ and s denote the sample mean and standard deviation. The Grubbs' test statistic is the largest absolute deviation from the sample mean in units of the sample standard deviation (NIST, 2013).

Appendix 5: Graphs of K- and L-function.

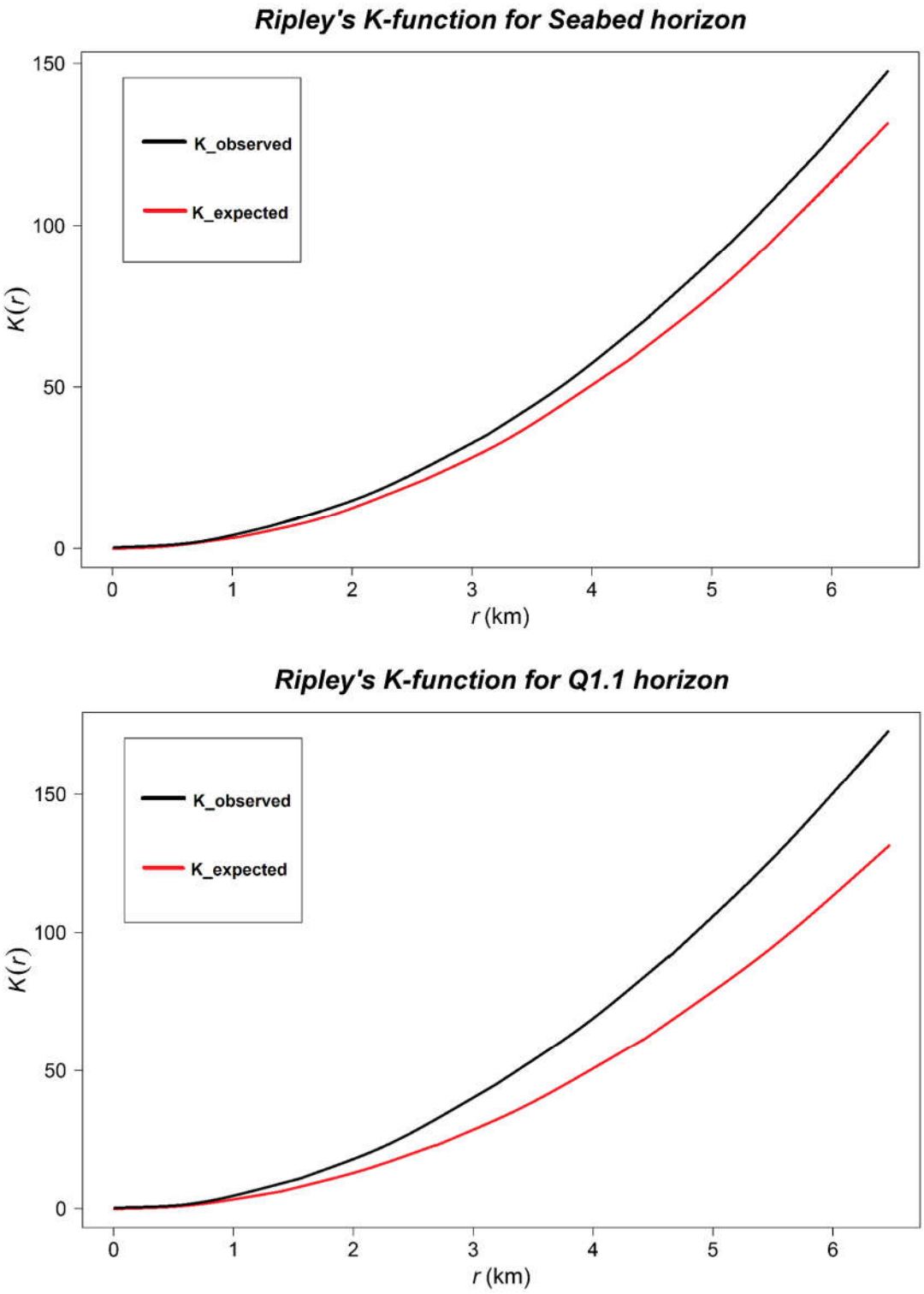

Figure 6.1: Ripley's K-function for Seabed and Q1.1 horizon. Results show shorter distances than expected.

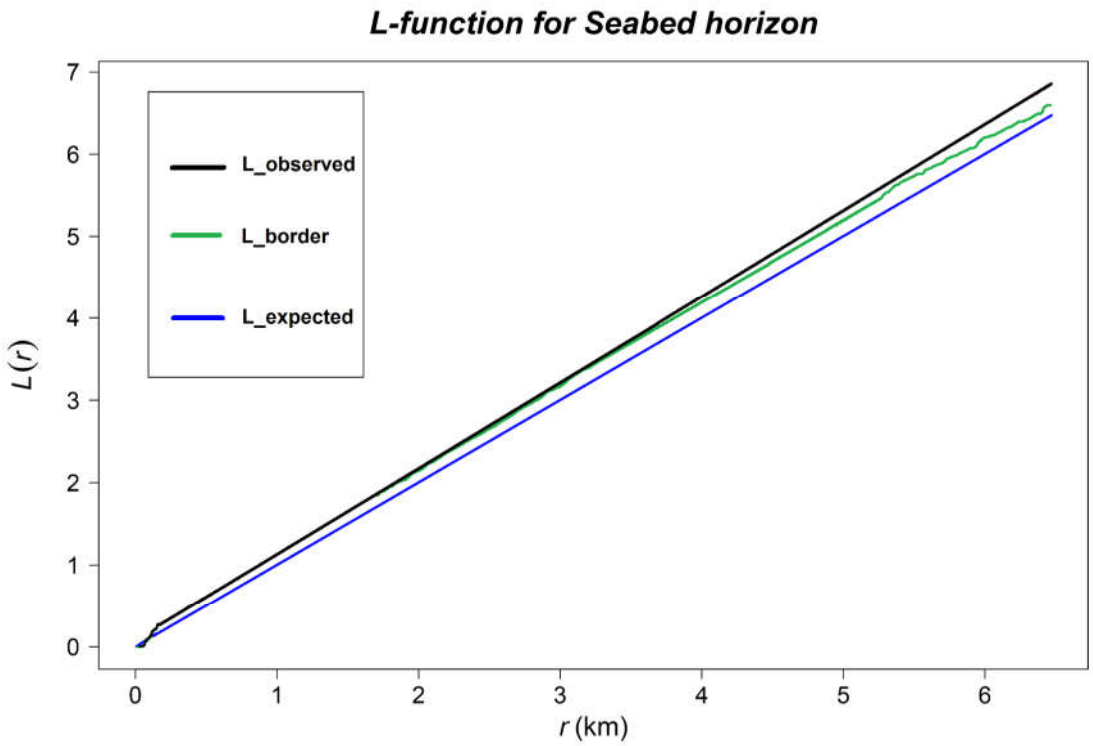

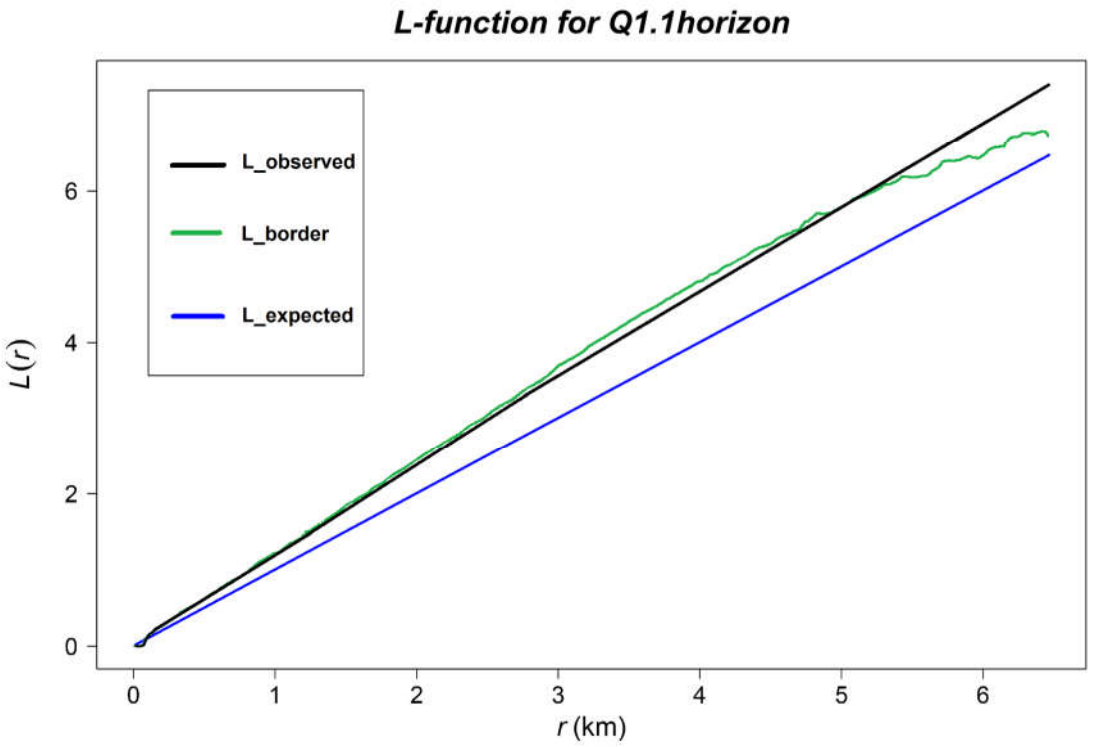

Figure 6.2: L-function for Seabed and Q1.1 horizon. Results show point pattern with the border edge correction changes to a random pattern past 6 km radius.

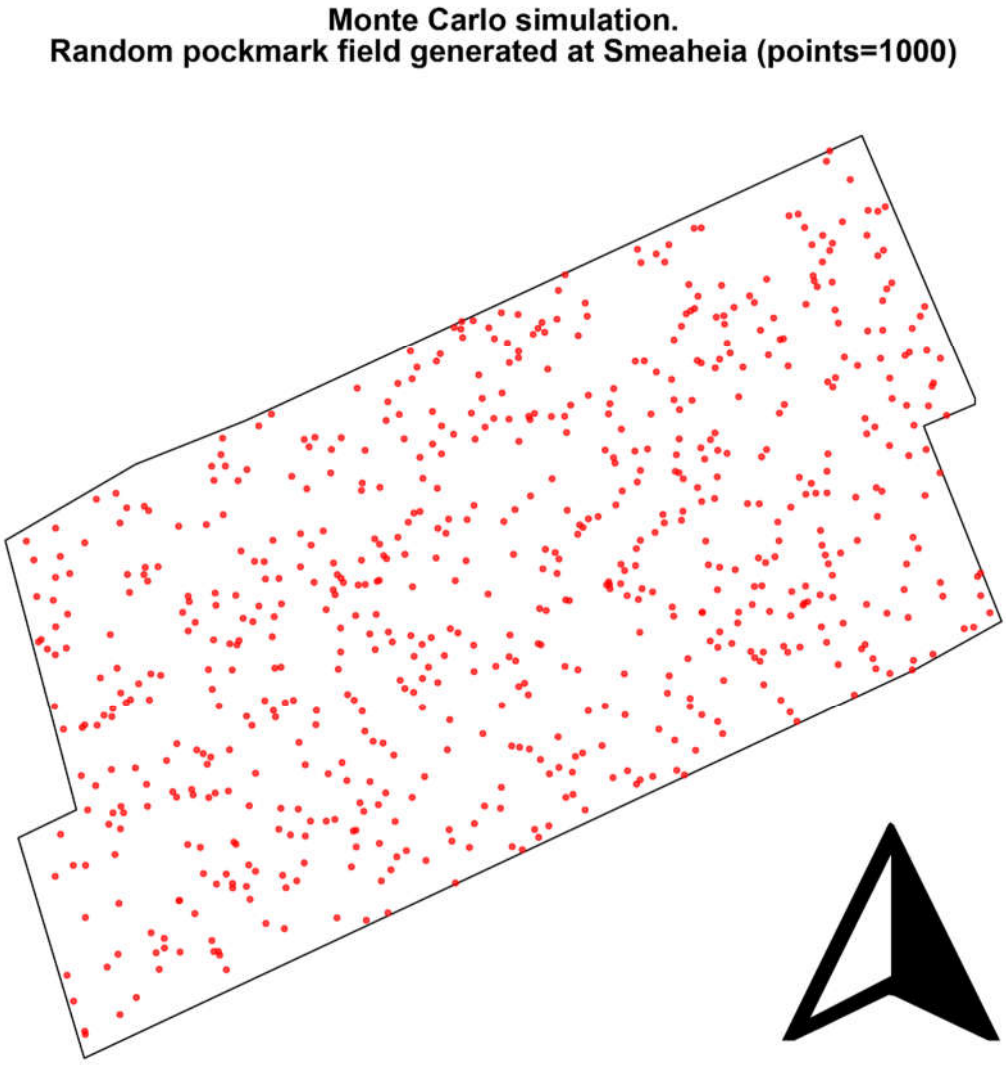

Figure 6.3: A field of randomly distributed pockmarks at Smeaheia generated for the calculation of expected point distances in a random pattern. The randomness was generated using a Monte Carlo simulation. The field has 1000 points although not all points are visible due to the resolution and view distance.

Appendix 6: Normality tests of horizon populations

Table 6.7: Shapiro-Wilk normality test of horizon data. This method tested against the assumption of normality. Null hypothesis assumed sample from a normal distribution; else it rejects the assumption if p-value is less than 0.05.

Shapiro-Wilk normality test	p-value	W-score	Normal distribution
SB_pop1_data$Width	2.808e-10	0.96764	Reject
SB_pop2_data$Width	0.2253	0.97238	Accept
SB_pop1_data$Area	< 2.2e-16	0.92066	Reject
SB_pop2_data$Area	9.275e-05	0.88912	Reject
Q11_pop1_data$Width	1.434e-10	0.96592	Reject
Q11_pop2_data$Width	0.08308	0.95394	Accept
Q11_pop1_data$Area	< 2.2e-16	0.92265	Reject
Q11_pop2_data$Area	0.003415	0.91397	Reject?
Q12_pop1_data$Width	4.14e-05	0.95983	Reject
Q12_pop2_data$Width	0.06478	0.95004	Accept
Q12_pop1_data$Area	1.664e-09	0.90475	Reject
Q12_pop2_data$Area	0.2757	0.8902	Accept
Q21_pop0_data$Width	2.183e-07	0.96453	Reject
Q21_pop1_data$Width	0.0009196	0.9919	Reject
Q21_pop2_data$Width	0.8445	0.99207	Accept
Q21_pop0_data$Area	0.0005698	0.98344	Reject
Q21_pop1_data$Area	4.751e-14	0.95208	Reject
Q21_pop2_data$Area	4.476e-06	0.90681	Reject
Q31_pop1_data$Width	4.904e-05	0.95356	Reject
Q31_pop2_data$Width	0.2959	0.97468	Accept
Q31_pop1_data$Area	9.718e-10	0.88254	Reject
Q31_pop2_data$Area	0.0109	0.94253	Reject
Q32_pop1_data$Width	1.906e-05	0.96079	Reject
Q32_pop2_data$Width	0.01187	0.91523	Reject
Q32_pop1_data$Area	6.216e-11	0.89288	Reject
Q32_pop2_data$Area	0.000777	0.86923	Reject

Table 6.8: Grubb test of horizon population data. U-value is ratio of sample variances. G-value is standard deviations from mean. Null hypothesis assumes no outliers in data sample. P-value of 1 confirms the null hypothesis, less than 0.05 rejects it.

Grubbs test	p-value	G-value	U-value	Outliers
SB_pop1_data$Width	1	5.43010	0.97554	No
SB_pop2_data$Width	1	4.05550	0.84811	No
SB_pop1_data$Area	1	4.94520	0.97893	No
SB_pop2_data$Area	1	3.84820	0.84518	No
Q11_pop1_data$Width	1	5.45330	0.97513	No
Q11_pop2_data$Width	1	3.73420	0.83295	No
Q11_pop1_data$Area	1	5.02020	0.97813	No
Q11_pop2_data$Area	1	3.63570	0.82849	No
Q12_pop1_data$Width	1	5.09720	0.92772	No
Q12_pop2_data$Width	1	3.61260	0.84075	No
Q12_pop1_data$Area	1	4.42570	0.94243	No
Q12_pop2_data$Area	1	3.95020	0.79626	No
Q21_pop0_data$Width	1	4.82100	0.96589	No
Q21_pop1_data$Width	1	5.206	0.980	No
Q21_pop2_data$Width	1	4.71320	0.88307	No
Q21_pop0_data$Area	1	4.80870	0.96603	No
Q21_pop1_data$Area	1	4.46230	0.98458	No
Q21_pop2_data$Area	1	3.90230	0.91668	No
Q31_pop1_data$Width	1	4.9344	0.9208	No
Q31_pop2_data$Width	1	4.15910	0.83332	No
Q31_pop1_data$Area	1	4.22130	0.93709	No
Q31_pop2_data$Area	1	4.28050	0.81515	No
Q32_pop1_data$Width	1	5.35560	0.92968	No
Q32_pop2_data$Width	1	3.69950	0.77672	No
Q32_pop1_data$Area	1	4.37610	0.94498	No
Q32_pop2_data$Area	1	3.03090	0.85229	No

Appendix 7: Graphical normality test with Q-Q plots

Q-Q plots Q3.2 URU horizon

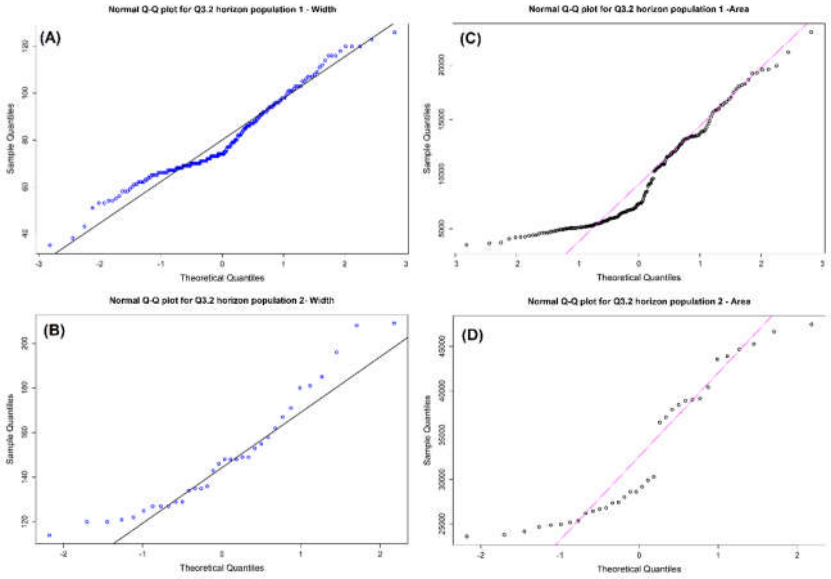

Figure 6.4: Q-Q plots for Q3.2 URU horizon. (A) Plot for population 1 width. (B) Plot for population 2 width. (C) Plot for population 1 area. (D) Plot for population 2 area.

Q-Q plots Q3.1 horizon

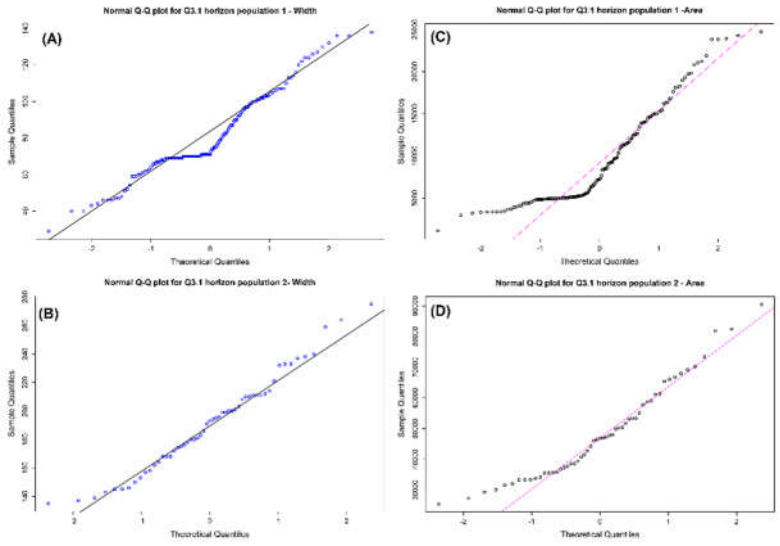

Figure 6.5: Q-Q plots for Q3.1 horizon. (A) Plot for population 1 width. (B) Plot for population 2 width. (C) Plot for population 1 area. (D) Plot for population 2 area

Q-Q plots Q2.1 horizon

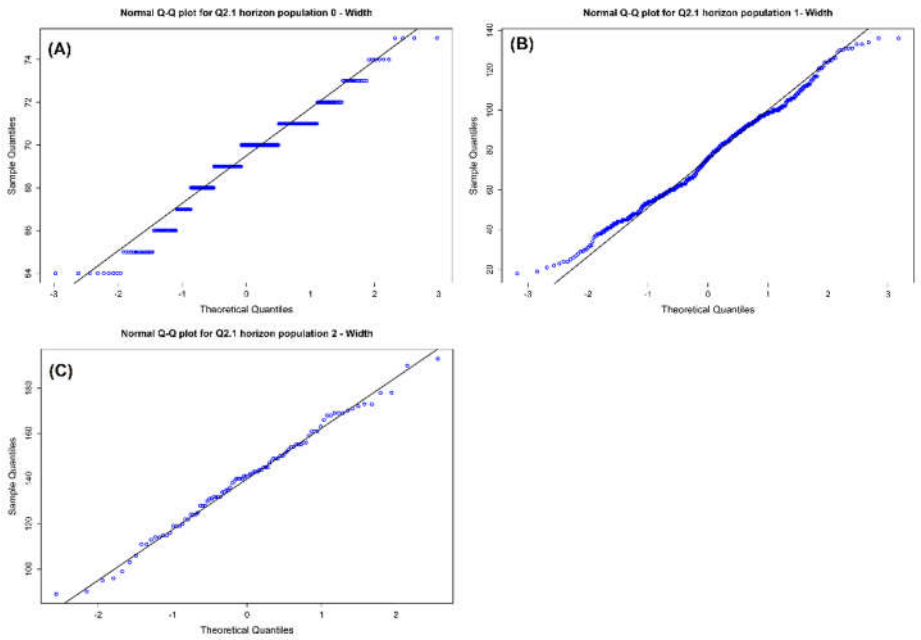

Figure 6.6: Q-Q plots for Q2.1 horizon width. (A) Plot for population 0 width. (B) Plot for population 1 width. (C) Plot for population 1 width.

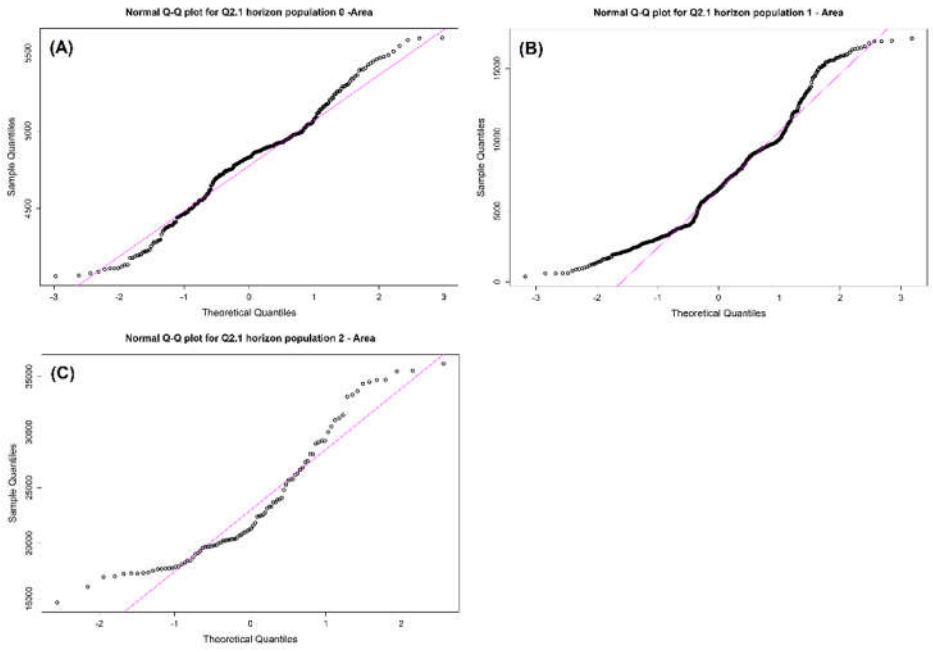

Figure 6.7: Q-Q plots for Q2.1 horizon area. (A) Plot for population 0 area. (B) Plot for population 1 area. (C) Plot for population 2 area.

Q-Q plots Q1.2 horizon

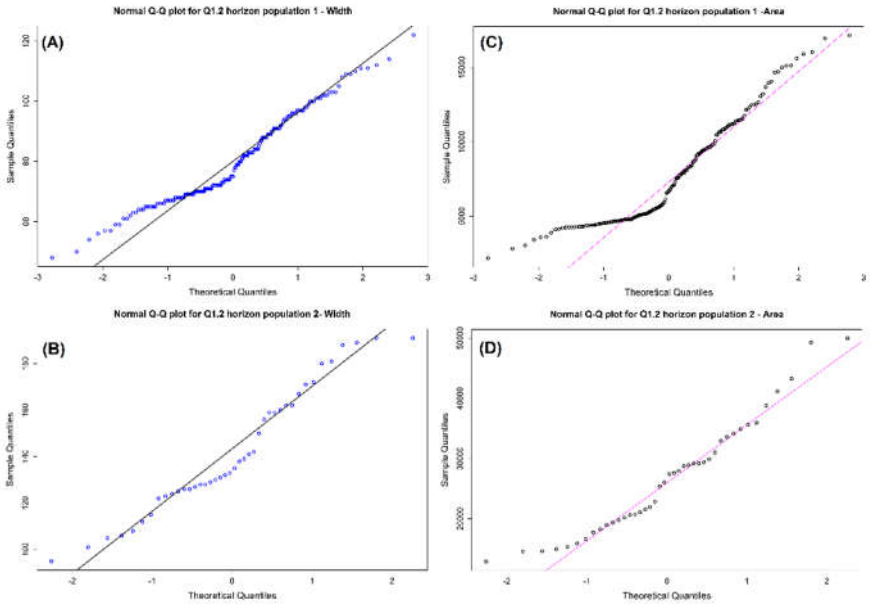

Figure 6.8: Q-Q plots for Q1.2 horizon. (A) Plot for population 1 width. (B) Plot for population 2 width. (C) Plot for population 1 area. (D) Plot for population 2 area.

Q-Q plots Q1.1 horizon

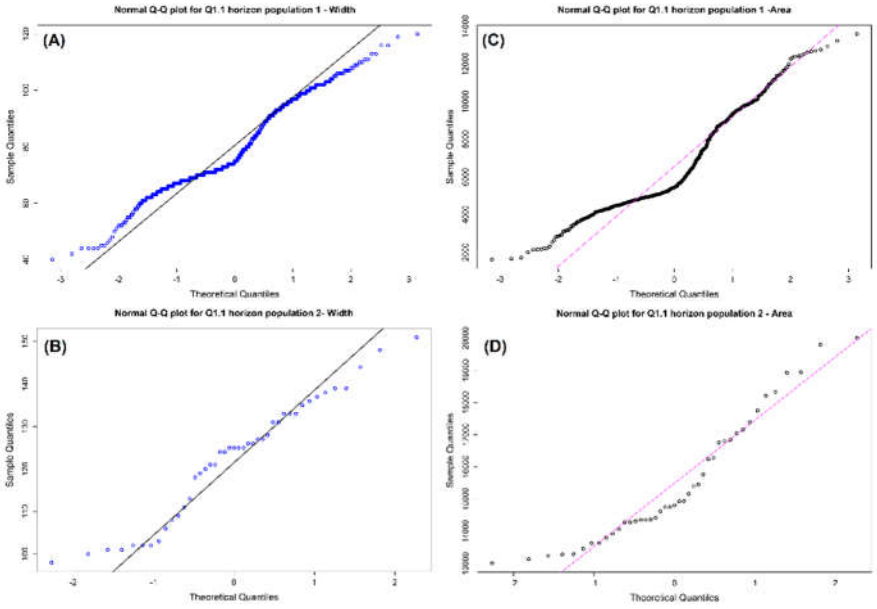

Figure 6.9: Q-Q plots for Q1.1 horizon. (A) Plot for population 1 width. (B) Plot for population 2 width. (C) Plot for population 1 area. (D) Plot for population 2 area.

Q-Q plots Seabed horizon

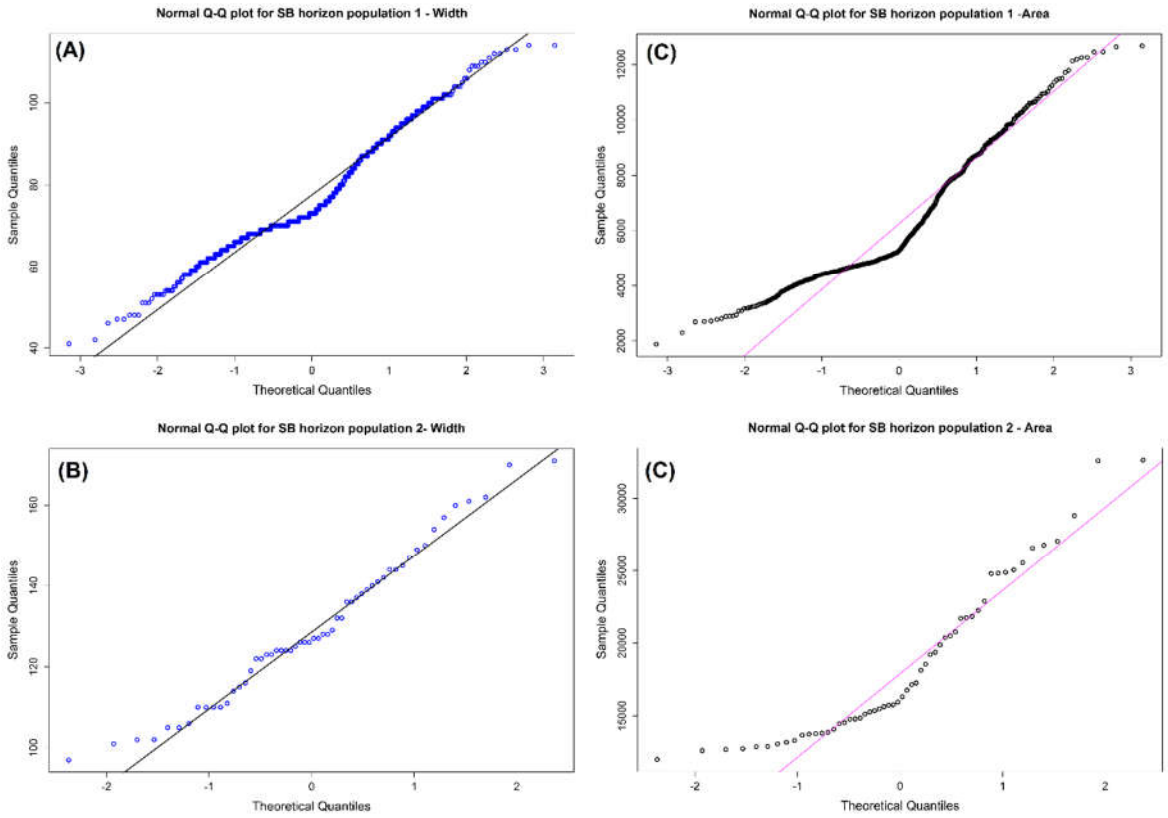

Figure 6.10: Q-Q plots for Seabed horizon. (A) Plot for population 1 width. (B) Plot for population 2 width. (C) Plot for population 1 area. (D) Plot for population 2 area.